University
of Glasgow

Hollyer, Tristan (2016) *MRI indices of functional recovery following intracerebral implantation of a human neural stem cell line in a pre-clinical model of ischaemic stroke.* PhD thesis.

http://theses.gla.ac.uk/7667/

MRI INDICES OF FUNCTIONAL RECOVERY FOLLOWING INTRACEREBRAL IMPLANTATION OF A HUMAN NEURAL STEM CELL LINE IN A PRE-CLINICAL MODEL OF ISCHAEMIC STROKE

TRISTAN HOLLYER

B.Sc (Hons) Biomedical Science (Pharmacology)
University of Aberdeen

Submitted in fulfilment of the requirements for the
Degree of Doctor of Philosophy (Ph.D)

Institute of Neuroscience & Psychology
College of Medical, Veterinary, & Life Sciences
University of Glasgow

October 2016

ABSTRACT

Stem cell therapy for ischaemic stroke is an emerging field in light of an increasing number of patients surviving with permanent disability. Several allogenic and autologous cells types are now in clinical trials with preliminary evidence of safety. Some clinical studies have reported functional improvements in some patients.

After initial safety evaluation in a Phase 1 study, the conditionally immortalised human neural stem cell line CTX0E03 is currently in a Phase 2 clinical trial (PISCES-II). Previous pre-clinical studies conducted by ReNeuron Ltd, showed evidence of functional recovery in the Bilateral Asymmetry test up to 6 weeks following transplantation into rodent brain, 4 weeks after middle cerebral artery occlusion.

Resting-state fMRI is increasingly used to investigate brain function in health and disease, and may also act as a predictor of recovery due to known network changes in the post-stroke recovery period. Resting-state methods have also been applied to non-human primates and rodents which have been found to have analogous resting-state networks to humans. The sensorimotor resting-state network of rodents is impaired following experimental focal ischaemia of the middle cerebral artery territory. However, the effects of stem cell implantation on brain functional networks has not previously been investigated.

Prior studies assessed sensorimotor function following sub-cortical implantation of CTX0E03 cells in the rodent post-stroke brain but with no MRI assessments of functional improvements. This thesis presents research on the effect of sub-cortical implantation of CTX0E03 cells on the resting- state sensorimotor network and sensorimotor deficits in the rat following experimental stroke, using protocols based on previous work with this cell line. The work in this thesis identified functional tests of appropriate sensitivity for long-term dysfunction suitable for this laboratory, and investigated non-invasive monitoring of physiological variables required to optimize BOLD signal stability within a high-field MRI scanner.

Following experimental stroke, rats demonstrated expected sensorimotor dysfunction and changes in the resting-state sensorimotor network. CTX0E03 cells did not improve post-stroke functional outcome (compared to previous studies) and with no changes in resting-state sensorimotor network activity. However, in control animals, we observed changes in functional networks due to the stereotaxic procedure. This illustrates the sensitivity of resting-state fMRI to stereotaxic procedures. We hypothesise that the damage caused by cell or vehicle implantation may have prevented functional and network recovery which has not been previously identified due to the application of different functional tests.

The findings in this thesis represent one of few pre-clinical studies in resting-state fMRI network changes post-stroke and the only to date applying this technique to evaluate functional outcomes following a clinically applicable human neural stem cell treatment for ischaemic stroke. It was found that injury caused by stereotaxic injection should be taken into account when assessing the effectiveness of treatment.

CONTENTS

LIST OF FIGURES

LIST OF TABLES

ACKNOWLEDGEMENTS

'There is much to know and life is short, a life without knowledge is not a life',
Baltasar Gracián.

AUTHOR'S DECLARATION

I hereby declare that, except where explicit reference is made to the contribution of others, this thesis is the result of my own work and has not been submitted for any other degree at the University of Glasgow or any other institution.

TRISTAN HOLLYER

LIST OF ABBREVIATIONS

4-OHT 4-hydroxytamoxifen

ADP Adenosine Diphosphate

AMPA α-amino-3-hydroxy-5-methyl-4-isoxazolepropionic acid

ANOVA Analysis of Variance

ARAT Action Research Arm Test

ATP Adenosine Triphosphate

AUC Area Under the Curve

BAT Bilateral Assymetry Test

BI Barthel Index

BOLD Blood Oxygenation Level Dependent

CBF Cerebral Blood Flow

CBV Cerebral Blood Volume

CC Corpus Callosum

CCL C-C motif ligands

CIMT Constraint-Induced Movement Therapy

CNS Central Nervous System

CPP Cerebral Perfusion Pressure

CPu Caudate putamen

CsA Cyclosporine A

CT   Computed Tomography

CTX-cell CTX0E03 cell

Cx   Cortex

DALY Disability-adjusted life year

DMN Default Mode Network

DTI   Diffusion Tensor Imaging

DWI   Diffusion Weighted Imaging

ECA   External Carotid Artery

EEG   Electro-encephalogram

EGF   Epidermal Growth Factor

EPI   Echo Planar Imaging

ER   Oestrogen Receptor

FA   Fractional anisotropy

FID   Free Induction Decay

FLASH Fast Low Angle Shot

fMRI   functional Magnetic Resonance Imaging

FOV   Field of View

FWHM Full-weight at half maximum

GABA γ-aminobutyric acid

GAP-43 Growth Associated Protein - 43

GFAP Glial Fibrilliary Acidic Protein

GP   Globus Pallidus

GPCR G-protein Coupled Receptor

GRE Gradient Refocused Echoes

H&E Haematoxylin & Eosin

HRF Haemodynamic Response Function

HUVEC Human Umbilical Vascular Endothelial Cells

ICA Internal Carotid Artery

ICAM-1 Intra-Celluar Adhesion Molecule-1

ICP Intra-Cranial Pressure

ILF Intra-Luminal Filament

IR Infra-red

Irf-1 Interferon Regulatory Factor-1

ISFs Infra-slow Fluctuations

LC Locus Coeruleus

LFP Local Field Potential

LTP Long-term Potentiation

MAP-2 Microtubule-associated protein 2

MCAO Middle Cerebral Artery Occlusion

MEG Magnetoencephalography

MMP Matrix Metalloproteinases

MRI Magnetic Resonance Imaging

MSC Mesenchymal Stem Cell

NACWO Named Animal Care & Welfare Officer

NF-κB Nuclear Factor-κB

NHP Non-Human Primates

NICE National Institute for Health and Care Excellence

NIHSS National Institute of Health Stroke Scale

NMDA N-Methyl-D-aspartate

NPC Neural Progenitor Cells

NVO Named Veterinary Officer

OA Occipital Artery

OEF Oxygen Extraction Fraction

PAM Paraformaldehyde

PE Poly-ethylene

PET Positron Emission Tomography

PISCES Pilot Investigation of Stem Cells in Stroke

PO Posterior Thalamic Nucleus

PtA Pterygopalatine Artery

RARE Rapid Imaging with Refocussed Echoes

RF Radio Frequency

RMS Rostral-Migratory Stream

ROI Region of Interest

ROS Reactive Oxygen Species

rs-fMRI resting-state functional MRI

SD Standard deviation

SE	Spin-echo
SGZ	Sub-Granular Zone
SMT	Sensorimotor Thalamus
SNR	Signal-to-noise ratio
SPM	Statistical Parametric Mapping
SVZ	Sub-Ventricular Zone
TBM	Tensor Based Morphometry
TE	Time to Echo
TNFα	Tumour Necrosis Factor-alpha
tPA	tissue Plasminogen Activator
TR	Time to repetition
TTC	2, 3, 5-triphenyltetrazolium chloride
VBM	Voxel Based Morphometry
VDM	Voxel Displacement Map
VEGF	Vascular Endothelial Growth Factor
VL	Ventro-lateral Thalamic Nucleus
VP	Ventro-posterior Thalamic Nucleus
VRF	Veterinary Research Facility
VLSM	Voxel Lesion Symptom Mapping
vWF	vonWillibrand Factor
WHO	World Health Organisation

INTRODUCTION

1.1 STROKE

Stroke is a term used to describe a wide array of central nervous system disorders associated with any cerebrovascular disorder resulting in an acute clinical presentation. These include sub-arachnoid and intracerebral haemorrhages, silent infarction, and ischaemic infarction determined via evidence of ischaemic injury within a vascular territory and with clinical symptoms lasting for greater than 24 hours or until death (Sacco et al., 2013). With high metabolic demands (requiring 15% of cardiac output) and limited energy reserves, the brain is highly sensitive to persistent perturbations in CBF (cerebral blood flow). As a consequence, the affected area of the brain dies leading to permanent loss of function with limited recovery.

1.1.1 *Stroke subtypes & epidemiology*

Stroke affects 15 million people worldwide (WHO). Cerebrovascular disease accounts for 6.3% of the global Disability Adjusted Life Years (DALYs) i.e. the total number of potential years lost by premature death due to disease, totalling 9.35 millions of years (Lopez et al., 2006). In the UK, stroke is believed to cost £3 billion a year with over 4000 deaths in Scotland in 2014 (Scottish Stroke Statistics, 2016) and a wider economic cost of £8 billion primarily due to the effect of permanent post-stroke disability. Although

the mortality rate from stroke has decreased by 39% in the last 10 years in Scotland (Scottish Stroke Statistics, 2016), over 50% of stroke survivors are left permanently disabled, leading it to be the greatest range of disability burden of any disease (Adamson et al., 2004).

The two main forms of stroke are occlusive ischaemic (80% incidence) or haemorrhagic (20% incidence), with each requiring its own unique form of clinical management (Heiss, 2010). Haemorrhagic stroke is typically caused by amyloid angiopathy (Thanvi and Robinson, 2006). Occlusive ischaemic stroke occurs when an embolus (coagulated blood) occludes a cerebral vessel permanently or transiently. Small vessel disease also causes ischaemic stroke but is mechanistically less well understood. The artery occluded determines the region of the brain affected and the resultant symptoms.

1.1.2   *Cerebral blood flow, autoregulation, and stroke*

The brain's dependence on a continuous supply of oxygen and glucose has led to the evolution of mechanisms to ensure blood supply is not perturbed. *Autoregulation* assures that across a range of systemic mean arterial blood pressures, cerebral perfusion pressure (CPP) is maintained. CPP is regulated by arteriolar diameter to control flow and volume (Lassen, 1959) via a plethora of factors, most importantly carbon dioxide, a potent vasodilator (Gibbs and Gibbs, 1935; Meng and Gelb, 2015). Other factors include hydrogen ion concentrations and vascular smooth muscle responses via sheer stress receptors (Lassen and Christensen, 1976). Many of these contributors are the product of the metabolic demand of the neurons. Indeed, coupling of the cerebral vasculature to the

neurons helps to maintain adequate function (see Section 1.4.1).

Autoregulation can be summarised as a ratio between CBF and CPP detailing the ranges at which it can be maintained (typically $60 - 150$ mmHg, Figure 1). Lower perfusion pressures will cause vasodilation and vasoconstriction at high pressure within the aforementioned limits. Out-with these limits, flow is no longer pressure-independent and hypo-/hyper-perfusion will occur.

Human CBF is approximately 60ml/100g/min (Steiner and Andrews, 2006) and 100ml/100g/min in the rat (Hernández et al., 1978). Autoregulation exists to protect the brain from ischaemic damage as a consequence of systemic blood loss, traumatic injury, haemorrhage or from high blood pressure which may limit oxygen extraction. Ischaemic stroke can cause a loss of autoregulation leading to hypoperfusion, contributing to stroke pathogenesis (Dohmen et al., 2007).

Following occlusion of a cerebral artery, CBF reduces across the vascular territory. In end-arteries, this reduction in perfusion is the most severe, however this is partly determined by the collateral vascular anatomy of the area where the converse may occur. Instantaneous reduction in perfusion pressure soon causes damage to the affected tissue (see below). The perfusion thresholds at which particular forms of damage/perturbations occurs were initially determined in the baboon (Branston et al., 1974; Astrup et al., 1977). Branston *et al.* showed that cortical evoked potentials on the somatosensory cortex decreased as a function of blood flow (measured by the hydrogen clearance method (Pasztor et al., 1973)), with complete failure of evoked responses at 15ml/100g/min. It was later demonstrated the CBF threshold for failure of cortical
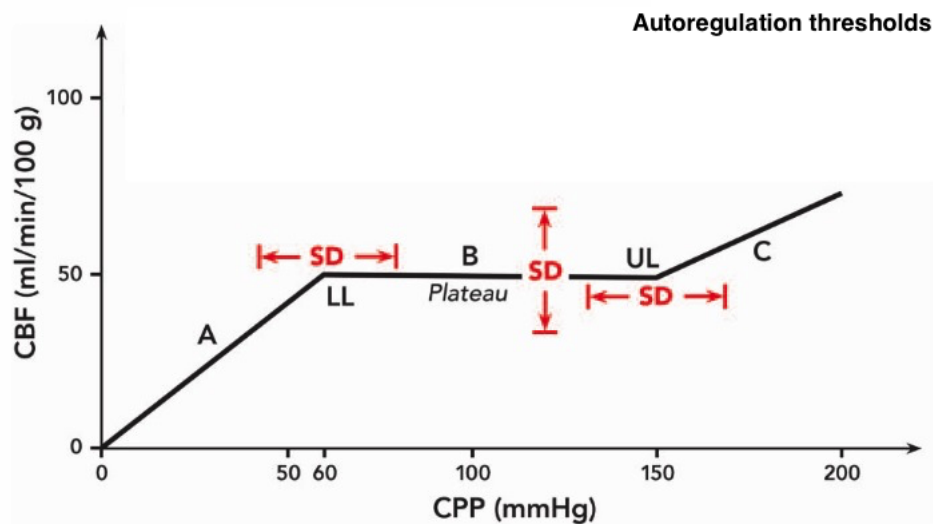
Figure 1: Illustration of cerebral autoregulation as a ratio of CBF and CPP in man. Autoregulation is pressure-independent along a range of approximately $60 - 150$mmHg (*Plateau*, **B**). CBF becomes pressure-dependent at the lower limit (LL, **A**), upper limit (UL, **C**), and standard deviation (SD, **SD**). Image adapted from Meng and Gelb (2015)

evoked potentials was less than that for the depolarisation of neurons caused by the release of intracellular potassium (Astrup et al., 1977). This confirmed earlier hypotheses of an ischaemic *'penumbra'* whereby at a certain level of reduced CBF, neurons are functionally inactive but are structurally uncompromised and therefore potentially salvageable. Astrup *et al.* determined the CBF threshold for the ischaemic penumbra to be between 10 and 17 ml/100g/min. Below this, cell death would occur rapidly and irreversibly. Between normal CBF (50ml/100g/min) and the upper limit for the ischaemic penumbra, the brain exists in a state called *benign oligaemia*. Here, there is reduced CBF and CPP but with no functional impairment due to increased oxygen extraction fraction (OEF, Lee et al. (2005)). Figure 2 illustrates the CBF thresholds at which these various pathologies occur.
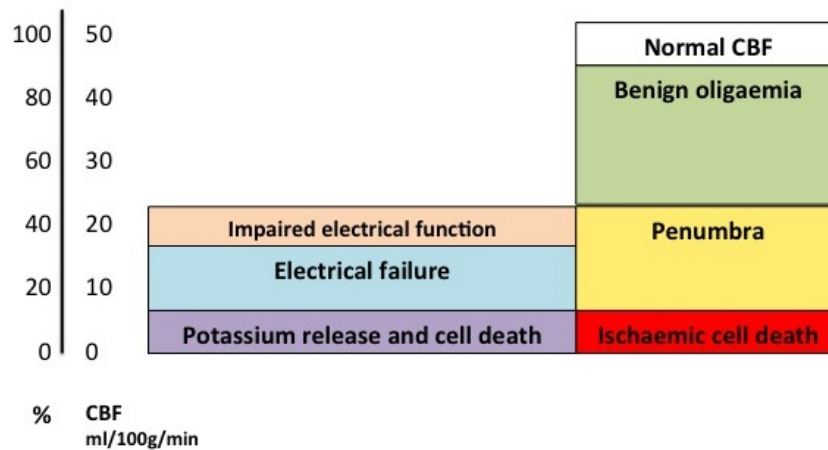
Figure 2: The CBF thresholds of cellular impairment and death. Cell death occurs below 10ml/100g/min; the penumbra at $10 - 17$ml/100g/min, and benign oligaemia $18 - 45$ ml/100g/min. Image adapted from non-human primate data from Astrup et al. (1977)

1.1.3 *Acute ischaemic stroke pathophysiology*

A severe reduction in cerebral blood flow following occlusion of a cerebral blood vessel impedes the delivery of oxygen and glucose to the local parenchyma known as the ischaemic core. As a consequence, a cascade of pathological mechanisms, beginning a few minutes after the reduction in perfusion come into play eventually resulting in the death of the tissue. The time course of the acute, and chronic, stroke pathological processes are detailed in Figure 3.

The initial insult & excitotoxicity

The interruption in normal perfusion very quickly leads to a depletion of limited ATP (adenosine triphosphate) reserves and a concurrent rise in ADP (adenosine diphosphate) after 30 seconds (Katsura et al., 1994). Unable to maintain membrane potentials (via the failure of Na^+/K^+-ATPase), intracellular concentrations of K^+ fall and cell membranes depolarise, activating voltage-

dependent Ca^{2+} channels, causing the release of glutamate into the extracellular space. Increases in glutamate (with limited re-uptake) activate ionotropic NMDA (N-methyl-D-aspartate), AMPA (α-amino-3- hydroxyl-5-methyl-4-isoxazole-propionate), kainate, and metabotropic glutamate receptors (mGLuR), (Beart and O'Shea, 2007), initiating excitotoxic effects. The NMDA receptor is permeable to Ca^{2+} and mGluR, causing release of Ca^{2+} from endoplasmic reticulum (ER) stores via the IP_3 (inositol triphosphate) pathways. Although the ER and mitochondria often act as sinks for intracellular calcium, overloading leads to formation of reactive oxygen species (via excessive nitric oxide production increasing peroxynitrite levels) and activation of calcium dependent proteins such as calpains and lipases; causing damage to cell membranes. The increased influx of sodium (and chloride) ions leads to passive influx of water into the cells causing a decline in ADC (Apparent Diffusion Coefficient), resulting in DWI (Diffusion Weighted Imaging) hyperintensities, following experimental and human cerebral ischaemia (Schlaug et al., 1997; Lansberg et al., 2001; Wegener et al., 2005). Gradually, several hours after ischaemia, intravascular water shifts to the extracellular space causing vasogenic oedema detected as T_2 hyperintensities on MRI, compromising perfusion, and increasing intra-cranial pressure (ICP, von Kummer et al. (2015)).

Acute inflammation

As soon as oxidative stress occurs, reactive oxygen species (ROS) activate the coagulation cascade (causing microvessel occlusions), the proteolytic complement system (Napoli, 2001), and the release of Interleukin-1α from the endothelium. Other pro-inflammatory cytokines such as Nuclear Factor -κB (NF-κB), Interferon Regulatory Factor 1 (Irf-1), and Tumour Necrosis Factor-alpha (TNFα) are

released by damaged cells (Iadecola and Anrather, 2011). Consequently, endothlial expression of ICAM-1 (Intercellular Adhesion Molecule-1), E-selectins, P-selectins, and Matrix metalloproteinase (MMP) release, coupled with regulation of junctional proteins, increase neutrophil and macrophage extravasation (Engelhardt and Sorokin, 2009). Within the brain, microglia change their morphology to active or phagocytic ameboid types within 4 hours following ischaemia also contributing to the inflammatory process. Splenomegaly is a well documented response to ischaemia with increases in production of the aforementioned cytokines and C-C motif ligands (such as CCL2, CCL3, and CXCL12) augmenting the local immune response in the brain (Liu et al., 2015).

Peri-infarct depolarisations

Within the anoxic ischaemic core, neurones remain permanently depolarised due to the loss of ATP and high extracellular concentrations of glutamate and potassium. Neurons within the peri-infarct area have been shown to exhibit spontaneous depolarisations where a slow transient increase in extracellular K^+ is followed by rapid spike in concentrations, at a high energetic cost (Nedergaard and Hansen, 1993; Fabricius et al., 2006). Mies and Hossmann (1993) demonstrated that the frequency of peri-infarct depolarisations in the rat correlated with an increase in infarct volume of 13 mm^3 per depolarisation.

Cell death

Both cell necrosis and apoptosis occur during ischaemic stroke. The respective fates of cells depends on their location within the ischaemic region. Cytotoxic oedema and plasma membrane degradation cause cell necrosis, a concurrent release of calcium from intracellular stores and an efflux of glutamate and intracel-

lular debris into the extracellular space. Necrotic cell death contributes to a positive feedback cycle of inflammation, cell damage, and death (Martin et al., 1998). Histological hallmarks of necrosis are cellular swelling, pyknosis, atypical organelle morphology, lysis, and vacuolation of the neuropil. Within the peri-infarct tissue, caspase dependent/independent apoptotic cell death dominates, primarily due the reduced severity of the ischaemic insult (Dirnagl et al., 1999). Mild ischaemic injury causes cytochrome-c and caspase production from 6 hours post-insult and subsequent cell death $24 - 72$ hours later (Endres et al., 1998). Apoptotic cells are characterised by the condensation of chromatin and cellular blebbing with maintained membrane integrity. The cell death process and their removal by microglia and macrophages occur within the first few hours following the ischaemic insult and persist up to several weeks later.

1.1.4 *Chronic ischaemic stroke pathophysiology*

As well as focal damage at the site of compromised cerebral perfusion, the ischaemic insult induces global changes in the brain out-with the affected territory. The changes include diaschisis, degradation of distal neural pathways (including the spinal cord), and concurrent plastic compensatory changes (Figure 3).

Degeneration of neural pathways

Although ischaemic stroke affects a localised region of tissue within a vascular territory, the neurons within that area which synapse with others or - in the case of white matter tracts - transit through to other regions of the brain, die or become functionally compromised. Both the thalamus and substantia nigra have been found to be atrophied several months post-stroke, with loss of
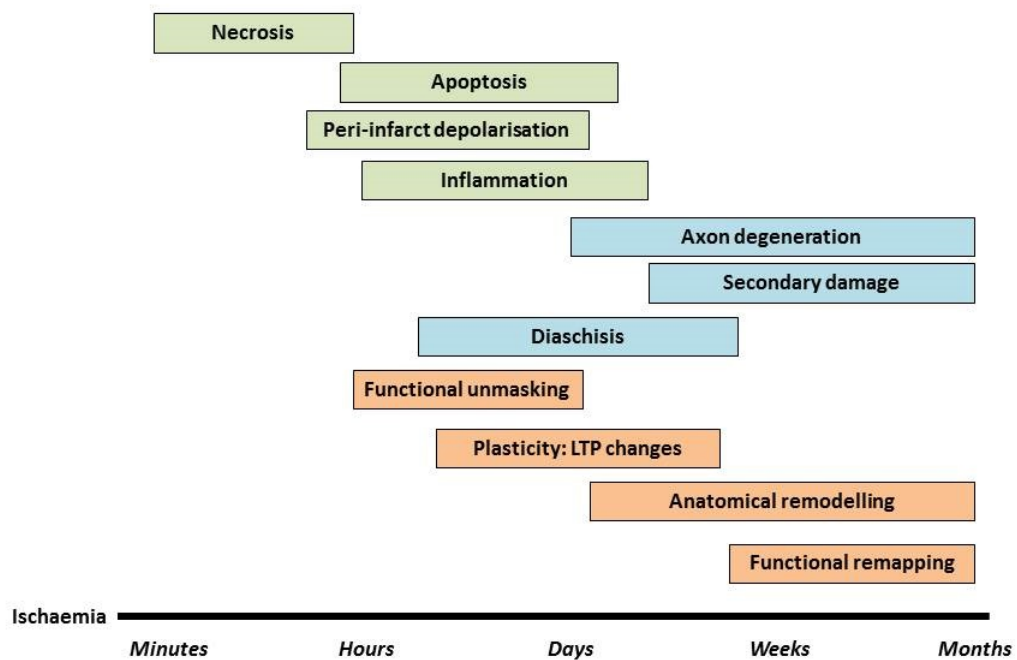
Figure 3: Time-course of stroke induced damage from the initial insult to several months later. Factors which contribute to the growth of the infarct are in green; pathological events remote from the infarct are in blue, and plastic responses in peach. Image adapted from Sist et al. (2012)

corticothalamic and thalamocortical pathways following MCA occlusion (Fujie et al., 1990; Hara et al., 1993; Abe et al., 2003). The ipsilesional thalamus has also been shown to have upregulated NMDA, and downregulated GABA receptors, suggesting a hyper-excitable state (Qü et al., 1998). Beyond the thalamus, post-stroke Wallerian degeneration of the cortical-spinal tract is a well described phenomenon with damage to the sensorimotor cortex inducing secondary damage to the corticospinal tract one-month following injury (Weishaupt et al., 2010). Diffusion Tensor Imaging (DTI) has shown a reduction in spinal cord fractional anisotropy (FA) at 30 days post stroke which correlated with deficits following motor assessments (Puig et al., 2010). Functional unmasking describes the unveiling of pre-existing, latent pathways has been found to occur within an hour post-stroke (Sigler et al., 2009).

Diaschisis

Diaschisis describes functional changes in areas of the brain remote from the site of damage (Seitz et al., 1999). Derived from the Greek roots of *shocked throughout'*, it is a symptom of the reaction to the ischaemic insult. Acutely, oedema in large infarctions causes swelling and compression of the contralateral hemisphere including the compression of the vasculature (O'Brien et al., 1974; Witte et al., 2000; Izumi et al., 2002), with compromised CBF and metabolism (Lenzi et al., 1982; Celesia et al., 1984) as well as impaired vascular reactivity to hypercapnia (Kågström et al., 1983; Dettmers et al., 1993). Electrophyisiological studies have demonstrated that focal stroke caused impaired GABA transmission in the contralesional hemisphere and the peri-infarct region (Buchkremer-Ratzmann and Witte, 1997) due to impaired translation (or post-translational modifications) of the GABA$_A$ receptor (Neumann-Haefelin et al., 1999).

Plasticity and functional recovery

The mammalian cortex is a complex network of reciprocal communications between functional areas. Although structural and functional recovery in the injured brain is poor compared to other organs, there is substantial evidence of an array of mechanisms which aim to adapt to focal injury.

Focal damage to a region of the cortex has compounding effects on the integration of the whole network. For example, lesioning of the M1 motor cortex leads to a dissociation of M1 from the whole somatosensory network, with impaired sensory and motor function (Friel et al., 2005). And loss of areas adjacent to the motor cortex causes deleterious changes in motor mapping (Gharbawie et al., 2005). Although the brain is most often perceived as

being organised into discrete functional areas, certain functions, such as the memory engram, are believed to be widely diffuse with multiple, adaptive pathways (Lashley, 1950; Bruce, 2001). Diffuse connectivity has also been demonstrated between sensory and motor areas of the cortex (Smits et al., 1991; Ferezou et al., 2007) and may therefore contribute to post-stroke recovery via functional unmasking.

PLASTICITY IN THE PERI-INFARCT REGION   Early studies in the squirrel monkey demonstrated that partial destruction of the M1 region causes remapping of digit representations in the surviving area (Nudo et al., 1996). The same applied following deafferentation subsequent to the removal of a digit (Merzenich et al., 1983). The evidence from Nudo *et al.* suggested that the re-mapping process is both an activity and competition based process. Soon after stroke, the peri-infarct environment becomes a growth-promoting region with increased expression in growth-associated genes such as GAP-43, p21, and *c-jun* balanced by the expression of growth-inhibing brevican (Carmichael et al., 2005). Stroemer et al. (1995) showed that GAP-43 (an axonal protein found in growth cones, indicative of sprouting) levels were increased in peri-infarct region up to 14 days post-cortical infarction. Synaptophysin (a presynaptic terminal vesicle marker of synaptogenesis) expression increased $14 - 60$ days post-stroke in the peri-infarct and contralesional cortex suggesting that synaptogenesis is part of the long-term recovery mechanism. VEGF (Vascular Endothelial Growth Factor), which has pro-angiogenic and neurotrophic properties, has been found to be upregulated in the peri-infarct region (Stowe et al., 2007). Neuroanatomical and *in vivo* optical studies have demonstrated that excitatory dendritic spines are capable of remodelling following brief periods of ischaemia, with

a cessation of blebbing and re-extension of previously retracted spines (Li and Murphy, 2008). In the long-term, dendritic spines have increased turnover rates (Brown and Murphy, 2008) and spine density is greater in regions far from the infarct due to the increased level of perfusion as distance from the infarct increases (Mostany et al., 2010).

The peri-infarct region has also been shown to exhibit a higher baseline firing rate (Schiene et al., 1996) and increased incidence of long-term potentiation (LTP) 7 days post-lesioning (Hagemann et al., 1998). It's likely that the degree of plastic recovery is dependent on the balance between growth-promoting and growth-inhibiting factors in association with the aforementioned competition, and the distance away from the ischaemic infarct.

OUTWITH THE PERI-INFARCT REGION   Post-stroke plastic mechanisms are not confined to the peri-infarct region. Improved recovery from stroke-induced aphasia is associated with increased activation in the contralateral Broca's area (Thulborn et al., 1999). However there is a balance between increased compensatory activity of the contralateral hemisphere with activity in adjacent regions of the ipsilesional hemisphere. Calautti et al. (2010) and Ward et al. (2003b) found that BOLD signal activity confined to the damaged hemisphere predicted a greater degree of recovery compared to increased activity in the contralateral cortex, particularly so in the case of large infarctions. In the rat contralateral M1 region, Hsu and Jones (2006) found increased MAP-2 and NMDA receptor subunit one expression 24 days after lesioning of the sensorimotor cortex. The density of both MAP-2 and NMDA subunits was also associated with an improved performance in the pellet reaching task, dependent on stroke volume. This sug-

gested that lesion dependent compensatory mechanisms were occuring in the contralateral hemisphere. Stroke volume dependent effects on resting-state and stimulus-driven fMRI responses in the rat have also been illustrated by vanMeer et al. (2010) & Weber et al. (2006), (see Chapter 5 for more details). It's therefore logical to conclude that in the case of large infarcts, tissue of similar function to that lost, i.e. if the whole vascular territory was destroyed, would be found in regions with a different vascular supply. This is in comparison to smaller infarcts where surviving peri-lesional tissue may have had a pre-existing functional relationship to the tissue lost. Although recovery mechanisms may restore behaviour to pre-stroke levels it's unlikely that the functionality is identical due to the loss of highly specific neurons, depending on the region damaged. It is also important to note that post-stroke recovery takes much longer in humans compared to animals (Murphy et al., 2009).

1.1.5   *Current clinical interventions*

The symptoms of stroke can occur suddenly and include hemiparesis/hemiplegia, hemianopsia, and aphasia. Public campaigns such as the 'Act F.A.S.T' by the NHS `http://www.nhs.uk/actfast/Pages/stroke.aspx` are aimed to reduce the time taken for patients to reach hospital. Diagnosis of stroke is typically assisted by non-contrast CT (Computer Tomography) or Diffusion-weighted MRI. If ischaemic stroke is confirmed then patients are assessed for blood vessel recanalisation via pharmaceutical thrombolysis or thrombectomy. tPA (tissue-Plasminogen Activator) is a protease which activates endogenous fibrinolytic plasmin. It is currently recommended for use up to 4.5 hours from symptom onset (Saver et al., 2009). The beneficial administration of tPA beyond 4 hours

has been found to be negligible (Whiteley et al., 2016).

Thrombectomy is the mechanical removal of a thrombus via an intravascular device to restore blood flow. If the thrombus can be identified by either CT or MRI angiography, then the thrombus can be removed via an intravascular device as per the recommendations in NICE guideline IPG548, `https://www.nice.org.uk/guidance/ipg548` and (Goyal et al., 2016). There is also substantial evidence to show that patient survival, independence, and functionality are improved if the patient is treated within a specialist acute stroke unit (Reviews, 2013).

Aside from thrombolysis or thrombectomy, another clinical treatment for large strokes is decompressive hemicraniectomy to allow for the herniation of the brain out of the skull, to avoid compression of healthy tissue (Lu et al., 2014). Methods of preventing reoccurence include aspirin administration, control of hypertension, high circulating cholesterol, and diabetes management where possible (Amarenco et al., 2004; Lawes et al., 2004; Ridker et al., 2005).

The functional deficits caused by stroke often improve and then stabilise (Jørgensen et al., 1995). Physiotherapy and speech & language therapy are often given with an aim to rehabilitate post-stroke. Methods such as constraint-induced movement therapy and electromyography biofeedback have shown some improvements when assessed systematically (Langhorne et al., 2009; Corbetta et al., 2010; Langhorne et al., 2011; Pollock et al., 2014).

1.1.6   *Animal models of ischaemic stroke*

Animal models are an invaluable resource for investigating the organ-wide and systemic effects of a pathology and/or therapeutic. In the case of stroke, they are essential for understanding the structural and functional changes which occur following focal injury. The middle cerebral artery (MCA) is the most commonly occluded vessel in humans (Heiss, 2016), and this is reflected in the *in vivo* models.

Rodent models of MCAO

Mice and rats are the most popular choice of species for pre-clinical stroke research due to lower relative costs, similar cerebrovasculature to man, the availability of co-morbid/genetically modified models, well understood physiology, and greater ethical acceptance compared to non-human primates (Macrae, 2011). Middle cerebral artery occlusion (MCAO) can be carried out by a range of mechanical or pharmaceutical methods.

The most popular method of MCAO is the intraluminal filament (ILF) method of mechanical occlusion (Koizumi et al., 1986a; Longa et al., 1989). Typically, the common carotid artery and its bifurcation is exposed and a nylon suture with a bulb at the proximal end inserted through the internal carotid artery into the Circle of Willis to the origin of the MCA. Occlusion can be permanent or transient with its withdrawal after a prescribed period of time simulating reperfusion. The ischaemic damage caused is primarily in the striatum and often the sensorimotor cortex (Figure 4). The method is popular due to the short procedural duration allowing for high throughput, and the absence of a need to perform a craniectomy. Occlusion can be confirmed by

Laser Doppler Flowmetry with reasonable success however the method still carries a large variance in infarct volume as well as a risk of vessel rupture and intracerebral haemorrhage (Schmid-Elsaesser et al., 1998). Oedematous swelling can cause death within 48 hours in large infarcts due to compression of the bulbar structures within the intact skull. In hypertensive rats, MCAO methods ethods which involve craniectomy lead lower mortality rates as the brain has space to expand, lowering intracranial pressure (Ord et al., 2012).

Other mechanical methods of MCAO include permanent occlusion of the MCA at proximal or distal locations via electrocoagulation (Tamura et al., 1981), or injection of an autologous blood clot (Kaneko et al., 1985). Electrocoagulation methods are more favourable for controlling infarct volume (by determination of which area of the MCA to occlude) and generation of favourable amounts of penumbra (Macrae, 2011), but require greater surgical skill and time.

Examples of pharmaceutical methods of MCAO are topical application of endothelin onto the MCA (Macrae et al., 1993), stereotaxic injection of endothelin into the brain parnechyma (Sharkey et al., 1993), intraluminal injection of thrombin (Orset et al., 2007), and photochemical generation of free radicals (and thus clot generation) via photo-excitation of Rose Bengal (Watson et al., 1985). The methods described above are an example of the wide array of models available depending on the nature of the scientific question poised. Disadvantages of rodent models include the lack of white matter, the limited cognitive behaviours compared to humans, and the lissencephalic nature of their brains in comparison to other mammals, including primates.
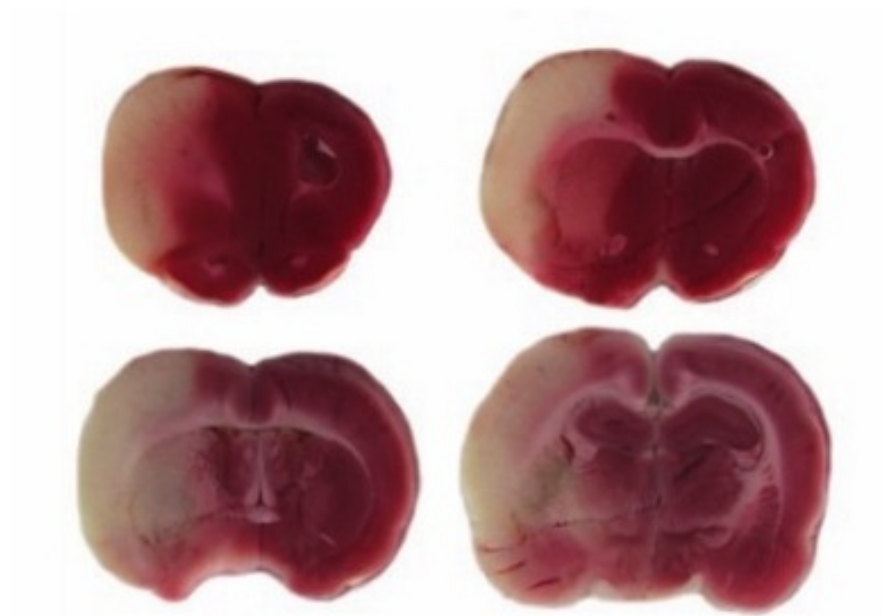
Figure 4: The extent of ischaemic damage in the striatum and the cortex and oedematous swelling of the infarcted hemisphere 48 hours following occlusion of the MCA via the intraluminal filament method. Brain tissue has been stained with TTC (2, 3, 5-triphenyltetrazolium chloride) which is dehydrogenated to red formazan in living mitochondria. Dehydrogenation is unable to occur in dead, infarcted tissue and as such, does not stain. Image adapted from Farr and Trueman (2011).

Non-human primates & other species

Non-human primates (NHPs) are phylogenetic cousins of humans. Commonalities within the brain include similar vascular anatomy (Fukuda and del Zoppo, 2003), greater white to grey matter ratio compared to rodents, a gyrencephalic cortex, and similar network structures. MCAO techniques have been applied to the marmoset (Freret et al., 2008) and baboon (Branston et al., 1974) as well as sheep (Wells et al., 2012), pigs (Sakoh et al., 2000), and cats (Feustel et al., 1981). However, the use of larger animals has greater housing and care costs. In particular, NHPs and cats attract a greater degree of public ethical criticism. These issues limit the volume of research in higher animals despite calls for greater use of these species to improve translation of pre-clinical therapeutic research to the clinic. There are still however caveats, for example the failure of the free-radial trapping agent NXY-059 to show clinical efficacy despite pre-clinical trials in primates as well as rodents (Shuaib et al., 2007).

1.1.7   *Assessment of post-stroke disability in humans*

Unilateral ischaemic stroke induces neurological deficits on the contralateral side to damage. Ischaemic damage to the MCA territory of the brain can present clinically as limb and/or facial hemiparesis or hemiplegia, ataxia, aphasia, spatial neglect and sensory loss (Symposium, 2016) with the majority of these symptoms successfully reproduced in rodent and primate models of ischaemic stroke (Ginsberg, 1996).

Patient recovery, after surviving the initial insult, is a complicated, non-linear process carried out by a variety of mechanisms

including compensation to the disability and substitution via reorganisation of surviving networks which requires patient-specific rehabilitation programmes (Langhorne et al., 2011). One technique used to rehabilitate upper limb hemiparesis is Constraint Induced Movement Therapy (CIMT, Grotta et al. (2004)), where the ipsilesional, healthy forelimb is restrained to force use of the hemiparetic limb. The EXCITE trial (Wolf et al., 2010) demonstrated equal improvement in arm motor function when treated 3-9 and 15-21 months post-stroke, with greater rate of improvement in the former treatment group. However, systematic analyses suggest that the reported benefits of such treatment is subject to small-study bias (Corbetta et al., 2010).

Contralateral control of the body is also complemented by ipsilateral pathways (Brus-Ramer et al., 2009). Some of the functions lost can be spontaneously restored via compensation by related regions of the affected network including the opposite hemisphere (Biernaskie et al., 2005). However, this compensation by the opposite hemisphere has been found to reduce the degree of activation within surviving areas of the network which in turn is attributable to poorer functional outcomes (Ward et al., 2003a).

Assessments of human disability

Various clinical measures exist to assess stroke-induced neurological deficits as well as the extent of the subsequent impairment. The National Institutes of Health Stroke Scale (NIHSS, `http://www.nihstrokescale.org/`) is a quantitative evaluation of stroke-induced neurological deficit (Brott et al., 1989), which has also been shown to be a good predictor of long and short-term outcomes (Adams et al., 1999). The Barthel Index (BI), from Mahoney and Barthel (1965), evaluates the degree of dependence

a patient requires during day-to-day living for example clean-ing, dressing, and climbing stairs. Such tests can be used as a means of assessing the efficacy of rehabilitative treatments. The Fugl-Meyer test (Fugl-Meyer et al., 1975) is a performance based assessment of impairment evaluating motor function, balance, joint mobility, and sensory function. Although comprehensive, the test is lengthy, taking approximately 30 minutes.

The Action Research Arm Test (ARAT, Yozbatiran et al. (2008)) assesses a patient's post-stroke hemiplegic limb function via their ability to move their arm and grasp, grip, and pinch various objects; providing an evaluation of their arm specific limitations on daily activity. A two point improvement in ARAT test score (moving a $25mm^3$ block) is currently being used as the primary outcome measure in the PISCES-II trial (NCT02117635).

1.2   STEM CELLS

1.2.1   *Stem cell biology*

Mammalian stem cells are classified by: a lack of specialisation, the ability to undergo mitotic division, and to differentiate into other cell types (Gage, 2000). The diversity of daughter cells to which they can differentiate depends on their position within a well established hierarchy. This hierarchy and concordant nomenclature is shown in Figure 5.

A zygote is the only totipotent mammalian cell type, with the ability to differentiate into any other cell type following implantation into the wall of a uterus. Upon development into a blastocyst, embryonic stem cells have the capability to form an entire organism, with the exception of the trophoblast cells of the placenta. As the development process continues, cell types become restricted to only those within a specific organ or tissue type, and following further signalling inputs and developments, specialised adult cells are generated. Within a mature organism, adult stem cells persist for the repair and/or renewal of almost all adult tissues with some restrictions. Recent technological advances have allowed for adult fibroblasts to be de-differentiated into pluripotent cells via the introduction of four 'reprogramming' genes: *Oct*4, *Soc*2, *c-myc, Klf*-4 (Takahashi et al., 2007).

Following the identification, characterisation, and induction of various stem cell sources, investigations have led towards assessments of their therapeutic role in transplantation (from exogenous or autologous sources) in the treatment of disease.

1.2.2   *Neural stem cells*

Until relatively recently it was believed that the adult brain is incapable of mitotic division. Indeed, the adult brain has a very limited capability to repair following injury in comparison to the dermis or the gastrointestinal tract. However, there exist two niches within which neural progenitor cells (NPCs) reside: the subventricular zone (SVZ), adjacent to the ependymal layer of the lateral ventricles (Johansson et al., 1999), and the smaller subgranular zone (SGZ) within the dentate gyrus of the hippocampus (Altman and Das, 1965; Eriksson et al., 1998). Several studies have also identified self renewing Glial Flibrillary Acidic Protein (GFAP) positive cells *in vitro* and *in vivo* (Laywell et al., 1999; Imura and Kornblum, 2003; Garcia et al., 2004). Subsequently, the purpose and role of neural stem cells within the forebrain have been investigated.
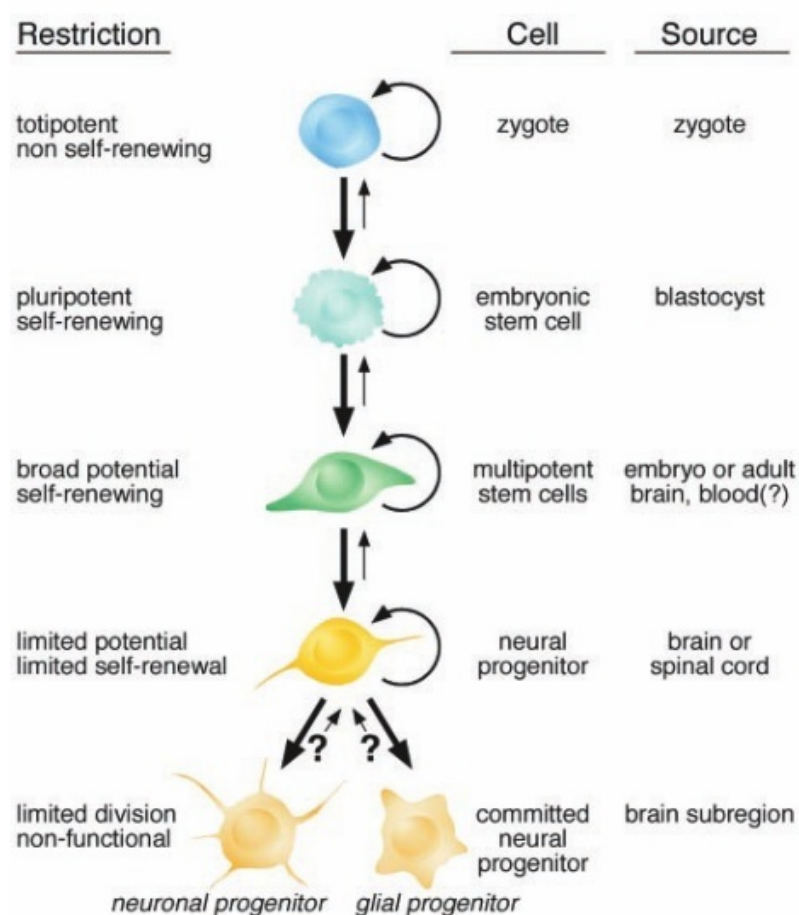
Figure 5: Illustration of neural stem cell lineage beginning from the totipotent zygote and the various stages of further specialisation with limitations to their subsequent fate. Small arrows in reverse direction infer the de-differentiation of cells to their parent type. Image adapted from Gage (2000).

Fates of Subventricular and Subgranular NPCs

Neural precursor cells are subject to a huge variety of signalling inputs during their growth, development, and integration to the adult nervous system (Abrous et al., 2005). Developing cells within the SGZ migrate only a short distance to the granular cell layer above, forming glutamatergic synapses and projecting axonal processes out to the CA3 neurons (Liu et al., 2003). SVZ precursors have been identified in rodents, non-human primates, and humans. In rodents these cells migrate towards the olfactory bulb alongside blood vessels via a chemorepulsion mechanism through what is known as the Rostral Migratory Stream (Lois and Alvarez-Buylla (1994), Figure 6). Once at the olfactory bulb, rodent SVZ precursors mostly differentiate into GABAergic granule cells, and integrate into the olfactory bulb circuitry (Belluzzi et al., 2003). There is some evidence for the presence of neural stem cells and a rostral migratory stream in non-human primates (Kornack and Rakic, 2001) and also the human brain (Curtis et al., 2007). However the studies in the latter remain controversial (Sanai et al., 2007). Human studies have found that the number of proliferative cells in the SVZ declines with age (Sanai et al., 2011), and do not integrate into the human olfactory bulb (Bergmann et al., 2012), but are found in the striatal areas adjacent to the SVZ (Ernst et al., 2014). There is also some evidence for neurogenesis in the cortex (Gould et al., 2001).

The biological requirement for neurogenesis in both the olfactory bulb and the dentate gyrus is speculative. Suggestions include the requirement for mammals to detect and process novel olfactory stimuli and the consolidation of learning, and memory, respec-

tively (Liu et al., 2003; Lazarini and Lledo, 2011).

Following brain injury, SVZ progenitor cells have been found to proliferate and migrate ectopically in response to chemoattractants such as Reelin (Hack et al., 2002; Parent, 2003). In the case of ischaemic stroke, neurogenesis has been found to increase in the SVZ ipsilateral to the site of injury (Parent et al., 2002; Arvidsson et al., 2002) and differentiate into cells initially positive for doublecortin (an immature neural maker). These ectopic cells have been found to migrate in chains, similar to the RMS, along blood vessels (Thored et al., 2007). There is also some evidence that this also occurs in human stroke with Ki-67 (proliferative marker) and doublecortin positive cells identified (Jin et al., 2006).
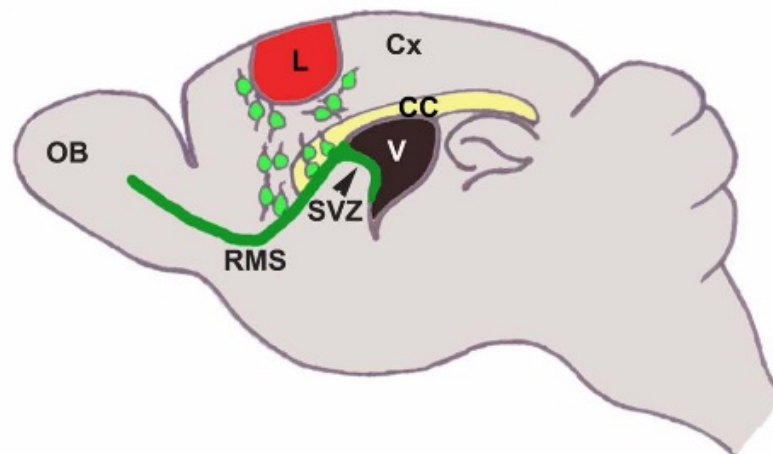
Figure 6: Illustration of the Rostral Migratory Stream (RMS, green) in the rodent brain. Normally, neuroblasts migrate along the RMS to the olfactory bulb (OB). In reaction to brain injury, these neuroblasts have been reported to migrate ectopically to the site of injury. Lesion (L), Cortex (Cx), Corpus callosum (CC), Ventricle (V). Image adapted from Saha et al. (2012).

1.2.3   *The Therapeutic Potential of NPCs*

With our limited capacity to treat neurodegenerative disease or to restore function after focal ischaemic damage with conventional pharmaceutical approaches, focus has turned to the potential role of stem cells due to their capacity to differentiate into the various cell types of the CNS. Current hypotheses define that stem cell treatments for CNS would either strive to re-establish connectivity via the replacement of damaged neurons, stimulating angiogenesis, or to provide additional trophic support for endogenous recovery mechanisms (Kornblum, 2007).

Stem cells as a novel treatment for ischaemic stroke

Stem cells offer an alternative potential opportunity to regain lost functionality (Lindvall and Kokaia, 2011; Sinden et al., 2012). The post-stroke brain is by no means a static environment and the pathological processes (described earlier) vary greatly from the moment of insult to the subsequent weeks and months As such, the optimal timing and dose to administer a stem cell therapeutic remains unknown. Previous clinical trials have focused on the use of autologous blood sourced mesenchymal stem cells (MSCs), which differentiate into neurons and glia, delivered intravascularly in the acute or sub-acute stages (Uccelli et al., 2008; Lee et al., 2010; Honmou et al., 2011). However, there is some controversy with this method as Detante et al. (2009) showed that technecium labelled human MSCs did not cross into the brain one week after MCAO.

Other investigations have focused on the chronic post-stroke period (da Fonseca et al., 2010; Bhasin et al., 2011). At this stage, the majority of dead tissue has been removed with the infarct

replaced by a CSF filled cyst, inflammation is reduced, and surviving tissue plasticity mechanisms are under way. Implantation of stem cells at this stage may therefore enhance the plastic compensatory approaches. Using neural stem cells (which have a more direct lineage to CNS cells compared to MSCs) seems a rational choice. However, this provides unique challenges in the sourcing and administration of such cells whereas autologous mesenchymal stem cells are far easier to isolate. Despite these challenges, both neural and mesenchymal stem cells are currently in clinical trials.

Steinberg et al. (2016) recently published the results of a Phase 1/2a clinical trial of allogenic bone marrow mesenchymal stem cells transfected with a Notch1 intracellular domain, which has a role in stem cell differentiation into neurons and glia (Lundkvist and Lendahl, 2001; Dezawa et al., 2004). The study demonstrated that intracerebral implantation of the cell line into the peri-infarct area, on average 22 months post stroke, lead to a mean decrease in NIHSS scores of 2 and a mean increase in the Fugl-Meyer motor function of 11.4% with no serious adverse effects of transplantation. However caution in interpretation is advised due to the uncontrolled study design which was also not powered to detect improvements in clinical scores.

1.2.4 *The neural stem cell line CTX0E03*

The CTX0E03 cell line is a neural stem cell line currently under clinical investigation as a treatment to improve functional disability in the chronic post-stroke phase (See Chapter 5). CTX0E03 (CTX) cells are a conditionally immortalised human neural stem

cell line manufactured in an automated environment to a clinical grade by ReNeuron Ltd.

Cell line generation and immortalisation

The CTX cell line was derived from cortical tissue of a single first trimester foetus (Bioscience Resources, USA) in compliance with ethical and legal guidelines (Pollock et al., 2006).

The function of a protein of choice can be controlled by its fusion to the hormone binding domain of a steroid hormone receptor (Picard, 1993). The oestrogen receptor (ER) is a steroid hormone of high interest for control of expression due to the relative ease in obtaining its ligand, 17β-estradiol, and the absence of endogenous ER in many tissues (Littlewood et al., 1995). However, due to the presence of oestrogen in many culture serums and the weak agonism of media component phenol red (Berthois et al., 1986), the ER, in its unadulterated form, is undesirable. A mutant murine ER (E525R) has no binding specificity with 17β-estradiol but has partial agonist activity with the anti-oestrogen drug metabolite, 4-hydroxytamoxifen (4OHT) (Danielian et al., 1993). The E525R mutant ERs expression is strictly dependent on the presence of 4OHT (Littlewood et al., 1995) and as such makes an ideal target for controlling protein function.

Conditional immortalisation was achieved via controlled expression of the *c-myc* protein. As an oncogene, c-myc is involved in cellular proliferation and apoptosis (Cerni, 2000). With concerns that the long-term maintenance of embryonic and primary stem cell lines can lead to genetic instability and tumourgenicity, a c-mycER$^{\text{TAM}}$ transgene was transfected via a retroviral vector. Clonal division of the neural stem cells was therefore permitted

in the presence of 4-hydroxytamoxifen in culture until a time of requirement whereby a 4-OHT free media can be used to silence the transgene and initiate differentiation (Stevanato et al. (2009), Figure 7). The integration site of the c-mycER^{TAM} transgene at a non-coding region of Chromosome 13, ensured the stability of the cell line up to 45 passages with a stable karyotype.
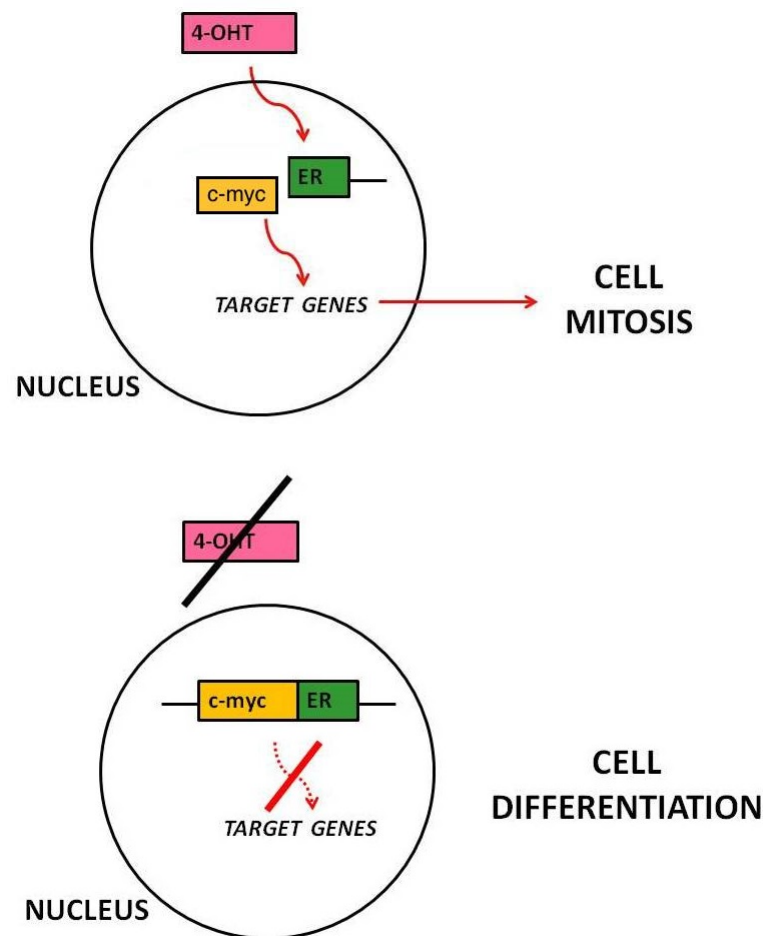
Figure 7: Diagram illustrating the dependence of CTX cell mitotic division with the conditional expression of c-Myc on agonism of the E525R receptor by 4-hydroxytamoxifen. **Top**, agonism of the E525R receptor with 4-hydroxytamoxifen in culture media permits clonal division of the CTX cells. **Bottom**, the absence of 4-hydroxytamoxifen from culture media induces differentiation and maturation of CTX cells.

CTX0E03 cell line characteristics in vitro and in vivo

Characterisation studies *in vitro* have found that CTX cells have the following phenotypes as described in Pollock et al. (2006) and Hicks et al. (2013). The human cells were identified in the post-stroke rodent brain by staining for the Human nuclear antigen (HuNuc, Figure 8).

   i *Neuron and astrocytic cell types.* Following the removal of 4-OHT from the cell culture media the cells ceased clonal division and underwent differentiation to β-III tubilin, Olig-2 (oligodendrocyte), and GFAP (Glial Fibrillary Associated Protein, astrocyte) positive cells, (Figure 9).

   ii *Pro-Angiogenic* CTX cells have been found to highly express VEGFA (Vascular endothelial growth factor A), EGF (Epidermal Growth Factor), TGFβ1 (Tumour Growth Factor Beta-1), HIF-1α (Hypoxia Inducible Factor 1-alpha), and other pro-angiogenic growth factors. CTX-cells showed co-staining in co-culture with HUVEC (Human Umbilical Vein Endothelial) cells and association with smooth muscle actin *in vivo* (Figure 10), suggesting that CTX cells may play a role in angiogeneis via direct interaction with vascular cells or via the release of pro-angiogenic factors.
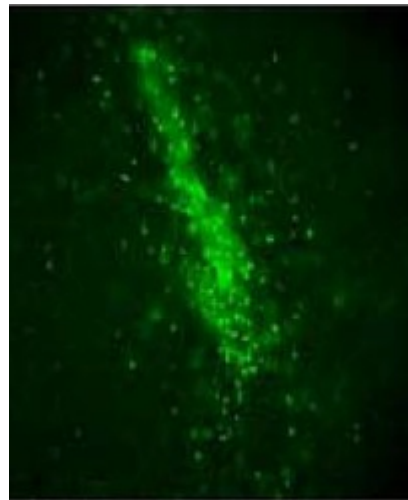
Figure 8: Confocal micrograph of HuNuc positive cells (green) in the ipsilateral striatum 5 weeks post-transplant. Image adapted from Pollock et al. (2006), scale bar not provided in publication.
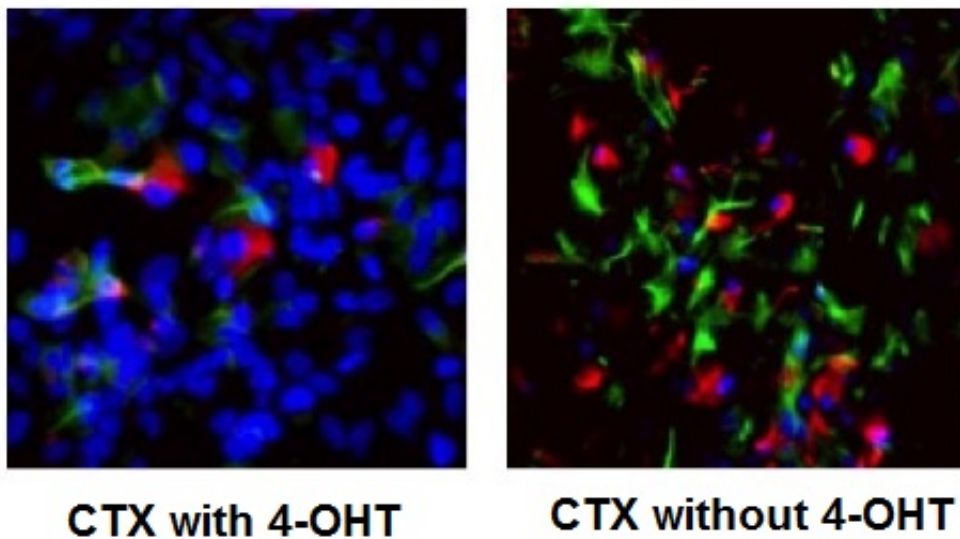
Figure 9: In vitro immunocytochemistry of CTX0E03 cell neural and astrocyte differentiation. Left: CTX-cells in culture in growth media with 4-OHT. Right: CTX-cells 7 days after removal of growth factors and 4-OHT. Stains: Hoesht nuclear (blue), βIII-tubulin (green), and GFAP (red). Image adapted from Pollock et al. (2006).

CTX - vWF *in vitro*   CTX - actin *in vivo*
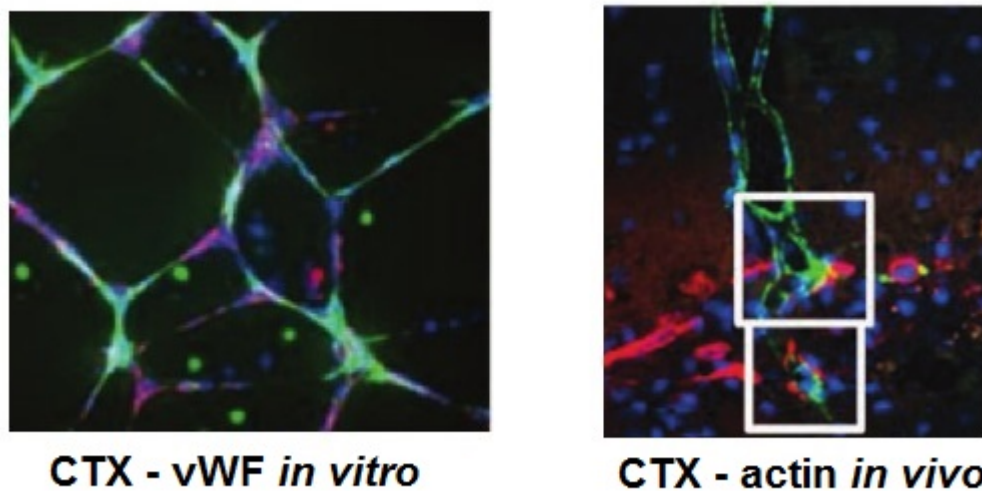
Figure 10: In vitro and in vivo immunocytochemistry of angiogenic properties of CTX0E03 cells. Left: HUVEC - CTX cell co-culture with HUVEC; von-Willebrand factor (purple); CTX cell human specific nestin (green). Right: CTX0E03 cells (red) in proximity to smooth muscle actin (green) highlited by white boxes. Images adapted from Hicks et al. (2013).

CTX0E03 *effects and the post stroke brain*

All published studies which have investigated the effect of CTX-cells in the post-stroke brain have done so with implantation at 4 weeks following focal cerebral ischaemia in Sprague Dawley rats (Pollock et al., 2006; Stroemer et al., 2009; Smith et al., 2012). Improvements in sensorimotor function of treatment groups have been assessed via the Bilateral Asymmetry (details in Chapter 3), and Rotameter tests.

The cell line has been shown to be safe in rodents up to 3 months post-transplantation; exhibiting positive dose-dependent efficacy up to doses of 450000 cells when implanted into the peri-lesional caudate nucleus (Stroemer et al., 2009).

CTX cell transplants increased the number of von Willebrand Factor positive cells at the peri-lesional implantation site at seven

days (Figure 10, Hicks et al. (2013)) and three months post-implantation (Stroemer et al., 2009). *In vivo*, CTX cells have been shown to differentiate into CD62 (endothelial marker) and Olig-2 positive cells (Figure 11); and caused up-regulation of endogenous & MAP-2 (Microtubule associatated protein), a mature neural marker (Stroemer et al., 2009).

The PISCES Clinical Trials

CTX cells are currently in a Phase II clinical trial (PISCES-II, NCT02117635) to determine whether an intracerebral dose of 20 million cells into the ipsilesional hemisphere recovers loss of function of the paretic arm 4 weeks following ischaemic stroke. The Phase I PISCES trial demonstrated no serious effects of CTX-cell transplantation (more details in Chapter 5).

CTX - CD31   **CTX - Olig-2**
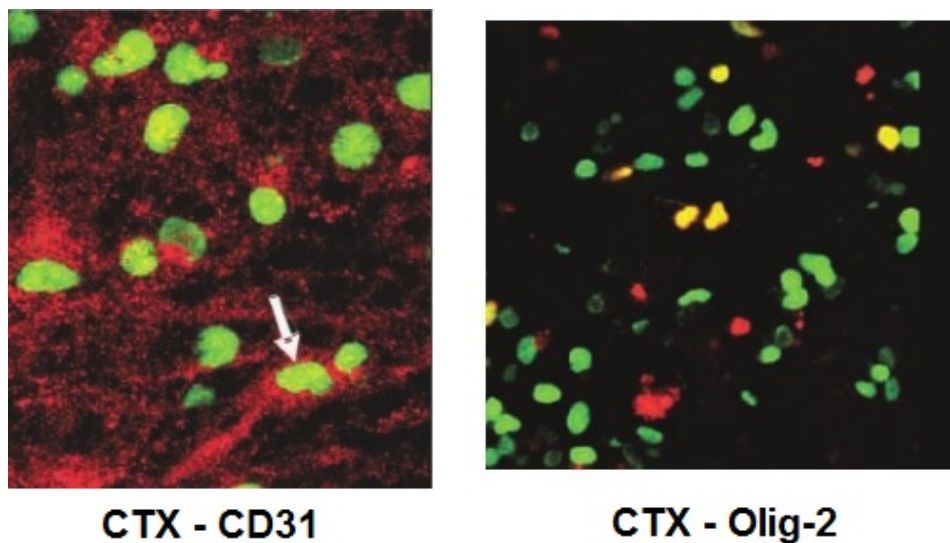
Figure 11: Confocal images of immunocytochemistry staining of 3 month post-MCAO rat brain sections. Left: CTX cell (HuNuc, green) co-staining with endothelial CD31 (red) cells showing as yellow. Right: CTX cell (HuNuc, green) co-staining with Olig-2 (red) cells, showing as yellow. Images adapted from Stroemer et al. (2009)

.

1.3 MAGNETIC RESONANCE IMAGING

1.3.1 *Magnetic resonance theory*

Nuclear Magnetic Resonance (NMR) is the phenomenon whereby nuclei (that possess spin) align with an external magnetic field, and precess, creating a net magnetisation (M_0). The precessional frequency (ω) of a nucleus within an external magnetic field (of strength B_0) is given in Equation 1, determined by a nucleus dependent constant known as the gyromagnetic ratio, γ.

$$\omega = \gamma B_0 \tag{1}$$

Protons excited by a radio-frequency (RF), or excitation pulse, of matching Larmor frequency i.e. on resonance frequency, tilts the net magnetization from along the B_0 axis (or z-axis) into the xy-plane, by inducing phase coherence among the nuclei. The time constants of the recovery back to equilibrium are known as T_1 and T_2 relaxation times respectively. T_1 is spin-lattice relaxation time, and T_2 is spin-spin relaxation time. T_2 is dependent on the interactions between spins. The measured signal decays over time due to the dephasing of the spins, caused by the local interactions of the spins as well as inhomogeneities in the external magnetic field. This decay is known as Free Induction Decay (FID). The rate of FID is given by T_2^* which is always less than T_2. Images acquired with T_2^* weighting are more likely to include susceptibility artefacts. They typically occur where there are caused ferrous depositions such as haemorrhages and air in the sinuses and ear canals.

Repetition time (TR) & Echo Time (TE)

The repetition time (TR) is the time interval between excitation pulses and will dictate the magnitude of the received signal and affect image contrast. Longitudinal magnetisation (M_z) at time TR compared to the original magnetisation (M_0) is determined by their respective T_1 values (Equation: 2)

$$M_z = M_0(1 - e^{\frac{-TR}{T_1}}) \tag{2}$$

The rate of decay of the $T_2{}^*$ signal is described in Equation 3. It can be seen that the time at which the signal is measured i.e. Echo Time (TE), will affect image contrast due to the T_2 values of different tissues.

$$e^{\frac{-TE}{T_2{}^*}} \tag{3}$$

Tissue composition, the determination of T_1 and T_2

Different tissues have different chemical compositions and structural components. As such, the behaviour of proton spins within each of these varies.

Fat protons are within large triglyceride structures surrounded by electroneutral carbon atoms compared to the more exposed protons of water molecules. As such, fat protons resonate at a lower frequency, realigning with B_0 faster, leading to lower $T1$. Water has a long T_2 due to the rapid rotation of the molecules across a wide range of frequencies whereas protons in solid structures such as muscle or bone have more restricted rotations and as such, shorter T_2 values.

Different tissues have differing T_1 recovery, and T_2 or $T_2{}^*$ decay times, and as such, the overall signal measured is a result of the density of protons in the sample. By varying the TR and TE, images with differing tissue contrast can be made. For example, by applying short TRs and short TEs, the T_2 relaxation effects are minimised and therefore allows for differentiation of structures based on their T_1 values. Longer TEs and TRs reduce T_1 relaxation effects and allow for T_2 or T_2^* contrast. F

1.3.2   *Application of MR theory to imaging*

Application of magnetic field gradients (thus differing the Larmor frequencies of the protons within an object) allows for spatial localisation. MRI was developed by Lauterbur, who named it zeugmatography. Further technological advances eventually led to the development of modern-day Magnetic Resonance Imaging (MRI).

MRI is based on the application of magnetic field gradients across a subject placed within the static field (therefore with differing Larmor frequencies across the subject) to derive the spatial information of the received signal. There are usually three primary gradients, applied in three orthogonal dimensions:

SLICE-SELECT GRADIENT (z AXIS):   By transmitting RF pulses of bandwidths with a centre frequency matching the Larmor frequency, spins are excited only within this region; determining the slice position. The slice thickness is determined by the bandwidth of the RF pulse and the strength of the slice selection gradient. The remaining two gradients determine the spatial localisation within the slice.

FREQUENCY-ENCODING GRADIENT (*x* AXIS):   During detection of the echo, following excitation, applying a gradient along the x-axis, protons will precess at different frequencies. As such, the rate of change of phase is proportional to the position along the x-axis.

PHASE-ENCODING GRADIENT (*y* AXIS):   The gradient applied for a short time along this axis between pulse and acquisition causes the transverse magnetisation to precess at different rates. Once turned off, the spins precess at the same rate, but with phase-offset proportional to their position along the y-axis.

The field of view (FOV) of an image is the spatial extent over which MR data are collected. The data within the FOV are divided into elements known as voxels. The size of the FOV and the voxels determines the image resolution.

The raw data acquired are digitally converted measurements for an echo from a given volume or slice. The raw data are stored as an array of complex numbers along the readout direction. Raw data matrices are generated with each row corresponding to the value of the phase-encoding gradient the was applied. Each point, the echo signal amplitude, can therefore be described as k_x, k_y for the time that the respective gradient is active. This is known as *k-space*, measured in s^{-1}. The central part of the matrix contains data acquired at low amplitude phase-encoding gradients and are mostly responsible for image contrast. The outer areas of the matrix are data acquired at high or low amplitude gradients and so generate high frequencies (see Equation 1), providing edge definition. To generate the image matrix, the complex data are

Fourier-transformed in both dimensions.

The Signal-to-noise ratio (SNR) of MRI data is determined by several variables including: hardware properties, proton density, voxel volume, receiver bandwidth, T_1, T_2, flip angle, TE, TR to name a few. Optimisation of these variables will improve SNR, and thus image quality.

Pulse sequences describe the manner in which RF pulses and gradients are applied which in turn determines the signal measured and the resultant images. Diverse sequences have been developed which permit investigations into various macro and micro-structural properties of tissues but also the metabolic and functional behaviours within all organs including the brain.

SPIN-ECHO SEQUENCES   A Spin-Echo (SE) sequence applies a 90° excitation pulse, flipping the magnetisation vector into the orthogonal plane. Due to the T_2^* effect, spins begin to dephase. Application of a 180° pulse will cause the spins the precess in the opposite direction, and to become in phase again. Spin re-phasing eliminates B_0 effects resulting in a T_2 weighted echo (Hahn, 1950). The TR and TE of the spin echo sequence will determine the contrast of the image as described above.

GRADIENT-ECHO SEQUENCES   Gradient echo/Gradient recalled echo (GRE) sequences were developed to decrease scan time. A short TR and small flip angle (less than 90°) are used with an echo generated via gradient reversal. The TE used and thuse the resultant signal will determine the amount of T_2^* weighting. However because of this, GRE images are confounded by a lower SNR compared to SE sequences with similar parameters.

ECHO-PLANAR IMAGING   Echo-planar imaging (EPI) sequences are very rapid acquisitions whereby k-space is filled following a single RF pulse by rapid switching of the frequency and phase-encoding gradients. Multi-shot EPI uses multiple excitations to fill k-space, increasing acquisition time but reducing susceptibility artefacts. EPI image contrast is determined by the TE when the phase encoding gradient is zero.

1.4 THE BOLD SIGNAL

Although now one of the staple methods to investigate brain function during activation and rest, the *Blood Oxygenation Level Dependent* (BOLD) signal is a reflection of a complex integration of cerebral blood flow, blood volume, and metabolic events in response to neuronal activation. Since the first identification of the BOLD signal 26 years ago (Ogawa, Lee, Nayak and Glynn, 1990), functional imaging studies have dominated the neuroscience and psychology literature. BOLD data are often presented as 'activated' voxels overlaid on anatomical maps to reflect spatiotemporal signal changes of statistical significance.

1.4.1 *Flow-metabolism coupling*

The mammalian brain is highly metabolically active, consuming 20% of the body's energy at rest (Mangia et al., 2008). The majority of ATP use is devoted to glutamate cycling and maintaining the cellular ionic gradients required for signal propagation and synaptic transmission. Functional hyperaemia is the phenomenon of the increase in blood flow in response to neuronal activation. The mechanisms by which functional hyperaemia is induced are multifaceted, further complicated by the varying distributions of energy consumption throughout different regions of the brain. Energy use within the cerebral cortex is distributed between synaptic transmission, housekeeping (non-signalling tasks), action potentials, and maintaining resting potentials estimated at 44, 25, 16, and 15 percent respectively (Howarth et al., 2012). Flow-metabolism coupling evolved to ensure active neurons and glia receive adequate blood supply to maintain normal function. We are now aware of a multitude of molecular signals which

work in concert to direct flow at the macro- and microscopic level to ensure that active regions are supplied with sufficient oxygen and glucose to function. These include glutamate, lactate, oxygen, arachdonic acid metabolites, and adenosine (Attwell et al., 2010). As a result, we are also beginning to unpick potential mechanisms by which flow-metabolism coupling dysfunction may occur, contributing to disease onset or pathology.

Prior to the early 1980s, it was conventionally believed that the blood flow response to neural activity was driven by metabolic demand in a linear fashion (Roy and Sherrington, 1890). However, measurements of cerebral blood flow (CBF), and oxygen extraction fraction (OEF) via Positron Emission Tomography (PET) imaging, using ^{15}O labelled water and molecular oxygen respectively, showed that the blood flow response to somatosensory stimulation exceeded metabolic rate by nearly 6-fold (Fox and Raichle, 1986). Although initially controversial, see Fox (2012), the term *functional hyperaemia* was termed to describe how activity at the cellular level within the brain is coupled with disproportionate increase in local blood flow.

The brain has a relatively constant oxygen extraction fraction (OEF) of 40% from the blood at rest (Gusnard and Raichle, 2001). During activation however, feed-forward mechanisms increase CBF to anticipate the increased demand for oxygen and glucose. For example, stimulation of the human V1 area resulted in a 15% increase in energy demand with a 60% increase in CBF (Lin et al., 2010). Consequently, functional hyperaemia causes a reduction in the OEF; the fundamental basis of the BOLD signal. For increasing metabolic demand, the oxygen gradient between blood and the tissues must be increased either by increasing capillary pO_2 or

decreasing mitochrondial pO_2. Therefore CBF is a determinant of tissue oxygen tension. However, even at a microscopic level, the interstitial pO_2 is not uniform (Leithner and Royl, 2014) and many models fail to consider the impact this has on local OEF and flow responses during activation. Hypotheses, such as the capillary transit time heterogeneity (CTH) hypothesis (Rasmussen et al., 2014) aim to provide a conceptual expansion of existing models.

1.4.2 *Functional hyperaemia & Identification of the BOLD signal*

Deoxyhaemoglobin is paramagnetic (Pauling and Coryell, 1936) and the susceptibility (the degree of magnetisation) of blood changes as a linear function of oxygenation (Weisskoff and Ki-ihne, 1992). As such, deoxygenated blood has a greater suscepti-bility compared to its oxygenated counterpart causing local field inhomogeneities within erythrocytes, the lumen contents, and surrounding tissues; shortening the net T_2^* in the voxel. One may initially believe that as a result of neural activity, the T_2 signal would decrease further as oxygen is extracted. However, as described above, functional hyperaemia causes a surplus of oxy-genated blood to be delivered to the region of activation thereby decreasing the concentration of paramagnetic deoxyhaemoglobin within the vessel lumen.

The contrast changes within the vessels of the hyper-/hypoxic ro-dent brain were first identified via a gradient echo pulse sequence at 7T (Ogawa, Lee, Nayak and Glynn (1990), Figure 12). Com-parisons between contrast during carbon monoxide inhalation (which has negligible contrast effects) and hypoxia, inferred that the contrast changes were generated by susceptibility differences between vessel deoxyhaemaglobin and the surrounding tissues.

This seminal paper spurred the hypothesis that MRI could be utilised to investigate activity in the brain.
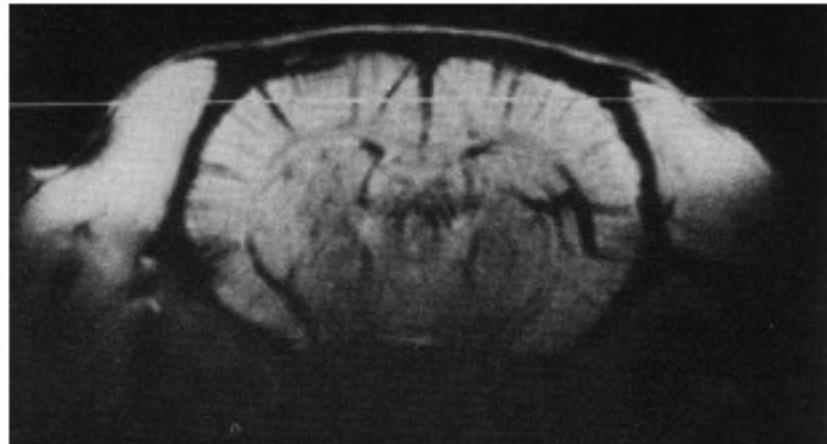
Figure 12: GRE image of an anoxic rat brain (ventilated on 100% N_2) at 7T (117x117x500μm). High levels of deoxyhaemoglobin within blood vessels caused increase in magnetic susceptibility and reduced T_2^* as shown by the contrast of the cortical vessels. Image adapted from Ogawa, Lee, Kay and Tank (1990).

1.4.3 *Neurophysiological contributors to the BOLD signal & the haemodynamic response*

Logothetis et al. (2001) were the first to demonstrate the neural basis behind the BOLD signal. Using simultaneous fMRI and intra-cortical electrophysiology, it was shown that increases in the Local Field Potential magnitude (LFP, up to 300μm from the electrode) were highly correlated with the haemodynamic response with some contribution of Multi Unit Action potentials (MUAs). The cortical BOLD signal represents regional inputs and processing in the voxel as well as excitatory and inhibitory interneurons. Excitatory inputs are either intrinsic signals from within the cortex or thalamocortical afferents to pyramidal cells

whereas inhibitory connections are short and local, possibly tuning the projecting neural outputs (Logothetis, 2003).

The temporal dynamics of the BOLD responses are typified by three phases (Figure 13): first a pre-stimulus dip, believed to be due to a short increase in deoxyhaemoglobin due to metabolic demands prior to hyperaemia (Hu and Yacoub, 2012). The second, positive response is the signal change to the functional increases in CBF and CBV which occurs 2-4 seconds post-stimulus. This is followed by the 'post stimulus undershoot', (van Zijl et al., 2012).

The resultant BOLD signal changes as a consequence of functional hyperaemia is typically weak, within 1-2% (greater at higher field strengths). As such, a substantial degree of image pre- and post-processing is required to detect changes in brain activity (see Section 1.4.6 below). To fit within the statistical models used in fMRI analysis, the data are often fitted to a *haemodynamic response function* (hrf).
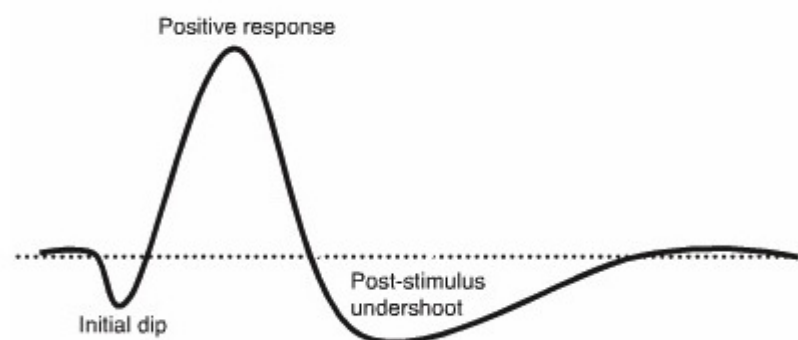
Figure 13: The temporal profile of the BOLD response. The response is characterised by an initial dip in the BOLD signal followed by a signal increase caused by the hyperaemic response. Lastly, the post-stimulus undershoot. Image adapted from Hu and Yacoub (2012).

The hrf assumes that the BOLD response following neural activation acts in a linear time-invariant relationship. There are various methods to model the hrf (Ashby, 2011). Data are often fitted to a function which models the hrf (Boynton et al., 1996). As shown in Figure 14, this function models the lag in peak response following the stimulus with a peak at approximately six seconds and a slow decay over a 20 second period. However, this function does not accommodate for the differences in the hrf seen throughout the brain (Aguirre et al., 1998), such as the delayed response seen in the prefrontal cortex (Schacter et al., 1997). As such, the model risks introducing bias in the task-based paradigms increasing the risk of false detection of activation (Ashby, 2011).

To make hrf models more flexible, canonical forms were generated with several variables which can be estimated (Boynton et al., 1996). Non-linear models were also generated since the BOLD response is not linear (Buxton and Frank, 1997). However, linearity holds without any substantial introduction of errors (Ashby, 2011). Non-linear methods have since been developed, however many require considerable computational power (Friston et al., 2000).

Applications of spin-echo BOLD and gradient-echo BOLD imaging

Most BOLD experiments are conducted using a GRE-EPI sequence. However, the signal is often mis-localised due to the draining of deoxyhaemoglobin rich blood into pial vessels and surface veins (Disbrow et al., 2000). Spin-echo (SE) sequences, as described earlier, eliminate T_2^* decay and can improve the spatial specificity of the BOLD signal to the parenchyma (Goense et al. (2007), Figure 15).
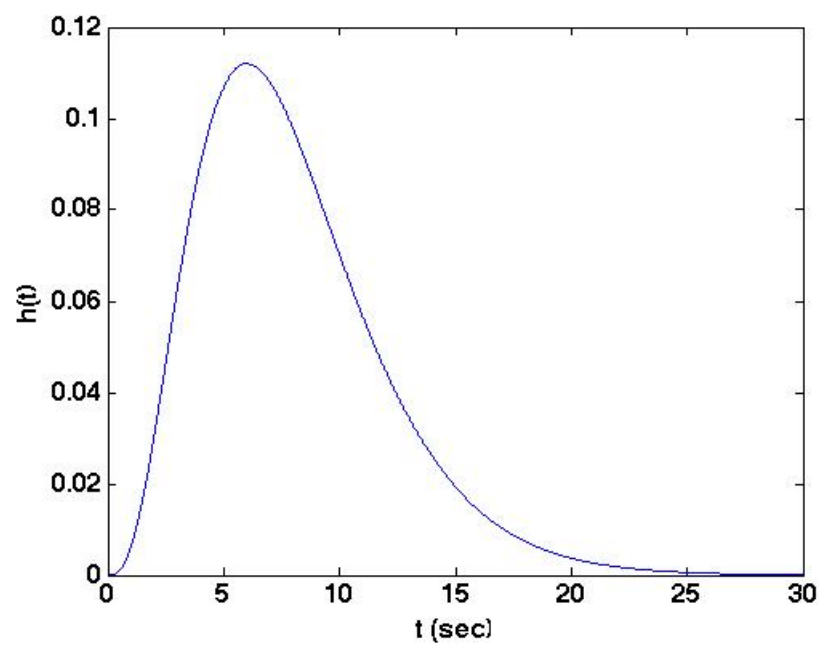
Figure 14: Mathematical model of the haemodynamic response function h(t), based on (Boynton et al., 1996) often used to model the BOLD response. Figure generated from MATLAB code provided in Ashby (2011).
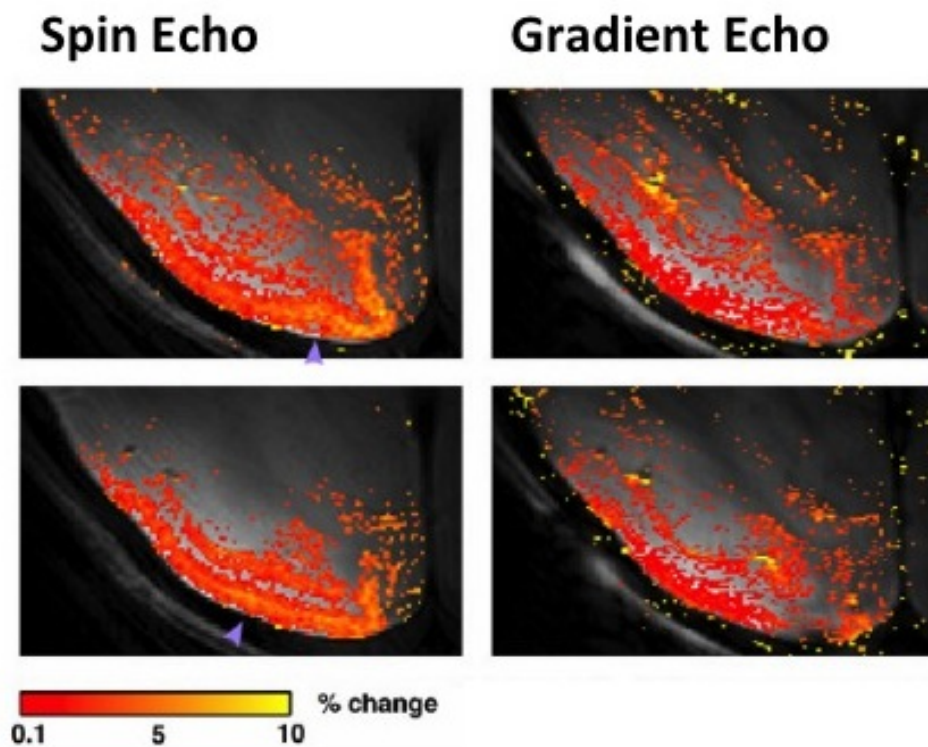
Figure 15: Spin echo (left) and Gradient echo (right) fMRI activation maps from the Macaque V1 acquired at 4.7T (SE $333x326\mu$m planar; GE $333x250\mu$m planar; both 2mm slice thickness). In the SE images, V1 activation is confined to the grey matter in Layer IV. GE-EPI activation showed maximal activation at the surface, illustrating GE-EPI sensitivities to the veins. Figure modified from Goense et al. (2007).

1.4.4   *BOLD imaging in animals*

A large number of functional imaging studies have been conducted in non-human primates (Logothetis et al., 1999; Disbrow et al., 2000; Goense et al., 2008). They are a preferable model for fMRI investigations compared to rodents due to their larger brain size, greater grey-to-white matter ratio, more homologous brain structure to humans, and their ability to be trained for conscious experiments for long periods of time. However, due to cost and low public approval, their use is limited to a few specialised centres. As a result, functional imaging studies in rats have increased in popularity. Although it is possible to train rats to remain still within an MRI scanner (Liang et al., 2015), anaesthesia or sedation is preferred with various compounds trialled, each with their own strengths and caveats for BOLD imaging (detailed in Chapter 4).

1.4.5   *The BOLD signal in the resting brain*

Great focus has been applied to understanding the mechanisms underpinning the intrinsic activity of the resting brain. PET, and later BOLD imaging, where the subject was invited to remain at 'rest' during imaging, showed that brain activity occupied a specific network known as the Default Mode Network (DMN, Raichle et al. (2001)) whose activity reduced during task driven activations. Resting BOLD fluctuations in bandwidths previously considered as noise (< 0.1 Hz) were first identified by Biswal (Biswal et al., 1995) across the human sensorimotor network. Additional resting cortical networks have subsequently been identified (Lowe et al., 1998; Hampson et al., 2002).

There are differing views on the neural basis of resting state BOLD imaging. Leopold et al. (2003) identified low frequency fluctuations in the local field power in the macaque visual cortex with high coherence between electrodes over 20mm apart. He et al. (2006) showed, using electrocorticography in humans, that slow cortical potentials (SCPs) - a combination of infra-slow fluctuations (ISFs) and δ frequency band of LFPs correlated with spontaneous BOLD fluctuations in several states. Schölvinck et al. (2010) demonstrated in the macaque that Local Field Potentials correlated with global cortical BOLD oscillations. The haemodynamic response correlated with frequencies in the gamma band (40-80 Hz) with a characteristic 6 second lag. There were also correlations with lower frequencies (2-15 Hz) with no lag. LFP-BOLD coupling was lower in variance and more strongly coupled when the monkey's eyes were closed.

Resting BOLD studies in rats

Rats have also been shown to possess resting state networks (Pawela et al., 2008) including the DMN (Lu et al., 2012) indicating conservation of this phenomenon across mammals even under light anaesthesia or sedation. Indeed, the rodent sensorimotor resting state network shows strong homology with neuroanatomy as seen in Figure 16.
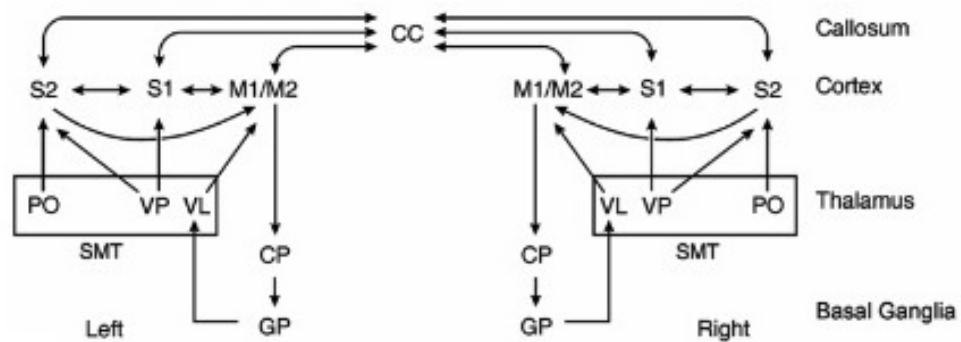
Figure 16: Illustration of the rodent sensorimotor network based on histological studies. Abbreviations: corpus callosum (CC), Primary/Secondary Motor area (M1/2), Primary/Secondary Sensory area (S1/2), caudate putamen (CP), globus pallidus (GP), sensorimotor thalamus (SMT), ventro-lateral thalamic nucleus (VL), ventral-posterior thalamic nucleus (VP), posterior thalamic nucleus (PO), Figure modified from Pawela et al. (2008).

1.4.6   *BOLD data Pre-processing*

Pre-processing of raw-functional data is an essential component of all functional MRI data analysis. In statistical terms, noise is the variability that does not fit the model, so by managing the variance through several pre-processing steps, the power of the data are increased.

MOTION CORRECTION: Motion shifts the spatial distribution of voxels leading to mismatches between TRs. Most correction methods use *rigid body registration*, which corrects for motion along three translational dimensions and three rotations. Using one volume as the standard, images from each TR are transformed to match it as closely as possible (Friston et al., 1995).

COREGISTRATION: Registration of functional data directly to an anatomical template carries the risk of registration being purely resolved by localisation with the edges of the brain, rather than including structures within the brain, due to the poor contrast of the EPI data set (Poldrack et al., 2011). Coregistration to a well recognised anatomical atlas with distinct structural delineations improves the spatial localisation of the regions of the brain involved in resting-state networks. The most popular coregistration method (also known as rigid-body transformation) is based on mutual information which aims to maximise the association between grouped voxel intensities (Collignon et al., 1995).

SPATIAL SMOOTHING: Spatial smoothing replaces a voxel value at each TR by a weighted average of its neighbours by the *full weight at half maximum* (FWHM) kernel. As such, high frequency noise over small areas is removed and by doing so, increases the SNR.

The data also become more normally distributed and therefore more rigorously fit to the statistical tests used in functional MRI analyses (Ashby, 2011).

TEMPORAL FILTERING: Temporal filtering smooths voxel data across the time series, removing either high frequency noise (low pass filter), or low frequency noise (high-pass filter).

FIELD-MAPPING AND DISTORTION CORRECTION: Echo planar imaging (EPI) is highly susceptible to geometric distortion due to B_0 inhomogenieties caused by sources such as the air within the ear canals, haemorrhages within the parenchyma, or implanted devices. These sources of susceptibility cause the greatest distortion in the phase direction due to the smaller bandwidth. As such, inhomogeneities cause shifts in voxel position, altering the shape of the brain. Distortion (often dissimilar between subjects) complicates EPI image intra-subject co-registration as well as co-registration to standard atlases. Field-mapping is a direct measurement of the inhomogeneities within a subject and is calculated by acquiring two 3D gradient echo images at different echo-times, calculating the phase difference between them, and dividing it by the difference in TE. From the phase, magnitude (a FLASH counterpart of the phase image), and functional volumes, a voxel displacement map (VDM) is calculated and the EPI volume subsequently unwarped (Jezzard and Balaban, 1995).

The pre-processing methods described above are analogous between human and non-human data sets. In the case of anaesthetised rodents, motion correction is not usually required, because the animal is unconscious and secured via ear and tooth bars.

1.4.7   *The Applications of BOLD imaging*

It is of no surprise that functional imaging has gained in popularity due to its ability to infer neural activity non-invasively. As such, the neuroimaging field in relation to cognition and disease has exploded in the last two decades (Bandettini, 2012). Resting state BOLD studies have often focused on the purpose of the Default Mode Network and its changes in disease states (Buckner and JR, 2008). Physical damage to the brain in the form of ischaemia, traumatic injury, or tumourigenesis all affect brain structure, and function as a consequence with resultant changes in functional networks (Honey and Sporns, 2008).

The effect of ischaemic stroke on the BOLD signal and functional networks has been extensively investigated. It's been found that ischaemic stroke causes a decline in the magnitude of the BOLD signal in the contralateral hemisphere following a finger tapping task (Pineiro et al., 2002). Findings such as these are unsurprising. Post-stroke responses such as the 'no reflow' phenomenon (Ames et al., 1968), impaired vascular responses to stimuli such as hypercapnia (Kågström et al., 1983), and the sustained constriction of capillary pericytes (Hamilton et al., 2010; Hall et al., 2014) all affect neurovascular coupling and the BOLD signal as a consequence. The loss of neurons, gliosis, loss of long range fibres, and subsequent cyst formation (detailed earlier) all have a direct consequence on neuroanatomy and function. However the adult brain is capable of some degree of plasticity which has been identified in both rats (Weber et al., 2008; vanMeer et al., 2010; van Meer et al., 2012) and in humans (Ward et al., 2003a,b; Dancause, 2006).

There is a general consensus that in the early stages of infarction, increased activity in the contralateral hemisphere (e.g. increased digit representation) is attributable to loss of horizontal callosal projections causing a reduction in interneuron inhibition (Dancause, 2006). The degree of involvement of the contralesional cortex in the post-stroke brain is believed to predict functional outcome (Weiller et al., 1993; Pineiro et al., 2001; Dijkhuizen et al., 2003; Ward et al., 2003b) with increasing involvement indicative of poor recovery.

However, the heterogeneity of infarct size, location and functional consequences following stroke make determining if there exists a typical response of the brain to injury, incredibly challenging.

1.4.8 *Summary*

Therapies for ischaemic stroke are currently mechanical or pharmaeutical recannalisation, preventing recurrence, or adaptive measures to cope with the subsequent disability. Stem cell treatments may provide a new means of limiting ischaemic injury, or improving disability in the chronic stages of the disease. CTX0E03 cells have previously shown to improve motor function following middle cerebral artery occlusion in rodent models (Stroemer et al., 2009; Smith et al., 2012). After Phase I evaluation suggested the cell line to be safe in human patients (Kalladka et al., 2016) the cell line is now in a Phase 2 clinical trial. Magnetic resonance imaging is a relatively safe means of investigating brain structure and function in both humans and pre-clinical models. Resting state fMRI is now a popular method to assess brain connectivity without the need for a stimulus. As the mechanisms of CTX-cell induced functional improvement are yet to be determined, resting-state

fMRI may provide a means to assess how the brain responds to stem cell transplantation. As there has yet to be a published study on resting state network changes following a stem cell therapy for stroke and few studies on the longitudinal changes in rat brain connectivity post stroke, this thesis will present novel data in this field.

1.5 HYPOTHESES

The hypotheses in this thesis are:

- The functional assessments chosen will be of suitable sensitivity to detect long-term post-stroke dysfunction.

- Non-invasive monitoring of end-tidal carbon dioxide, and other variables, will be achievable within a high-field MRI scanner.

- Intracerebral transplantation of CTX0E03 cells into the peri-infarct region will generate sensorimotor functional improvements (as seen previously) with concordant changes in the post-stroke resting-state network.

1.6 AIMS

The aims of the experiments in this thesis are thus as follows:

- To assess a range of behavioural tests suitable for the detection of long-term post-stroke sensorimotor dysfunction.

- The development of an anaesthesia and physiological monitoring protocol suitable for longitudinal fMRI studies and rodents.

- Investigating the effect of a neural stem cell therapy for ischaemic stroke on resting-state fMRI networks and functional outcome.

METHODS

2.1 LEGISLATION AND WELFARE

All procedures involving animals were performed under the Animals (Scientific Procedures Act), 1986, under UK Home Office Project Licence, 60/4449, ('Pre-clinical stroke and experimental MRI', Prof I.M.Macrae, University of Glasgow). Stem cell handling and transplantation was approved by the University of Glasgow Genetically Modified Organisms Safety Committee (GMSC) under reference number GM223/INP/MM_1. Materials brought into the Biological Services Veterinary Research Facility were approved following Risk Assessment by the Biological Services Safety and Records Officer, in file under serial number 380. All procedures were performed by Tristan Hollyer (PIL: 60/13076) unless stated otherwise.

The animals used in all experiments were adult male out-bred Sprague Dawley strain of laboratory rat (*Rattus norvegicus*). Animals were housed in maximum groups of 4 under a 12 hour light/dark cycle (7am/7pm, local time) in identical plexiglass containers with sawdust, nesting material, and a cardboard cylinder. Access to water and food pellets was *ad libitum* during licensed procedures unless stated otherwise. In all surgical procedures, body temperature was monitored and maintained at $37 \pm 0.5\,^{\circ}\mathrm{C}$ using a rectal probe coupled to a homeothermic heat blanket (Harvard Apparatus).

2.2 SURGICAL PRACTICE

2.2.1 *Aseptic technique*

Aseptic technique was followed for all surgical procedures as defined in the Project Licence 'Background Information on Programme of Work & Local Appendices' and are summarised below.

Equipment, operator, and the surgical bench

The surgical bench, cork-board, and surrounding area were disinfected using 70% ethanol. Sterile drapes were then placed over the bench and cork-board with autoclaved surgical instruments and swabs placed on them. Non-thermostable items such as the Doccol intraluminal filaments were sterilised by immersion in a cold sterilant (Medistel$^{®}$) for a minimum of 30 min and then rinsed with sterile saline. In between surgeries, tools were scrubbed in Decon$^{®}$90, rinsed with water, and the tips resterilised by placement in a hot-bead steriliser for a minimum of 15 seconds (Germinator 500, Cell Point Scientific), or placed in a bench-top autoclave. Prior to surgery, the operator scrubbed and washed their hands, nails, and wrists via a standard hand washing procedure using 4% chlorhexidine digluconate hand scrub (Hydrex, Ecolab). Sterile gloves and clean scrubs and gown were worn for all procedures.

Preparation of the animal

The surgical site of the anaesthetised rat was clipped of hair in a location distant from the surgical area. The skin was then disinfected using a swab soaked with 0.5% w/v Chlorhexidine digluconate in 70% w/v ethanol solution (Hydrex$^{®}$Clear, Ecolab).

Pre-operative analgesia was then administered as described in Section 2.2.2.

2.2.2 *Analgesia*

Ropivacaine (10mg/ml), (Naropin, GSK), was used as a line-block analgesic (1-2mg/kg) for recovery procedures including stereotaxic implantation (Section 5.3.5) and transient Middle Cerebral Artery Occlusion (Section 2.3.1). Naropin was administered subcutaneously onto the prepared surgical site in the anaesthetised animal prior to incision.

2.2.3 *Anaesthesia*

For all surgical procedures, rats were transferred from their housing cages in the VRF to the surgical suites within the Wellcome Surgical Institute or the Glasgow Experimental MRI Centre (GEM-RIC). Following recording of body weight, the animals were anaesthetised in an anaesthetic chamber (Baxter Healthcare Ltd, UK) with 5% isoflurane in a mixture of oxygen and nitrous oxide at 30% and 70% respectively; delivered at a rate of 1 l/min. Anaesthesia was maintained either via a nose-cone (0.5 l/min) or via endotracheal intubation (Section 2.3.2) with 2-3% isoflurane at the same oxygen-nitrous oxide gaseous mixture. Depth of anaesthesia was confirmed by the absence of any withdrawal reflexes to pinching of the ventral aspect of the hindpaw, typically absent within 4-5 min from the start of anaesthesia. This reflex was assessed frequently throughout all surgical procedures. If a withdrawal reflex was present, surgery was halted temporarily and delivered isoflurane levels increased to a level suitable to inhibit this reflex.

2.3 SURGICAL PROCEDURES

Surgical procedures were undertaken either in the Wellcome Surgical Institute or the GEMRIC theatre suites.

2.3.1 *Transient Middle Cerebral Artery Occlusion*

Transient middle cerebral artery occlusion (tMCAO) was performed via the intraluminal filament method, first described in Koizumi et al. (1986b) and reviewed in (Macrae, 1992, 2011), as shown in Figure 17. Viewing through a bench-top microscope (Wild/Leica M650), an incision was made down the midline of the prepared ventral neck using an #11 scalpel blade and the underlying fascia and the left ventral region adjacent to the trachea exposed. The masseter, omohyoid and cleidomastoid muscles were dissected apart to expose the common carotid artery (CCA). Two 4-0 stutures were placed around the CCA approximately 10 mm apart; the tie most distal from the heart approximately 5mm from the bifurcation of the CCA to the external carotid artery (ECA) and internal carotid artery (ICA). This tie was loose compared to the more proximal tie which was secured around the vessel permanently. Loose ties of 4-0 silk suture threads were placed around the ECA between the branches of the occipital and ascending pharyngeal arteries and also the occipital (OA) and Internal carotid (IC) arteries. A 4-0 silk thread was sometimes used to isolate the pterygopalatine artery (PtA) at its bifurcation from the ICA. The purpose of these ties was to occlude retrograde blood flow and manipulate the vasculature to provide the best visual field for insertion of the intraluminal filament. Ties were placed under tension and manipulated using Halsted Mosquito forceps. Using micro-scissors, an incision was made between the

two ties on the CCA and an intraluminal filament (purchased from Doccol Corp., MA) of appropriate size, (see Table 1) was carefully inserted through the CCA and ICA to the origin of the MCA. This was confirmed by the filament encountering resistance at an insertion length approximately 22 mm from incision site. Once the filament was inserted correctly, the distal CCA and ICA ties were secured to retain the filament; all other ties were removed.

Sham MCAO

Sham MCAO procedures were performed to account for the affect of the surgery on functional performance. As according to Stroemer et al. (2009), sham surgery was performed by repeating the exact procedure as described above with the exception of the complete insertion. In this case, the filament was only inserted to the bifurcation of the internal carotid artery and the pterygopalatine artery (approximately 8mm) and withdrawn after the equivalent occlusion time.
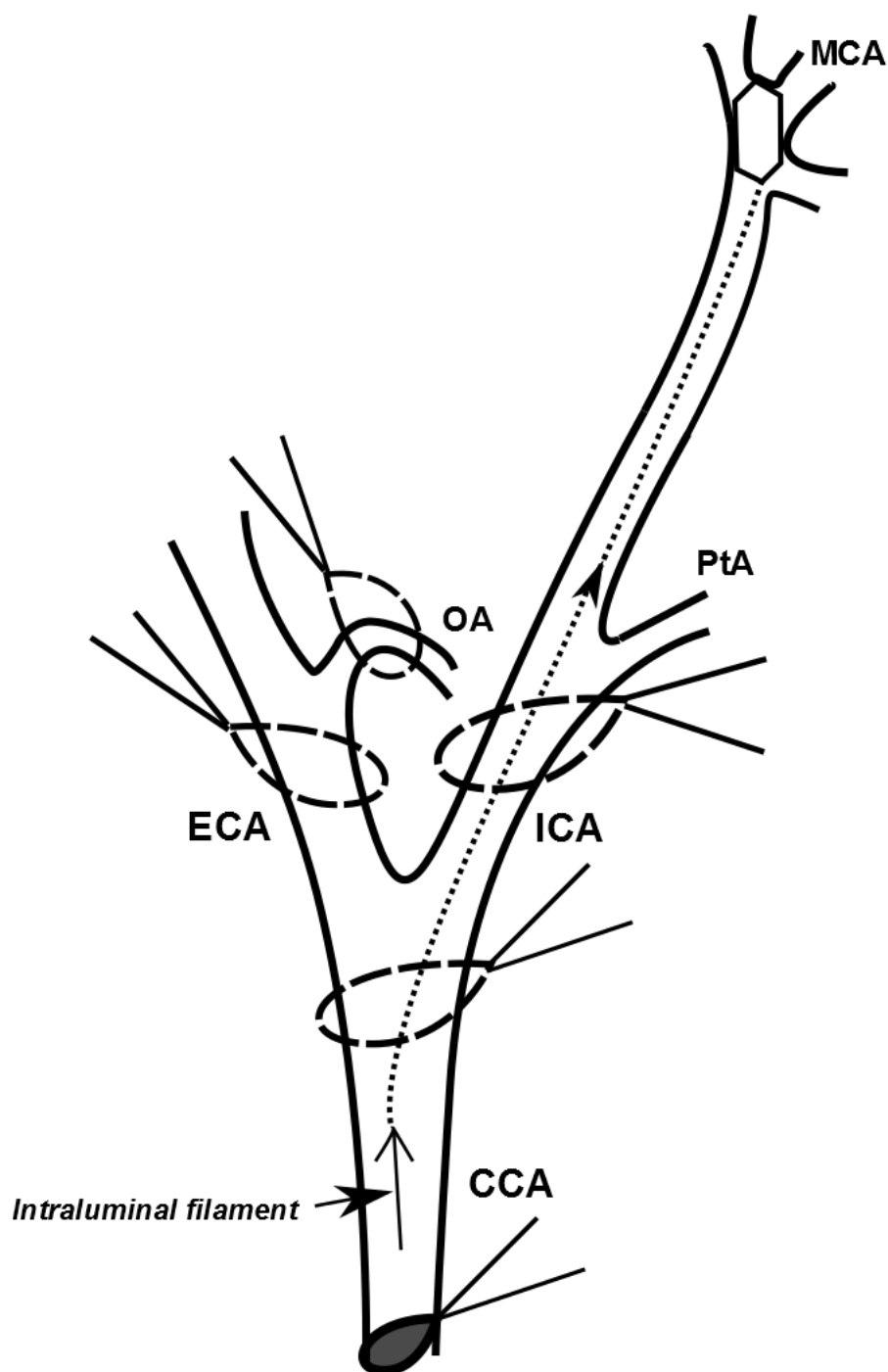
Figure 17: Illustration of intraluminal occlusion of the left middle cerebral artery when viewed inferiorly. The intraluminal filament was inserted distal to the bifurcation of the CCA and guided up through the ICA to the origin of the MCA. Dashed loops represent loose ligatures; solid loops represent permanent ligatures around the vessels.

Animal Weight (g)	Coat diameter (mm)	Suture USP no.	Coat Length (mm)
280-330	0.37, 0.39	4-0, 5-0	3-4, 4-5, 5-6
330- 400	0.41	4-0, 3-0	3-4, 4-5, 5-6

Table 1: Recommended intraluminal filament dimensions for MCAO as recommended by, and purchased from Doccol

In situ recovery for confirmation of correct placement of the intraluminal filament.

As described in Stroemer et al. (2009); to confirm that the intraluminal filament had successfully reduced blood flow to the middle cerebral artery territory of the affected hemisphere, the incision was temporarily closed using Michel clips and the animal recovered from anaesthesia with the intraluminal filament *in situ*. At 60 minutes following insertion of the filament, three tests sensitive to ischaemic damage within the MCA territory were conducted:

- Tail lifting/contralateral forelimb test: the rat was lifted by the base of its tail. Successful occlusion of the MCA in an animal would lead to contralateral forelimb flexion, contralateral body twisting, or hemiparesis.

- Circling test: lifted by the base of its tail with the forepaws remaining in contact with the surface, an animal with a successful MCA occlusion would tightly circle.

- Vibrissae evoked forelimb placement test: brushing the vibrissae over a raised surface initiated a step-up reflex of the corresponding forelimb. Successful MCA occlusion removed this reflex on the side contralateral to the ischaemic insult.

This procedure also allowed for the overlapping surgeries to maximise throughput and reduce time under anaesthesia.

Post-MCAO Surgical Care

The standard post-operative care procedure (Section 2.4) was followed with the following exceptions to dietary monitoring. As detailed in Modo et al. (2000), rats were provided with three softened dietary pellets for the first 24 hours after surgery. Food intake and defecation were monitored on a scale of 0 to +3 with 0 being no food eaten or defecation to +3 being all food eaten with obvious signs of urination and defecation for the first 72 hours. For the first 48 hours following surgery, 2.0 ml of 0.9% saline were given subcutaneously twice a day to prevent dehydration and aid recovery. Additional supportive fluids - either 0.9% saline or 2 ml 50% glucose:saline solution (Baxter Healthcare Ltd) or food enriched with Complan (Heinz) - were given on a discretionary basis. Recovery progress was recorded on ReNeuron form 023-*V*03 'Post-Operative Record Sheet Following MCAO'.

2.3.2 *Endotracheal intubation*

For procedures where endotracheal intubation was required, intubation equipment was made using a 16G IV cannula (AniCath^{TM}, Millpledge). A stylus was made by removing the bevel of the needle using wire cutters and creating an acute bend at the midpoint; the cannula itself comprised the endotracheal tube, as shown in Figure 18.

The animal was first deeply anaesthetised, described in Section 2.2.3, before being transferred to the surgical bench. Placed supine, a loop of 2-0 suture thread attached to a corkboard by a 19 gauge needle was placed around the rat's upper incisors. Once secure, the board and the rat were raised up to a vertical angle

(75-90 degrees) so that the rat was hanging from its incisors with its mouth partially open. A fibre optic light was positioned on to the dorsal aspect of the neck to help illuminate the larynx and the upper trachea; the tongue moved aside using forceps and the oral cavity dried with a cotton bud.

The endotracheal tube, supported by the stylus was then carefully placed through the throat and into the trachaea, the stylus removed, and the tube connected to an Ugobasile volume-driven ventilator (Harvard Bioscience). Correct placement was confirmed by a synchronisation of lung inflation with the ventilator. If this was not the case, the intubation tubing was likely to be in the oesophagus, and as such, the tube was removed and reinserted. Once correctly inserted, the intubation tube was secured by a small suture made in the lip and depth of anaesthesia assessed. Ventilation parameters were typically set to 60-70 breaths/min with an inspired/expired volume of 2.5-3.5 ml with gasesous mixtures described above in Section 2.2.3.

Endotracheal intubation is a preferred method of anaesthesia delivery for certain procedures as by controlling the volume and rate of inhaled gases precisely, the suppressive effects of isoflurane on respiration are limited and physiological parameters (e.g. arterial pCO_2 and pO_2) can be more accurately controlled. Care was taken to avoid trauma to the palette and larynx and the animal reanaesthetised if reaction to laryngeal stimulation was observed.
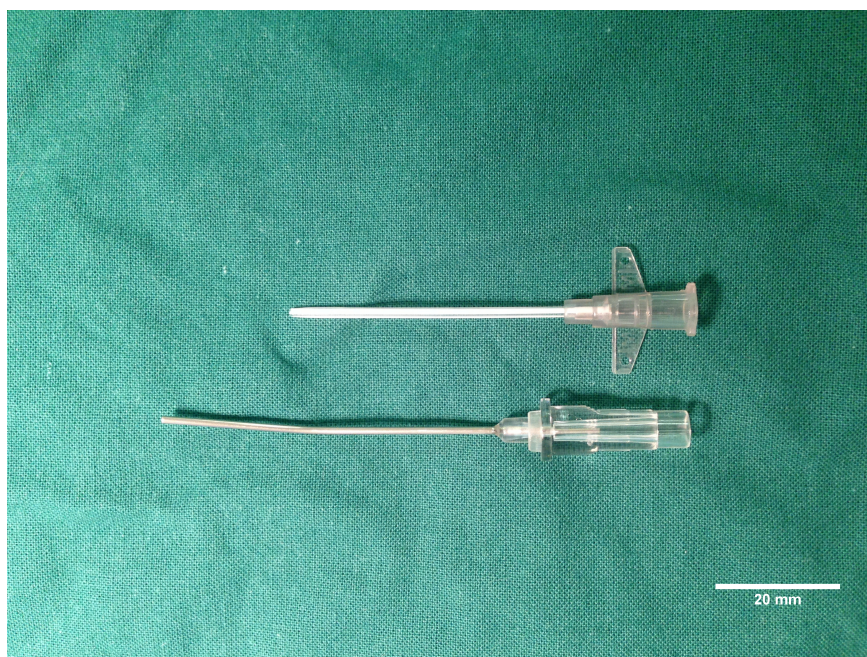
Figure 18: Photograph of the modifications made to the IV cannula (AniCath$^{\text{TM}}$, Millpledge) to create the endotracheal tube (top) and stylet (bottom). Scale bar: 20 mm.

2.3.3   *Arterial and venous cannulation*

Both arterial and venous cannulations followed the same procedure with the respective blood vessel. As such, the procedure in this section will refer to both the femoral artery and vein as 'the vessel'. The leg was secured and the inguinal region shaved and disinfected as described in Section 2.2.1. Following incision, the components of the femoral sheath (vein, artery, and nerve) were dissected apart (with care taken to avoid trauma to the femoral nerve) and two 4-0 silk suture threads placed around the vessel and tied at proximal and distal ends of the exposed vessel. An arteriotomy directed towards the proximal aspect of the vessel was made and a 0.93 mm internal diameter PE-tubing catheter (connected to a 1 ml syringe containing heparinised saline (1000units/ml) was inserted into the lumen. Once secured, the catheter was flushed with heparinised saline and connected to a transducer with blood pressure and heart rate recorded in real-time using Biopac acquisition software. At regular intervals, blood samples were taken ($75 - 100\mu l$) and analysed for pH, oxygen and carbon dioxide partial pressures (pO_2, pCO_2) and $\%O_2$ saturation using a clinical blood gas analyser (RAPIDLab$^{\text{TM}}$248 System, Siemens).

2.4   RECOVERY & POST-OPERATIVE CARE

Post-operative care followed a standard procedure unless stated otherwise.

Immediately after surgery, 2.0 ml of 0.9% saline was given subcutaneously and the time of recovery from anaesthesia recorded. The animal was then transferred to a cage lined with AD pads and placed in a designated recovery room. Softened food pellets provided in a small plastic weighing boat on the floor of the cage. For the remainder of the recovery period, cages were cleaned and animals weighed daily, with a mash of softened pellets supplemented with Complan (Nutricia) given in addition to dry pellets *ad libitum* until pre-operative body weight was regained. As dictated in the Project Licence, if body weight dropped to below 25% of pre-operative weight the Named Animal Care and Welfare Officer (NACWO) or Named Veterinary Officer (NVO) were notified immediately and the animal's future in the study determined on an individual basis.

2.5 BEHAVIOURAL PROCEDURES

2.5.1 *Habituation to Handling*

Following delivery to the Veterinary Research Facility (VRF), and prior to formal assessments, the rats were acclimatised for seven days in the assessment to become accustomed to the handing and restraint methods applied in the behavioural assessments. Familiarisation to human interaction and handling helped to reduce anxiety and stress in the animals, which in turn, permitted more reliable data acquisition.

2.5.2 *Transient Global Neurological Assessments*

A ten-point scoring system, adapted from Modo et al. (2000), provided an acute assessment of global neurological sequelae following MCAO/Sham surgery. The assessment included the following tests described here, as if performed by a neurologically impaired animal.

- *Grasping*: By placing a bar under both forelimbs, in line with the animal, the animal fails to grasp the bar simultaneously with both forepaws.

- *Placing reaction*: The animal was placed on the edge of a platform or table where one side of the body is alongside the edge. When pulling each limb gently in turn off the edge, the animal fails to spontaneously replace the displaced limb back on to the platform.

- *Visual placing*: When lowering it slowly down towards the edge of the cage keeping its forelimbs free, the animal does not reach both forelimbs towards the cage.

- *Righting reflex* placed in a supine position, the animal would not spontaneously right itself.

- *Horizontal bar test*: By placing the animals forelimbs on to a bar approximately 30 cm above the surface, the animal is unable to hang on for a maximum of 3 seconds.

- *Spontaneous mobility*: When placing the animal on an open surface in a familiar environment it fails to move and explore the surroundings within 10 seconds of placement.

- *Circling*: Following focal cerebral ischaemia, circling behaviour was exhibited in the direction of the contralesional hemisphere either spontaneously, or when its hindlimbs are raised up by lifting from the base of the tail.

These tests were binary in their nature; a score of 1 confirming a deficit and a score of 0 confirming its absence. The remaining three points of the test were evaluated by the 'Tail Lifting Test'; a modification from the Bederson scale. The test evaluated the extent of dysfunction induced by MCAO, scored from 0 to 3 by the following criteria:

- 0 - no apparent dysfunction

- 1 - flexion of the contralateral forelimb

- 2 - body twisting to the contralateral side of damage

- 3 - hemiparesis

Such acute assessments are suitable for determining the extent of post-surgical impairment as well as an indicator of the degree of dysfunction generated by the stroke. They are not, however, deemed adequate in identifying permanent neurological dysfunction due to the tendency for rodents to spontaneously recover (Modo et al., 2000).

2.5.3 *Behavioural Assessments*

The identification of assessments suitable to evaluate long-term sensorimotor dysfunction caused by experimental stroke is described in Chapter 3.

2.5.4 *Statistical analysis of behavioural data*

As described in Matthews et al. (1990), the application of a two-sample statistical test at each time-point in data acquired serially is statistically incorrect: the data points are not independent of one another in temporal and subject terms. As such, Matthews and colleagues suggest the use of summary measures of repeated measurements data, in particular, the 'Area under the curve' (AUC) measure. An AUC value provides a summary of each animal's sensorimotor function (depending on the test). The mean results from each group can then be compared with relative ease using an appropriate t-test/ANOVA or their non-parametric equivalent.

All behavioural data results for each animal were summarised by an individual AUC value and group comparisons made accordingly on GraphPad Prism 6 software.

2.6 PERFUSION FIXATION

Transcardial perfusion fixation was performed for future histological analysis of CTX cell, control groups, and pilot tissue. Animals were first deeply anaesthetised (described in Section 2.2.3) and then maintained on 3% isoflurane via a face mask. The thoracic

cavity was opened by an incision at the xiphoid process of the sternum, the diaphragm incised, and the ribs cut at their postero-lateral aspect using blunt dissection scissors. The ribcage was then retracted superiorly to provide full access to the cavity. The heart was held loosely with Halsted Mosquito forceps, a cannula derived from a blunt 16G needle was inserted through the apex of the heart into the aorta. During insertion of the cannula, heparinised saline (10 ml/l) was running through it at a pressure of $80 - 100$ mmHg. Once positioned correctly, the right atrium was incised using sharp micro-dissecting scissors for complete circulatory exsanguination. Once the saline perfusate was clear of blood (approximately 200-300 ml), 4% paraformaldehyde (PAM) was perfused at the same pressure stated above. Satisfactory fixation was confirmed by spontaneous limb movements followed by the onset of tissue rigour after 200-300 ml of PAM perfusion.

2.6.1 *Post-perfusion tissue preparation & paraffin embedding*

Following perfusion fixation (Section 2.6), the carcass was decapitated and the head immersed in 4% PAM for a minimum of 24 hours to limit dark neuron artifacts (Cammermeyer, 1961; Jortner, 2006). Following immersion, the brain was removed and immersed in 4% PAM indefinitely until batch embedding. The embedding procedure was preceded by immersion on 70% ethanol for 24 hours and then processed by the protocol detailed in Table 2.

Step	Reagents	Duration(min)
1	70% Ethanol	60
2	95% Ethanol	60
3	95% Ethanol	60
4	100% Ethanol	60
5	100% Ethanol	60
6	100% Ethanol	60
7	Xylene	60
8	Xylene	60
9	Xylene	60
10	Paraffin	60
11	Paraffin	60
12	Paraffin	60

Table 2: Steps of the automated embedding process.

2.7   MAGNETIC RESONANCE IMAGING

A standard protocol was followed for preparing the animal for non-functional magnetic resonance imaging. All imaging experiments were carried out on a Bruker Biospec 7T/30cm system with a BGA12 integrated 400mT/m gradient (ID) system with integrated 'FASTMAP' shimming. Details of the scanning protocols used are in the respective study chapters.

2.7.1   *Standard preparation for Magnetic Resonance Imaging*

Animals were anaesthetised (as described in Section(2.2.3) and maintained via a facemask or endotracheal intubation (Section 2.3.2). The animal was placed prone within an MR compatible Perspex cradle (Bruker Biospin) and the head secured using ear and tooth bars. Body temperature was monitored via a rectal probe and maintained at $37\,^\circ$C via a closed-circuit heated water system (Cole-Parmer Polystat®) on the surface of the cradle and by a blanket placed over the dorsal surface of the body. Respiration rate was monitored using a pressure sensor (Graseby™) placed on the base of the cradle. All physiological parameters were monitored and recorded using a Biopac MP150 Acquisition System and Acq*Knowledge* software.

A four channel phased-array surface coil was secured level over the dorsal aspect of the head and the cradle then placed within the bore of the magnet. Positioning and alignment of the animal within the bore was verified by pilot scans.

Animals were required to be positioned within the cradle and the magnet as reproducibly as possible to ensure that the inter and intra-subject data sets were as uniform as possible. This was done by marking on the cradle its appropriate depth within the bore and making sure that the animal's head was as level as possible.

IDENTIFICATION OF FUNCTIONAL ASSESSMENTS SENSITIVE TO LONG TERM SENSORIMOTOR DYSFUNCTION

3.1 INTRODUCTION

3.1.1 *The Rodent Somatosensory Cortex*

The mammalian cerebral cortex is a highly organised, layered structure, with layers varying in function and specificity in the processing of information input, output, and signalling between associated cortical areas and sub-cortical structures (Felleman and Essen, 1991). Each layer is unique in its cytoarchitecture, energetics, connectivity and vascular supply (Patel, 1983) and each differs in its responses to its respective inputs (Dunn et al., 2005). Layer IV, the major input-layer, has denser microvasculature, is the most metabolically active, and appears to be responsible for initiating the haemodynamic response, with hyperaemia propagating up towards the surface layers (Tian et al., 2010).

The rodent neocortex shares the same anatomical hallmarks and nomenclature attributable to most other mammals. The somatosensory representation of the body is embossed within the S1 region, with a large proportion dedicated to the Vibrissae (Figure 19). Other major subdivisions of S1 are the forelimb (S1FL) and hindlimb (S1HL) areas. S1 has some partial overlap with the motor cortex with reciprocal communications to/from

the thalamic Ventroposterial lateral (VPL) and Ventroposterior medial (VPM) nuceli terminating in Layer IV (Donoghue et al., 1979). The sensory representation of the whole body is further replicated in S2 latero-caudal to S1.
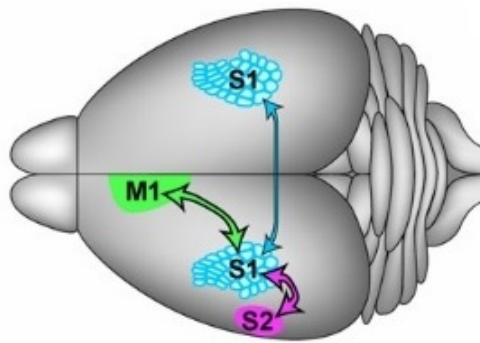
Figure 19: The Rodent Somatosensory Cortical Topography. The topography of the rodent S1 is dominated primarily by the vibrissae Barrel Cortex (blue). Barrel Cortex cortical connectivity exists between the contralateral Barrel field and the ipsilateral S2 and M1. Figure adapted from Petersen (2007).

The Vibrissae and the Barrel Cortex

The rodent vibrissae (whiskers) are an essential component of the animal's sensory system (Figure 20). Touch and object localisation is determined by contact of rhythmic whisking of the vibrissae in combination with freely ranging head and body movement (Kleinfeld et al., 2006). A large azimuthal plane is covered by anterior-posterior whisking and superior-inferior planes covered by dorso-ventral whisks (Bermejo et al., 2002).

Stimulation of the vibrissae causes depolarisation in sensory neurons of the infraorbital branch of the trigeminal nerve via mechanogated ion channels (Petersen, 2007). The sensory neurones form glutaminergic synapses within trigeminal nuclei 'barrelettes' in the brain stem which in turn project to their respective

barreloids in the VPM (Veinante and Deschênes, 1999). VPM neurons project to their discrete somoatotomic location in Layer IV of the Barrel Cortex.

The Barrel Cortex is the sensory subfield of S1 where each large vibrissa is somatopically mapped by individual neuronal functional representations (Woolsey and der Loos, 1970), Figure 20B. Processing of inputs from the vibrissae can be small and involve discrete populations of neurons, or wide ranging, demonstrating the wide range and plasticity of these cortical responses to differing stimuli (Frostig, 2006). Integration of the vibrissae system occurs through several nested feedback loops:

- the brainstem (including whisking rhythm generation, (Nguyen and Kleinfeld, 2005).

- via thalamic nuclei VPM to S1 and S2; a paraleminiscal pathway through the posterior medial nucleus to the superior colliculus, M1, S1 and S2; and a direct leminiscal pathway from the VPM to the Barrel Cortex.

- corticocortical projections with thalamocortical mediation.

Extensive labelling studies have shown that relay cells of the thalamic central lateral nucleus have projection to the striatum and both S1 and M1 vibrissae areas (Deschênes et al., 1996). Overlapping inputs from these areas to the dorso-lateral striatum provide evidence for an integrative role of the basal ganglia.

Cortical processing of signals from Barrel Cortex are both unilateral and bilateral. Corticocortical connections exist via glutaminergic neurons. Unilaterally there are projections to S2 and M1 with some callosal connectivity (Petreanu et al., 2007).
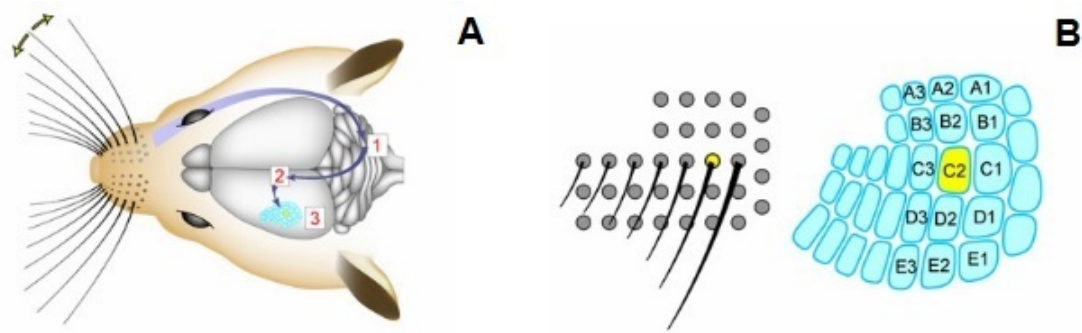
Figure 20: The Rodent Barrel Cortex. (A) Stimulation of a vibrissa causes excitatory input into the trigeminal ganglia (1), the VPM (2) and consequently to the Barrel Cortex (3). (B) Vibrissae have specific somatotopic maps on the contralateral cortex. Figure adapted from Petersen (2007).

Short periods of intraluminal MCAO induce damage primarily to the striatum. As such, corticothalamic inputs through the dorsol-lateral striatum are most often damaged by MCAO. Longer occlusion times will often involve infarction of the cortex. The resulting sensorimotor deficits detail the complexities of the sensoirmotor system neural circuity and its vulnerabilities to damage.

3.1.2   *Rodent skilled forelimb use*

Skilled forelimb use (reaching, grasping, and manipulation) is a homologous function across many species, apparently emerging in the early stages of tetrapod evolution (Iwaniuk and Whishaw, 2000).

The skilled reaching movement occurs in several stages driven firstly by upper arm positioning and abduction to pronate the palm followed by supination at the wrist to present food to the mouth (Whishaw and Pellis, 1990). The individual digits of the forehand make a series of complex movements during the reaching task including flexion, reaching, and *'arpeggio'* grasping motions (Whishaw and Gorny, 1994). The movement is coordinated via a synergy of several pathways including the cortical spinal, rubrospinal, tectospinal, and reticulospinal tracts (Iwaniuk and Whishaw, 2000). Within the forebrain, comprehensive lesioning studies have shown that the caudate-putamen, motor cortex, and the substantia nigra all share a role in skilled forelimb use (Whishaw et al., 1986).

Although the motor cortex (M1) is typically spared during MCAO due to anterior cerebral artery supply, motor function is often impaired due to damage of subcortical structures with circuits linked to M1 leading to changes in the forelimb representation in the cortex (Gharbawie et al., 2005).

3.1.3   *Assessing Post stroke disability in rodent models*

The neurological deficit induced by focal cerebral ischaemia can be broadly divivded into two categories: transient global deficits,

and long term sensorimotor or cognitive deficits (Modo et al., 2000). The former (assessed by tests such as the Bederson score, see earlier) provides a useful means to confirm the acute onset of stroke induced deficits and the presence of oedema. However, it has been demonstrated that rodents will spontaneously recover and/or compensate with the unimpaired limb to mask these deficits (Caleo, 2015).

Functional tests aim to detect the asymmetry induced by unilateral ischaemic brain damage with a primary focus on motor function and sensory neglect (Schaar et al., 2010). These include: the Staircase test (Montoya et al., 1991), the 'Vermicelli Handling Test (Allred et al., 2008), The Cylinder Test Schallert et al. (2000), The Bilateral Asymmetry Test (Schallert and Whishaw, 1984), The Vibrissae Evoked Forelimb Reaching Test (Brooks, 1933) and The Corners Test (Zhang et al., 2002).

With the overall aim of most candidate treatments being to restore functions lost due to stroke, it is essential to select assessments capable of demonstrating the persistent deficits caused by ischaemic stroke, with no susceptibility to adaptation or masking and with limited user bias (Schallert, 2006). In the case of CTX0E03 cell transplantation into the chronic post-stroke brain, tests must be sensitive enough to detect long-term disabilities but to a sufficient degree to detect subtle functional improvements.

3.2 AIMS

The aims of the experiments in this chapter were to identify sensorimotor assessments of suitable sensitivity to detect long-term functional deficits caused by middle cerebral artery occlusion. The selection of several appropriate tests was essential to investigate, in future longitudinal assessments, the potential functional improvements following CTX0E03 treatment.

3.3 METHODS

The strain, sex, age, habituation, handing, MCAO, post-operative care, and global neurological scoring procedures are described previously in the Methods chapter.

3.3.1 *Functional assessments of post-stroke sensorimotor dysfunction*

Sensitive assessments capable of detecting permanent sensorimotor dysfunction following focal cerebral ischaemia were essential for detecting predicted functional improvements subsequent to CTX0E03 transplantation. Various tests were piloted to evaluate their sensitivity and specificity to such deficits.

THE CORNERS TEST.   As described in Zhang et al. (2002), the Corners Test assesses the ability of a rodent to spontaneously rear up and turn to exit a 90° corner. This reflex is initiated when the vibrissae on each side are simultaneously stimulated by contact with the sides of the wall and involves a combination of vibrissae sensation, forelimb and postural functions (Barth et al., 1990). A

neurologically healthy rodent will have a turning preference of 40-60 % towards a particular side (Figure 21). Following focal striatal damage by left MCAO, rats exhibit a turning bias to the left.

A section of cardboard (approximately 50x100 cm) was folded centrally to create a 90 degree angle. Each rat was introduced to the corner ten times and the direction of exit recorded, with at least a 60 second interval between assessments. The percentage of turns to the left was calculated. Rats were tested prior to, and following MCAO. Any animal with a preferential turning bias (greater than 60% in either direction) prior to surgery was excluded. Some rats became intolerant in the latter half of the experimental period resulting in fewer than ten assessments being made. The percentage of turns to the left was calculated from the maximum number of successfully completed trials.
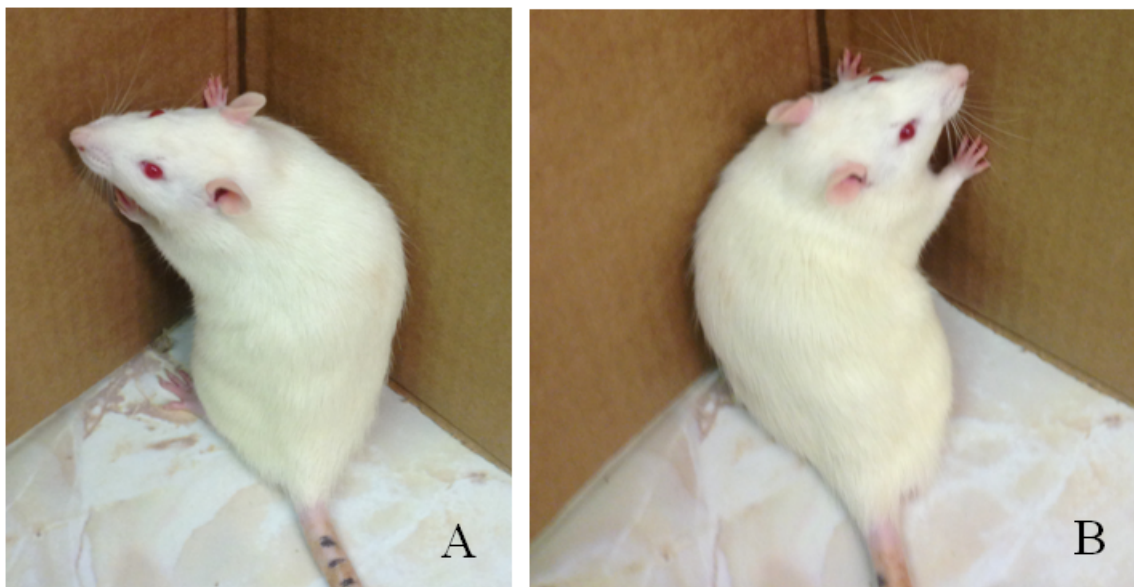
Figure 21: Photograph of a rat performing the Corners Test. Animals which had undergone left MCAO exhibited a turning preference towards the ipsilateral (A) over the contralateral (B) side of damage.

THE BILATERAL ASYMMETRY (STICKY LABEL) TEST.   Focal injury of the cortex or striatum can result in tactile extinction and sensory neglect; a deficit whereby simultaneous bilateral stimulation generates an absence in sensation to the contralateral stimulus locus until the ipsilateral stimulus is removed. When the neglect is only partially resolved, it is known as obscuration (Benton and Levin, 1972; Abramsky et al., 1971). The Bilateral Asymmetry Test (or Sticky Label Test) is a popular test for assessing tactile extinction and sensory neglect and was utilised in previous assessments of sensorimotor recovery following CTX0E03 transplantation following experimental stroke (Stroemer et al., 2009; Smith et al., 2012). It was therefore apt that this test was trialled to determine whether similar results were achievable in our laboratory environment.

The rats were scruffed and 14 mm diameter circular adhesive labels (Ivy Stationary) were attached to the ventral aspect of both forepaws (Figure 22). The paws where then pressed gently between the handler's fingers simultaneously to remove any placement bias and the animal placed into a testing box. The rats then attempt to remove the labels with their tongue or teeth. Performance was recorded using a digital video camera (Panasonic HX-WA20) with the paw of first contact and the times of label contact and removal noted. The maximum recording time was defined as 180 seconds. Failure to either contact or remove the labels within the allotted time was given the maximum time of 180 seconds. The video data were analysed and the time to remove the label (removal time), defined as length of time taken following first contact to successfully remove the label.
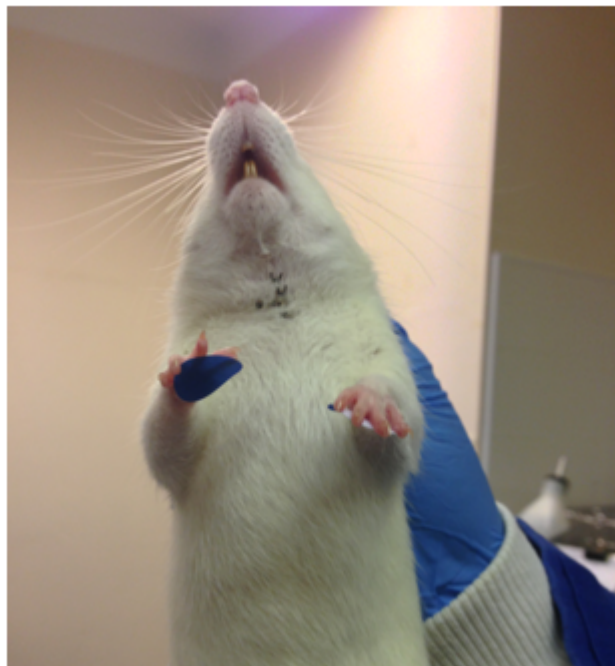
Figure 22: Photograph of a rat being prepared for the Bilateral Asymmetry (Sticky Label) test. The animals were held by the scruff of the neck; 14mm diameter labels applied to the ventral surface of each forepaw and the paws pressed simultaneously before recording responses.

staircase (paw reaching) test.   The staircase test evaluates the skilled reaching, grasping, and retrieving abilities of rats or mice. Designed by Montoya et al. (1991), diet restricted animals were presented bilaterally with 3 sugar pellets (TestDiet, MO) per step, on a series of descending stairs (7 in total). The pellets were only accessible from a narrow, enclosed plinth, allowing for independent assessment of each forelimb (see Figure 23). Diet restriction of animals was necessary to motivate them to perform the test during training and testing. Ischaemic damage to the MCA territory affects both sensory and motor pathways including damage to the corticospinal tract, affecting forelimb function. Advice from Dr Rebecca Trueman, (University of Nottingham) was sought in the design of this assessment.

Following the published diet restriction protocol in Farr and Trueman (2011), approximately 8-10 dietary chow pellets (10-13 g) per animal were provided on the floor of the cages each day. This caused a reduction to, and maintenance of body weight to 85-90% of their starting weight and was sufficient to motivate the animals to perform. Each animal's weight was recorded three times a week. If their weight dropped below 85% of starting weight, they were separated from their cage mates for 24-48 hours and fed additional diet to allow their weight to improve, before being returned to their group housing. Small amounts of sugar pellets were also provided before the training period to reduce any neophobia.

Diet restriction was introduced 5-7 days prior to training. During the training phase, each step of both staircases was filled to capacity with sugar pellets. The rats were then placed in the apparatus for 15 minutes. This allowed them to become familiar with the

testing environment and the pellet retrieval task. The training was conducted twice a day over a 5 day period. The number of pellets retrieved was not recorded during the training phase.

Following training, baseline performance values were acquired over 5 consecutive days with the baseline number of pellets considered to be the median number of pellets retrieved from each step (max 3). Animals which failed to successfully retrieve any pellets due to an inability to habituate to the testing environment were excluded from the study. Following acquisition of baseline data, the animals were returned to an *ad libitum* diet until surgery. Once animals had regained their pre-surgery weight, diet-restriction was re-initiated for the remainder of the experimental period.
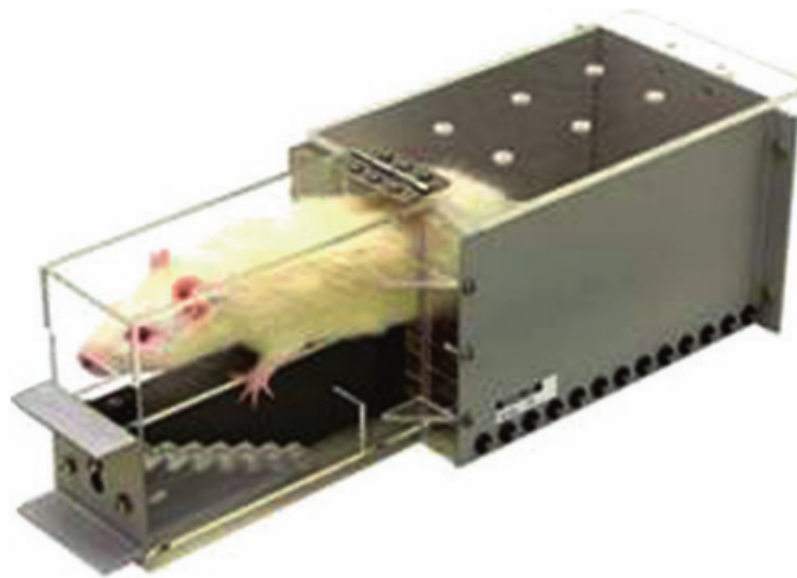
Figure 23: Photograph of an adult rat performing The Staircase Test. Rats are only able to obtain sugar pellets from each side with the respective forelimb. Image adapted from Farr and Trueman (2011).

THE VIBRISSAE EVOKED FORELIMB (WHISKERS) TEST.   This test assessed the reflex which occurs when the vibrissae are brushed upwards along a surface (Brooks, 1933). Animals were held with the hind limbs supported and the forelimb contralateral to the testing side, restricted. The animal's vibrissae were then brushed upwards along the end of a bench. In a naïve/sham animal, the forelimb ipsilateral to the stimulated vibrissae reached up to make contact with the bench surface (Figure 24). As mentioned previously, intraluminal MCAO generates primarily a striatal infarction. As such, neurons from the VPM to the Barrel cortex are vulnerable to damage. The vibrissae evoked forelimb test is therefore an assessment of striatal damage. Left MCAO leads to a failed response to right whisker stimulation. Animals were tested on each side three times with successful performance marked

as '0' and a failed response as '1'. Results were presented as '% failed responses'.
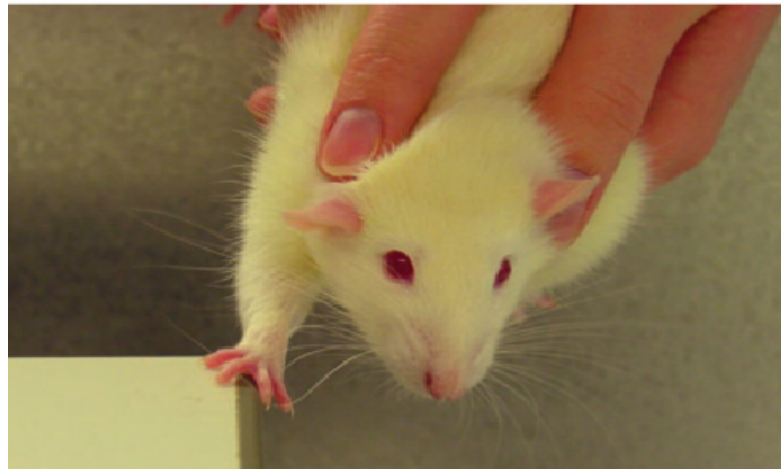
Figure 24: Photograph of an adult rat performing Vibrissae Evoked Forelimb (Whiskers) Test. A neurologically healthy rodent would place the forelimb ipsilateral to the stimulated vibrissae up onto a surface. Image adapted from Farr and Trueman (2011).

THE ADJUSTING STEPS TEST. Forelimb akinesia following MCAO was assessed using a modified version of the adjusting steps test used in (Olsson et al., 1995; Mine et al., 2013), (Figure 25). The animal was supported with one right forelimb free and its hind limbs restrained. The free forepaw was moved in a forehand and backhand direction with the number of bracing steps/hops made over a 0.9 m distance over 5 seconds counted. The test was conducted twice in both directions and the median value in each direction evaluated as a measure of the overall performance.
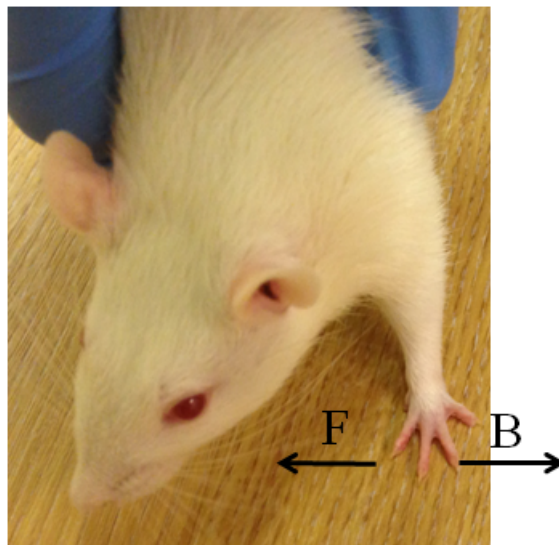
Figure 25: Photograph of an adult rat performing the Adjusting Steps Test. The free forepaw was dragged 0.9 m along a surface in the direction of the forehand (F) and the backhand (B) over a duration of 5 seconds. A neurologically healthy rodent's limb would undertake a series of steps/hops whereas a focal ischaemic infarction negated this reflex.

3.3.2 *Histology*

For assessments of the ischaemic infarct, brain were removed and stained using Haematoxylin and Eosin (H &E). Haematoxylin and eosin stain cellular nuclei and cytoplasm, respectively. Brains were extracted from euthanized rats 7 days post-stroke, fresh frozen in isopentane at $-40°$C for 10min and then mounted and embedded for tissue sectioning (20μm) on a cryostat at $-19°$C. Sections were collected at 8 stereotaxic levels (relative to bregma rostral-caudally) representing the regions of the forebrain supplied by the middle cerebral artery (Figure 26). The sections were then stained with H&E, mounted with DPX and covered with glass coverslips. Images of the sections were taken using a Micro Nikkon 55mm camera using MCID software (Figure 27).
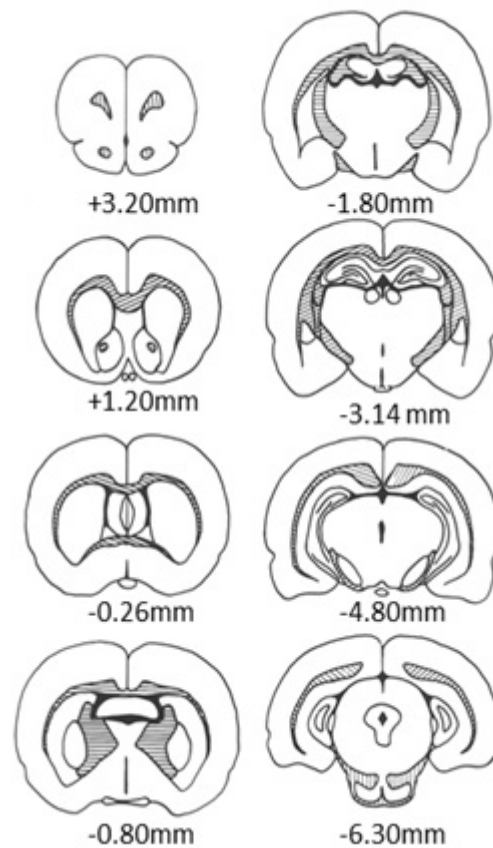
Figure 26: Illustration of the eight coronal levels of the relative to Bregma (mm) based on (Konig and Klippel, 1963) used by Osborne et al. (1987) to illustrate regions of forebrain vulnerable to infarction following middle cerebral artery occlusion.
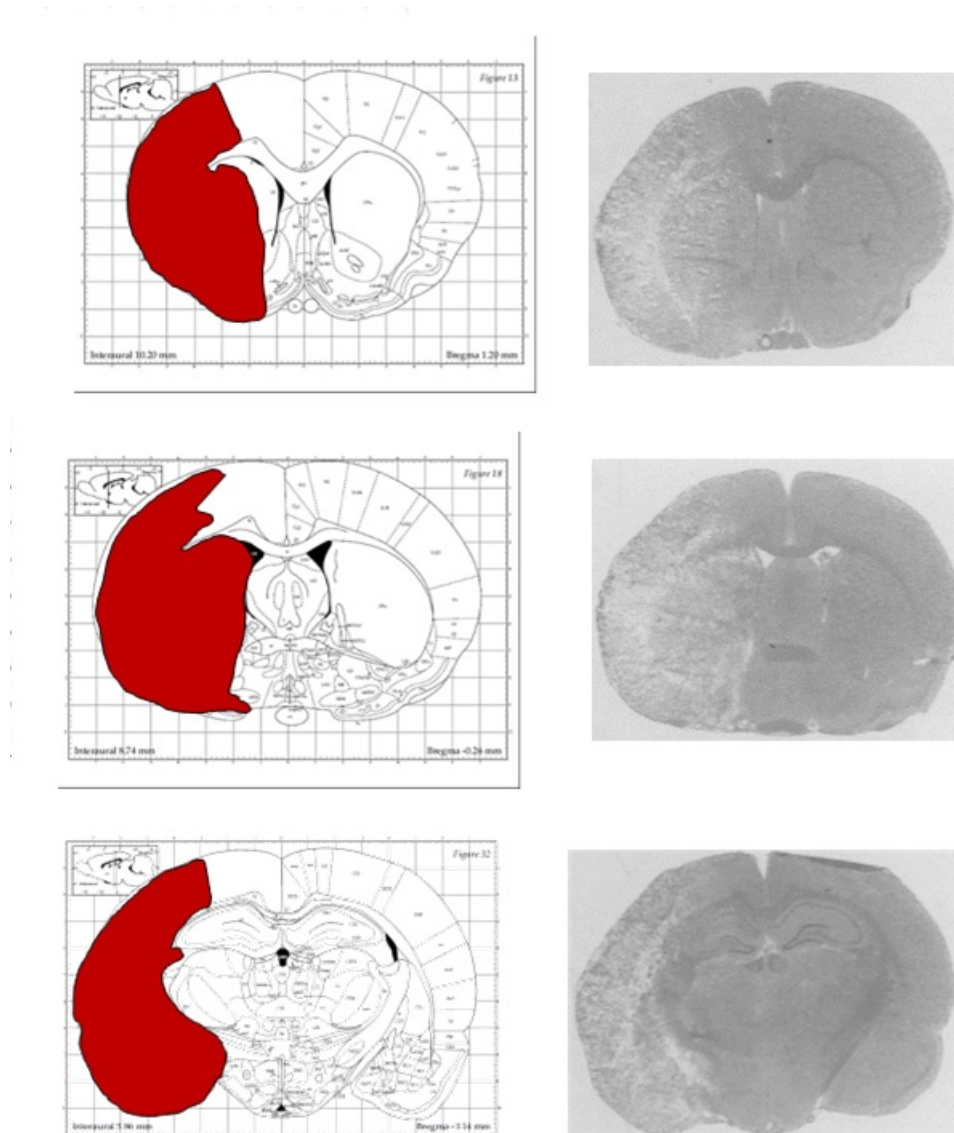
Figure 27: Determination of the infarct 7 days post-MCAO from MCID photographs. The ischaemic infarct was measured from photographs of the relevant slides (right). The distribution of the infarct is shaded in red on coronal plates from the Paxinos and Watson (2006) atlas (left).

3.3.3   *Study design*

The sensitivity of functional assessments was assessed at three time periods post-MCAO in series. Animals were randomly assigned to MCAO or Sham surgery.

ACUTE TO SUB-ACUTE (7 DAYS):   70 min transient MCAO (tMCAO) was conducted (as described earlier), followed by daily global neurological and vibrissae reflex assessments, functional assessments on days -1, 2 and 7. Brains were removed and infarct volumes were quantified from haematoxylin and eosin (H&E) stained sections at stereotaxic 'levels' of the MCAO territory defined in Osborne et al. (1987). n = 5 and 8 for Sham and MCAO groups respectively, unless otherwise stated.

SUB-ACUTE TO CHRONIC (21 DAYS):   70 min tMCAO with functional assessments on days -1, 2, 7, 14, and 21. Infarct volumes were quantified from T_2 weighted RARE MR images acquired on day 7 post-MCAO. n = 7 and 16 for Sham and MCAO groups respectively.

CHRONIC (12 WEEKS):   90 min tMCAO with assessments on day -1 and at weekly intervals. Infarct volumes were quantified from T_2 weighted RARE MR images acquired between 4 and 8 weeks post-MCAO. n = 10 in both Sham and MCAO groups.

MRI imaging

Animals were prepared and positioned as previously described. T_2weighted RARE (Rapid imaging with Refocused Echoes) imaging was used for high resolution anatomical imaging for delin-

eation of the ischaemic infarct (TR=600ms, TE=46.62ms; planar resolution of 100μm; 16 slices of 750μm thickness). Following imaging, the animal was removed and recovered in its home cage.

3.3.4 *Statistical analysis*

All data are presented as mean $\pm$ standard deviation or median $\pm$ interquartile range, as an appropriate means of displaying the distribution of the data. To ascertain at which time post-stroke functional assessments were no longer sensitive to sensorimotor dysfunction, Sham and MCAO groups, and their respective time points were compared via One-way ANOVA or the non-parametric equivalent Kruskal-Wallace test with the relevant correction for multiple comparisons. Corner, Adjusting Steps, Bilateral Assymetry tests at 7 days were assessed with thr Kruskal-Wallace test and with One-way ANOVA at 21 days to assess at which time point the test lost sensitivity. For tests conducted daily and the 12 week study, the summary measure of area under the curve (AUC) was evaluated for each animal and the group means compared Matthews et al. (1990). Conventional statistical measures such as Student's t-test/ANOVA are unsuitable for serial data sets as they do not take into account the likely correlation and dependence between time points. AUC and other summary measures use the individual subject as the 'basic unit' (Matthews et al., 1990) and use the results of the whole data time series to summarise the individual responses. The individual responses can then be pooled according to treatment groups and the means compared by conventional measures.

3.4 RESULTS

3.4.1 *Assessments sensitive up to 7 days post-MCAO*

Acute and sub-acute post-stroke global neurological and functional deficits were assessed in 8 and 5 male SD rats following 70 min and Sham tMCAO, respectively. Global neurological score was assessed daily. Functional assessments were conducted in a main cohort of rats on days -1, 2 and 7 pre/post-surgery. These included:

- The Corners test.

- The Adjusting Steps test trialled in a sub-cohort of two Sham and five tMCAO animals.

- The Bilateral Asymmetry Test / Sticky Label Test (BAT), trialled in a sub-cohort of two Sham and five tMCAO animals.

- The Whiskers Test: assessed daily in a sub-cohort of two Sham animals and all eight tMCAO animals.

Fresh-frozen, H&E stained, 20μm sections of tissue were manually delineated from optical MCID images. The mean infarct volume was 130 ± 94mm^3, (Figure 28). There were no abnormalities in the Sham animals.

Transient MCAO produced global neurological deficits which persisted over 7 days following 70min tMCAO ($p < 0.0001$, Figure 29).
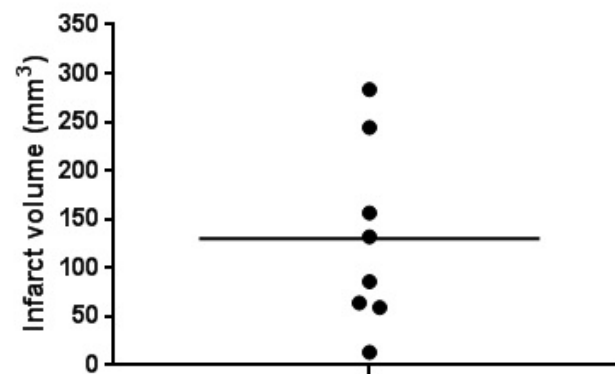
Figure 28: Infarct volumes quantified from H&E sections taken across the MCA territory following 70min tMCAO. Mean volume: $130 \pm 94\text{mm}^3$ (mean $\pm$SD).
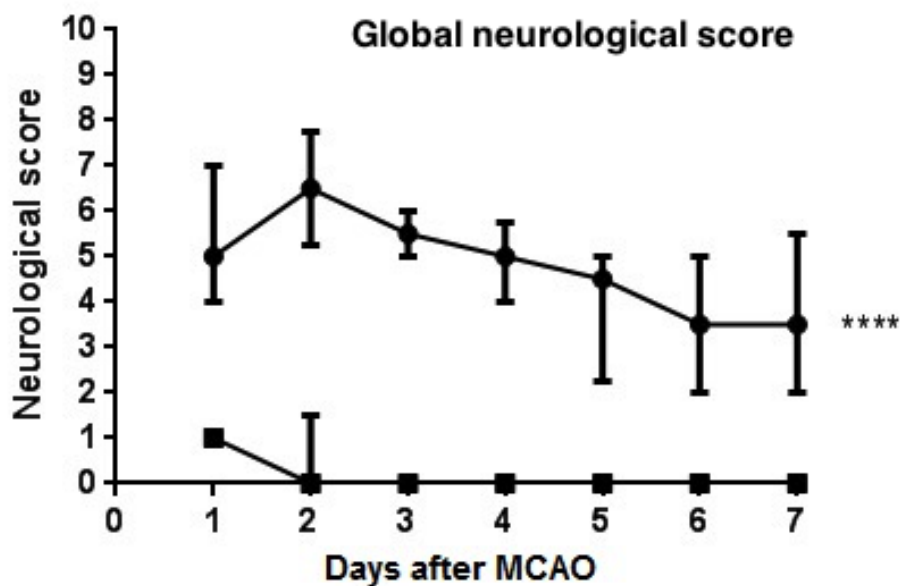
Figure 29: Daily Global Neurological Scores following Sham (■) or 70min tMCAO (●). 70min tMCAO caused distinct neurological impairment throughout the experimental period ($p < 0.0001$); Unpaired t-test of Group AUC values. Sham (n= 5), tMCAO (n= 8) Data presented as Median $\pm$ Interquartile range.

In the Corners test, all rats which underwent tMCAO exhibited an increased turning bias towards the ipsilateral side of damage when exiting a 90 degree corner (p< 0.01, Figure 30). Sham animals showed no change in turning bias (p> 0.05).
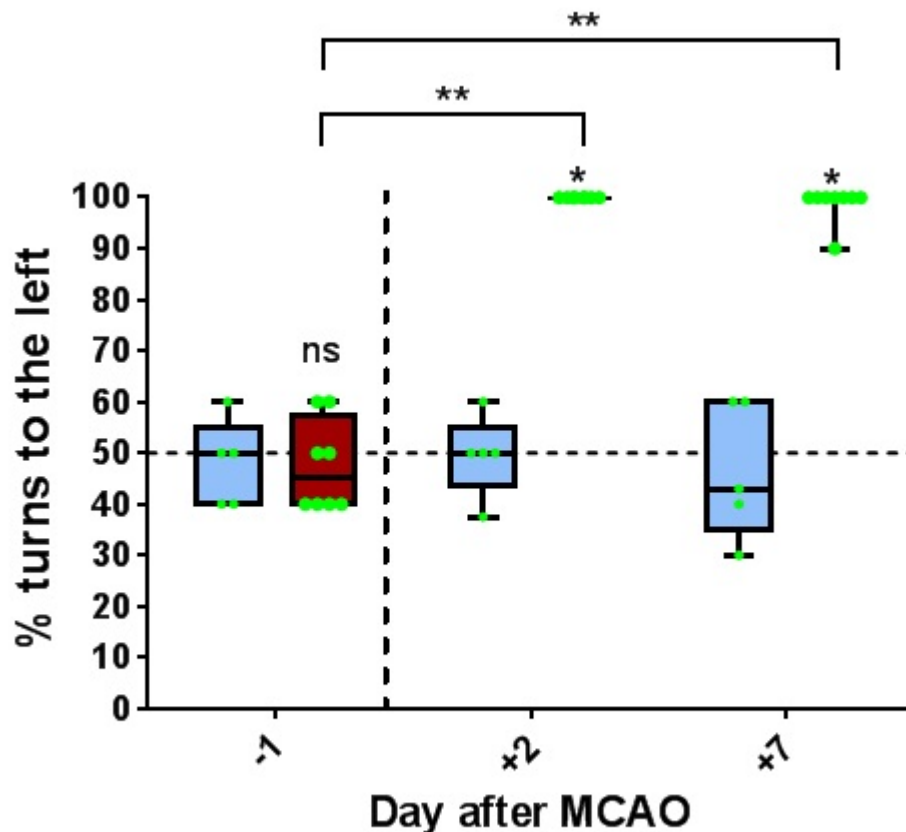
Figure 30: The percentage of turns to the ipsilesional side (left) at days −1, 2 and 7 following Sham (blue) or 70min MCAO (red) during the Corners Test. There were no pre-stroke differences (p> 0.05). 70min tMCAO caused distinct neurological impairment with persistent turning to the left compared to Sham animals at the same time points (*, p< 0.05) and compared to baseline values (**p< 0.01); Kruskal-Wallace with Dunn's multiple comparisons test. Data presented as Box &Whiskers plot with minima and maxima and individual data points superimposed in green. Sham (n= 5), tMCAO (n= 8).

The number of adjusting steps/hops taken when the right (contralesional/affected) and left (ipsilesional/unaffected) forelimb was dragged laterally and medially from the body across a surface for a distance of 0.9m. No significant changes in lateral stepping actions were found 2 and 7 days post tMCAO with either forelimbs ($p > 0.05$, Figure 31). 7 days post tMCAO, there was a significant decline in the number of medial adjusting steps in the right forelimb only (Figure 32).

Figure 31: The number of adjusting steps made when the left (top) and right (bottom) forelimbs are dragged **lateral** from the midline on days -1, 2 and 7 following Sham (black) or 70min tMCAO procedure (red). There was no effect of tMCAO on lateral stepping movements of either forelimb at any time point (p> 0.05); Kruskal-Wallace with Dunn's multiple comparisons test. Data presented as Box & Whiskers plot with minima and maxima and individual data points superimposed in green. Vertical dashed line represents MCAO at day zero. Sham (n= 2), MCAO (n= 5).
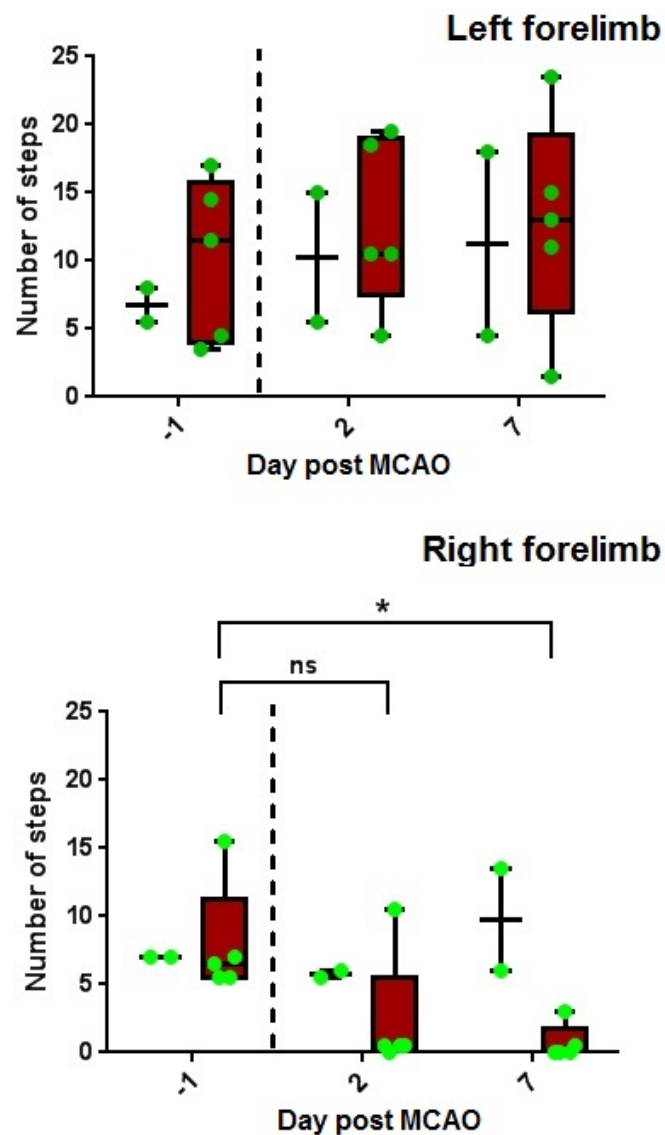
Figure 32: The number of adjusting steps made when the left (top) and right (bottom) forelimbs are dragged **medial** from the midline on days -1, 2 and 7 following Sham (black) or 70min left tMCAO procedure (red). There was no effect of MCAO on medial stepping movements of the left (ipsilesional) forelimb. MCAO caused a reduction in the number of steps made with the contralesional (right) forelimb at 7 days compared to baseline (p< 0.05); Kruskal-Wallace with Dunn's multiple comparisons test. Data presented as Box & Whiskers plot with minima and maxima and individual data points superimposed in green. Vertical dashed line represents MCAO at day zero. Sham (n= 2), MCAO (n= 5).

The Vibrissae Evoked Forelimb / Whiskers test was trialled daily post-stroke and sham procedure (Figure 33). There was no effect of left tMCAO on forelimb raising reflexes on the ipsilesional side compared to Sham-operated controls ($p > 0.05$). Contralesional right forelimb raising was permanently impaired by MCAO in comparison to Sham-operated controls.

Figure 33: The percentage failed forelimb placing reflexes following upward vibrissae stimulation of the ipsilesional side (left, top) and contralesional side (right bottom) at days 1 to 7 following Sham (•) or 70min left tMCAO procedure (■) procedure. There was no effect of MCAO on reflex ability on the ispilesional side. 70min MCAO caused distinct neurological impairment of the contralesional forelimb reflex compared to Sham animals at the same time points (***, p= 0.002), Unpaired t-test of AUC values. Sham (n= 2), MCAO (n= 8).

Stroke induced sensory neglect and tactile extinction was trialled by the Bilateral Asymmetry Test (Figure 34). The time taken to remove the label from the ipsilesional (left) and contralesional (right) forepaws were measured. There were no differences in any assessments of the MCAO group (p> 0.05).

Figure 34: The time taken for removal of the adhesive label from the ipsi- and contra-lesional forepaw in the bilateral asymmetry test. There was no statistically significant effect of MCAO on the removal times from the ipsi- and contra-lesional forelimb however, there was a clear trend for an increased removal time on the contralesional forepaw (p> 0.05, Kruskal-Wallace). MCAO Contralesional (■), MCAO Ipsilesional (■), Sham Contralesional (▲), Sham Ipsilesional (▲). Vertical dashed line represents MCAO at day zero. Sham (n= 2), MCAO (n= 4).

All functional assessments showed evidence or trends for sensitivity to unilateral sensorimotor dysfunction in the acute and sub-acute post-stroke period. The small number of sham control animals and absence of pre-surgical measurement of the vibrissae reflexes warrant further investigation, with a larger number of animals and an extension of the study period out to the early chronic phase of post-stroke pathology. As such, all tests were examined for sensitivity to post-stroke dysfunction up to 21 days.

3.4.2   *Assessments sensitive up to 21 days post-MCAO*

With the Corners, Adjusting Steps, Whiskers and Bilateral Asymmetry assessments showing evidence for sensitivity to post-stroke dysfunction in the first seven days post-insult, all were assessed for sensitivity out to 21 days. It also provided an opportunity to continue to develop surgical skills.

T_2 weighted RARE MRI was carried out 7-12 days post-stroke to provide quantification of the infarct. The mean infarct volume was $107 \pm 82\text{mm}^3$ (Figure 35), with no statistical difference compared to the 7 day study above ($p > 0.05$, two-tailed unpaired t-test). It can be seen that the infarct volumes are biomodal in their distribution with some large strokes involving cortical areas.
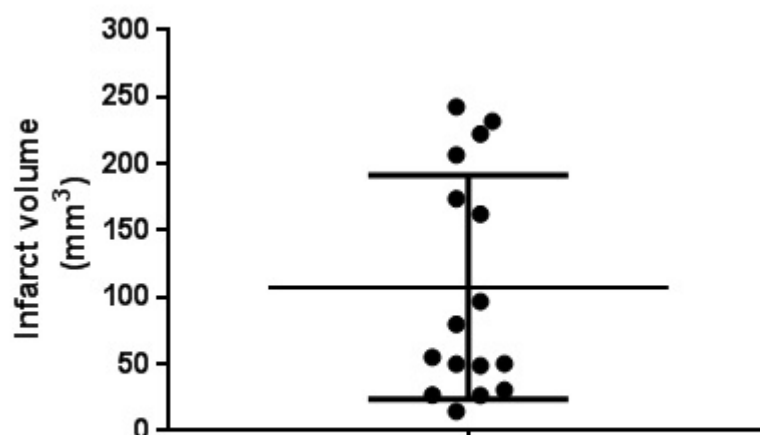
Figure 35: Infarct volumes quantified by manual delineation of T_2 hyperintensities from RARE images acquired 7-12 days following 70 min tMCAO. Mean volume: $107 \pm 82\text{mm}^3$ (mean $\pm$SD).

In the Corners test, all rats which underwent tMCAO exhibited an increased turning bias towards the ipsilateral side of damage from days 2 to 14 post-stroke compared to sham controls and baseline, (Figure 36). The inter-quartile range and median stroke-induced turning biases increased over this period and at 21 days there was no difference between stroke and sham animals. Sham animals showed no change in turning bias from days -1 to 21, (p$>$ 0.05).
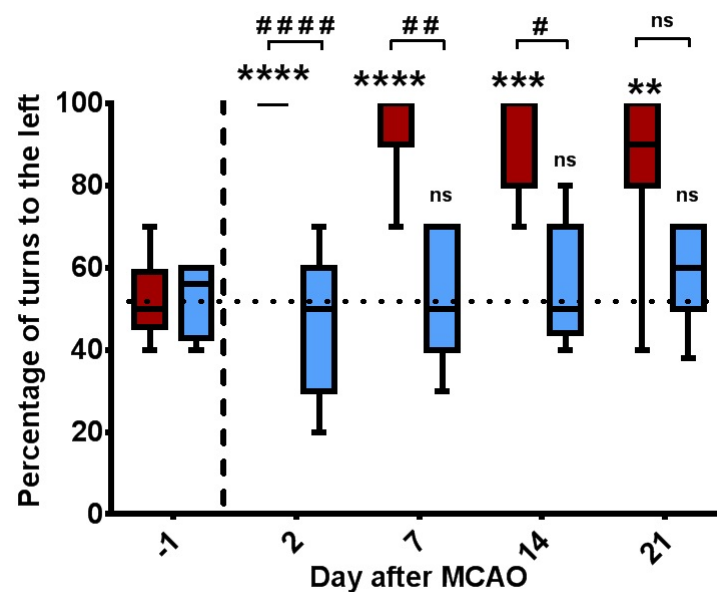
Figure 36: The percentage of turns to the ipsilesional side (left) at days -1, 2, 7, 14 and 21 following Sham (blue) or 70min tMCAO (red) during the Corners Test. There were no pre-surgical differences and no change in Sham animal performance. 70min tMCAO caused distinct turning bias compared to baseline. Compared to Sham animals at the same time-points, tMCAO animals showed left-turning bias up to 14 days post-occlusion (####, p$<$ 0.0001; ##, p$<$ 0.01; #, p$<$ 0.05; ns, p$>$ 0.05) and compared to pre-MCAO values (****, p$<$ 0.0001; ***, p$<$ 0.001; **, p$<$ 0.01; ns, p$>$ 0.05); Kruskal-Wallace test with Dunn's correction for multiple comparisons. Data presented as Box &Whiskers plot with minima and maxima. Vertical dashed line represents MCAO at day zero. Sham (n= 7), tMCAO (n= 16).

The lateral and medial adjusting steps of the right forelimb were counted on days -1, 2, 7, 14 and 21 post-MCAO or Sham surgery. Lateral steps were only impaired on days 2 and 7 compared to both the Sham group and baseline values and compared to baseline on day 14 only ($p > 0.05$, Figure 37). There were no significant changes in lateral stepping actions at 21 days post tMCAO compared to sham and baseline ($p > 0.05$). Medial stepping motions (Figure 38), were permanently impaired compared to baseline values ($p > 0.0001$) and to the Sham group ($p < 0.01$, Days 2, 7, and 14; $p < 0.05$, Day 21). There were no significant changes in Sham group performances across timepoints ($p > 0.05$).
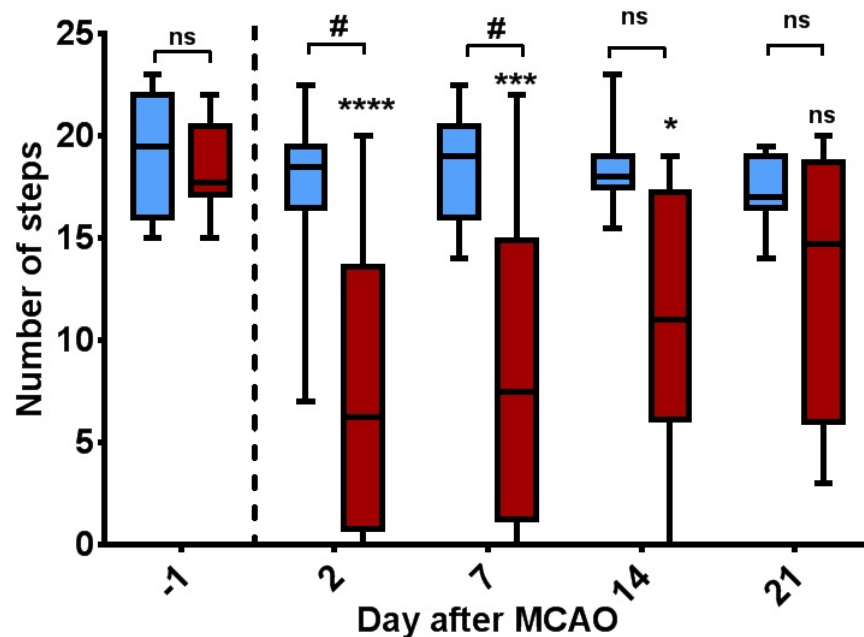
Figure 37: The number of adjusting steps made when the right forelimb is dragged **lateral** from the midline on days -1, 2, 7, 14, and 21 following Sham (blue) or 70min left tMCAO procedure (red). tMCAO impaired lateral stepping movements up to day 7 compared to Sham controls. (#, $p < 0.05$; ns, $p > 0.05$) and up to 14 days compared to baseline measurements (****, $p < 0.0001$; ***, $p < 0.001$; ns, $p > 0.05$); Kruskal-Wallace test with Dunn's correction for multiple comparisons. Data presented as Box &Whiskers plot with minima and maxima. Vertical dashed line represents tMCAO at day zero. Sham (n= 7), tMCAO (n= 16).
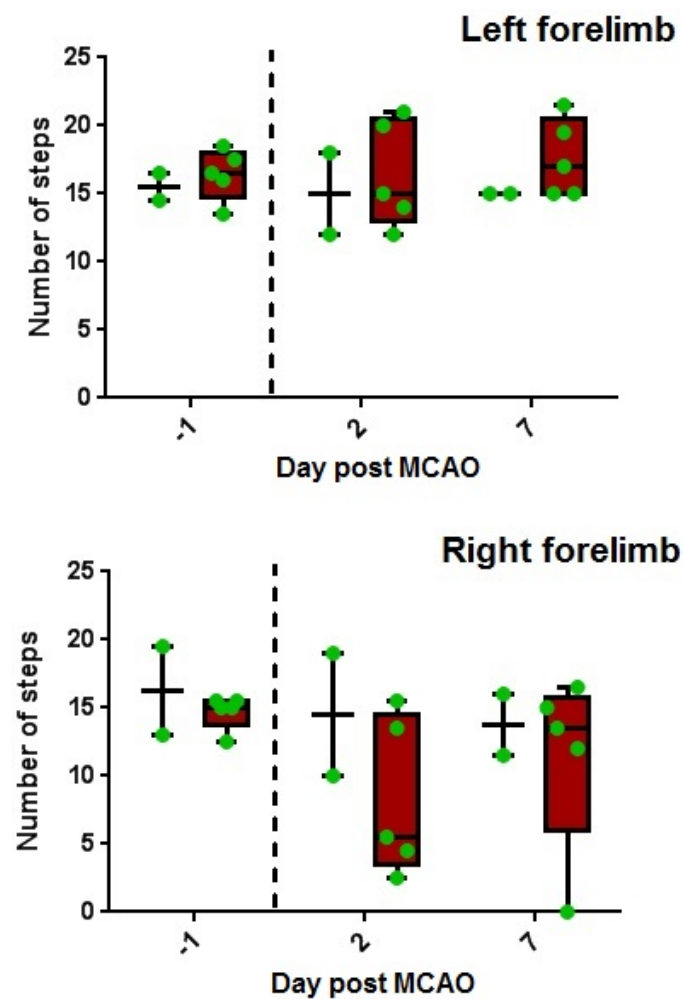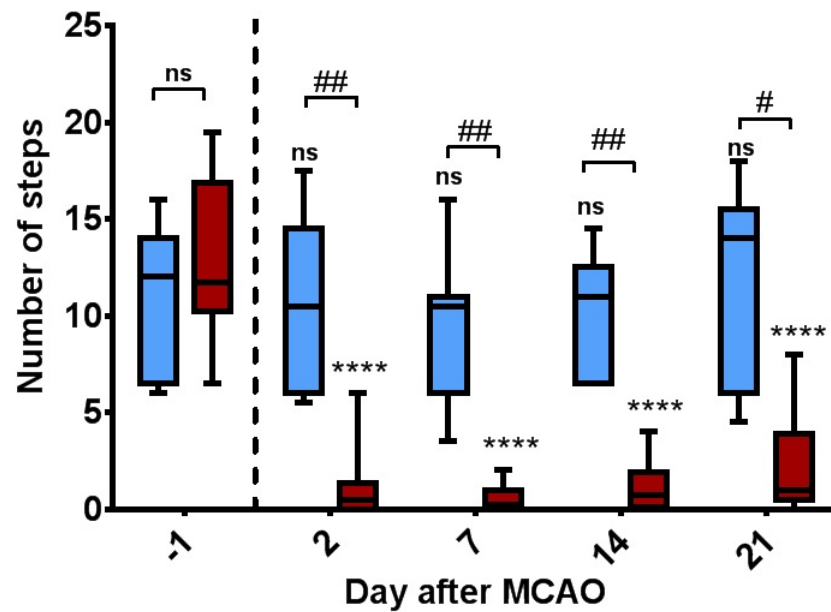
Figure 38: The number of adjusting steps made when the right forelimb is dragged **medial** from the midline on days -1, 2, 7, 14 and 21 following Sham (blue) or 70min left tMCAO procedure (red). MCAO impaired medial stepping motions compared to Sham controls (##, p< 0.01; #, p< 0.05; ns, p> 0.05) and consistently compared to baseline (****, p< 0.0001; ns, p> 0.05). Kruskal-Wallace test with Dunn's correction for multiple comparisons. Data presented as Box &Whiskers plot with minima and maxima. Vertical dashed line represents MCAO at day zero. Sham (n= 7), MCAO (n= 16).

The sensitivity of the Vibrissae evoked forelimb / Whiskers test to stroke-induced dysfunction on both ipsilesional and contralesional hemispheres was trialled on days -1, 2, 7, 14 and 21 post-stroke and sham procedure (Figure 39). There was no effect of left tMCAO on forelimb raising reflexes on the ipsilesional side compared to Sham-operated controls ($p > 0.05$). However, it can be seen by the large variability in the results that some animals did have a failed ipsilesional forelimb raising response but it was not statistically significant. Contralesional right forelimb raising was impaired by tMCAO in comparison to Sham-operated controls at all time points with no evidence of spontaneous recovery ($p > 0.05$).
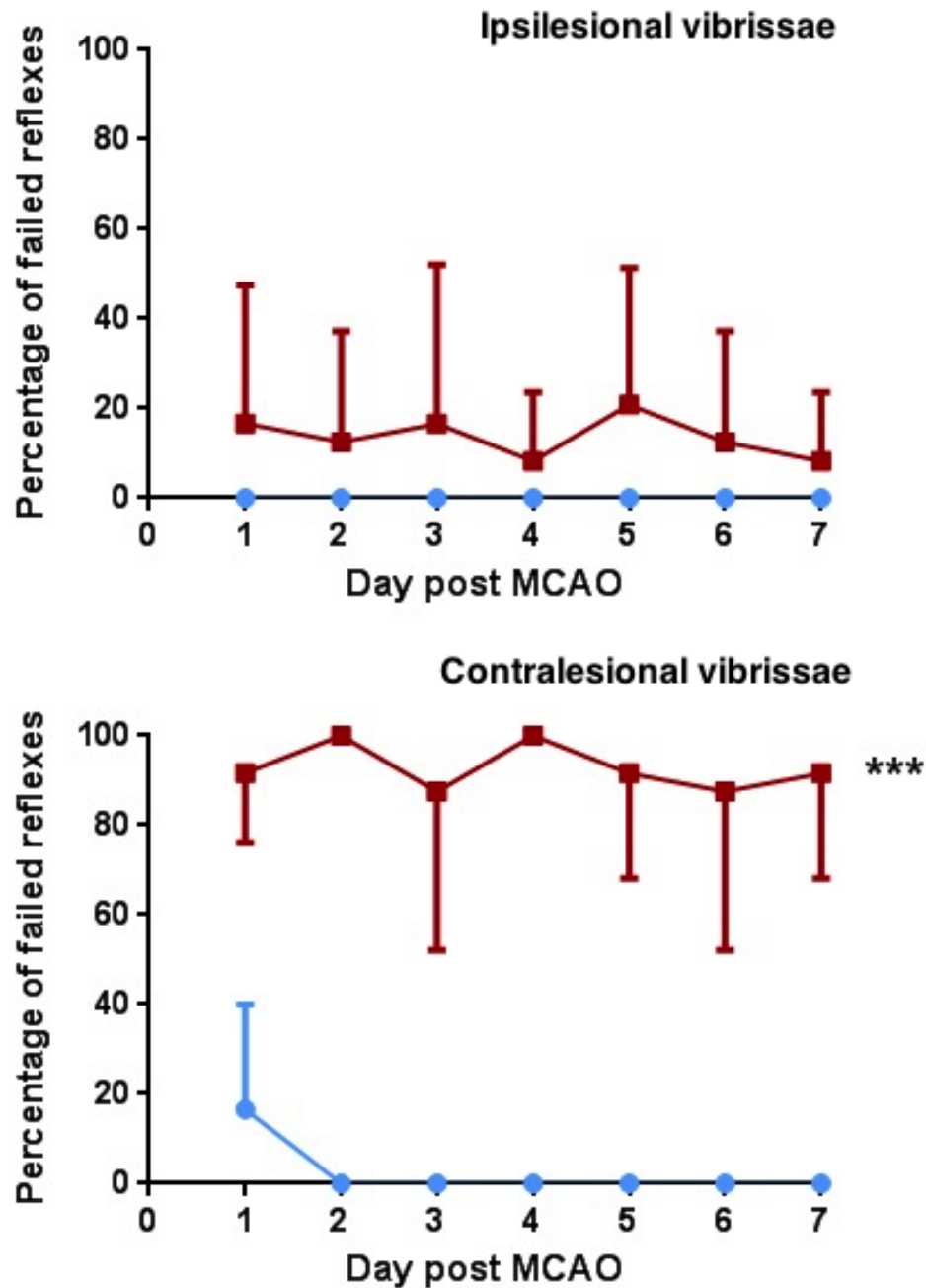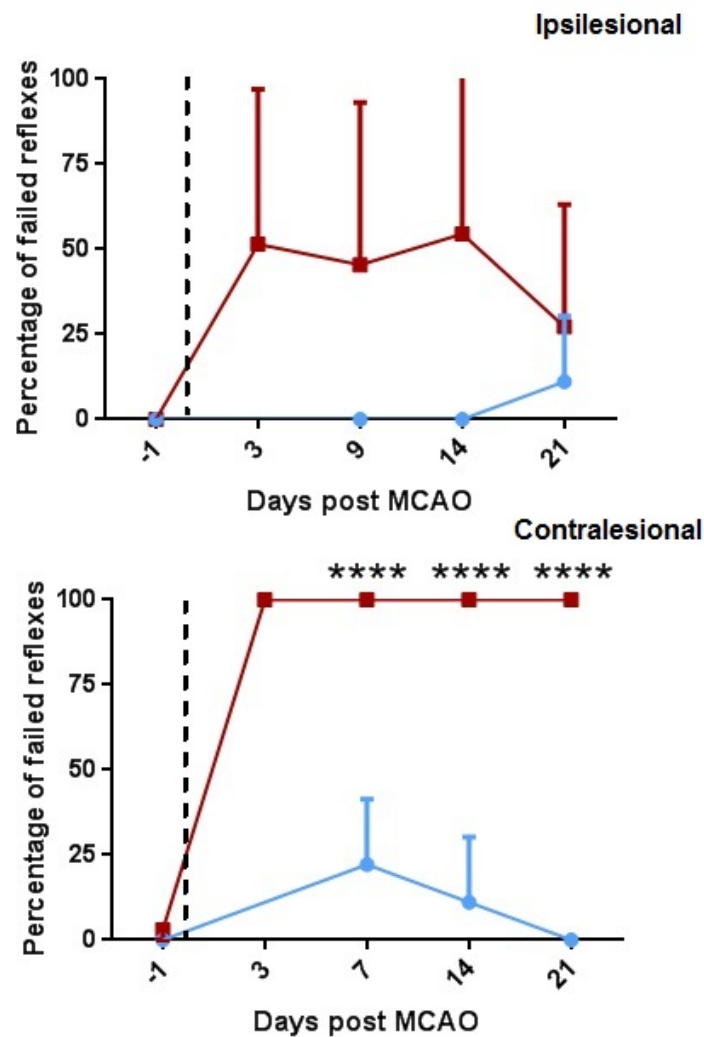
Figure 39: The percentage failed forelimb placing reflexes following upward vibrissae stimulation of the ipsilesional side (left, top) and contralesional side (right bottom) at days −1, 2, 7, 14 and 21 following Sham (blue) or 70min tMCAO (red) procedure. There was no effect of tMCAO on reflex ability on the ispilesional side (ns, $p > 0.05$). 70min tMCAO caused neurological impairment of the contralesional forelimb reflex compared to Sham animals at the same time points (****, $p < 0.0001$) and compared to baseline values; One-way ANOVA with Bonferroni's correction for multiple comparisons. Data presented as mean±SD. Vertical dashed line represents tMCAO at day zero. Sham (n= 3), MCAO (n= 11).

The sensitivity of the bilateral asymmetry test to detect sub-acute to early-chronic dysfunction was trialled days -1, 2, 7, 14 and 21 post-stroke and sham surgery (Figure 40). Sham surgery had no effect on label removal times ($p > 0.05$). The time to remove labels from both contralesional and ipsilesional forepaws was significantly impaired by stroke at Day 2 only ($p < 0.0001$ & $p < 0.01$ respectively) compared to Sham groups and baseline. At all other post-stroke time-points there were no differences in removal times compared to sham-surgery controls and baseline times ($p > 0.05$).
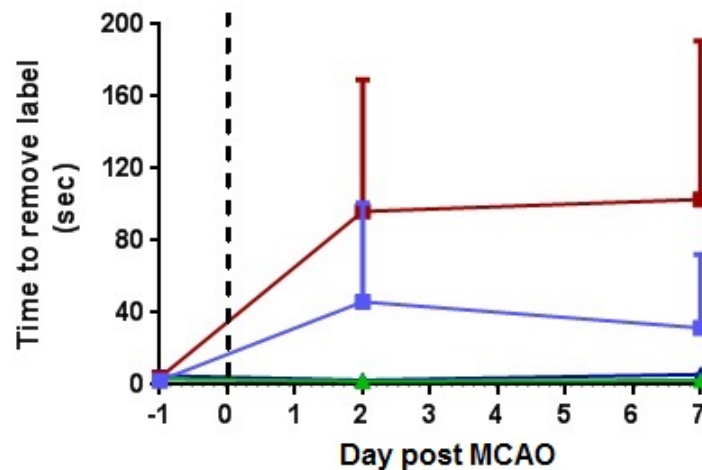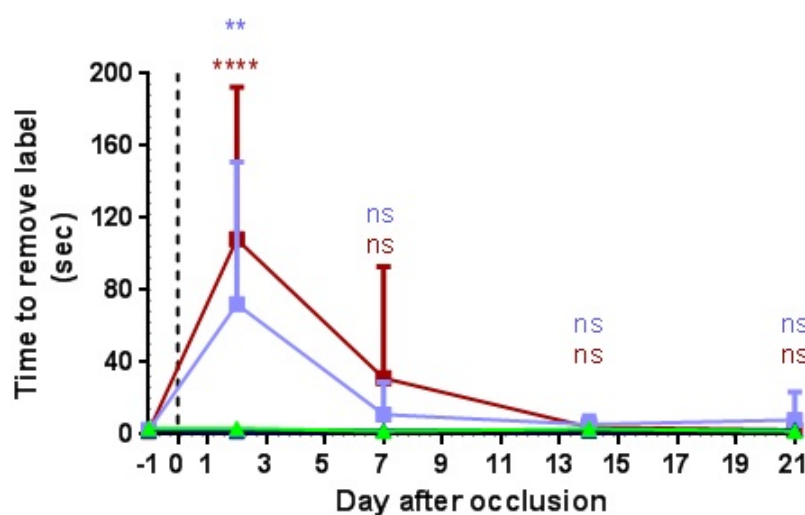

Figure 40: The time taken for removal of the adhesive label from the ipsi- and contra-lesional forepaw in the bilateral asymmetry test at days -1, 2, 7, 14 and 21 post-tMCAO or Sham procedure. 70min tMCAO increased label removal times on both ipsilesional and contralesional forepaws 2 days post-surgery compared to baseline and Sham equivalents (****, $p < 0.0001$; **, $p < 0.01$). There were no differences between baseline or sham removal times at any other timepoints. tMCAO Contralesional (■), tMCAO Ipsilesional (■), Sham Contralesional (▲), Sham Ipsilesional (▲). Data presented as mean±SD. Vertical dashed line represents tMCAO at day zero. Sham (n= 7), tMCAO (n= 16).

There was a loss of sensitivity to detect a deficit in the Corners and Bilateral Asymmetry tests compared to Sham controls by days 21 and 7, respectively. They were henceforth excluded from future use. The Whiskers and medial Adjusting Steps tests continued to show evidence for sensitivity to unilateral sensorimotor dysfunction in the sub-acute to early-chronic post-stroke period. The larger n-numbers, pre-stroke data, and sham controls for all tests increased the statistical power of these results.

The Whiskers and Medial Adjusting steps tests were selected as tests for sensitivity in the long-term chronic post-stroke period up to +12 weeks following MCAO.

3.4.3 *Assessments sensitive up to 12 weeks post-MCAO*

Due to the binary nature of the Whiskers test scoring and risks of handler bias in The Adjusting Steps test; The Staircase test (Montoya et al., 1991) was also trialled for use, due to previous evidence of its sensitivity to long-term disability and limited user bias (Trueman et al., 2011; Farr and Trueman, 2011).

Previous studies found the onset of post-CTX cell improvements from 6-8 weeks following transplant with assessments continuing up to 12 weeks post-transplant (Stroemer et al., 2009; Smith et al., 2012). Therefore finding assessments with continued sensitivity to post-stroke dysfunction up to 3 months following the ischaemic insult was essential before conducting a longitudinal study involving CTX0E03 cell transplantation.

Following a series of failed strokes in earlier pilot work, the MCA occlusion time was increased to 90 min for this study. The

Whiskers and Adjusting Steps tests were carried out 1 week prior to, and weekly after stroke surgery. The Staircase test was carried out 1 week prior, and fortnightly post-stroke surgery.

All infarct volumes in this study were of small volume (23.5 $\pm$ 21mm^3) occupying the caudate putamen only (Figure 41). Possible reasons for this are discussed below.
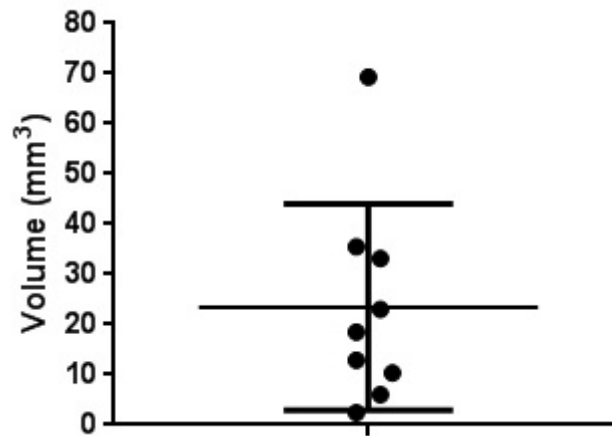
Figure 41: Infarct volumes quantified by manual delineation of T$_2$ hyperintensities from RARE images acquired 4-10 weeks following 90 min MCAO. Due to an administrative error, one animal did not undergo imaging. Mean volume: 23.5 $\pm$ 21mm^3 (mean $\pm$SD).

Following the success of the Adjusting Steps test to demonstrate stroke induced forelimb akinesia up to 21 days following the ischaemic insult, its robustness was assessed over a 12 week period following MCAO/Sham procedure (Figure 42). Sham animals demonstrated no change in right forehand stepping function following surgery. Animals which underwent 90 min left tMCAO demonstrated immediate dysfunction followed by a mean recovery of stepping function to 40% to baseline performance (+56% compared to performance at week 1). Comparisons of mean group AUC values showed that left tMCAO induced persistent deficits in medial stepping actions compared to sham surgery only ($p < 0.0001$), with no effect on lateral stepping ($p > 0.05$), (Figure 42).
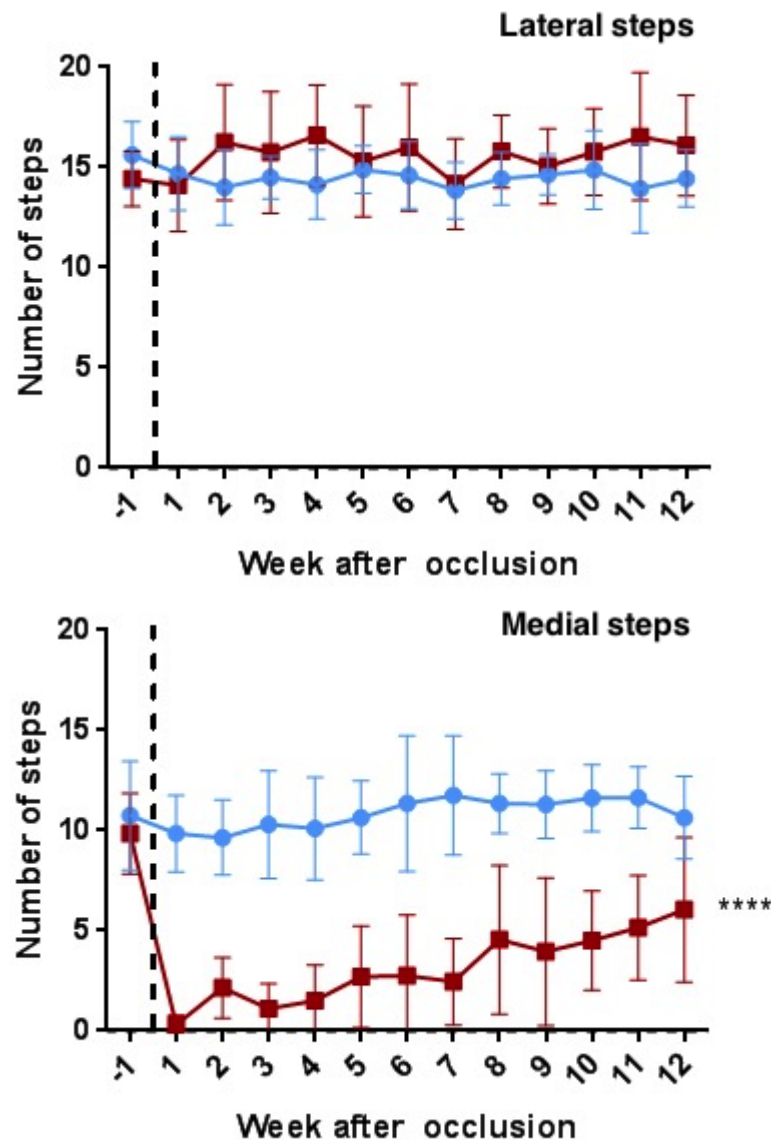
Figure 42: The number of adjusting steps made when the right forelimb is dragged lateral (top) and medial (bottom) from the midline following Sham (●) or 90min left tMCAO procedure (■) measured at -1 week prior to surgery and weekly intervals thereafter. There was no effect of tMCAO on lateral stepping movement ($p > 0.05$). Medial steps were permanently impaired by left tMCAO (****, $p < 0.0001$) with a mean recovery of 40% by week 12. Data presented as mean ±SD, group mean AUC comparisons via unpaired t-test. Sham (n= 10), MCAO (n= 10).

From earlier Whiskers Test experiments it was found that left MCAO will lead to a failed forelimb response to right whisker stimulation. Although shown to be highly sensitive in earlier assessments, we assessed this reflex deficit up to 12 weeks post-MCAO. Left MCAO induced deficit of right vibrissae evoked forelimb raising function was persistent and permanent with very little evidence of spontaneous functional recovery (Figures 43) compared to Sham controls ($p < 0.0001$) even in cases of small infarctions (Figure 41). There was no permanent effect on left forelimb raising ($p < 0.05$).
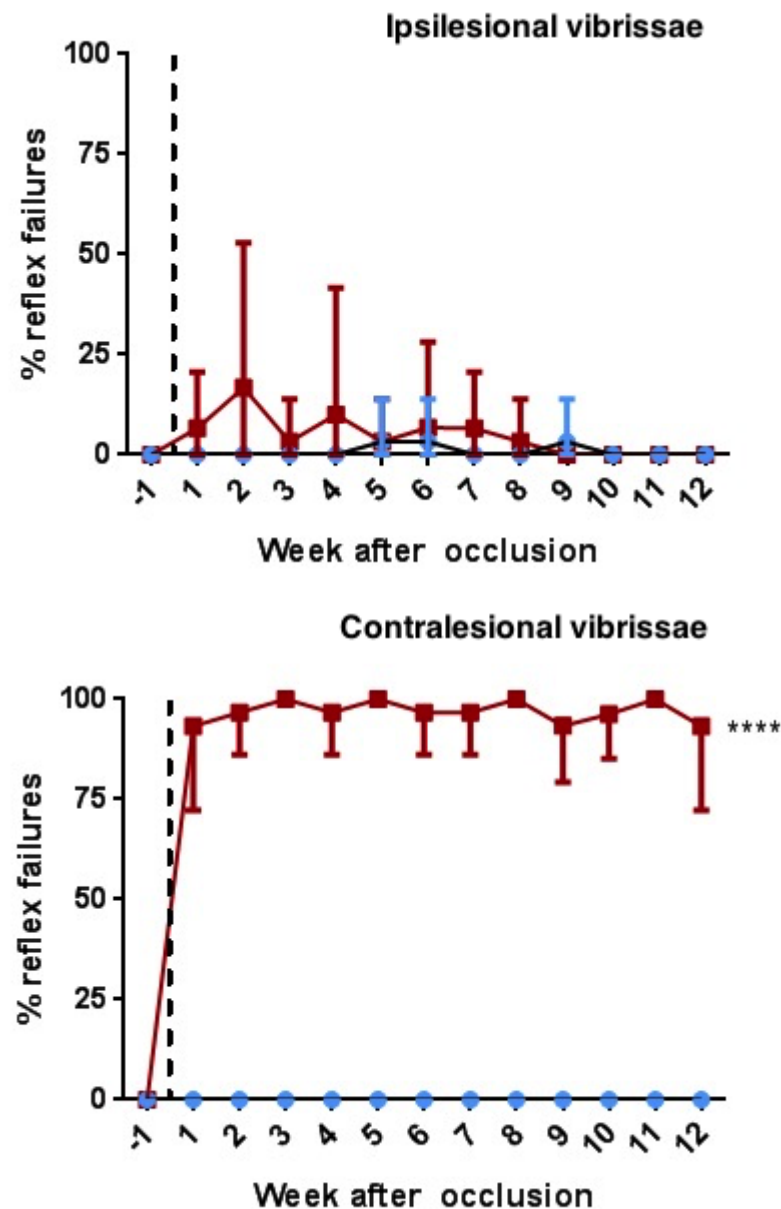
Figure 43: The percentage failed homotopic forelimb placing reflexes following upward vibrissae stimulation of the ipsilesional side (left, top) and contralesional side (right, bottom). Sham (●) or 90min left tMCAO animals (■) were tested at -1 week prior to surgery and fortnightly intervals thereafter. There was no effect of tMCAO on reflex ability on the ipsilesional side ($p > 0.05$). 90min tMCAO caused permanent neurological impairment of the contralesional forelimb reflex compared to Sham animals points with no recovery (****, $p < 0.0001$). Group mean AUC values compared by two-tailed unpaired t-test. Data presented as mean $\pm$SD. Sham (n= 10), MCAO (n= 10).

With the requirement for a robust sensorimotor test with sufficient sensitivity to detect long-term stroke-induced deficits, the Staircase test was piloted over a period of 12 weeks following 90min left tMCAO (Figure 44). Diet-restricted animals were trained to retrieve sugar pellets from a 7-step bilateral staircase (3 per step), accessible with the homotopic forelimb only. Sham animals demonstrated no change in their ability to retrieve pellets using the right forepaw following surgery. Animals which underwent 90 min left tMCAO demonstrated immediate dysfunction followed by a limited recovery to 50% to baseline (20% compared to performance at week +2) in right forelimb pellet retrieval. Long-term sensitivity of the Staircase test was evaluated by calculated individual animal AUC values and comparing group means. Both tests showed that left MCAO induced persistent deficits in right forelimb pellet retrieval compared to sham surgery ($p < 0.0001$).
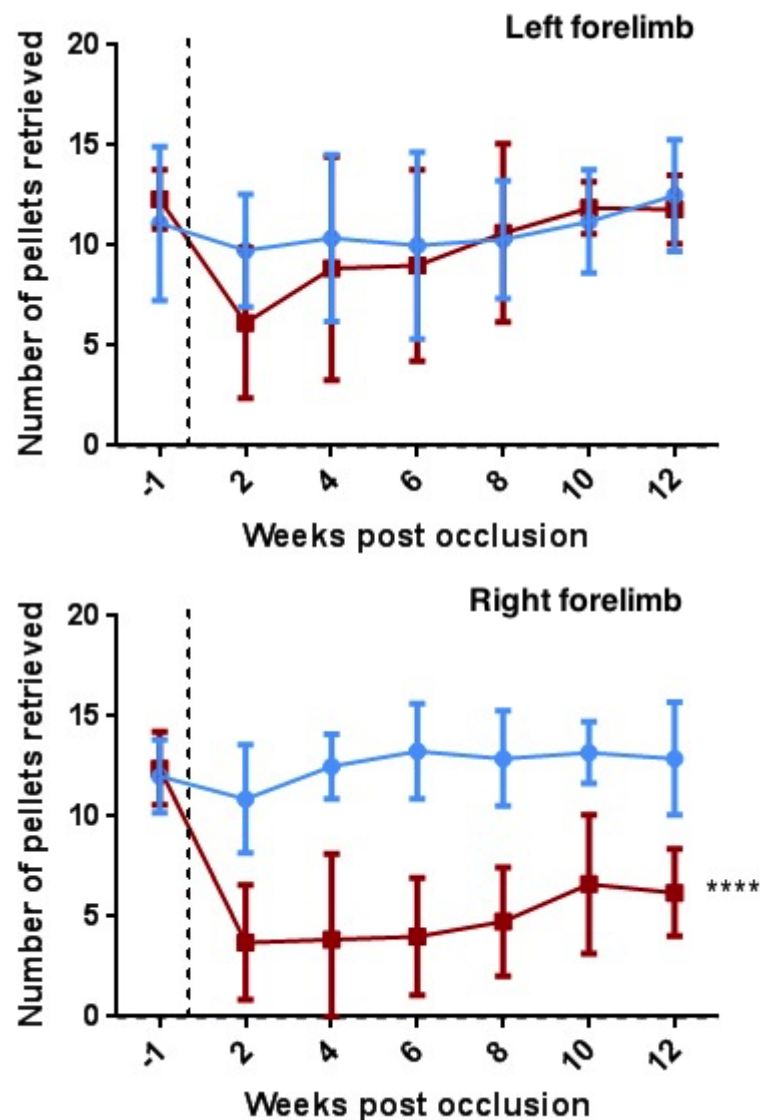
Figure 44: The number of pellets retrieved with the ipsilesional (left, top) and contralesional (right, bottom) forelimbs following Sham (●) or 90min left tMCAO procedure (■) measured at -1 week prior to stroke surgery and fortnightly intervals thereafter. There was no effect of tMCAO on left forelimb retrieval ability ($p > 0.05$). 90min tMCAO caused a sustained deficit in pellet retrieval ability with the right forelimb (****, $p < 0.0001$) with a mean recovery of function of 20% by week 12 compared to week 2. Group mean AUC comparisons via two-tailed unpaired t-test. Data presented as mean ±SD. Sham (n= 10), MCAO (n= 10).

3.5 DISCUSSION

Identification of assessments appropriate for long-term stroke-induced deficits was an essential task before undertaking a longitudinal study with CTX0E03 cell treatment and MRI. Tests had to be able to expose dysfunction consistently, and repeatedly as well as being able to detect any beneficial, or indeed detrimental, effect of the stem cell implantation.

In this chapter, the Bilateral Asymmetry Test (BAT), Corners, Adjusting Steps, Vibrissae evoked forelimb raising, and later the Staircase tests were assessed for sensitivity to tMCAO-induced sensorimotor function. The BAT and Corners test were no longer sensitive to sensorimotor dysfunction by 21 days post-stroke. The remaining tests, as well as the Staircase test, were shown to be suitable up to 84 days post-stroke.

7 & 21 day assessments

The global neurological scoring system, based on Modo et al. (2000) and Bederson et al. (1986), was assessed daily (Figure 29). There was a peak global deficit at Day 2 post-stroke. Scores then plateaued at Days 6 and 7, a finding consistent with previous investigations (Modo et al., 2003). However, such assessments are known to lose sensitivity in the later post-stroke phases (Schaar et al., 2010) as the acute pathology resolves and masking behaviour (in the rat) ensues. Modifications of the scales are present, often with greater maximum scores to limit the ceiling effect (Emma Reid, personal communication). Compared to Sham controls, this battery of tests provides a useful means of acutely determining whether tMCAO has been successful or not and the overall welfare of the animal. Animals with consistently high

impairments are unlikely to survive in the long-term and should be euthanised on welfare grounds.

The Corners test, showed tMCAO-induced left turning bias up to 14 days post-ischaemia (Figures 30 & 36). Bouët et al. (2007) had similar findings in the mouse with a loss in sensitivity by Day 24 compared to the previous assessment at Day 8 in comparison to Sham controls suggesting a role of spontaneous recovery. These results contrast with Shen et al. (2006) and Zhang et al. (2002) who showed turning biases up to 28 and 90 days in the post-stroke rat and mouse respectively. In both of these studies, tMCAO animals had mean infarct volumes of approximately 35% of total brain volume, similar to data presented in this thesis. It is likely that differences in results are due to the subjective nature of the assessment, whereby animal subjects often require encouragement to perform and often adapted to the testing environment and as such was discontinued from further investigations.

The Bilateral Asymmetry test is a popular sensory motor assessment of MCAO-induced dysfunction due to its ability to evaluate tactile extinction and obscuration (Schallert and Whishaw, 1984) with various modifications to assess the magnitude of sensory dysfunction (Soleman et al., 2012). There are multiple ways of analysing the data gathered from such experiments including, the latency between removal and contact time between forepaws, the time taken to remove, and the time taken to detect the label. The test has proven popular in rodent stroke studies (Modo et al., 2000; Virley et al., 2000; Freret et al., 2006; Stroemer et al., 2009; Smith et al., 2012; Soleman et al., 2012). There are however, variations on methodology including the use of a bracelet of adhesive tape around the wrist rather than a circular label on the

dorsal aspect of the paw (Stroemer et al., 2009). This makes the task more challenging for an impaired rodent as well as more time consuming. Such methods are likely to make the BAT more sensitive to dysfunction; often a circular label on the forepaw is relatively easy for an animal to remove. It was found in this study that the bilateral asymmetry test was not sensitive to sensorimotor dysfunction beyond 7 days post-MCAO, contrary to other published research (Figures 34 & 40). The method of MCAO used in the majority of the studies referenced earlier was the ILF method similar to this thesis however Soleman et al. (2012) used the parenchymal endothelin-1 model in aged rats. As well as differences in stimulus used, analysis of the BAT is often up to assessor interpretation and as such leaves it open to bias, especially when the animal makes multiple attempts to remove the label, and animal habituation is likely. The lack of apparent sensitivity of the Bilateral Asymmetry test and high risk of user bias led to the cessation of any further investigation of this test beyond 21 days post-stroke.

Counting the number of adjusted steps has been shown to be a marker of long term dysfunction. Previous studies showed that MCAO leads to a decline in the number of adjusting steps made by the forepaw in a lateral direction to the midline (Vendrame et al., 2004; Mine et al., 2013). In the above experiments, followingt MCAO there was no change in the number of lateral steps after 14 days and in-fact a consistent decrease in the number of medial adjusting steps (Figures 31, 32, 37 & 38).

The Vibrissae evoked forelimb (Whiskers) test is sensitive to striatal, as well as cortical damage (see above). It was found that this assessment is highly sensitive to MCAO-induced damage

with consistent, failed reflexes at all time points for the respective investigations (Figures 33, 39, & 43), even in the case of small infarctions (Figure 41). The noted deficits on the ipsilesional side were unexpected (Figure 39) and were likely to be an effect of the surgery, in rare cases, or complacency due to the animal becoming habituated to the task. When taken out to 12 weeks post-stroke (Figure 43), the variance in atypical ipsilesional forelimb placement declines over a 6 week period, suggesting recovery of impairment. The test has previously been shown to be indicative of sub-cortical damage, and capable of detecting rehabilitation following experimental treatments (Barth and Stanfield, 1990; Schallert et al., 2000; Stroemer et al., 2009). Due to its high sensitivity and the ease of which the test is conducted (with little chance of bias, due to its binary scoring) and its use in previous CTX-cell studies (Stroemer et al., 2009) the test was a good candidate for use in the future longitudinal imaging study.

12 week assessments

In this series of experiments, animals in the tMCAO group had small mean infarcts of 23.5mm^3 involving the striatum only (Figure 41) likely due to partial occlusion of the MCA or high collateral flow. Despite this, sensorimotor deficits were detectable and persistent. This may be due to the susceptibility of white matter to ischaemic damage (Pantoni et al., 1996; Goldberg and Ransom, 2003) and as such, important neuroanatomical white matter structures such as the internal capsule and anterior commissure within the subcortical MCA territory. These neuroanatomical structures as well as regions of the caudate putamen all contain white matter tracts involved in inter- and intra-hemispheric communication and even a small lesion is likely to cause sensorimotor defects. Indeed, it has been shown that small focal lesions induced by

intracranial administration of endothelin-1 can lead to structural and functional deficits (Frost et al., 2006; Lecrux et al., 2008). It is therefore feasible that antero- and retero-grade degradation of sensorimotor pathways can occur without evidence of a T_2 weighted lesion being apparent on imaging.

Compromised dexterity is often the most long-lasting deficit reported by patients (Bouët et al., 2007) so use of a test which assesses dexterity, such as the Staircase test is a clear choice when evaluating the theraputic potential of any treatment. The Staircase test, Adjusting Steps, and whiskers test were all assessed for sensitivity up to 12 weeks post-MCAO.

All three behavioural tests showed adequate sensitivity in detecting long term sensorimotor deficits up to 12 weeks following focal cerebral ischaemia induced via the intraluminal filament model (Figures , 42, 43, & 44). The small volumes of sub-cortical damage lead to partial recovery in staircase and adjusting steps performance by 20% and 56% respectively. However, spontaneous recovery can be expected (Schallert et al., 2000; Rossini et al., 2003; Schaar et al., 2010). In a casual observation, some animals with the larger infarcts often showed the least degree of recovery although this was not always consistent. There was no overall regain of forelimb placing function following vibrissae stimulation.

The results indicate that these three functional assessments are suitable for investigating recovery of function following intracerebral implantation of CTX0E03 cells. Functional recovery has previously been shown in the vibrissae evoked forelimb test at 12 weeks following implantation of CTX cells (Stroemer et al., 2009). The other two tests have previously been published in investiga-

tions of cellular therapeutics for stroke and other neurological disorders (Olsson et al., 1995; Döbrössy and Dunnett, 2005) but not for the CTX line for treatment of chronic ischaemic stroke. The hypothesis to be tested is that the cell treatment group of animals will show partial recovery in performance over a similar time course to that of previous studies; approximately from 5-8 weeks following transplantation (Stroemer et al., 2009; Smith et al., 2012). By using three sensorimotor tests in combination with multi-modal MRI, effects of the stroke and/or stem cell therapeutic have a good chance of being identified.

ESTABLISHING NON-INVASIVE PHYSIOLOGICAL MONITORING FOR FUNCTIONAL IMAGING UNDER MEDETOMIDINE SEDATION WITH ISOFLURANE

4.1 INTRODUCTION

Functional imaging studies are often met with various technical and physiological challenges (see Introduction Chapter). Due to the sensitivity of the BOLD signal to arterial pCO_2 and other physiological variables (Logothetis et al., 1999), it was essential that all physiological variables were monitored and kept within range to ensure robust, and reliable data were acquired. It was therefore necessary that before undertaking a longitudinal functional imaging study, confidence was needed that systemic physiological variables, most crucially, arterial pCO_2, could be monitored and adjusted repeatedly and non-invasively. Previous studies have used urethane, ketamine-xylazine mixtures or α-chloralose with or without conjunctive administration of pancuronium bromide for the detection of resting-state or stimulus specific BOLD signal changes (Williams et al., 2010). However, these compounds are unsuitable for serial imaging studies due to the requirement for intravenous delivery, muscle paralysis, and the risk of seizures and generally poor, or no recovery (Lukasik and Gillies, 2003).

The longitudinal nature of the planned CTX-cell study (Chapter 5) required methods to non-invasively monitor physiological parameters. The aims of the experiments outlined in this chapter were therefore to develop and optimise an anaesthesia protocol, using the veterinary pharamceutical medetomidine, for *in vivo* functional imaging based on well established protocols by Weber et al. (2006) and Lu et al. (2012). There was also an aim to establish non-invasive monitoring of end-tidal (ET)-CO_2, heart rate, and SpO_2 whilst maintaining appropriate physiological control during mechanical ventilation. Both of these were to ensure the reliable acquisition of resting-state fMRI data in future studies.

An End Tidal (ET) Capnograph and an MRI compatible pulse oximeter (Nonin) were investigated as non-invasive means of evaluating ET CO_2, heart rate, and SpO_2 respectively. Comparisons were made between conventional invasive measurements and non-invasive ones made with the trial equipment.

4.1.1   *Physiology and Pharmacology of Medetomidine*

The alpha-2 adrenoreceptor ($\alpha 2$ receptors) agonist, medetomidine, is a well documented drug of choice for *in vivo* functional imaging (Weber et al., 2006; Lu et al., 2012). An understanding of its mechanism of action provides an insight into its suitability and an appreciation for the side-effects which accompany its use.

Alpha-2 adrenoreceptors in the central nervous system

$\alpha 2$ adreoreceptors are a $G_i/_o$ subtype of the adrenergic G-protein coupled receptors (GPCR), (Bylund, 1988; Alexander et al., 2008), whose primary mechanism of action is via the inhibition of adenylyl cyclase with subsequent reduction in cAMP levels within cells.

In situ hybridisation studies have identified the location of all three of the $\alpha 2$ receptor sub-types (A, B and C) in various structures within the brain (Scheinin et al., 1994), making them clear targets of interest for neuropharmacological intervention. In the study mentioned above, $\alpha 2$A receptors were found to be highly localised to the locus coeruleus (LC) in the hindbrain. The LC contains the highest density of noradrenergic neurones in the brain with projections throughout the CNS. Its primary purpose is the promotion of wakefulness via projections to other nuclei responsible for alertness (Samuels and Szabadi, 2008), inhibition of regions involved in REM sleep (Hou et al., 2002), and the cerebral cortex (Jones and Yang, 1985). The release of noradrenaline from LC neurones is co-regulated with μ-opioid receptors (Nakai et al., 2002). It is therefore unsurprising that the LC has been a region of interest for pharmacological intervention either via targeting neuronal autoreceptors (surface receptors of the transmitting neuron) altering synaptic behaviour, or by acting on LC target neurones.

Effects of Alpha-2A agonism & the Requirement for Physiological Control under Medetomidine Sedation

Agonism of $\alpha 2$ receptors with clonidine or medetomidine generates sedative effects (Buerkle and Yaksh, 1998; Savola et al., 1986; Hedenqvist et al., 2000). Although not often used in human medicine, medetomidine and its enantiomer, dexmedetomidine, are frequently used as pre-operative sedatives in veterinary practice and pre-clinical research (Sinclair, 2003). Hypotension is a marked effect of centrally acting $\alpha 2$ agoinsts with subcutaneous, intravenous or intramuscular administration demonstrating respiratory depression and bradycardia in out-bred strains of rats. The hypotensive, respiratory, and bradycardic effects of alpha-2 agonists *in vivo* require careful monitoring so as to ensure phys-

iological parameters do not deviate towards deleterious ranges, even under appropriate dosing. This is of particular importance for blood pressure, and arterial pCO$_2$. Cerebral vasculature has a limited capacity for autoregulation out with a systemic blood pressure range of 70-160 mmHg (Hernández et al., 1978) and CO$_2$ has a pronounced vasodilatory effect on arterioles at partial pressures above 45 mmHg (Kety and Schmidt, 1948). There is no evidence of medetomidine causing marked changes to the BOLD signal related to neural activity compared to α-chloralose or ketamine-xylazine mixtures in the default mode or sensorimotor networks (Magnuson et al., 2010; Lu et al., 2012). However, as the BOLD signal is highly sensitive it was important to develop an optimal range of parameters, under a suitable means of ventilation, by which all relevant physiological variables were monitored and controlled within adequate ranges.

4.1.2 *End Tidal Capnography*

Carbon dioxide, a potent cerebral vasodilator, is an important variable to maintain within a range of 35-45mmHg in arterial blood. Arterial blood gas (ABG) measurements for arterial partial pressures of CO$_2$ (p$_a$CO$_2$) are accurate but invasive and discrete. Due to limitations in the amount of blood that can be withdrawn for longitudinal studies, capnography is a suitable alternative as it is a non-invasive and continuous means of ascertaining physiological p$_a$CO$_2$.

The structure of carbon dioxide lends itself to optical measurements in the infrared (IR) spectrum with an absorption at $4.3\mu m$. Therefore, the concentration of carbon dioxide in a sample of gas can be calculated by comparing the IR intensity prior to, and
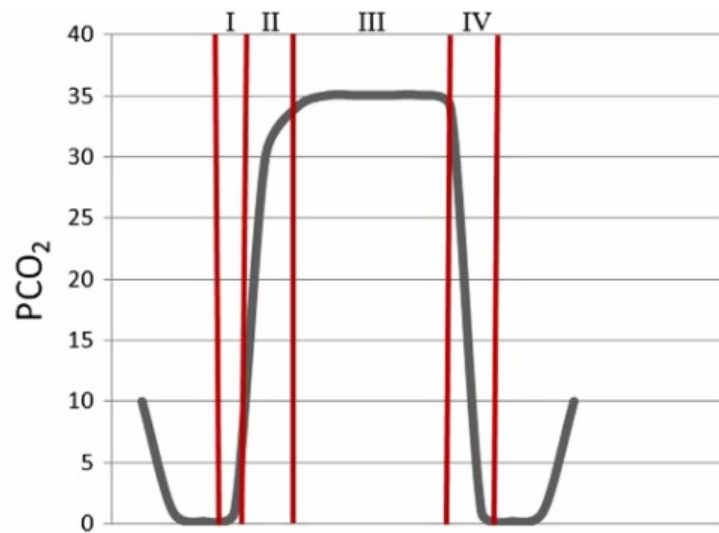
Figure 45: Model capnogram from (Thawley and Waddell, 2013) in normal physiological scenarios divided into four phases. I, exhalation of dead space gas; II, exhalation of a mixture of dead space and alveolar gases; III, exhalation of alveolar gases (the end of which is the End Tidal value); and IV, inspiration. $P_a CO_2$ in mmHg.

following passage through the sample. CO_2 is typically measured as % or mmHg. The standard waveform for a normal capnogram is detailed in Figure 45.

There are two main methods of capnography for artificially ventilated animals. These are defined in terms of the position of the sensor to the ventilation pathway: Side-stream, and main-stream. A main-stream device measures pCO_2 directly from the airway with no time delay. Side-stream analysis samples expired air from the ventilation tubing, causing a time delay with peak End-tidal CO_2 (ET-CO_2) readings out of phase with the breathing rate. The time delay can be exacerbated by the length of the sampling line.

4.2 METHODS

4.2.1 *Experimental animals*

Naïve, male Sprague-Dawley rats weighing 315-420g were used in this pilot study. Experiments were carried out with the animal in the MRI cradle on the bench-top, simulating the scenario of the animal being in the scanner bore. All experiments were non-recovery.

4.2.2 *Anaesthesia protocol*

The medetomidine administration protocol published in Lu et al. (2012), in turn based on Weber et al. (2006), was chosen as it was shown to be robust and reproducible.

Rats were initially anaesthetised according to the standard protocol described in Section 2.2.3 with the exception of using medical air instead of nitrous oxide. The animals were then intubated and cannulated (Sections 2.3.3 and 2.3.2), and transferred to the cradle and maintained under 2% isoflurane by mechanical ventilation at 1 l/min of medical air, supplemented with O_2 at 24-27% of inhalation volume measured using an oxygen sensor (Viamed, UK).

Stock solutions of medetomidine (Domitor, Orion Pharma) and reversal drug, atipamezole (Antisedan, Orion Pharma), were supplied at 1 mg/ml and 5 mg/ml respectively and stored at room temperature. The animals were weighed and aliquots of the stock solutions were diluted in saline to 100 μg/kg/ml and at 100

μg/kg, respectively.

A syringe containing 10 ml of the medetomdine solution was mounted onto a syringe pump (Fresenius Kabi, Injectomat MC Agilia®) and connected to a cannula inserted into the subcutaneous space of the shaved flank. A 0.5 ml bolus dose of medetomidine was administered subcutaneously and isoflurane levels gradually reduced to, and maintained at 1%. 15 minutes following the bolus, the subcutaneous infusion was started at 1 ml/hour.

Recovery from sedation

Whilst still on the ventilator, medetomidine sedation was reversed by subcutaneous injection of 100 μg/kg atipamezole. Once signs of conciousness began to appear (after 3-5min), the intubation tube was removed and the animal recovered in individual housing cages overnight before being returned to group housing.

4.2.3   *Ventilation and side-stream capnography*

The animals required artificial ventilation as the medetomidine administration at the doses described suppressed spontaneous breathing in our Sprague-Dawley rats.

Side stream sampling of a closed ventilation system introduces challenges in maintaining adequate ventilation due to the relatively large volumes sampled from the circuit compared to the lung volume of the rat (minute volume 27ml/min/100g (Strohl et al., 1997)) which reduces the ventilation pressure. As such, two different ventilators were tested with an aim to determine which one could accommodate the challenges that side-stream sampling

brings.

Two capnographs were also assessed (details in Table 3 and below). With each ventilator set up, end-tidal gases were sampled from the expiration line, with an example shown in Figure 46.

1. Ugo-Basile Volume Cycling Ventilator (Harvard Apparatus): A prescribed tidal volume is delivered via a cylinder-piston assembly with the motor speed determining respiration rate.

2. SAR-830 Dual Volume/Pressure Cycling Ventilator (CWE Instruments): Pressure driven ventilators offer more precise control of *in vivo* ventilation by offering management of the specified inspiration pressure (cm H_2O), flow rate (cc/min), inspiration time (T_i, ms) and rate (bpm). The ventilator will inspire to a specific pressure at a specified flow and rate; the latter is overridden if T_i is greater than the reciprocal of the rate. Tidal volume can be calculated as the product of flow and inspiration time or conversely, the required flow rate can be calculated as twice the product of the tidal volume and respiration rate. Expiration depends on the compliance of the lungs.

Parameter	CAPSTAR-100	microCAPSTAR
Measurement range (% CO_2):	$0 - 10$	$0 - 9.9$
Accuracy (mmHg):	*n/a*	1.1
Response Time (ms at 50ml/min):	130	150
Sample Flow Rate Range (ml/min):	$10 - 50$	$5 - 20$

Table 3: Specifications for the CAPSTAR-100 and microCAPSTAR (both CWE Instruments).
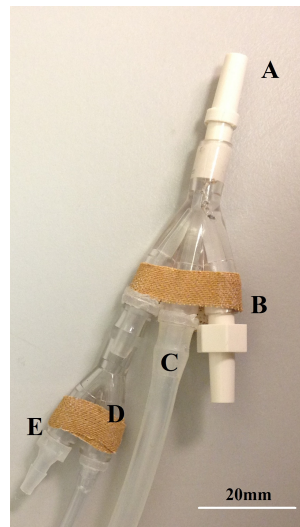
Figure 46: Photograph of the Three-way Luer connector (internal diameter 4.1mm) used for artificial ventilation and end-tidal sampling when ventilating with the SAR-830 Pressure cycling system. (A) Male Luer connection to the intubation tube; (B) inspiration line; (C) connector for airway pressure sensor; (D) Luer-Y connector with capnograph sampling line attached; (E) expiration line. The tubing for volume-cycling ventilation had a similar set up with the exception of the use of a two-way Luer connector.

4.2.4 *Pulse Oximetry*

Once the animal was secured within the cradle, the pulse oximeter was attached to the hindpaw of the non-cannulated limb and secured using tape (Leukoplast).

4.2.5 *Data analysis*

This study involved the sampling of physiological data at various time points both within, and between groups. The data below are summarised in two parts:

  i The group means of the average physiological variable for each animal were compared to assess whether there were any large differences between ventilation-capnograph paradigms.

 ii To determine which paradigm ensured the greatest stability of each variable over the duration of experiment, the respective standard deviations of each experimental variable were compared by one-way ANOVA, with Tukey's test for multiple comparisons.

To assess how well the End-tidal CO_2 measurements agreed with the arterial blood gas values, the data were assessed by the Bland-Altman method (Bland and Altman, 1999) corrected for multiple comparisons within each individual (Bland and Altman, 2007). The term *'bias'* is used to define the mean difference between the two measurement methods, which has its own variance. Ninety-five per cent of the expected differences between measurements can be expected to be found within the 95% *Limits of agreement*. It is these limits which are corrected for multiple comparisons within individuals by multiplying the variance by a factor which

reflects the number of observations made (further details are in the aforementioned reference).

The above method was chosen as it is inappropriate to assess agreement between measurements using a correlation coeffiecient as such values signify the strength of a relationship between two independent variables, not their agreement. Correlation coefficients also have a high incidence of false positives and depend on the range of the data (see Bland and Altman (1986)). End-tidal carbon dioxide measurements were expected to be slightly lower than arterial gas measurements due to alveolar dead space, as such, one will expect a small bias which represents this physiological constraint.

Statistical advice for this study was sought from Dr J. McClure, Institute of Cardiovascular and Medical Sciences, University of Glasgow.

4.3 RESULTS

Three experimental set-ups were tested:

1. Volume-cycling ventilator with CAPSTAR-100 (n=4)

2. Pressure-cycling ventilator with CAPSTAR-100, (n=3)

3. Volume-cycling ventilator with Microcapstar, (n=6)

The mean durations of these experiments were 191, 168, and 189 minutes for each experimental group, respectively.

During the experimental period, changes of the tidal volumes and percentages of inspired oxygen delivered to each animal to maintain p_aCO_2 and pO_2 within normal ranges ($35 - 45$mmHg), and (min. 80mmHg) respectively. The accuracy and effect of side stream-sampling of expired air by capnographs on arterial blood gases were investigated.

4.3.1 *The effect of medetomidine on heart rate and measurement accuracy of the pulse oximeter.*

Heart rates were monitored via the femoral artery cannula transducer (Section 2.3.3) and the pulse oximeter attached on the opposite foot (Section 4.2.4).

The effect of medetomidine bolus on heart rate

Medetomidine is known to induce bradycardia. This was confirmed in 7 animals with measurements of heart rate before the bolus (2.5% isoflurane) and after the start of the infusion (1% isoflurane, 15 minutes later) via the arterial cannula. A subcutaneous bolus of 50μg/kg medetomidine caused a mean reduction

in heart rate of 71 ± 41bpm (SD), (Figure 47).
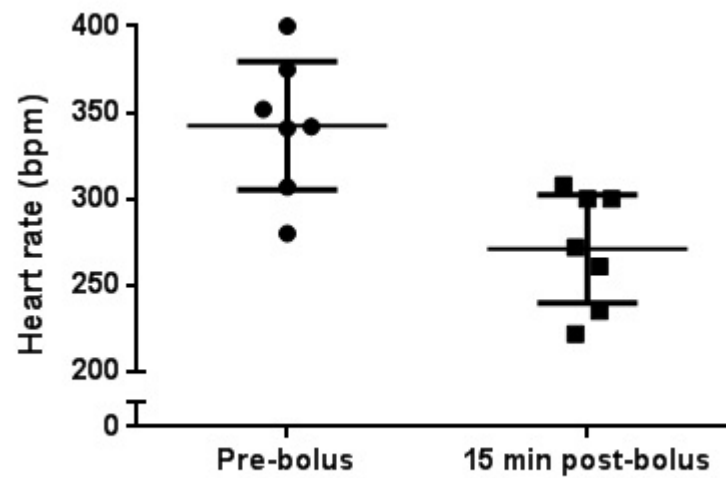
Figure 47: Heart rates recorded via femoral artery cannula prior to subcutaneous administration of medetomidine bolus ($50\mu g/kg$) and 15 min later when the subcutaneous infusion ($100\mu g/kg$) was initiated.

Agreement between Pulse Oximeter and Arterial line on heart rate measurement

The use of a non-invasive MRI compatible pulse oximeter capable of accurate heart rate measurements is obvious benefit for longitudinal functional imaging studies. Simultaneous measurements of heart rate from the arterial line transducer and the pulse oximeter were compared.

As shown in Figure 48, the low bias and small limits of agreement between measurements satisfied us that linear regression with 95% prediction intervals between the two would confirm the ability of the pulse oximeter to accurately measure heart rate.
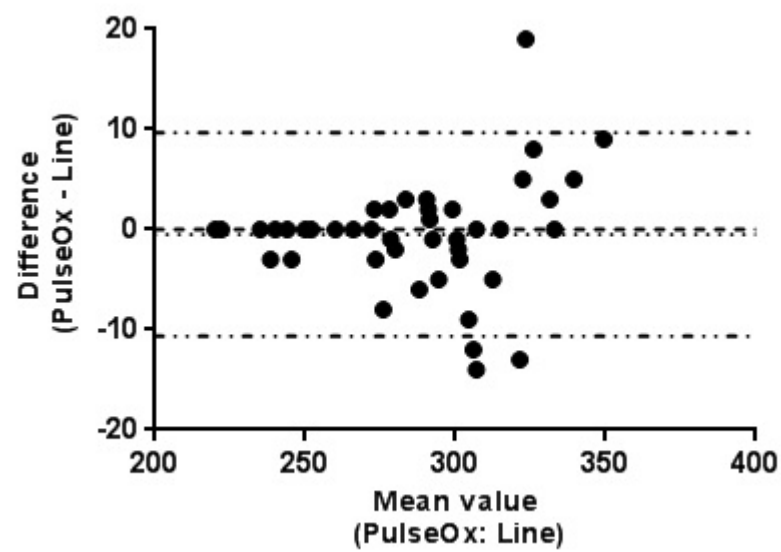
Figure 48: Bland-Altman plot of the bias and 95% limits of agreement between simultaneous measurements of heart rate from a femoral arterial line and pulse oximeter attached to the contralateral hindpaw. Bias = -0.48 and 95% Limits of agreement (corrected) = -10.64 to 9.68

4.3.2   *Arterial pO$_2$ changes and agreement between Arterial O$_2$ saturation and SpO$_2$*

Since the BOLD signal depends on deoxyhaemoglobin levels, arterial partial pressures of oxygen are another variable essential to maintain during functional imaging. Arterial oxygen pressures must be maintained to at least 80 mmHg to avoid hypoxia. Hyperoxia does not perturb the BOLD signal until pressures of over 200 mmHg are reached, where paramagnetic free oxygen then begins to dissolve in blood plasma (Tuunanen and Kauppinen, 2005).

Arterial oxygen levels in artificially ventilated animals depend on the levels of oxygen in the inhaled gases as well as on tidal volumes (Figures 49 50, 51& 62, and Table 4).
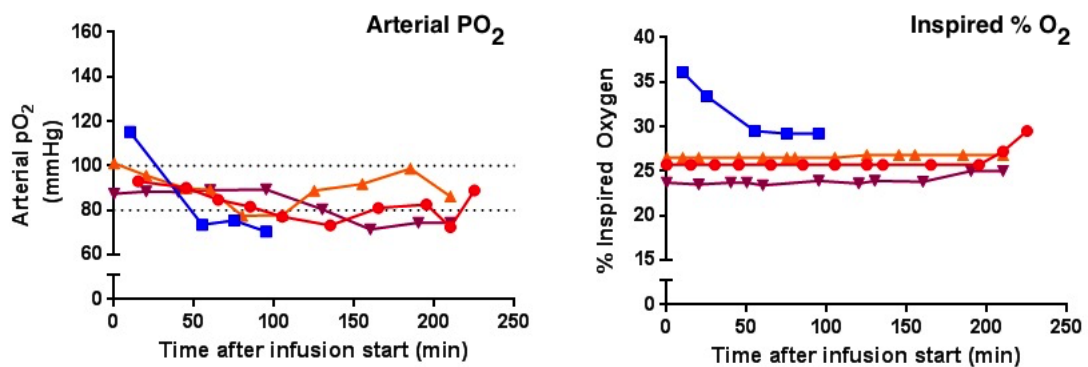
Figure 49: Changes in Arterial pO$_2$ with respect to inspired O$_2$ (right) while ventilated using the Volume-cycling ventilator with CAPSTAR-100 sampling. Animal 1(●); Animal 2 (■); Animal 3(▲); Animal 4(▼).
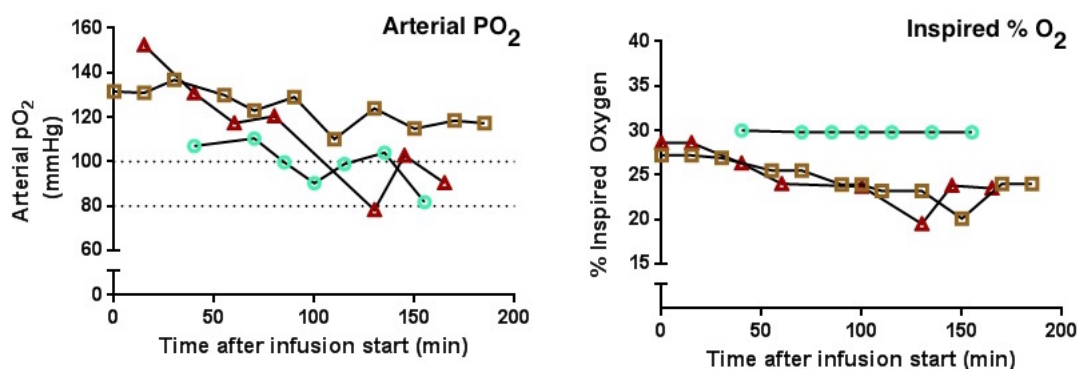
Figure 50: Changes in Arterial pO$_2$ with respect to inspired O$_2$ (right) while ventilated with the Pressure-cycling ventilator with CAPSTAR-100 sampling. Animal 7($\circ$); Animal 8 ($\square$); Animal 9($\triangle$).
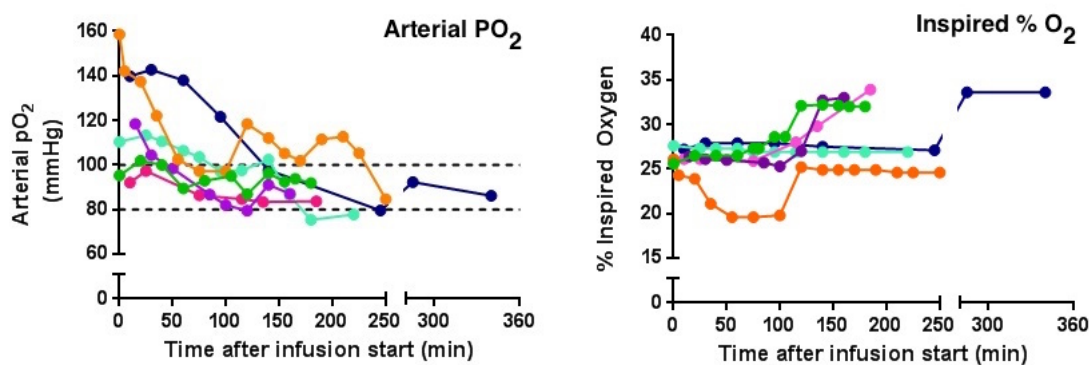
Figure 51: Changes in Arterial pO$_2$ with respect to inspired O$_2$ (right) while ventilated using the Volume-cycling ventilator with Microcapstar ET-CO$_2$ sampling. Animal 12 ($\bullet$); Animal 13 ($\bullet$); Animal 14 ($\bullet$); Animal 15 ($\bullet$); Animal 16 ($\bullet$); Animal 17 ($\bullet$).

Mean pO_2 levels were maintained above 80mmHg for all experiments (Figure 52). However, animals in the Volume-CAPSTAR group (Figure 49) were frequently mildly hypoxic even with increases in tidal volume. The percentage of inspired oxygen for each group are summarised in Table 4.

Variable	Vol-CAP	Press-CAP	Vol-microCAP
Inspired O_2 (%)	27.0 ± 3.2	26.4 ± 3.0	27.5 ± 2.1
Tidal Volume (ml)	6.8 ± 1.1	7.2 ± 2.7	5.3 ± 0.5

Table 4: Ventilation parameters. Vol-CAP (n=4), Press-CAP (n=3), Vol-microCAP (n=6). Data presented as mean±SD.

In the experiments with the pressure cycled ventilator and the Microcapstar (Figures 50 & 51), all animals began the experiments with pO_2 levels greater than 90mmHg despite similar levels of inhaled oxygen. The pressure-ventilated paradigm caused higher mean pO_2 than the volume driven experiments with the CAPSTAR-100 too. (Figure 52). The partial pressures of oxygen throughout these experiments were all equally variable (Figure 53).
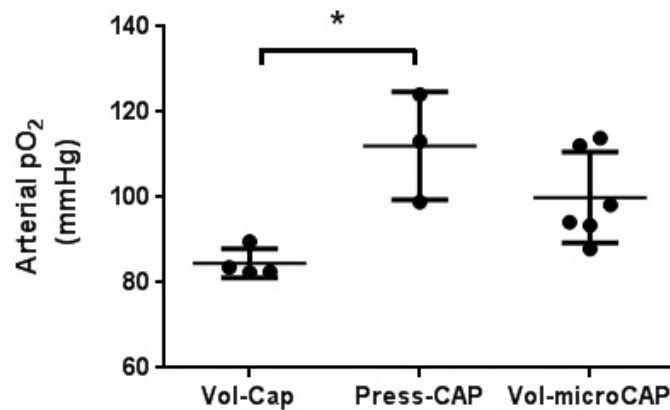
Figure 52: Summary graph of the Mean arterial pO_2 over the duration of the experiment for each animal. Animals in the Volume-CAPSTAR100 group had, on average, lower arterial pO_2 compared to the Pressure-cycling group, $p < 0.05$ (One-way ANOVA with Tukey's multiple comparisons test). Data presented as mean$\pm$SD.

Figure 53: Standard deviations of each animal's pO_2 throughout the course of their respective experiment. The SD provides an indication of the variability of the pO_2 in response to changes in inspired oxygen. No statistically significant differences were identified between groups (One-way ANOVA). Data presented as mean±SD.
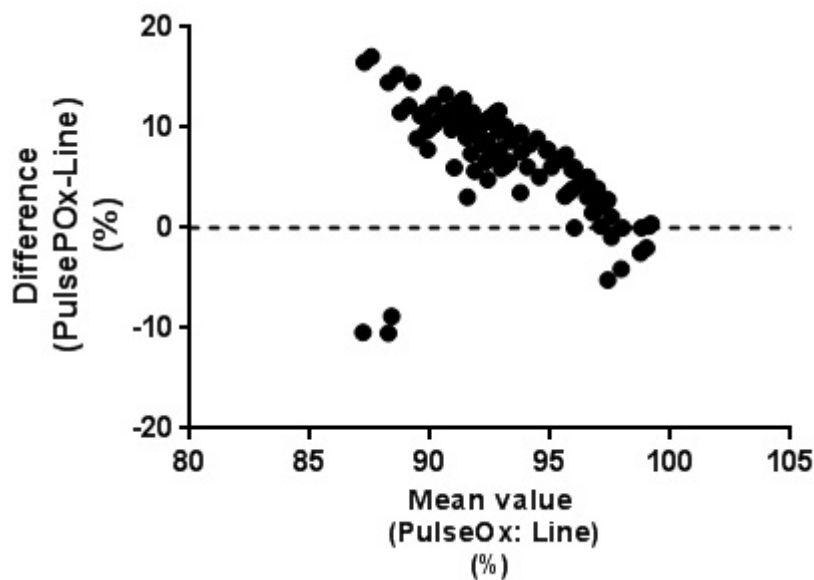
Figure 54: Bland-Altman plot assessing the agreement between blood oxygen saturation measurements by non-invasive pulse oximeter measurements and from arterial blood sampling from a femoral artery cannula.

From Figure 54 it can be seen that the differences between oxygen saturation measurement values vary according to the size of the measurement, shown by the downward slope in the data: in other words, the variance in the measurements increases as measured values decrease. This would not be resolved by a logarithmic transformation of the data. Bland and Altman (1999) recommended "modelling the variability in the SD of the [differences] ... based on absolute residuals from a fitted regression line". This means that the variability of the variances in measurements are fitted to a regression line i.e. adjusting for the differences between measurements, to establish a more robust measure of agreement.

The differences (D) between measurements were regressed against the average (A) values of O_2 saturation (Equation 4). To calculate the limits of agreement of this relationship, ie, the variation about the line of best fit, the residuals (R) of the differences are then regressed against the average values (Equation 5). If the relationship between R and A is not significant, the standard deviation of the adjusted differences is the SD of the residuals. If the relationship is significant, the SD of the residuals is multiplied by $\sqrt{\frac{\pi}{2}}$ and Equations 4 and 5 combined.

$$D = b_0 + b_1 A \tag{4}$$

$$R = c_0 + c_1 A \tag{5}$$

In the case of Figure 54, the resultant regression based on Equation 4 was:

$$D = 98.2 - 0.98A \tag{6}$$

The residuals of Equation 6 were not significantly different from the average measurements. As such, the 95% limits of agreement for this regression were:

$$98.2 - 0.98A \pm 1.96 \times 4.15 \tag{7}$$

With this 95% agreement limit and a slope of approximately 1, inference can be made of good agreement between measurement options. As such, it was determined that the pulse oximeter provided accurate measurements of blood oxygen saturation.

4.3.3   *Requirements to modify ventilation parameters to maintain p_aCO_2*

Arterial carbon dioxide levels are a fundamental variable in cerebral blood flow investigations due to its potent effect on cerebral blood flow. Tidal volumes were adjusted throughout the experimental periods with an aim to achieve normal, stable physiological variables. Within-group changes are illustrated in Figures 56, 57, 58, and summarised in Figures 59, 60, 61, and 62. Group tidal volumes are summarised in Table 4.

Experiments were conducted using the conventional volume cycling ventilator with End-Tidal sampling with the CAPSTAR-100, (Figure 56). All animals were acutely hypercapnic at the start of the experiment with ventilation volumes gradually increased to compensate. Volume changes were made slowly to avoid over-inflation and damage of the pleural tissues. The return to normocapnia proved challenging due to the side-stream sampling by the capnograph, taking up to 120 min with tidal volumes of up to 8.5ml required. The reduction in ventilation volume and subsequent hypercapnia in Animal 1 was intentional in order to acquire resting-state data under hypercapnia. The experiment involving Animal 2 was terminated because the animal became intolerant to the anaesthesia protocol.

CAPSTAR-100 side-stream sampling with pressure cycling ventilation was evaluated to ascertain whether delivery at constant peak inspiratory pressure would compensate for pressure loss caused by the capnograph. However, responses to ventilation were highly variable, (Figure 57). More frequent changes in tidal volume were required to keep arterial blood gases within the normal range compared to the constant volume ventilator (Figure

62). This could have been due to our relative inexperience in using this particular set-up.

The Microcapstar samples at smaller volumes compared to the CAPSTAR-100 and was evaluated in 6 animals using the volume-cycling ventilator. Any requirements to change tidal volumes were far lower than with the other set-ups (Figures 58 & 62). This did not limit difficulties in maintaining normocapnia. Mean arterial pCO_2 values (Figure 59) and mean tidal volumes (Figure 60) were varied in each experiment. No differences were found in the variability of p_aCO_2 between the three experimental paradigms (Figure 61) despite there being differences in the the tidal volume variances (Figure 62).

4.3.4 *Comparison of End-tidal CO_2 measurements in relation to arterial pCO_2*

As described in Section 4.3.3 above, it was necessary to see whether we could reliably measure end-tidal CO_2 using side-steam capnography as a non-invasive means of ascertaining pCO_2. At times of arterial blood sampling, we simultaneously recorded the ET-CO_2 for comparison. It is known that the end-tidal pCO_2 is 3-5mmHg lower than the arterial pCO_2 due to the alveolar dead-space (Larson and Severinghause, 1962), so we expected a similar bias in our measurements. The results of these comparisons are summarised in Table 5 with individual group results described in Figure 55.

All experiments showed substantial bias with both capnograph set-ups consistently under-reading ET-CO_2. Although the micro-CAPSTAR showed the lowest measurement bias compared to the

arterial pCO_2, it had the widest limits of agreement (Figure 55C). As Figure 55B shows, using a Pressure-cycling ventilation unit caused a smaller bias in ET-CO_2 readings with the CAPSTAR-100 compared to the conventional ventilator (Figure 55A), however as discussed above (Figures 58 & 60) we experienced far greater challenges in delivering a consistent tidal volume (Figure 62) to maintain a normal range of arterial pCO_2 with equal variance as the other experimental paradigms (Figure 61).

Variable	Bias $\pm$ SD	95% Limits of agreement (corrected)
Vol-CAP	38.00 ± 7.40	$21.9 - 54.0$
Press-CAP	18.05 ± 4.01	$10.15 - 25.95$
Vol-microCAP	14.24 ± 12.35	$-11.20 - 39.68$

Table 5: Summary of the Bias and limits of agreement for arterial pCO_2 measurements compared to ET-CO_2. Limits of agreement were adjusted for multiple comparisons.
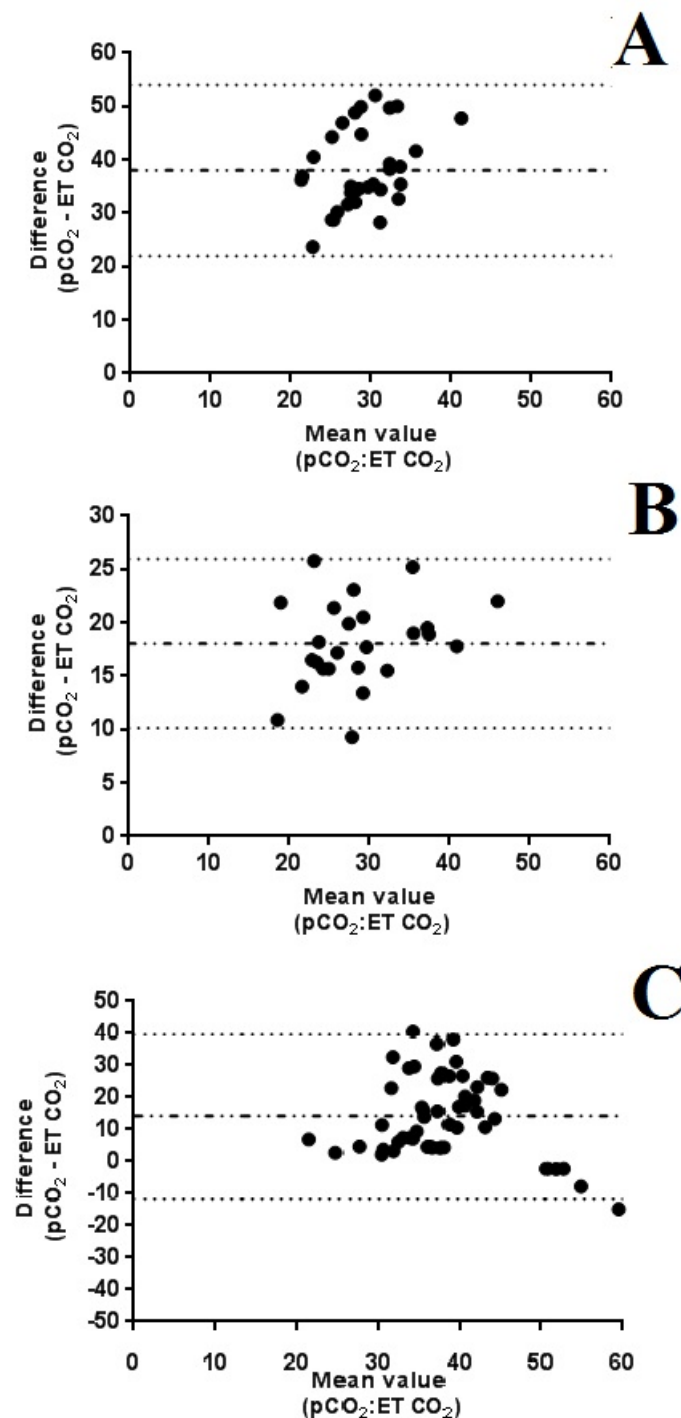
Figure 55: Bland-Altman plots comparing p_aCO_2 measurements made via arterial blood gases and side-stream capnography. Bias represented by the central dashed line and 95% limits of agreement by the dotted lines. 'Vol-Cap' group (**A**); "Press-Cap' group (**B**); and 'Vol-microCap' (**C**).

4.3.5 *Arterial pCO$_2$ changes*
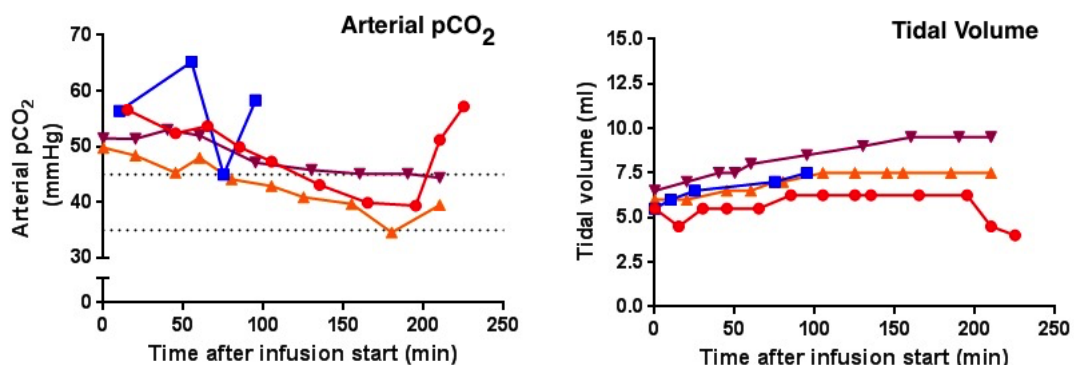
Figure 56: Arterial pCO$_2$ changes using CAPSTAR-100 sampling (left) and changes made to tidal volume (right) in response to p$_a$CO$_2$ changes under volume cycling ventilation. Animal 1(●); Animal 2 (■); Animal 3(▲); Animal 4(▼).
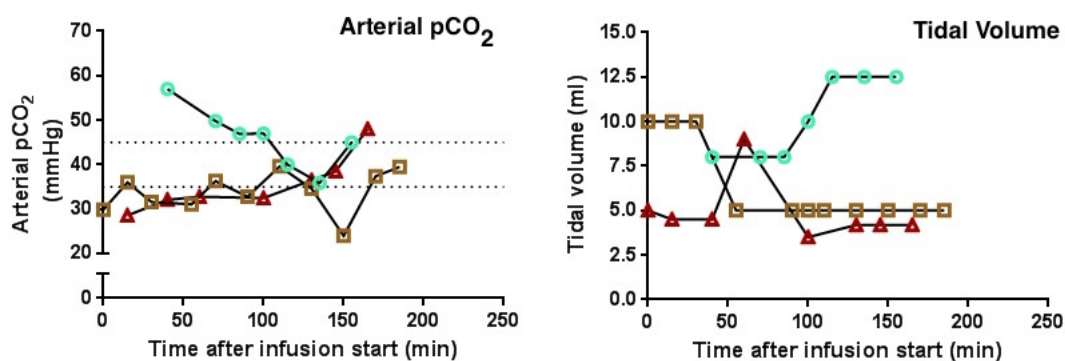
Figure 57: Arterial pCO$_2$ changes and changes made to tidal volume in response (right) using CAPSTAR-100 sampling under Pressure-cycling ventilation. Animal 7(○); Animal 8 (□); Animal 9(△).
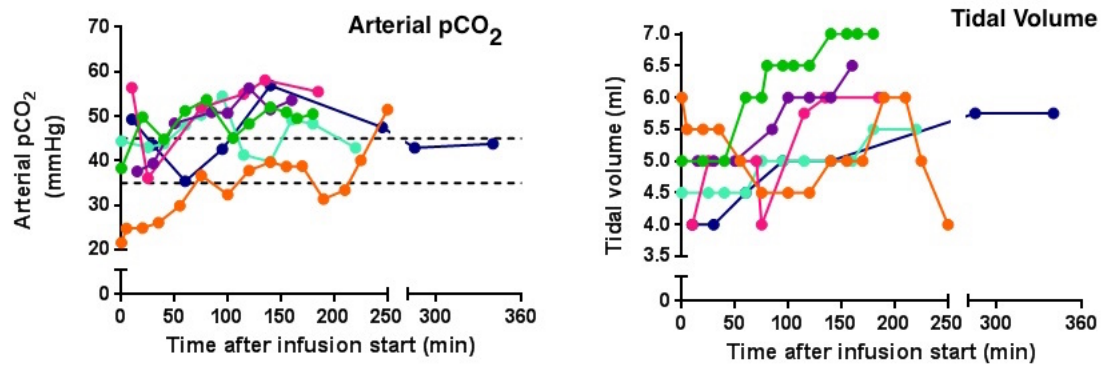
Figure 58: Arterial pCO₂ changes and changes made to tidal volume in response (right) using the Volume-cycling ventilator with Microcapstar sampling. Animal 12 (●); Animal 13 (●); Animal 14 (●); Animal 15 (●); Animal 16 (●); Animal 17 (●).
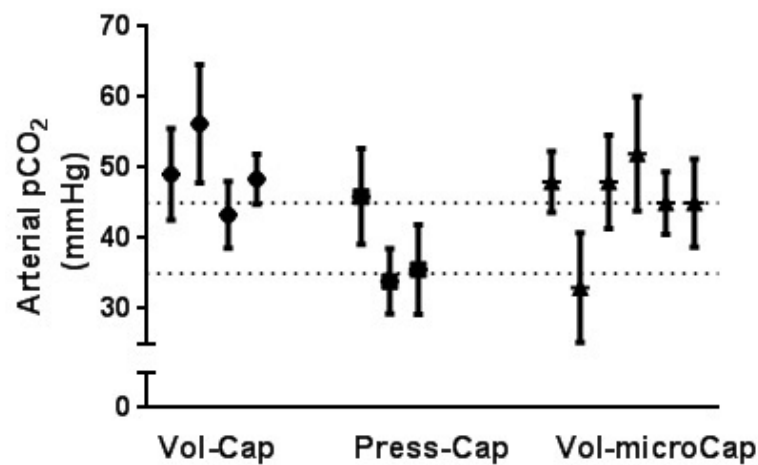
Figure 59: Summary graph of the Mean arterial pCO₂ of each animal for the duration of the experiment. Vol-CAP (n=4), Press-CAP (n=3), Vol-microCAP (n=6). Data presented as mean±SD.
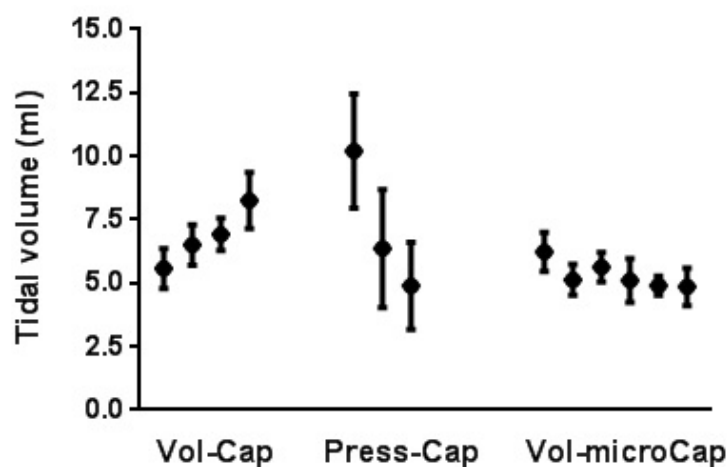
Figure 60: Summary graph of the Mean Tidal volumes delivered to each animal for the duration of the experiment. Vol-CAP (n=4), Press-CAP (n=3), Vol-microCAP (n=6). Data presented as mean±SD.
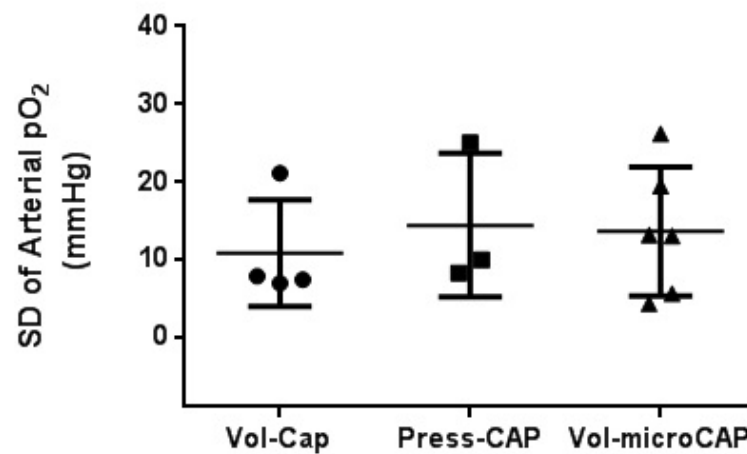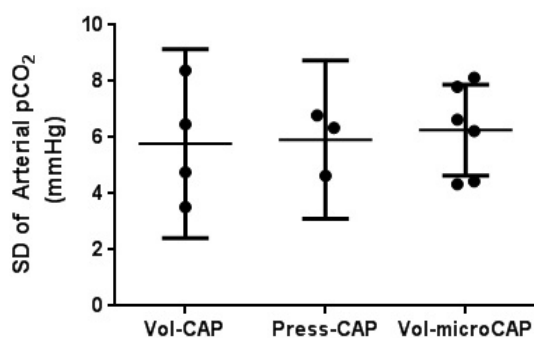

Figure 61: Standard deviations of each animal's p_aCO_2 throughout the course of their respective experiment. The SD provides an indication of the variability of the p_aCO_2 throughout the individual experiment. No statistically significant differences were identified between groups (One-way ANOVA). Data presented as mean±SD.
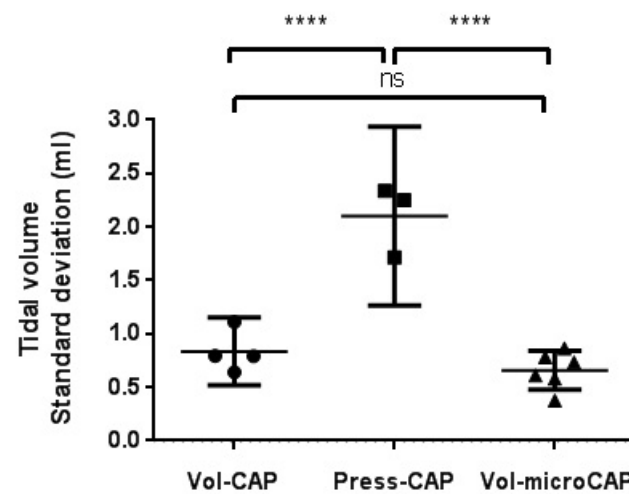
Figure 62: Standard deviations of each animal's tidal volume throughout the course of their respective experiment. The SD provides an indication of the variability of the changes required to maintain normal p_aCO_2 for each set-up. Differences were seen when comparing the volume-cycling paradigms to the pressure-cycling experiments (****, $p < 0.0001$) but not between volume cycling setups ($p > 0.05$); One-way ANOVA with Tukey's multiple comparisons test. Data presented as mean$\pm$SD.

4.3.6   *Summary of Physiological variables*

Table 6 below summarises the aforementioned and other physiological variables measured during the experimental periods.

Variable	Vol-CAP	Press-CAP	Vol-microCAP
Heart Rate (bpm)	306 ± 13	270 ± 13	264 ± 30
MABP (mmHg)	101 ± 21	94 ± 6	81 ± 12
Body Temperature (°C)	37.4 ± 0.1	36.9 ± 0.1	37.3 ± 0.3
Arterial pCO_2 (mmHg)	49.25 ± 5.31	38.47 ± 6.52	45.72 ± 6.3
Arterial pO_2 (mmHg)	84.56 ± 3.43	112.1 ± 12.65	99.99 ± 10.65
pH	7.37 ± 0.05	7.48 ± 0.05	7.41 ± 0.05

Table 6: Average physiological variables collated from the start of the medetomidine infusion to the end of the experiment. Vol-CAP (n=4); Press-CAP (n=3); Vol-microCAP (n=6). Vol-CAP (n=4), Press-CAP (n=3), Vol-microCAP (n= 6). Data presented as mean±SD.

4.4   DISCUSSION

We aimed to optimise methods of monitoring End-tidal CO_2, heart rate, and SpO_2 in order to carry out longitudinal functional imaging noninvasively. End-tidal capnography and pulse oximetry were compared against measurement of arterial blood gases and blood pressure measurement via femoral artery transducer. Methods for compensation of changes in ventilation pressure caused by side-stream CO_2 sampling were also investigated.

As previously shown, medetomidine exerted a pronounced bradycardic effect (Figure 47). However, mean arterial blood pressure was maintained at homeostatic levels (Table 6).

During the first series of experiments, substantial challenges were encountered in maintaining normoxia and normocapnia (Figures 49, 52, 56, and 59). With the animal being in the prone position in the cradle, collapse of the lungs (atelectasis) by artificial ventilation caused hypoxia and hypercapnia. This was exacerbated by the high volume of sampling by the CAPSTAR-100 (minimum 10 ml/min) reducing the overall pressure in the ventilation circuit. The higher mean heart rates and lower blood pH of this group are likely to be explained by the persistent hypercapnia (Table 6).

Attempts to maintain a constant tidal volume and a fixed peak expiratory pressure during ventilation using the SAR-830 ventilator proved troublesome due to our inexperience with the unit (Figures 57, 60, and 62). ET-CO_2 sampling with this setup was no more beneficial than using the volume-cycling ventilator (Figures 55b and Table 5). There was no time to further investigate the use of this set-up. There were no challenges in maintaining sufficient oxygenation (Figure 50).

Variations in pO_2 (Figure 53), p_aCO_2 (Figure 61) and tidal volumes (Figure 62) during the course of each experiment, are largely attributable to our attempts to maintain variables within normal ranges. The large variances are mostly explained by challenges caused by the lengths of the ventilation line, and the sample line (described below).

Overall, none of the configurations tested measured ET-CO_2 in a manner which reliably represented the arterial pCO_2 (Section 4.3.4). As such, predicting a change in measured ET-CO_2 with linear regression (and the relevent 95% prediction intervals) to a reasonable degree of accuracy to true arterial pCO_2 was impossi-

ble.

ET CO_2 is typically 3-5 mmHg less than arterial pCO_2 due to alveolar dead space (Larson and Severinghause, 1962). However, the length of the sampling line from the ventilator expiration line to the sensor (outside the MR bore) has a length of 7m; the recorded sample is substantially lower than the expected ET CO_2. Aside from line-length, leakage and turbulence caused by the additional sampling line and connectors will generate challenges in ventilation and sampling. Compliance of ventilation tubing may also have an effect on physiological maintenance, especially with the lengths required to ventilate in the scanner. Softer, more compliant tubing will be more elastic under ventilation pressure changes, as such reducing flow through the system whereas more resilient tubing will maintain a more consistent ventilation pressure. Artificial ventilation is a closed circuit system with gases delivered and extracted at specified volume and/or pressure. By the addition of a side-stream sampling line, drawing expired gases at a prescribed rate, overall pressure within the circuit decreases.

Based on the results of the experiments above, it was decided that end-tidal capnography for MRI imaging required further optimisation to be able to be used effectively. Further optimisation would need more time than what was available to complete the longitudinal CTX cell investigation. We therefore chose to omit the capnography and measure arterial pCO_2 via femoral artery blood sampling. Cannulation of the artery also permitted continuous measurement of mean arterial blood pressure. Upon recovery of the animal, we were able to seal the arteriotomy in the femoral artery using diathermy forceps and successfully reperfuse the

hind-limb . As the pulse oximeter demonstrated good agreement in measurements of heart rate and SpO_2, it was deemed suitable for use in future studies.

The future work is now being carried out to continue to optimise end-tidal capnography of rats using an MRI compatible set-up. The details of the aforementioned results are being considered in the design of these experiments.

MRI INDICES OF FUNCTIONAL RECOVERY FOLLOWING CTX0E03 CELL TRANSPLANTATION AFTER ISCHAEMIC STROKE

5.1 INTRODUCTION

The brain is required to integrate and respond to a huge amount of external and internal stimuli. It is commonly accepted that distinct neural populations of the brain (nodes) interact with each other in networks which coordinate in response to stimuli, forming the basis of cognition and behaviour (Mišić and Sporns, 2016). Ischaemic damage to the brain can disrupt these networks, leading to functional and cognitive impairment.

With the failures to advance acute interventions beyond that of thrombolytics or mechanical removal of emboli to limit the extent of injury (Hacke et al., 2008; Kalra, 2010), attention has turned towards the use of stem cells as a means of recovery and/or repair of the post-stroke brain. Stem cells' inherent multipotency, and their proliferative capacity and trophism in response to injury suggest that they may be suitable as a therapeutic in the later stages of stroke (Sinden et al., 2012).

BOLD imaging (see Introduction Chapter) is the most popular modality used to study brain network connectivity during activation and rest (Fox and Raichle, 2007). As such, it provides

a means in which to assess the functional network changes in disease states as well as the brain's responses to therapeutics.

5.1.1   *Resting state fMRI and the post-stroke brain*

Within the resting brain, there exist temporal correlations in low-frequency BOLD signals between spatially distinct, but functionally associated regions. This extended the well-established stimulus-driven fMRI methodology into one where patients are simply asked to remain motionless and 'at rest' during imaging (Biswal et al., 1995; Auer, 2008). Similar findings have been shown using Positron Emission Tomography (PET) (Horwitz et al., 1984; Friston et al., 1993) and electrophysiological methodologies such as electrocorticography (He et al., 2006). Histological and neuroanatomical investigations (such as Diffusion Tensor Imaging) have supported functional connectivity hypotheses with relevant structural connectivities within the brain cytoarchitecture (Bressler and Menon, 2010).

Recognition of the dynamic behaviour of the resting brain during health and aberrations in disease have clinical potential in both diagnosis and prognosis. The conservation of resting-state networks among species including rodents (Pawela et al., 2008; Lu et al., 2012), allows detailed *in vivo* experiments to probe the direct mechanisms of brain connectivity in disease states.

Stroke is a sudden and focal injury to a region of the brain with global consequences. Network changes post-stroke are not restricted to the peri-infarct region. Whole brain changes in connectivity have been identified in various regions of the brain (Kim et al., 2015; Vallone et al., 2016) associated with the symptoms

of diaschisis (dysfunction in areas remote from the infarct locus (Seitz et al., 1999)).

Post-stroke disability can make task-based fMRI paradigms (such as finger tapping) challenging for patients. Other issues regarding task based functional imaging for stroke subjects are the limitations of the task paradigm to a certain network within a specific time frame, therefore neglecting the global and temporal changes in the BOLD signal throughout the brain (Carter et al., 2012). The absence of a stimulus paradigm in resting-state imaging can improve the practicality of investigating disabled stroke patients.

By assessing post-stroke connectivity with resting state-fMRI (rs-fMRI), it is hoped that it can become a useful methodology for identifying the structural and functional correlates of stroke-induced dysfunction, the resultant plasticity changes, as well as predicting long-term clinical outcome and any improvements following candidate therapies (He et al., 2007; Westlake and Nagarajan, 2011).

Resting state fMRI & Stem cell therapy

With several cell-based therapies currently under trial for either acute or chronic post-stroke interventions (Sinden et al., 2012), there is a need for methodologies which complement functional assessments in evaluating treatment effects. Non-invasive techniques such as EEG, MEG, and rs-fMRI are therefore suitable candidates for studying the local and global responses to cell therapy. Successful integration of cellular therapeutics into existing brain structures requires, differentiation and integration of the cell product into their respective lineages, for example: functioning neurons, forming synapses within existing networks;

angiogenesis of capillary beds with functionally relevant neurovascular coupling; or myelination of new or existing damaged neurons by oligodendrocytes. However, there is a growing consensus that rather than integration into the host neural network, cell therapies are more likely to provide a more trophic environment in which endogenous recovery mechanisms can act (Bliss et al., 2007; Stroemer et al., 2009). Successful transplantation integration/trophism/endogenous recovery should therefore be detectable by non-invasive modalities, potentially by changes in BOLD signal behaviour during rest and activity. Invasive mechanisms of investigation such as intracerebral electrophysiology are restricted to *in vivo* models but are still pertinent in examining the effects of cell-based therapies.

5.1.2   *CTX0E03 cells in clinical trial*

CTX0E03 cell treatment for chronic post-stroke disability is currently in clinical trials. The completed Phase I safety trial (PISCES, NCT01151124), showed no deleterious clinical effects of varying doses of CTX cell implantation into the peri-infarct basal ganglia (Kalladka et al., 2016). The 11 male patients demonstrated a median NIHSS score improvement of 2, but with variable changes in modified Rankin Scale (improvement in 3 patients, no change in 7 and worsened in 1 patient). However, the absence of blinding and randomisation, small sample size, considerable clinical care of the patients and lack of control subjects in this study, warrants extreme caution in the interpretation of these results. The trial found no cell-related adverse effects and a Phase II trial, (PISCES-II, NCT02117635) is currently under way with a primary outcome measure of an improvement in the 'Action Research Arm Test' (ARAT, Yozbatiran et al. (2008)). The ARAT test will assess pa-

tients who cannot retrieve and place a 25mm³ block with their
paretic arm prior to transplantation of 20 million cells, and again
6 months later.

Resting state fMRI in rodents

There are few investigations into chronic post-stroke changes
in rat resting-state networks measured by BOLD MRI (vanMeer
et al., 2010; van Meer et al., 2012) and no known studies where this
technique has been used to assess functional changes following a
stem cell treatment for stroke. Earlier *in vivo* studies found that
CTX0E03 cells improved functional recovery with some evidence
of angiogenesis and neurogenesis (Smith et al., 2012; Hicks et al.,
2013). Prior to this thesis, MRI had only been used in relation to
CTX cell therapy for infarct delination, volumetric changes and
Deformation-based morphometry (Smith et al., 2012). The use
of resting state-fMRI to study the post-stroke, stem cell-treated
rodent brain was therefore a novel opportunity to investigate
whether functional changes identified by behavioural assessments
correlated with MRI-derived metrics of brain functionality. These
could then determine whether such metrics would be applicable
to future stem-cell studies in both animal models and humans.
The study in this chapter was therefore a novel investigation
which complements previous and on-going clinical trials using
the same cell line.

5.2 AIMS

The aims of this study were as follows:

i To use resting state fMRI to characterise the effects of stroke
   on resting-state networks

ii To identify resting state fMRI indices of any functional recovery, identified by three functional assessments following CTX0E03 transplantation into the peri-infarct brain.

iii To use the protocol from the previous studies (Stroemer et al., 2009; Smith et al., 2012) in order to test the reproducibility of the findings and apply rs-fMRI to investigate changes in the post CTX0E03 cell treated ipsilesional caudate nucleus.

5.3 METHODS

5.3.1 *Longitudinal study design*

Three experimental groups were included in the study with an intended n= 12 for each:

- Sham MCAO - HypoThermasol vehicle

- 90 min MCAO - HypoThermasol vehicle

- 90 min MCAO - CTX0E03 cells in HypoThermasol

Animals were randomised into experimental groups using randomisation software (`http://www.randomization.com`) and recoded post-transplantation, blinding the experimenter during subsequent functional assessments. Animals were recruited to the study on a staggered basis with the whole study lasting 8 months. Previous studies identified the onset of functional recovery from 6 weeks following CTX cell transplantation (Stroemer et al., 2009; Smith et al., 2012). As such, the post-transplantation imaging experiments were conducted 6 weeks after cell or vehicle transplantation. Behavioural assessments were conducted prior to MCAO/Sham and stereotaxic surgeries and fortnightly after.

Details of all experiments, procedures, and their relevant timing are described in Table 7 below.

Procedures	Time point (weeks)
Functional test training	-6 to -5
MCAO/Sham Surgery	-4
Post-stroke MRI & Functional assessment	-1
Immunosuppression	-1 day $+14$ days
CTX cell/vehicle transplant	0
Post-transplant functional assessments	$2, 4, 6, 8, 10, 12$
Post-transplantation MRI	6
Perfusion fixation	12

Table 7: Longitudinal study design in chronological order based on weeks preor post- Hypothermasol vehicle or CTX0E03 cell transplantation (Week 0).

5.3.2 *Functional assessments*

The functional assessments used were the Staircase, Adjusting Steps, and Whiskers tests as piloted and detailed in Chapter 3.

5.3.3 *Anaesthesia and sedation*

Animals are artificially ventilated during MRI procedures and anaesthetised via a nose cone for MCAO and Stereotaxic surgery. The detailed protocols (and their optimisation) are described in Chapters 3 & 4.

5.3.4   *Middle cerebral artery occlusion*

The protocols for MCAO, analgesia, post-operative care are described previously in the Methods chapter. All rats underwent 90min left tMCAO or Sham procedure.

Modification of the transient MCAO procedure

Following the incidence of five consecutive failed occlusions using the Stroemer method described in Section (2.3.1), it was decided not to recover the animals from anaesthesia with the filament *in situ*. Instead, the incision was closed with Michel clips, and the animal maintained under anaesthesia and monitored using a Pulse Oximeter (Mouse OxPlus, Starr Life Sciences) attached to the hindpaw. The instrument measured Heart Rate, Breathing Rate, Pulse Distension, Breath Distension and SpO_2. These variables, including rectal temperature and percentage of inhaled isoflurane were monitored continuously and recorded at 10 min intervals following placement of the intraluminal filament. By keeping the animal under anaesthesia for the entire duration of the MCA occlusion, mean arterial pressure was lower than if the animal were conscious, reducing the likelihood of collateral flow into the occluded MCA territory.

5.3.5   *Stereotaxic implantation of CTX0E03 cells*

Delivery and Storage of CTX0E03 cells.

CTX cells in Hypothermasol (HTS) vehicle were delivered from ReNeuron in 50μl cryovials (10x10x40 mm) at 50000 cells/μl, in a cryobox (130x130x50 mm, Nalgene®) via a liquid nitrogen cooled

dry shipper. They were then transferred for long term storage into a liquid nitrogen storage unit at $-196\,^{\circ}$C.

Determination of stereotaxic coordinates for implantation.

In previous rat studies (Stroemer et al., 2009; Hassani et al., 2012; Smith et al., 2012), CTX0E03 cells were grafted into the ipsilesional caudate putamen at the following two sites:

- AP -1.3 mm, L -3.5 mm, V $+6.5$ mm

- AP -1.8 mm, L -4.0 mm, V $+6.0$ mm

Antero-posterior (AP) and lateral (L) were relative to Bregma and ventral (V) relative to the dura mater (Figure 63). It should be noted that as the left middle cerebral artery was occluded, rather than the right MCA as in the previous studies, the lateral coordinates were switched to positive indices as per the convention of coordinates on the left being positive. All other coordinates remained the same.

Previous studies were conducted with no knowledge of the location and volume of the ischaemic infarct. As such, it was not known whether the CTX cells were grafted into the ischaemic lesion until histological analysis was conducted. In this study, we were able to quantify the volume and location of the ischaemic infarct using T_2 weighted magnetic resonance imaging (Section 5.3.8). By doing so, we could ascertain whether the ischaemic infarct (T_2 hyperintensities) had encroached the area of the striatum where CTX cells would normally be grafted and modify their implant location if necessary.
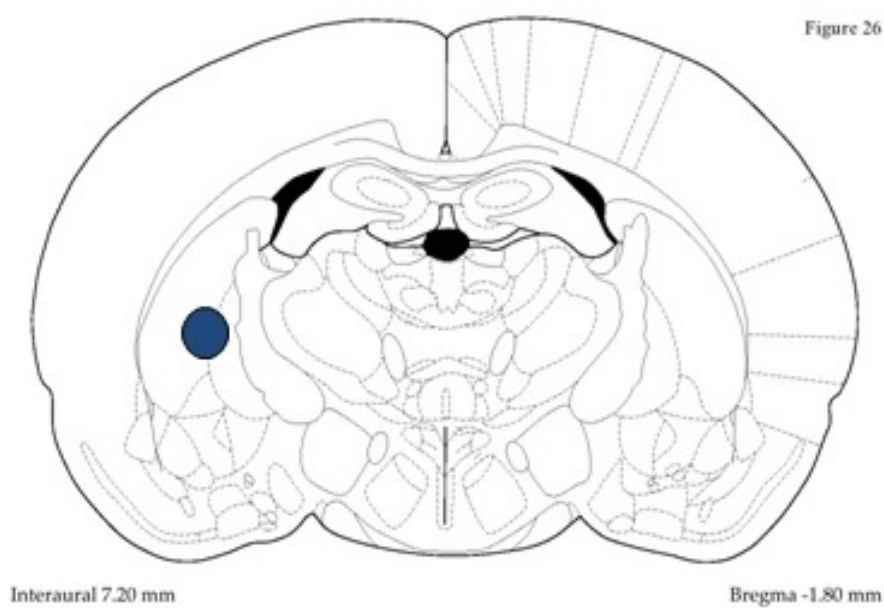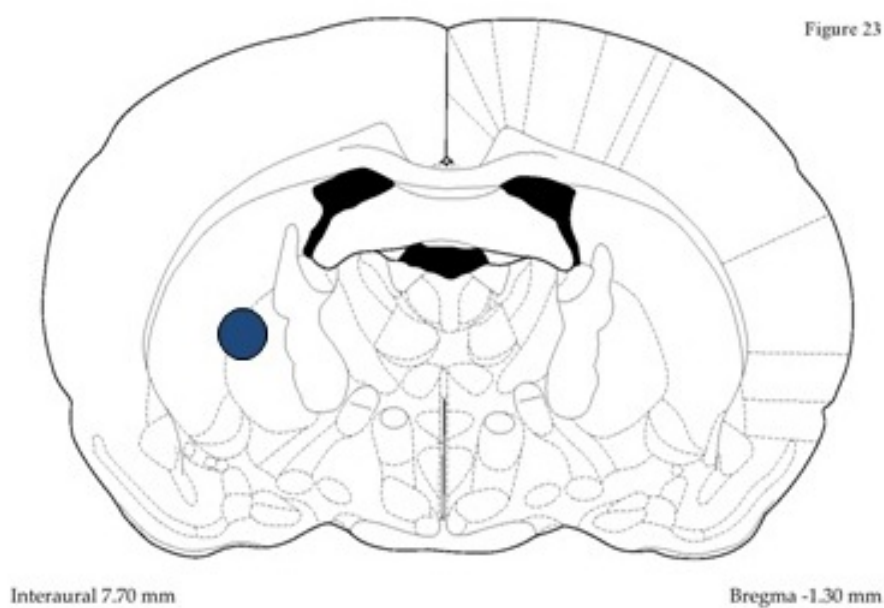
Figure 63: Diagrams taken from the Paxinos Atlas (Paxinos and Watson, 2006) with blue circles illustrating the stereotaxic implantation coordinates as previously defined in Stroemer et al. (2009), Hassani et al. (2012), & Smith et al. (2012). Both coordinates determined that the CTX cells were implanted into the ipsilesional striatum.

Using the methodology described in Bible et al. (2009), the location of the default coordinates for implantation were located on the respective image slices using a home-made MATLAB script. The distance of the coordinates from the manually identified mid-line on the dorsal surface of the brain (in millimetres) was calculated (10 pixels/mm). Lines were then plotted onto the image of a lateral width and ventral depth corresponding to the implantation coordinates (Figure 64). When infarcts encroached the predefined coordinates, the coordinates were altered by moving them to a more dorsal or caudal location but still aiming to keep the implantation site within the striatum. The implantation site was checked and recorded for all animals, including Sham and MCAO-Vehicle groups.
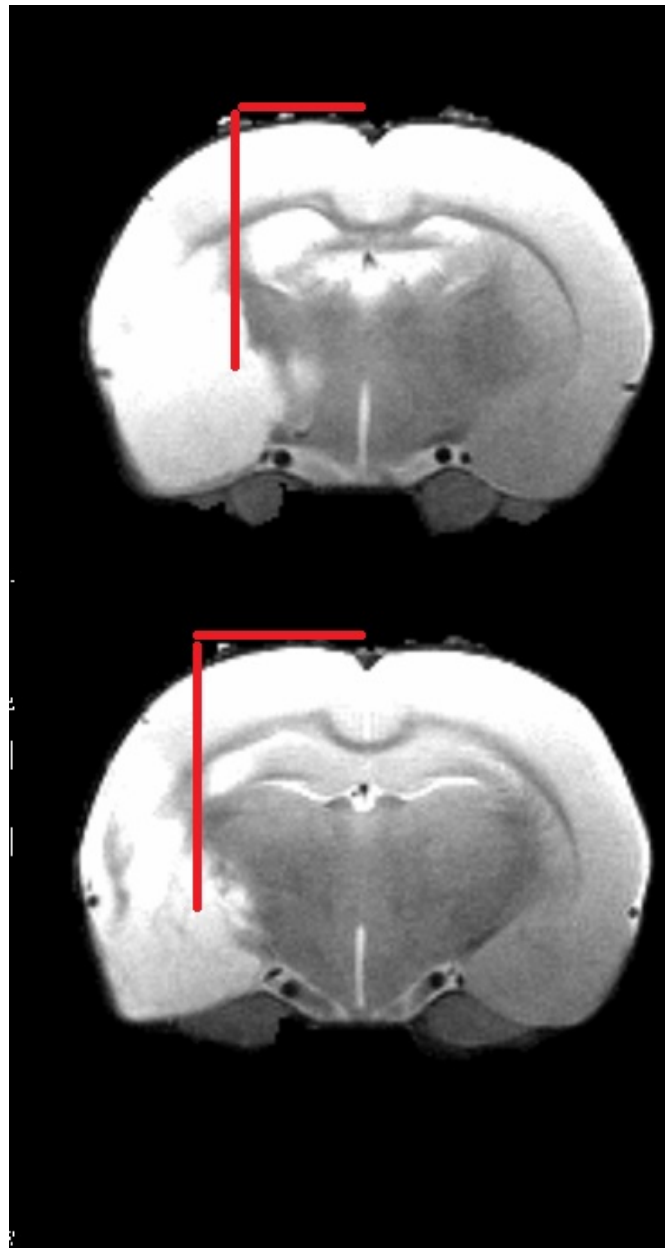
Figure 64: Example of determining whether the ischaemic infarct encroached the pre-defined implantation coordinates. Lines were plotted over the T_2 weighted RARE image lateral from the manually determined mid-line and then ventral from that point at the two rostro-caudal levels for implantation. Here infarcts (hyper-intensities) were present at the implantation site and for transplantation, the coordinates would have been altered to a more antero-dorsal location but still ensuring grafting into the ipsilesional striatum.

Preparation of the intracerebral needle.

Cells were transplanted using a 50μl Hamilton syringe with needle attached. Prior to loading for transplantation, the syringe barrel and needle were flushed with Medistel®, left for 30 min, and then flushed several times with sterile saline.

Handling and Preparation of CTX0E03 for Injection

Prior to transplantation, vials were removed from storage and transferred on dry ice to the Wellcome Surgical Institute operating theatre. Using gloves sprayed with 70% ethanol, the vials were removed from dry ice and the suspension allowed to thaw at room temperature. The 50 μl Hamilton syringe was secured in the stereotaxic frame, placed within a motorised syringe pump (KD Scientific), and loaded with HypoThermasol (HTS).

Cell Grafting

The rat was anaesthetised and prepared for surgery as described in Sections 2.2.3 and 2.2.2. The tips of the disinfected ear bars were dipped in local anaesthetic cream (EMLA, AstraZeneca), ocular lubricant applied (Lacrilube, Allergan) and the animal placed into the stereotaxic frame (Kopf 900 Series). Following administration of analgesia, a midline incision was made and the fascia removed using a bone scraper. The scalp was retracted by securing Spencer Wells clips to long 4-0 suture threads at anterior and posterior aspects of the scalp either side of the incision. The origin of the left temporalis muscle was also partially retracted using the bone scraper to improve access to the skull for the craniotomy. Any bleeding from capillaries and pial vessels was stemmed using pressure applied with sterile cotton buds. Stereotaxic coordinates were derived using a digital frame reader (Stoelting, IL). Once Bregma was located, the syringe needle was aligned with it and a

zero point set. The needle was then positioned to the prescribed coordinates (see above) and the location marked on the skull. The syringe was then raised clear of the skull to provide room for the craniotomies.

The craniotomies were performed using a dental drill (NSK) using a 0.2 mm diameter drill bit under saline to prevent heat damage to the underlying tissue. Once complete, the dura was punctured to prevent impeding the needle's passage. Approximately 15-20 μl of the CTX0E03 suspension was drawn up, the needle lowered into the brain at the prescribed depth, raised 0.01 mm to provide a space for the graft, and 4.5 μl injected at a rate of 1 μl/min. Following grafting, the cannula was left *in situ* for three minutes to allow permeation of the suspension, before slowly retracting the needle.

Once grafting was complete, the scalp was sutured, 5 ml of glucose/saline (two 2.5ml doses, Baxter Healthcare Ltd) administered subcutaneously, and immunosupression administered as described in Section 5.3.6. The standard post-operative care protocols (Section 2.4) were also followed.

5.3.6 *Immunosuppression*

Immunosuppression was required due to the xenograft nature of the cell transplants. The following drugs, and their concentrations, were prepared and administered subcutaneously post-transplantation are described below. Both drugs were formulated in a Category II hood in the Veterinary Research Facility. The administration protocol matched that of all previous *in vivo* CTX0E03 cell investigations.

Methylprednisolone sodium succinate (SoluMedrol, Pfizer)

20 mg/kg subcutaneously on days -1, 0 (day of transplant), and daily for 14 days. Stock solutions of 31.25mg/ml were prepared with sterile water and refrigerated prior to use.

Cyclosporine A (CsA) (Sandimmune, Novartis)

Cyclosporine A (Sandimmune, Novartis) in Kolliphore EL (Sigma) vehicle was formulated to a dose of 10mg/kg. Cyclosporine was administered on days -1, 0 , and +1 post-transplantation and three times a week subsequently for 14 days. Due to the viscous nature of the CsA-Kolliphor solution, subcutaneous administration via a 21G, needle was required as the force pressure through any smaller gauge needle caused the needle to detach from the syringe. The flanks on either side of the rats were shaved; the injection site alternated between doses, and the skin subsequently monitored for lesions.

All immuno-compromised animals were kept in pairs (wherever possible) in filter topped cages within the shared holding room for the duration of the treatment.

5.3.7   *Protocol for longitudinal MRI study*

Due to time constraints in optimising end-tidal capnography to provide reliable, non-invasive indication of arterial pCO_2 (detailed in Chapter 4), arterial cannulation and blood sampling was used to ensure physiological variables remained within normal ranges. Animals enrolled in the study were anaesthetised, intubated, cannulated, sedated and prepared as described in earlier Sections: 2.2.3, 2.3.2, 2.3.3, 2.7.1, 4.2.2, and 4.2.4 respectively. The imaging sequences detailed below were conducted in order and

arterial blood samples ($80\mu l$) were taken between a minimum of three, and a maximum of six times during the experiment. Ventilation parameters were modified, when necessary, to ensure normal physiological variables. The anaesthesia protocol with 1% isoflurane and medetomidine infusion is identical to the protocol in Section 4.2.2.

The following variables were recorded throughout the experiment:

- Body temperature (via rectal probe maintained between 36.5 and 37.5 °C using a water heating blanket).

- Mean arterial blood pressure (via arterial line).

- Heart Rate (via arterial line and pulse oximeter).

- SpO_2 (via pulse oximeter).

- Arterial O_2 saturation (via arterial blood sample).

- Arterial pO_2 (via arterial blood sample; normal range: 80-100mmHg).

- Arterial pCO_2 (via arterial blood sample; normal range: 35-45mmHg).

- Breathing rate (via respiration sensor).

- Arterial blood pH (via arterial blood sample; normal range: 7.45-7.55.

- Ventilation volume (via an Ugo-Basille volume cycling ventilator, ml).

- Percentage inhaled oxygen (via a Viamed oxygen sensor) .

Time of samples and scans were recorded relative to the initiation of the medetomidine infusion.

5.3.8   *Imaging sequences and specifications*

Animals were reproducibly positioned and coil positioning veri-fied using a FLASH sequence. Local shimming was conducted using a fieldmap based algorithm ('MAPSHIM'). A fieldmap was acquired after shimming to be able to apply distortion correction (TR=30ms, TE=2 and 5.8ms at an isotropic resolution of $250\mu m$). A 20-minute DTI 4-shot diffusion weighted spin-echo EPI (SE-EPI) sequence was also carried out, however due to time constraints, its analysis is beyond the scope of this thesis (TR=4500ms, TE= 36ms, in-plane resolution of 200μm, and 15 slices of 1mm thick-ness). Diffusion measurements were made in 36 directions with b-factors of 0, 600 and 1000 s.mm^2. T_2-weighted RARE (Rapid imaging with Refocused Echoes) imaging was used for high reso-lution anatomical imaging for delineation of the ischaemic infarct and for co-registration to the anatomical template (TR=5000ms, TE=55ms, in-plane resolution of 100μm, 15 slices of 1mm thick-ness). Resting BOLD fluctuation were measured using Single-shot EPI (TR=1200ms, TE=16ms, in-plane resolution of 500μm and 15 slices of 1 mm thickness) experiments with 500 repetitions and 20 dummy scans, totalling 10minutes. Total scan duration, including positioning times, took between approximately 70-90 minutes.

Post-imaging recovery from anaesthesia and sedation

Following completion of the imaging experiments the animal was returned to the operating theatre. The arterial cannula was removed and the arteriotomy sealed (to allow restoration of flow) using diathermy forceps (Eschmann) - performed by Lindsay Gallagher - and the wound sutured. Whilst still on the ventilator, medetomidine sedation was reversed by intraperitoneal injection of 100μg/kg atipamezol. Reversal typically took 3-5 minutes

following administration. Once signs of consciousness began to appear (e.g. resistance to intubation, hindpaw twitching and restoration of pinch reflexes) the intubation tubing was removed and the animals were recovered overnight in individual cages, with fresh softened diet before being returned to group housing.

5.3.9 *Data analysis*

Serial behavioural performances were analysed via group comparisons of individual Area under the Curve (AUC) values as described in Section (3.3.4). Group mean infarct volumes were compared by Student's two-tailed t-tests. Physiological data acquired at the time of the resting-state imaging in all three groups were compared by One-way Analysis of Variance (ANOVA) with Bonferroni correction for multiple comparisons.

Graphs and their respective statistical analyses were generated using Prism 5 software (GraphPad Software Inc). All data are presented as mean±standard deviation unless stated otherwise.

Infarct volume measurements

Ischaemic infarcts were measured from the T_2 weighted RARE images taken at weeks -1 and $+6$ post-transplant. Composite images of mean infarct distribution were calculated using MATLAB and MRICRO.

Resting state BOLD analysis

As described in Section 1.4.6, BOLD data requires several pre-processing steps before statistical analysis can be performed. These include: the detection and removal of artifacts, spatial normalisation and smoothing of the data. Following pre-processing,

statistical models can then be fitted to the data and networks derived and quantified.

Before detailing the pre-processing pipeline, the co-registration template used will be described below.

Schwarz MRI atlas in Paxinos Space & Regions of Interest

Seed-based region of interest (ROI) analysis was used to determine resting-state networks. Here, seed ROI voxels are are identified in a pre-determined region of functional and/or anatomical interest. The mean signal time series from this ROI is then correlated with all other brain voxels across the whole time series. Voxels with time-series correlations greater than the determined statistical threshold (see 5.3.10) are then overlaid onto the already coregistered anatomical template. The location of the seed ROI will determine the resting-state network which is identified (see Section 1.4.5).

The Paxinos & Watson Stereotaxic Rat brain atlas (Paxinos and Watson, 2006), is a widely used standard atlas for *in vivo* neurosciences. The atlas accurately details the anatomical structures of the brain with coordinates based on distances from the midline, bregma, and the interaural line. An MRI template, based on 97 structural scans of Sprague-Dawley rats aligned in Paxinos space, has been developed by Schwarz et al. (2006). It is freely available and was used for data coregistration and ROI determination. The Schwarz atlas template dimensions were: Matrix, 96x96x30mm^2, and Resolution 0.19x0.19x0.8mm^3.

Given that the PISCES II trial aims to investigate the efficacy of CTX cells on the improvement of sensorimotor dysfunction

post-stroke, seed-regions were focused on the S1 Forelimb (S1FL), Barrel Field (S1BF) areas and the primary motor cortex (M1) in both hemispheres (see Figure 65). The voxels from each internal structure from the Paxinos atlas are assigned an integer value allowing for derivation of structurally relevant unilateral and bilateral regions of interest (ROIs) which were extracted using homemade MATLAB scripts.
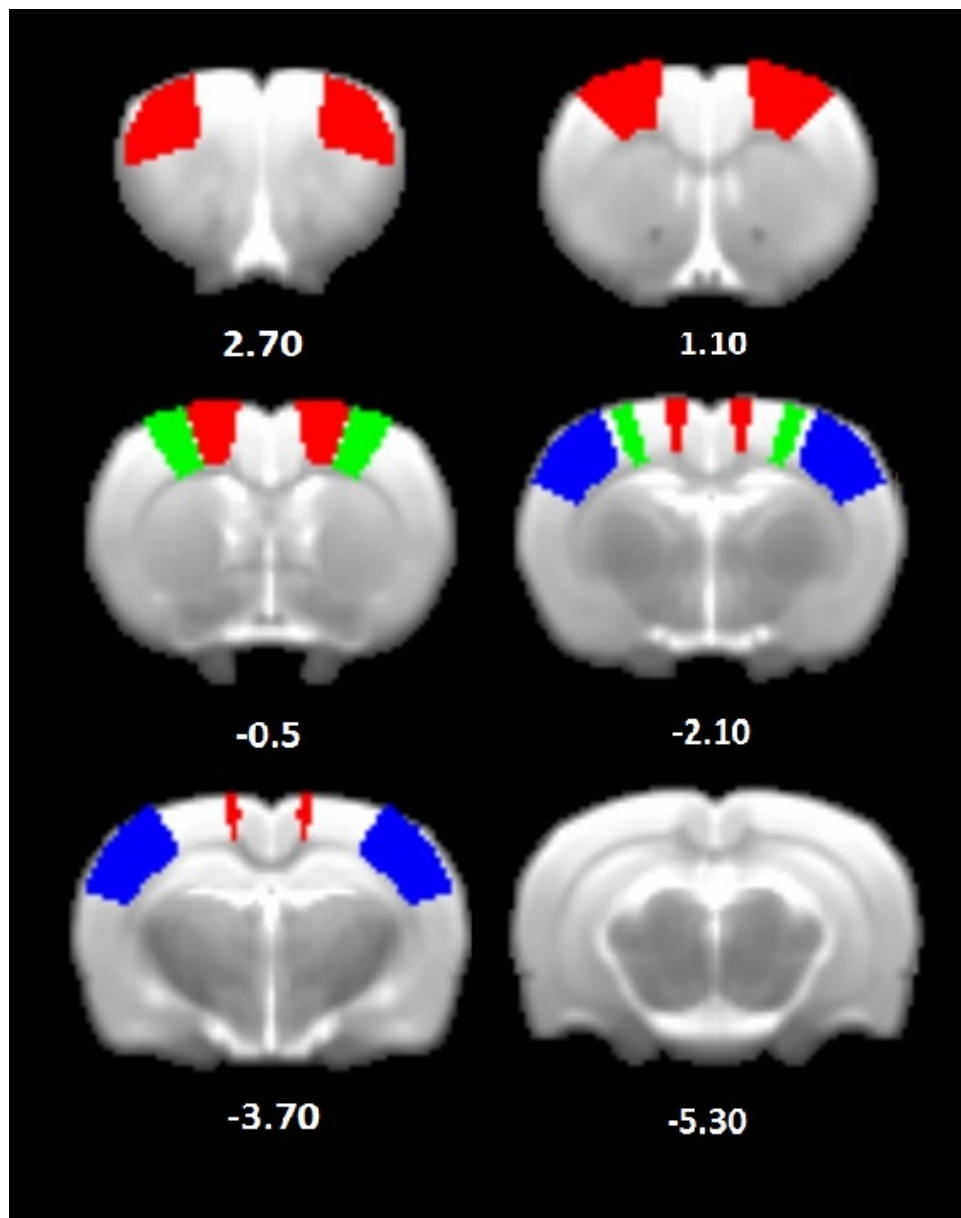
Figure 65: Location of the Regions of Interest (ROIs) used for seed-based correlations of the resting state data. M1 (red), S1FL (green), and S1BF (blue). The position of slices relative to Bregma in millimeters are noted below.

Image pre-processing

Pre-processing and network identification of the MRI data was conducted using SPM12 (Wellcome Department of Cognitive Neurology, London, UK `http://www.fil.ion.ucl.ac.uk/spm`) and the DBAPI toolbox as detailed below. MATLAB 2014a was used in all cases.

Resting-state data were initially triaged for SNR and motion artifacts using the Aedes Toolbox (University of Eastern Finland) for MATLAB (The MathWorks®). Using this package, the signal to noise ratio (SNR) of each dataset was assessed to determine if the data were of satisfactory quality (over 50), and the time series examined for motion artifacts.

All image header voxel dimensions were then augmented by a factor of ten (thus, comparable with human brain dimensions), to ensure compatibility with SPM12 using the DBAPI toolbox (details in Section 5.3.9).

Prior to functional connectivity analysis, images were pre-processed in the order detailed below and in Figure 66. By pre-processing the data through multiple steps we ensured robust spatial localisation of the functional data.

Coregistration and Normalisation to the Schwarz template:

With the Schwarz et al. (2006) atlas defining the image origin as bregma, the origin of the Resting-state and T_2 data sets were manually changed to the same location. As demonstrated in Figure 66 the methods stated in Goense et al. (2008) were used. Coregistration was performed as described in Collignon et al. (1995). The coplanar T_2 weighted RARE acquired at each experiment was

co-registered to the Schwarz template. The resting-state EPI data sets and magnitude images of the fieldmap were also coregistered to the RARE, so by proxy, both the frequency component of the fieldmap and the resting-state dataset were co-registered to the Schwarz template.

Distortion Correction:

Prior to co-registration, the frequency and magnitude components of the fieldmaps were manually extracted and rescaled using homemade MATLAB scripts. A voxel displacement map (VDM) of the phase distortion was then calculated using SPM (Jezzard and Balaban, 1995; Jenkinson, 2003). Following co-reigstration, the resting-state data were then unwarped in the phase direction (Superior-Inferior).

Skull stripping:

The RARE data were skull stripped using the 'Brain extraction toolbox, (bet) in (Smith, 2002). The fieldmaps were resliced to match the RARE and then brain voxels extracted using the skull-stripped RARE images as a mask. To extract the brain data from the functional images, skull stripped RARE images were resliced to match the EPI data, and all volumes skull stripped using a homemade MATLAB script.

The 'Data Processing & Analysis of Brain Imaging (DPABI) Toolbox

The 'DPABI for Rat' toolbox (which implements SPM functions Yan and Zang (2010)), was used for final pre-processing steps and network derivation. It is a semi-automated pipeline analysis toolbox, allowing for batch processing of rs-fMRI data. Through the toolbox, the following pre-processing steps were performed:
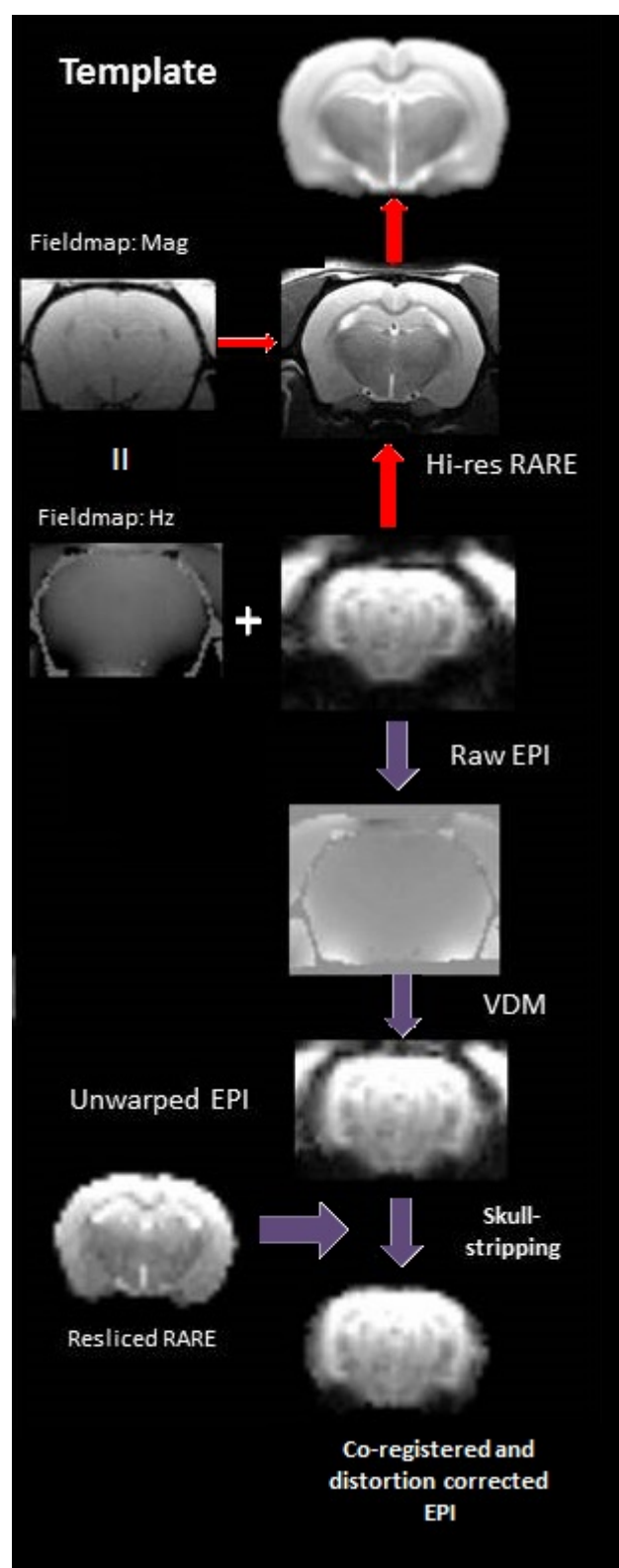
Figure 66: Pre-processing pipeline of EPI data. Red arrows represent coregistration. Purple arrows represent transformation processes. Abbreviations: Mag (Magnitude), Hz (frequency), VDM (Voxel displacement map).

- **Spatial filtering** Smoothing was carried out using the default Gaussian FWHM (Full-weight half-maximum) of $[666]$ mm defined in SPM12 .

- **Temporal Filtering** A bandpass filter of $0.01 - 0.08$ Hz was applied to the data.

5.3.10 *Statistical analysis of resting state data*

Using the seed-regions defined above, global correlations were derived. The correlation coefficients were then transformed via Fisher's transformation, automatically in DPABI (Z', Equation 8), to better fit the normal distribution.

$$Z' = \frac{1}{2} \ln \frac{(1+r)}{(1-r)} \tag{8}$$

Global maps & Inter-ROI comparisons

Group mean global maps were generated by averaging group correlations derived from the S1FL seed region across the time-series. To generate the figures on MRICRO, voxels were overlaid on the Schwarz template and a statistical significance threshold of $r \geq 0.30; Z' \geq 0.310, (p < 0.00001)$ then applied. The group mean time series between ROIs were also compared to each other and then the aforementioned statistical threshold applied.

5.4 RESULTS

5.4.1 *Attrition*

25 out of a total 49 animals either died or were excluded during the study according to *a priori* criteria (Table 8). Following 5 consecutive failed MCA occlusions the surgical method was modified as described above (Section 5.3.4). Two cases of infection were found: One following CTX cell transplantation which was complicated by severe bleeding from the skull; the other from an infection acquired from the femoral cannula blood pressure transducer. Following both incidents, aseptic standards were improved and recurrence prevented. Miscellaneous deaths included loss of spontaneous breathing during anaesthesia (x2) and one termination during surgery due to an emergency evacuation of the building.

A total of 8 animals were recruited for each group and successfully completed the study.

Cause	Number (% of total cases)
Failed MCAO	7(28)
Haemorrhage	7(28)
Exceeded licence severity	3(12)
Infection	2(8)
Death during intubation	2(8)
Failed baseline functional assessments	1(4)
Miscellaneous	3(12)

Table 8: Cause, and number of attrition cases during the study.

5.4.2   *Body weights and physiological variables*

Body weights of all animals were recording regularly through out
the study (Table 9). During the MCAO procedure, animals were
monitored via a pulse oximeter (detailed in Section 5.3.4) above.
The following variables were maintained with their respective
ranges: Rectal temperature ($37.0 - 37.4°C$), Heart Rate ($355 -
375\text{bpm}$) , Breathing Rate ($46 - 54\text{br/min}$), SpO_2 ($98.6 - 99.0\%$),
inhaled isoflurane ($2.0 - 2.4\%$).

Body weight at time point	Sham-Vehicle	MCAO-Vehicle	MCAO-CTX cell
Pre-MCAO/Sham	325 ± 31	329 ± 19	327 ± 16
7 days post-MCAO	364 ± 35	314 ± 17	309 ± 36
Pre-Stereotaxic	387 ± 38	349 ± 28	334 ± 38
Post-immunosuppression	361 ± 26	342 ± 35	316 ± 26
Study end point (still diet restricted)	375 ± 49	335 ± 36	319 ± 31

Table 9: Body weights of study animals at different stages throughout the
longitudinal study. n=8 for each group. Data presented as mean±SD.

5.4.3   *Infarct volumes of Vehicle and CTX cell groups*

Ischaemic infarctions were measured manually from T_2 weighted
RARE images acquired one week prior to, and six weeks following
CTX cell or vehicle transplantation (Figure 67). There were no
statistical differences between stroke groups at either time point.
Between time points there was a mean reduction in total infarct
volume of $7.1 \pm 13.4 \text{ mm}^3$ and $9.1 \pm 6.1 \text{ mm}^3$ in the MCAO-Vehicle
and MCAO-CTX groups, respectively (Figure 67C, $p > 0.05$).
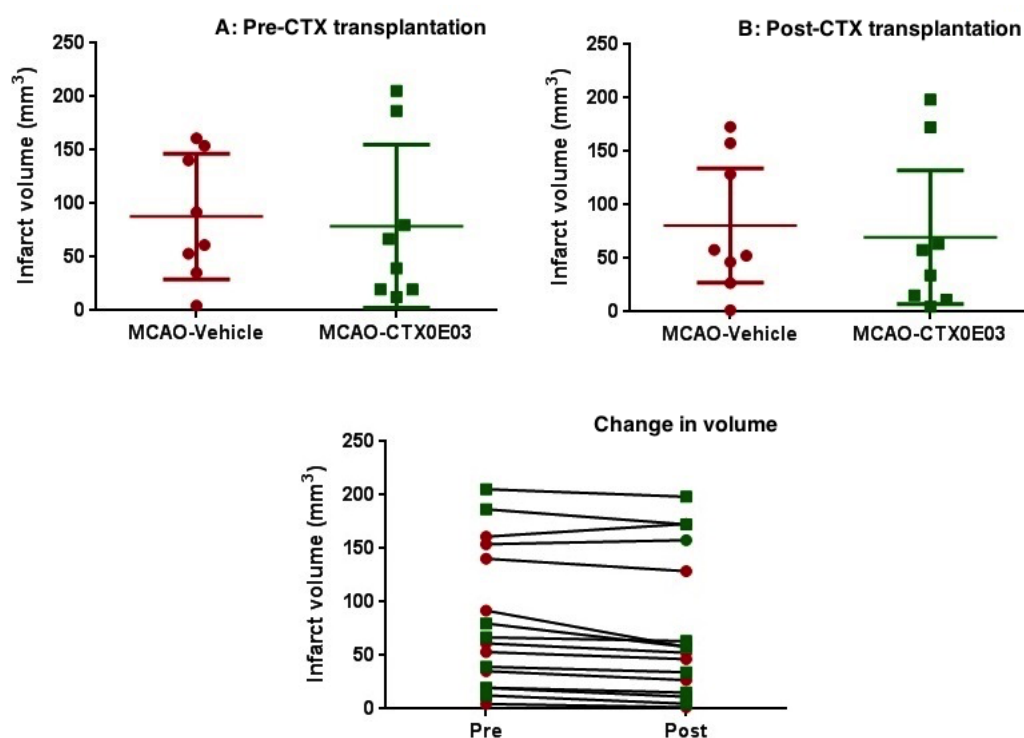
Figure 67: Ischaemic infarct volumes of both stroke groups, three weeks post MCAO surgery (A), and six weeks following CTX cell or vehicle transplantation. There was a mean decrease in infarct volume between time points (C). No statistical differences were found between group means (p> 0.05). Student's two-tailed paired t-test. Data presented as mean± SD.

5.4.4   *Functional asssessments*

All functional assessments were performed following a period of training prior to MCAO; 3 weeks after MCAO; and at 2 week intervals following CTX0E03/vehicle transplantation over 12 weeks.

The Staircase Test

Diet-restricted animals' ability to reach, grasp, and retrieve sugar pellets was assessed via The Staircase Test (Montoya et al., 1991), and the number of pellets retrieved with each forepaw was counted. Left hemisphere MCAO impaired pellet retrieval ability of both forelimbs (Right $p < 0.0001$, Left $p < 0.01$, in both MCAO groups, Figure 68). No recovery of function was seen during the period of functional assessment. CTX-cell transplantation led to no improvement in pellet retrieval using either forelimb. Sham animals showed a mean, but not significant, decrease in right forelimb pellet retrieval following stereotaxic injection compared to the post-surgical test at week -1. There was no effect of stereotaxic injection on pellet retrieval with the left forelimb.
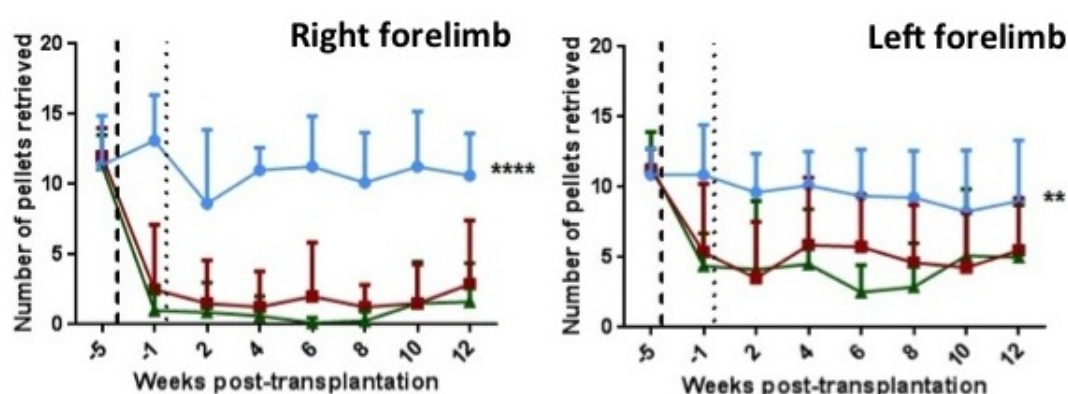
Figure 68: The effect of CTX0E03 cell transplantation on pellet retrieval in The Staircase Test. Baseline data were acquired prior to left tMCAO (dashed line) and cell/vehicle transplantation (dotted line), and every two weeks subsequently. (Left) the number of pellets retrieved with the right forelimb, (Right) the number of pellets retrieved with the left forelimb. Sham-Vehicle (n = 8, •); MCAO-Vehicle (n = 8, ■); MCAO-CTX0E03 cell (n = 8, ▲). Individual performance summarised using AUC analysis and group Sham compared to MCAO-veh and MCAO-CTX groups. There were no differences between the two MCAO groups. means compared with One-way ANOVA, **** p< 0.0001, ** p< 0.01. Data presented as mean ±SD.

The Adjusting Steps Test

The capability of animals to perform compensatory steps when the contralesional (right) forelimb was dragged lateral, and medial to the midline was evaluated (see Chapter 3 for details). There was no effect of MCAO or CTX cell transplantation on stepping ability when the right forelimb was dragged lateral from the midline, ($p< 0.05$, Figure 69). MCAO permanently impaired the medial stepping ability of rats in both stroke groups ($p< 0.0001$) with no evidence of functional improvement in the CTX cell transplantation group, ($p> 0.05$). Ipsilesional forelimb data were not acquired as pilot data showed no effect of MCAO on stepping ability.
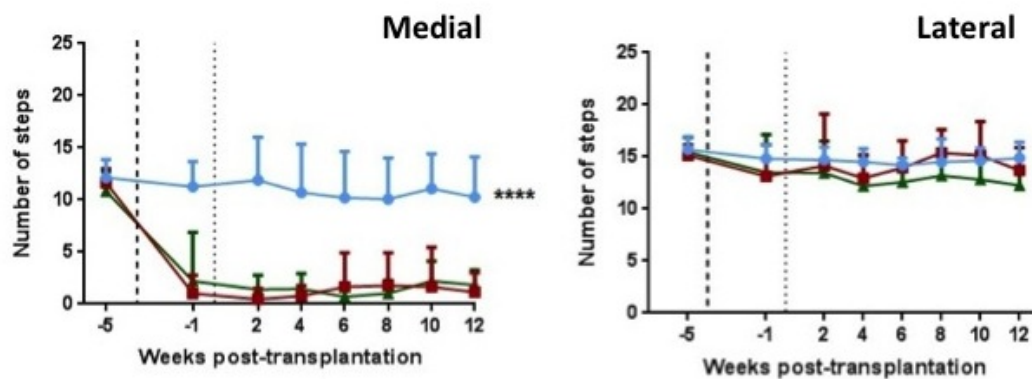
Figure 69: The effect of CTX0E03 cell transplantation on right forelimb function in The Adjusting Steps Test. Baseline data were acquired prior to MCAO (dashed line) and stem cell/vehicle transplantation (dotted line), and every two weeks subsequently. (Left) the number of adjusting steps made in the medial direction, (Right) the number of adjusting steps made in the lateral direction.
Sham-Vehicle (n = 8, •); MCAO-Vehicle (n = 8, ■); MCAO-CTX0E03 cell (n = 8, ▲). Individual performance summarised using AUC analysis and group means compared with One-way ANOVA, **** $p< 0.0001$ with Sham compared to MCAO-veh and MCAO-CTX groups. There were no differences between the two MCAO groups. Data presented as mean ±SD.

The Whiskers Test

The ability of animals to reflexively place their forelimb following upward homotopic vibrissae stimulation was evaluated. There was no effect of MCAO or CTX cell transplantation on the percentage of failed reflexes on the left side ($p > 0.05$, Figure 70). Transient MCAO caused a permanent failure in placing reflexes of the right (contralesional) forelimb ($p < 0.001$) with no improvement garnered by CTX cell transplantation, ($p > 0.05$, Figure 70). Sham animals showed a mean, but not significant, increase in reflex failures in weeks 2 to 10 following stereotaxic injection of HypoThermasol.
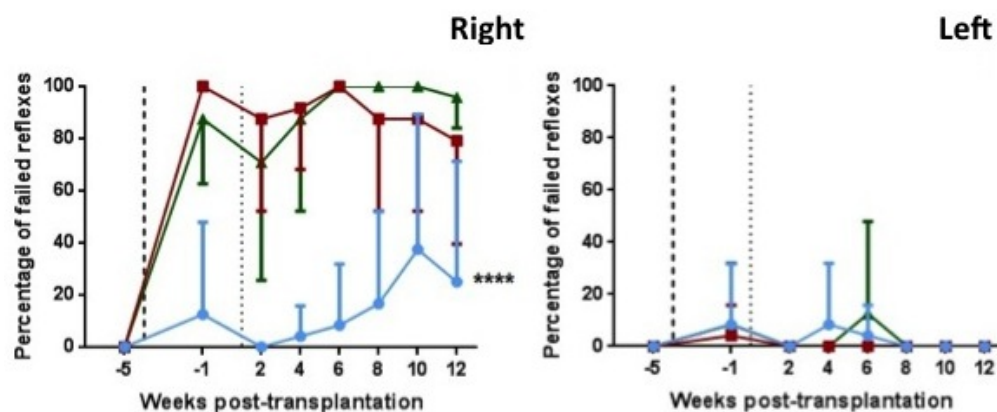
Figure 70: The effect of CTX0E03 cell transplantation on right and left forelimb placing failures, following stimulation of the homotopic vibrissae. Baseline data acquired prior to MCAO (dashed line) and stem cell/vehicle transplant (dotted line), and every two weeks subsequently. Sham-Vehicle (n = 8, ●); MCAO-Vehicle (n = 8, ■); MCAO-CTX0E03 cell (n = 8, ▲). Individual performance summarised using AUC analysis and group means compared with One-way ANOVA and Bonferroni's correction for multiple comparisons. **** $p < 0.0001$. Data presented as mean ±SD.

5.4.5 *CTX0E03 transplantation and resting-state networks*

Sham, MCAO-Vehicle and MCAO-CTX cell treated groups all underwent resting-state fMRI under medetomidine anaesthesia at 3 weeks following MCAO or Sham surgery, and again at 6 weeks following implantation of Hypothermasol vehicle or CTX cells. Resting-state data were assessed for quality, unwarped, pre-processed as described earlier, and global sensorimotor maps and inter-ROI correlations derived via seed-based analysis.

Exclusions

Three data sets from the pre-transplant Sham-Vehicle and one from the pre-transplant MCAO-Veh group were excluded due to surface coil failure leading to poor SNR. One animal from the MCAO-CTX group had an infarct so large that the resulting structural deformations were too large to correct and allow for accurate coregistration and as a result, the entire data set was removed. A technical error in the rectal thermometer caused an under-reading of body temperature and overheating of one animal in the post-transplant Sham-Vehicle group; the data set was consequently excluded.

Physiological variables during functional imaging

Physiological variables were acquired during imaging to ensure that at the time of the resting-state imaging, variables were within normal ranges appropriate for detection of the BOLD signal (Tables 10 & 11). The cannula in one pre-transplantation and in one post-transplantation MCAO-Veh group animal failed at the pre-resting state sampling time point. Ventilation parameters were maintained and resting-state network quality control of both data sets indicated no deleterious issues. There were some statistical

differences between mean variable values between groups. However the data range was within physiological norms and was no cause for concern. Post-transplant weights of the MCAO groups were lower than their Sham counterparts.

Variable	Sham-Vehicle	MCAO-Vehicle	MCAO-CTX cell
Time from infusion start (min)	73 ± 16	79 ± 15	78 ± 20
Body weight (g)	377 ± 36	342 ± 24	$331 \pm 32^*$
Temperature °C	36.9 ± 0.6	37.1 ± 0.3	$37.5 \pm 0.3^*$
Heart Rate (bpm)	235 ± 12	246 ± 14	258 ± 21
MABP (mmHg)	100 ± 8	$91 \pm 3^*$	$89 \pm 7^*$
$PaCO_2$ (mmHg)	45.6 ± 5.0	42.8 ± 2.8	42.7 ± 3.5
PaO_2 (mmHg)	99.1 ± 12.6	89.5 ± 15.5	103.3 ± 13.9
pH	7.421 ± 0.03	7.439 ± 0.03	7.417 ± 0.01
Inspired O_2 (%)	27.4 ± 1.8	27.7 ± 1.3	26.5 ± 0.9

Table 10: Physiological variables at the time of Resting state fMRI (minutes after the start of medetomidine infusion). Imaging protocol carried out 3 weeks after MCAO/Sham surgery and 1 week before stem cell transplantation. * represents statistical differences compared to the Sham-Vehicle Group ($p < 0.05$, One-way ANOVA with Bonferroni correction for multiple comparisons). Sham-Vehicle (n= 5), MCAO-Vehicle (n= 6), MCAO-CTX (n= 7). Data expressed as the mean±SD.

Variable	Sham-Vehicle	MCAO-Vehicle	MCAO-CTX cell
Time from infusion start (min)	84 ± 21	81 ± 14	91 ± 34
Body weight (g)	402 ± 37	$349 \pm 40^{*}$	$335 \pm 29^{**}$
Temperature $°C$	37.0 ± 0.3	37.1 ± 0.4	37.3 ± 0.2
Heart Rate (bpm)	225 ± 10	228 ± 28	234 ± 22
MABP (mmHg)	93 ± 10	88 ± 7	87 ± 8
PaCO$_2$ (mmHg)	42.2 ± 4.0	42.9 ± 4.4	39.5 ± 2.3
PaO$_2$ (mmHg)	106.8 ± 20.3	99.5 ± 11.1	106.9 ± 15.5
pH	$7.483 \pm 0.04^{\dagger}$	7.443 ± 0.05	$7.473 \pm 0.05^{\dagger}$
Inspired O$_2$ (%)	27.4 ± 2.13	29.3 ± 3.9	28.3 ± 2.4

Table 11: Physiological variables at the time of Resting state fMRI (minutes after the start of medetomidine infusion). Imaging protocol carried out 6 week following stem cell transplantation. * $p< 0.05$, ** $p< 0.001$, statistical differences compared to the Sham-Vehicle Group; (One-way ANOVA with Bonferroni correction for multiple comparisons). † $p< 0.05$, statistical difference between the Pre-transplant variable of the same group Sham-Vehicle (n= 7), MCAO-Vehicle (n= 7), MCAO-CTX (n= 7). Data expressed as the mean$\pm$SD.

Naïve networks and thresholding

During optimisation of the resting state sequence and anaesthesia, naïve rats were placed under medetomidine-isourane anaesthesia and resting state fMRI data were acquired as described above. All physiological variables were in range and SNR was over 50. The same pre-processing and analysis pipeline was used, apart from unwarping. As seen in Figure 71, animals had a complete bilateral sensorimotor network across the whole cortex.

As stated above, a correlation coefficient threshold of 0.3 (0.31, after Z′ transform) was chosen for network identification. Figure 71 demonstrates the effecting of varying statistical thresholds on sensorimotor network identification. Low statistical thresholds ($\rho = 0.1, 0.2$) increase the false positive rate (Type I error) with noise voxels identified as statistically significant. Alternatively, high thresholds ($\rho = 0.4$) increase the false negative rate (Type II error), often negating voxels contralateral to the seed region limiting significant voxels to the ipsilateral hemisphere.
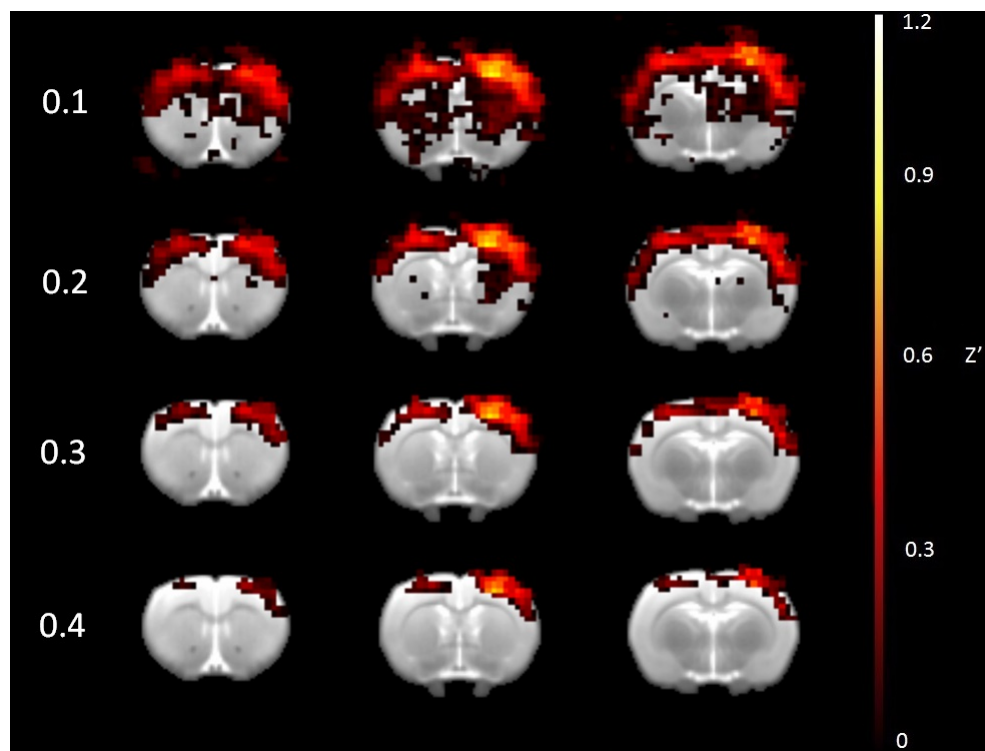
Figure 71: Mean global maps of the cortical resting-state sensorimotor networks of two naïve rats at varying correlation coefficient thresholds (left). The choice of correlation coefficient threshold determines ratio of voxel Type I and II errors.

Challenges with the ischaemic hemisphere

During the analysis process it became clear that despite robust coregistration, in animals where the infarct involved the dorso-lateral cortex, contamination of any seed ROIs voxels with CSF from within the ischaemic infarct and/or expanded ventricles would lead to maps with spurious correlations with other areas of high CSF (Figure 72). The high T_2^* signal of CSF within the infarct caused falsely high correlations between bilateral homologous ROIs. Infarct volumes in both stroke groups were highly variable (Figure 67) and as such, seed ROIs were either clear, partially, or fully contaminated by CSF in a non-consistent manner. Masking of the ischaemic infarct from the resting-state data was unsuccessful due to partial volume effects and smoothing. As a result, attention was focused on the intact contralesional (right) hemisphere, as detailed below.
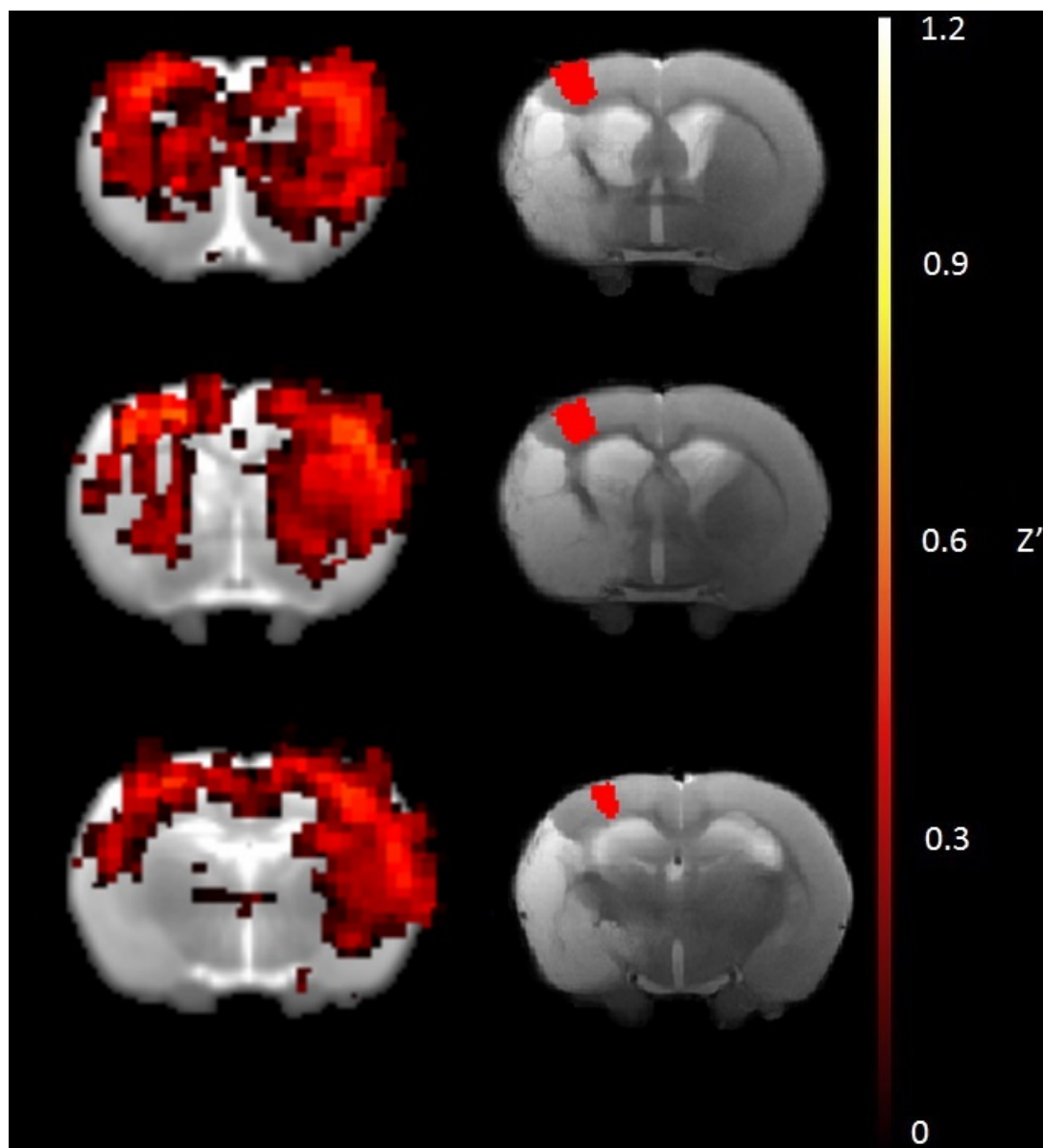
Figure 72: Global resting state map demonstrating the effect of brain deformation with white matter entering into the left S1FL seed ROI (red, right hand side). Brain distortion causes contamination of the ROI with white matter/CSF leading to correlations between the infarct, white matter, and the ventricles. Global comparisons based on the left S1FL thresholded at Fisher transformed correlation coefficient of 0.31 (left), the respective T_2 weighted RARE slices with S1FL seed ROI overlaid in red (right). Data from one animal. Colourbar represents the normalised correlation coefficient (Z') of the resting-state voxels.

The effects of CTX0E03 transplantation on resting state sensorimotor networks

Animals were transplanted with CTX0E03 cells or HypoThermsol vehicle (Sham, and MCAO controls) in the peri-infarct region as described earlier. Resting-state fMRI was conducted 1 week prior to, and 6 weeks following, transplantation.

Resting-state sensorimotor networks were derived using the right S1FL region as a seed for global correlations. Sham-Vehicle animals showed bilateral correlations of the sensorimotor cortex similar to a healthy/naïve sensorimotor network, 3 weeks following surgery (Figure 73). 6 weeks following CTX cell transplantation, the bilateral sensorimotor network was disrupted, likely due to the stereotaxic injection of Hypothermasol vehicle. This disruption was not reflected in the animal's functional ability with no significant effect on performance in behavioural tests (Figures 68, 69, and 70).

3 weeks following 90 min left tMCAO, the sensorimotor network was largely intact in the MCAO-Vehicle group (Figure 74) but not so in the MCAO-CTX group (Figure 75). There was some restoration of contralateral connectivity post-CTX cell transplantation and a small increase in connectivity around the seed following transplantation (Figure 75). As seen in the Sham group, stereotaxic implantation of Hypothermasol caused disruption of the resting network with a loss of left-hemisphere connectivity in both groups (Figures 74 and 75). However, as stated earlier, there was no detected functional improvement in behavioural tests following CTX cell transplantation.
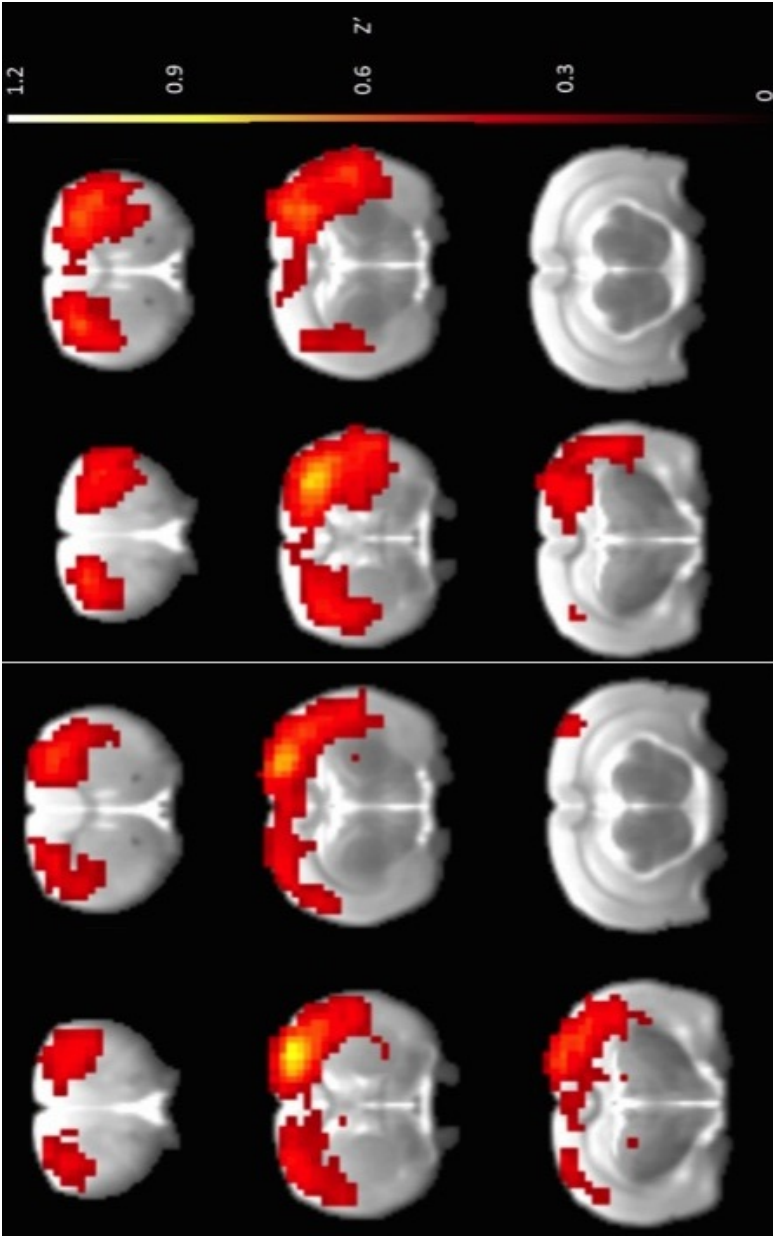
Figure 73: Sensorimotor resting-state network of the Sham-Vehicle group. **Left**: 3 weeks following 90 min Sham tMCAO; 1 week prior to stereotaxic injection of Hypothermasol vehicle into the left striatum (n= 5). **Right**: 6 weeks following stereotaxic injection of Hypothermasol vehicle. (n= 7). Global comparisons based on ROI in right S1FL thresholded at Fisher transformed correlation coefficient of 0.31. Resting state networks were derived using the DPABI toolbox and images generated using MRICRO.
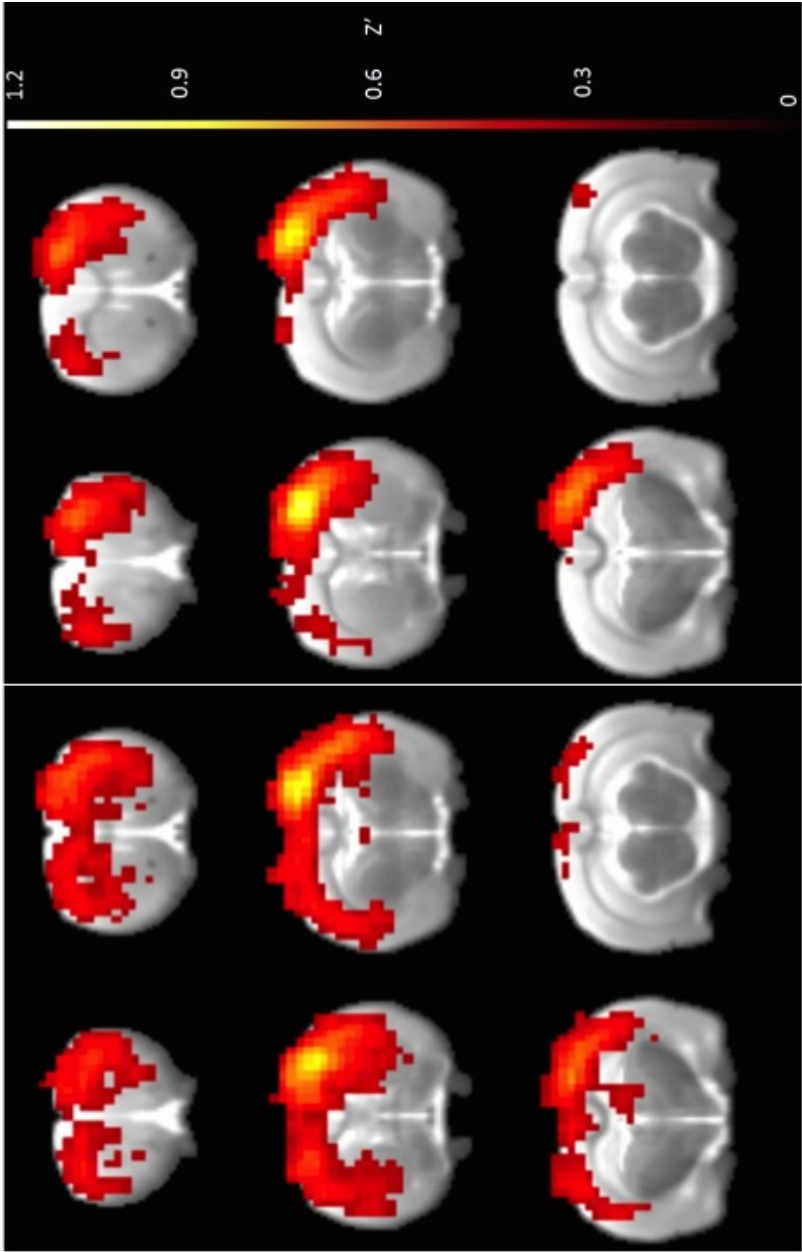
Figure 74: Sensorimotor resting-state network of the MCAO-Vehicle group. **Left**: 3 weeks following 90 min tMCAO; 1 week prior to stereotaxic injection of Hypothermasol vehicle into the left striatum (n= 7). **Right**: 6 weeks following stereotaxic injection of Hypothermasol vehicle (n= 8). Global comparisons based on ROI in right S1FL thresholded at Fisher transformed correlation coefficient of 0.31. Resting state networks were derived using the DPABI toolbox and images generated using MRICRO.
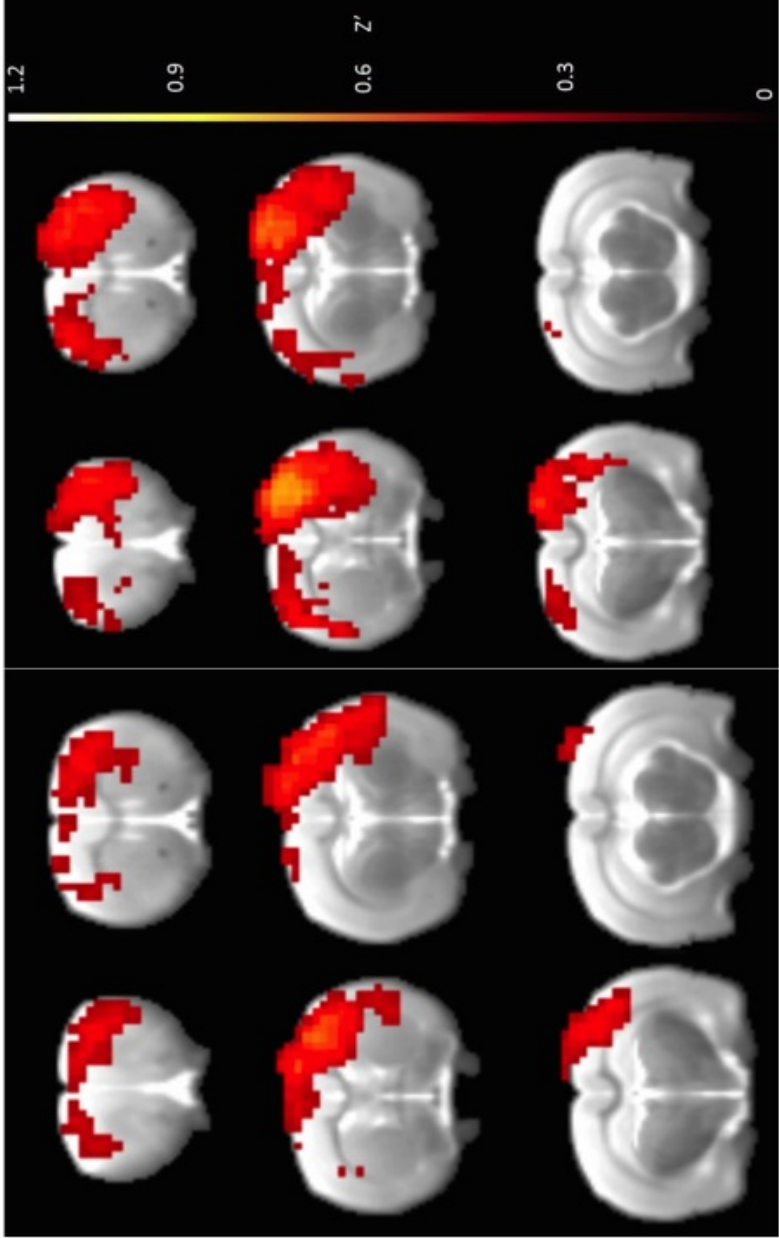
Figure 75: Sensorimotor resting-state network of the MCAO-CTX cell treated group. **Left**: 3 weeks following 90 min tMCAO; 1 week prior to stereotaxic injection of CTX0E03 cells into the left striatum (n= 7). **Right**: 6 weeks following stereotaxic injection of CTX0E03 cells (n= 7). Global comparisons based on ROI in right S1FL thresholded at Fisher transformed correlation coefficient of 0.31. Resting state networks were derived using the DPABI toolbox and images generated using MRICRO.

Resting-state sensorimotor networks and infarct location

With previous studies reporting post-stroke sensorimotor network recovery being dependent on the size of the ischaemic infarct (Weber et al., 2006; vanMeer et al., 2010) and with no evidence of behavioural or network recovery in the above results, the effect of infarct distribution on network connectivity was investigated.

Therefore, MCAO-Vehicle and MCAO- CTX animals were pooled and then re-grouped according to whether the ischaemic infarct encompassed the subcortical tissue or entorhinal cortex area only, or was more extensive and involving areas of the sensorimotor cortex (Figure 76). Four animals from the vehicle treated and one from the CTX cell treated group had large infarcts which involved the sensorimotor cortex (141 ± 48mm^3, mean$\pm$SD). Four animals from the vehicle treated and six from the CTX cell treated group had infarcts contained within the striatum and entorhinal cortex only (42 ± 30mm^3, mean$\pm$SD).
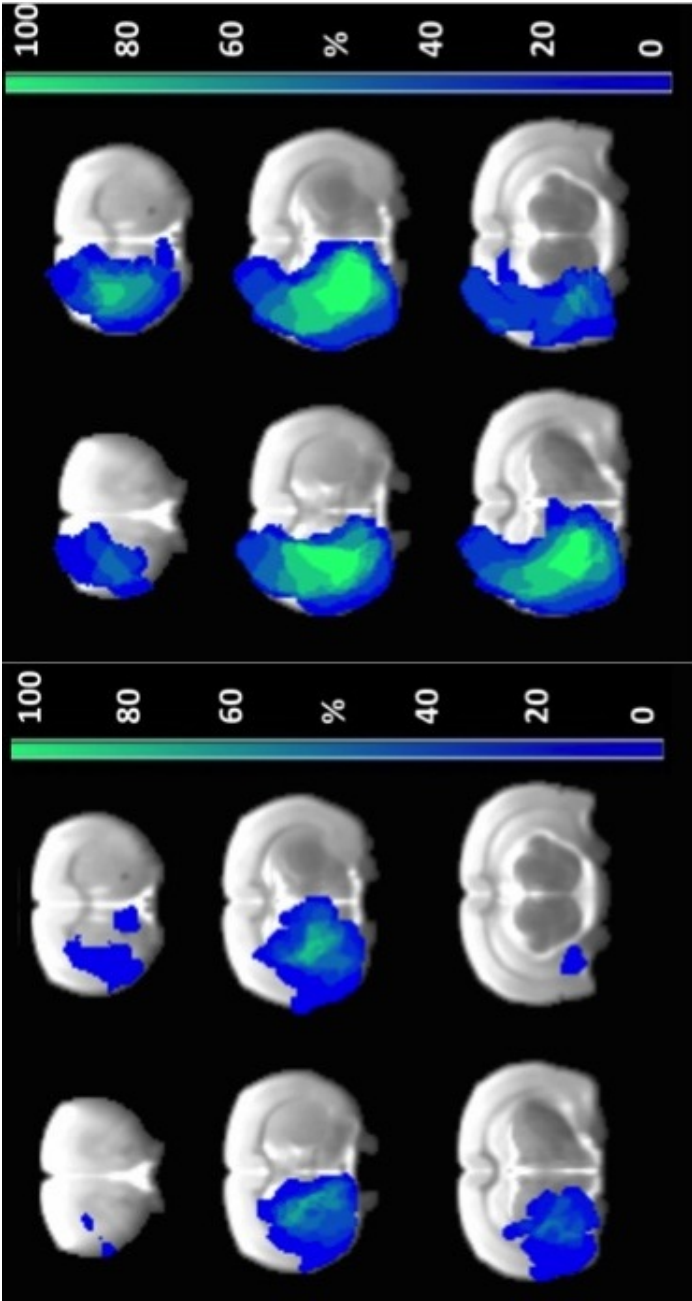
Figure 76: The percentage of voxels which contained ischaemic infarct and grouped according to infarct distribution. **Left**: Animals with subcortical strokes where ischaemic infarcts involved the striatum and/or the entorhinal cortex. (n= 10). **Right**: Animals with infarcts encompassing the striatum, entorhinal and the sensorimotor cortex. The percentage distribution of ischaemic infarcts which affected the sensorimotor cortex (n= 5). The infarct distribution was calculted on MATLAB and images generated using MRICRO.

Three weeks post-stroke, animals with infarcts confined to the left striatum and entorhinal cortex had a partial bilateral sensorimotor network and strong correlations with the whole right sensorimotor cortex (Figure 77). In animals with large infarcts, correlations were mostly restricted to the contralesional cortex around the seed with some contralateral correlations(Figure 78).

As mentioned earlier, it was seen in all treatment groups that stereotaxic injection appeared to disrupt bilateral connectivity of the resting sensorimotor network. When grouping based in infarct location, stereotaxic injection caused small changes in post-stroke networks in both groups with a loss of remaining contralateral networks which previously existed. This was more pronounced in the group with large infarcts involving the sensoirmotor cortex (Figure 78). There was also an increase in the ipsilesional intrahemispheric correlations in this group.
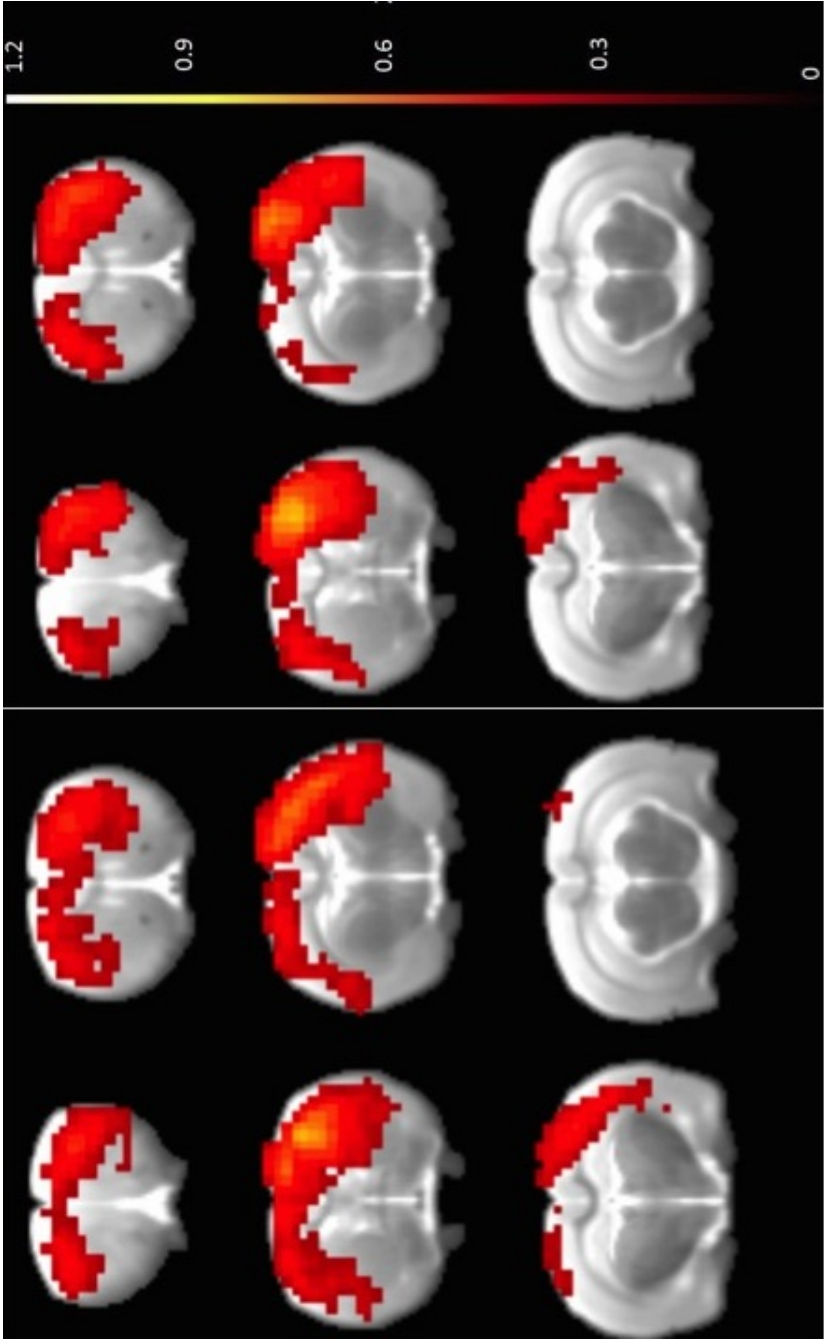
Figure 77: Mean global resting-state cortical sensorimotor network of pooled pre-CTX cell/vehicle transplant stroke group animals with infarcts confined to the striatum and entorhinal cortex. **Left**: 3 weeks following 90 min tMCAO; 1 week prior to stereotaxic injection of CTX0E03 cells into the left striatum (n= 10). **Right**: 6 weeks following stereotaxic injection of CTX0E03 cells (n= 10). Global comparisons based on ROI in right S1FL thresholded at Fisher transformed correlation coefficient of 0.31. Resting state networks were derived using the DPABI toolbox and images generated using MRICRO.
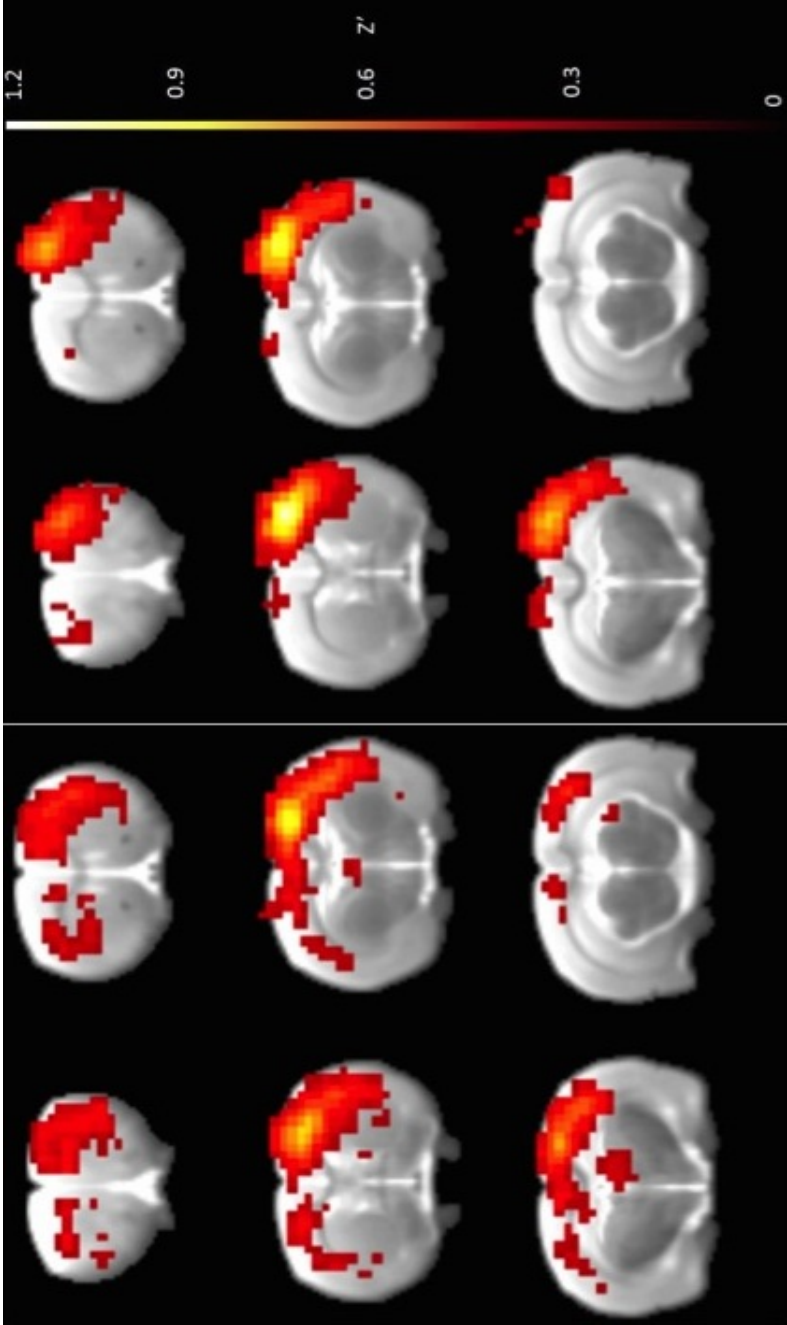
Figure 78: Mean global resting-state cortical sensorimotor network of pooled pre-CTX cell/vehicle transplant stroke group animals with infarcts confined to the striatum, entorhinal cortex and sensorimotor cortices. **Left**: 3 weeks following 90 min tMCAO; 1 week prior to stereotaxic injection of CTX0E03 cells into the left striatum (n= 5). **Right**: 6 weeks following stereotaxic injection of CTX0E03 cells (n= 5). Global comparisons based on ROI in right S1FL thresholded at Fisher transformed correlation coefficient of 0.31. Resting state networks were derived using the DPABI toolbox and images generated using MRICRO.

Connectivity correlations with the left S1FL

In Sham-vehicle treated animals, the absence of stroke and the challenges it caused (described in Figure 72) were not present. As such the left S1FL region of the cortex could be used as as seed region. Here the bilateral sensoriomotor network was detectable prior to the Hypothermasol vehicle transplantation (Figure 79).

Following stereotaxic implantation of HypoThermasol (Figure 79) scarring and bleeding generated by the procedure caused susceptibility artefacts and distorions near the seed region. As such, spurious correlations were generated.
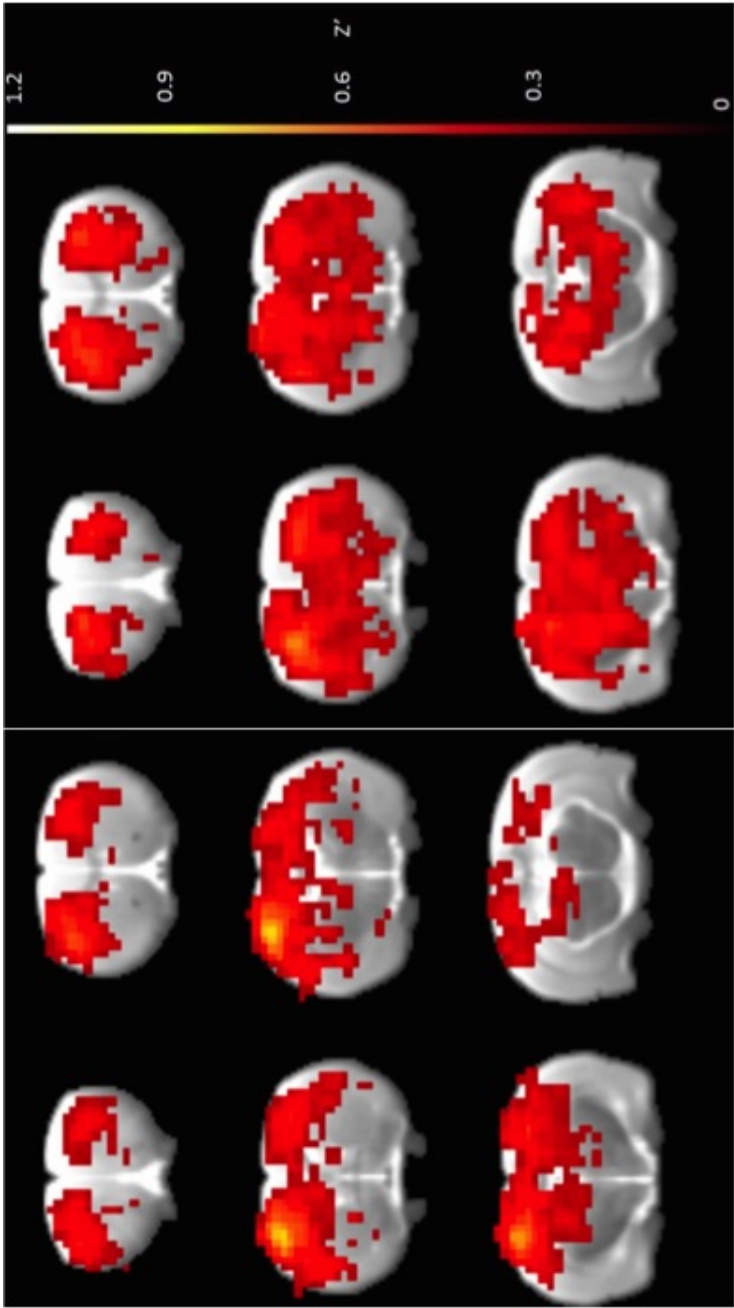
Figure 79: Mean global resting-state cortical sensorimotor network of Sham-vehicle transplant stroke group animals. **Left**: 3 weeks following 90 min Sham tMCAO; 1 week prior to stereotaxic injection of CTX0E03 cells into the left striatum (n= 5). **Right**: 6 weeks following stereotaxic injection of CTX0E03 cells (n=7). Global comparisons based on ROI in left S1FL thresholded at Fisher transformed correlation coefficient of 0.31. Resting state networks were derived using the DPABI toolbox and images generated using MRICRO.

Intra-hemispheric connectivity of the contralesional hemisphere

Intrahemispheric connectivity between different regions of the sensorimotor cortex was evaluated to determine whether resting-state fluctuations in the non-infarcted hemisphere change in response to stroke in the long-term. Correlations were assessed as previously described, by treatment group and pooled infarct location. Correlations between M1 (Figure 80) and S1BF (Figure 81) regions and the homotopic S1FL were compared. No differences were found between any groups at any time points with no effect of infarct size or CTX-cell treatment on intra-hemisphere connectivity.
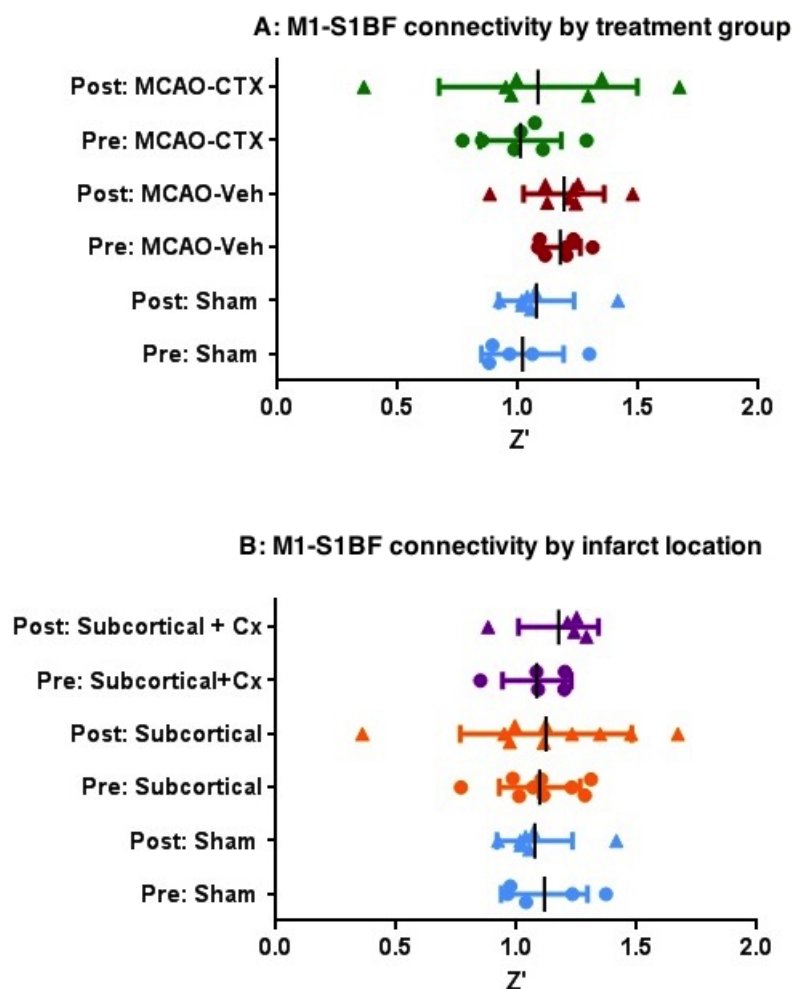
Figure 80: Intrahemispheric connectivity (Fisher transformed correlation coefficients Z′) of the contralesional M1 and S1FL regions of the sensorimotor cortex. Pre- and post-transplantation data displayed by treatment group (A) and pooled stroke volume location (B). There were no statistical differences between any groups and any time points (One-way ANOVA with Bonferroni correction for multiple comparisons, $p > 0.05$). Data are displayed for individual animals along with the mean and SD. Error bars: mean±SD.
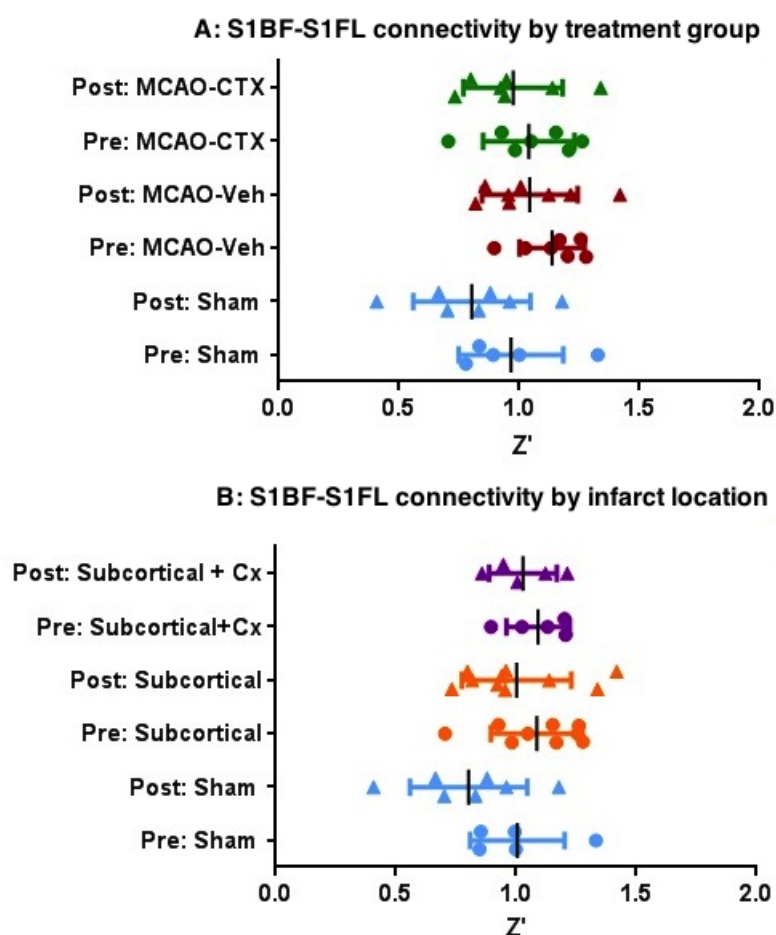
Figure 81: Intrahemispheric connectivity (Fisher transformed correlation coefficients Z') of the contralesional S1BF and S1FL regions of the sensorimotor cortex. Pre- and post-transplantation data displayed by treatment group (A) and pooled stroke volume location (B). There were no statistical differences between any groups and any time points (One-way ANOVA with Bonferroni correction for multiple comparisons, p> 0.05). Data are displayed for individual animals along with the mean and SD. Error bars: mean±SD.

The sensorimotor network of an animal with a failed MCAO

One animal was excluded from the longitudinal study due to a failed-MCAO and used for a terminal optimisation study under the same anaesthesia protocol, gradients, sequence, preprocessing, and analysis pipeline detailed above. The failed MCAO surgery had occurred 3 weeks earlier, as such, the animal was scanned at an analogous time as all animals recruited into the longitudinal study. Functional assessments showed no evidence of stroke-induced functional deficits, i.e. preserved vibrissae evoked forelimb function, which were confirmed by the absence of an ischaemic infarct on the T_2 weighted RARE. Figure 82 shows that there was an absence of the bilateral sensorimotor resting-state network similar to the animals that had undergone MCAO.
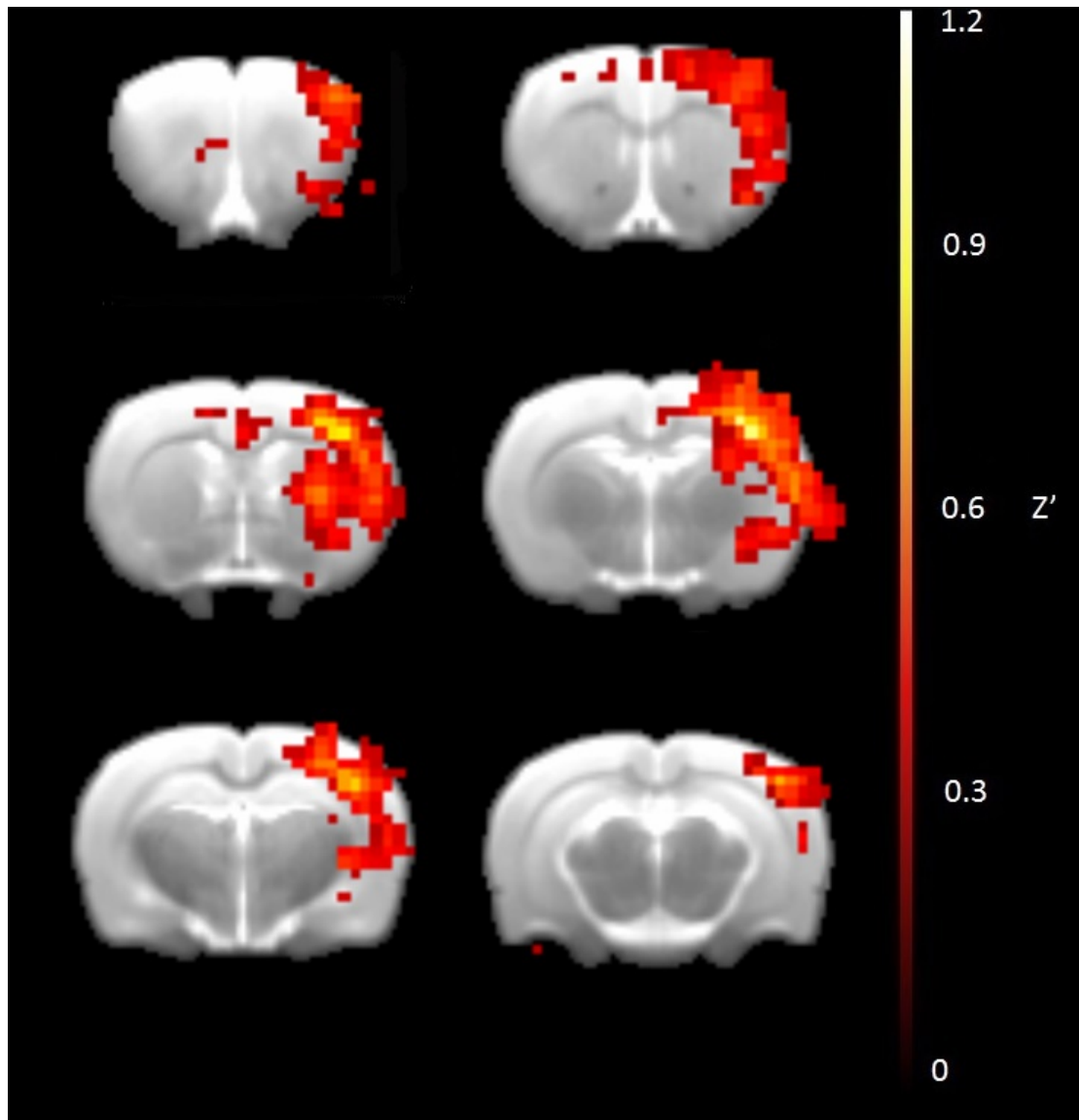
Figure 82: Mean global maps of the cortical resting-state sensorimotor networks of an animal with failed MCAO, with no evidence of functional deficits or ischaemic infarction on T_2 weighted MRI. Global comparisons based on ROI in left S1FL thresholded at Fisher transformed correlation coefficient of 0.324.

5.5 DISCUSSION

5.5.1 *The lack of functional improvement following CTX-cell treatment*

There was no evidence of sensorimotor functional improvement (Figures 68, 69 & 70) or changes in the resting-state sensorimotor network following CTX0E03 transplantation (Figure 75). This is contrary to previous studies using the same model of stroke and same stem cell line (Pollock et al., 2006; Stroemer et al., 2009; Smith et al., 2012) for which there are many potential causes.

Firstly, the stem cells may not have been successfully transplanted. This can be confirmed by histological analysis to identify any surviving cells or markers of differentiation as used in previous work. Secondly, damage caused by the needle tract may have offset any potential therapeutic effect of the stem cell placement (details below). In comparison to previous studies, functional MRI using medetomidine was used. Dexmedetomidine been reported to be neuroprotective at the acute stage via intravenous infusion (Jolkkonen et al., 1999), and there is no evidence on the effects of multiple medetomidine administrations over a long period of time. However the effect of multiple surgeries throughout the study cannot be discounted. One potential issue is the study design. By randomisation of treatment groups with small n numbers, there is a risk of an unequal distribution of small and large strokes. This was the case in this longitudinal study (Figure 67). Randomisation was not carried out in earlier CTX-cell studies. This increases the inter-group variability, potentially generating noise which may obscure any stem cell related effect. Allocating animals to treatment groups based on infarct volume to ensure

equal variance between groups could be considered for future studies.

5.5.2 *Functional assessments and the absence of spontaneous recovery*

Left transient MCAO induced sustained right forelimb impairment identified via the Staircase, Adjusting Steps, and Whiskers tests (Figures 68, 69, & 70). The main finding is that CTX cell transplantation generated no improvement in MCAO induced sensorimotor dysfunction in all three behavioural assessments used. In this longitudinal study there was no evidence of spontaneous recovery in either stroke group, despite evidence of this in the earlier pilot study (Chapter 3). Caleo (2015) also showed no spontaneous recovery in animals with ischaemic stroke induced by intracerebral endothelin-1. The MCAO-control group in Stroemer et al. (2009) also showed no spontaneous recovery. Blinding and randomisation of study animals reduces experimenter bias. As such, the spontaneous recovery seen in the pilot study may be attributable to bias, as the study was not blinded. Where infarctions are restricted to small volumes of tissue (such as in the 12-week pilot study), it is possible that the greater volume of surviving tissue has a greater capacity for repair of damaged circuits compared to large infarctions encompassing large structures and nuclei.

The absence of spontaneous recovery may also be attributable to the stereotaxic injection of CTX cells or HypoThermasol (HTS) vehicle. Following stereotaxic injection of HTS in the sham animals, there was an observed (but not statistically significant) reduction in right pellet retrieval (Figure 68) coupled with a loss of bilateral functional connectivity in the area of the cortex approximate

to the site of transplantation (Figure 73). When seeded in the left S1FL, some bilateral connectivity seems apparent (Figure 79) however this may be due to contamination of the ROI with the needle tract (containing blood/glial scarring/distorted white matter/ventricles), leading to spurious correlations. Differences in the implantation site due to the varied infarct volumes may have also contributed to these differences.

Inserting the injection needle in the brain causes an injury. Cortical stab injuries, biopsies, and electrode placements have been shown to cause microglial and macrophage recruitment and astrocytic scarring for up to 8 weeks, with a subsequent reduction in the counts of both cell types (Potter et al., 2012; Hampton et al., 2004). There is limited published research on the functional and anatomical consequences of stab injury. Stereotaxic injection into the caudate nucelus will damage both the overlying cortex, overlying vasculature, and the corpus callosum.

With the corpus callosum having a role in interhemispheric communication, it is unsurprising that damage caused by a stereotaxic procedure, may disrupt interhemispheric bilateral correlations in the BOLD signal. There is some qualitative evidence that correlations around the right S1FL seed region increased after stereotaxic needle insertion through the left hemisphere (Figures 75 & 78). Potter et al. (2012) showed that beyond 8 weeks post-stab injury, astrocytes and microglial cell counts decreased. It may be that at the time of the post-transplant scan (6 weeks after surgery), inflammation and scarring was still present, impeding connectivity and functional outcome. However the plateau in the Sham-vehicle pellet retrieval numbers beyond 4 weeks post-surgery (Figure 68)

suggests otherwise.

It is possible that the damage caused by stereotaxic implantation of CTX0E03 cells or HTS vehicle generated an additional source of noise in the behavioural data, clouding any functional improvements generated by the stem cells, although this was not seen in the Bilateral Assymetry test in previous work (Stroemer et al., 2009; Smith et al., 2012). Histological staining and immunocytochemistry of the implantation site and needle tract would confirm the presence of scarring, inflammation, and damage to the cortex and corpus callosum. The study by Frost et al. (2006) on the capsular endothelin-1 infarct model showed no functional impairments of saline injection into the posterior limb of the internal capsule compared to baseline performance.

Previous *in vivo* studies involving CTX cell transplantation (Stroemer et al. (2009) & Smith et al. (2012)) all used the Bilateral Asymmetry and Rotameter tests to assess post-transplantation functional recovery. The Bilateral Asymmetry test did not detect any long-term sensorimotor dysfunction in our hands (Chapter 3) and there were no facilities for Rotarod assessments. The Staircase, Adjusting Steps, and Whiskers test were piloted and selected for longitudinal assessment of post-stroke function, and deemed sensitive enough to detect functional recovery following CTX cell transplantation.

The Staircase test (Montoya et al., 1991) is a sensitive assessment of post-stroke dysfunction in rodent models due its ability to assess forelimb function independently with limited assessor bias. However, the gross summation of pellets retrieved that are used as a metric of performance, lack sensitivity in the fine aspects of

motor control. It was common to observe rats attempting pellet retrieval but failing to and displacing them to other steps. Colour coding of the pellets relative to their original step has shown to increase the sensitivity of the staircase test to impairments in dexterity in focal ischaemia and Parkinsonian models (Kloth et al., 2006). In the single pellet reaching task the animal is trained to reach forward for a single pellet and retrieve it. Although this assessment can be subject to the same rudimentary assessments as the Staircase test, detailed biometric assessments have been developed to fully elucidate the changes in all the components of the reaching act (lifting, reaching, pronation, grasping, supination and single digit movements), (Gharbawie et al., 2006; Alaverdashvili et al., 2008; Alaverdashvili and Whishaw, 2008). Such analyses further expand the data available from a simple task, but also allow investigations into compensatory mechanisms following injury.

Chronically diet-restricted rats performing the Staircase test often exhibited rushed and frantic behaviour when retrieving the pellets. It is therefore likely that this behaviour may have decreased the number of pellets the rats were able to retrieve had they been calmer. Because the Staircase limits the task retrieval to the individual forelimb, compensatory mechanisms such as increased use of the unimpaired forelimb or dexterous modification were undetectable. The Vermicelli test (Allred et al., 2008) or single pellet reaching task (see above) with additional biometric analyses could be more sensitive methods for detecting functional improvements following CTX0E03 cell transplantation which are likely to be more subtle than more gross assessments like the Staircase test. Where a range of tests are employed, the fewer that demonstrate a positive effect of therapy, the less likely the therapy

will translate to induce benefit in patients. Therefore tests such as the single pellet reaching task or Staircase test should be sufficient to determine whether a candidate therapy will translate.

5.5.3 *The ischaemic infarct*

CTX0E03 cells implanted into the peri-infarct region did not affect infarct volume (Figure 67). Conventional thought is that stem cell transplantation/administration does not replace volumes of dead tissue but instead provides a greater trophic environment for endogenous repair mechanisms to function (Bliss et al., 2007; Stroemer et al., 2009). As such, the current results are unsurprising. Small reductions in infarct volume over time are expected due the loss of the structural integrity of the infarcted hemisphere and the intraventricular pressure induced expansion of the ventricles into the territory. Mean infarct volumes in this study were markedly larger compared to volumes observed in pilot studies (Chapter 3). This is likely due to differences in the method of MCAO used, with the Stroemer method (conscious assessments of MCAO with the filament *in situ*), and the modified method used for this longitudinal study (Section 5.3.4). The mean arterial blood pressure (MABP) of awake rats is higher than in those under isoflurane anaesthesia (Buñag and Butterfield, 1982; Masamoto et al., 2009a). As such, recovery of the animal with the filament *in situ* is likely to lead to an increase in collateral flow to the occluded territory, maintaining penumbra viability, and reducing the volume of infarcted tissue. Lower MABP under anaesthesia will limit collateral flow to the occluded territory, leading to a larger infarct volume.

Animal models of ischaemic stroke allow for greater control in infarct location and volume compared to the highly variable human population. However they are not without their caveats. Intraluminal filament occlusion of the MCA at its origin is highly variable due to the risk of partial occlusion and perfusion into the MCA territory by Heubner pial anastomoses and other vessels (Heubner, 1874) makes the probability of cortical infarction difficult to predict (Brozici et al., 2003). The distribution of the ischaemic infarcts is often bimodal, between restriction to subcortical structures and those involving the sensorimotor cortex, as seen in the results in this Chapter. This has previously predicted the degree of spontaneous recovery with larger infarcts impairing recovery (Weber et al., 2008) & (vanMeer et al., 2010).

The location of an MCA territory infarct is therefore an important variable which can in part be determined by the model used. The vast majority of optical and electrophysiological studies investigating spontaneous recovery focus on cortical remapping and plasticity due to limitations of the techniques (Nudo, 1999). It is important to recognise that plasticity mechanisms in the cortex are likely to be different compared to the basal ganglia and thalamus (both of which contain a higher percentage of white matter compared to the cortex) because of the different respective functional roles. Models of ischaemic stroke such as the distal diathermy, topical endothelin, or photocoagulation methods (Macrae, 2011) generate focal cortical infarcts capable of generating long-term sensorimotor deficits. Although not without their own respective caveats, generation of lesions specific to the cortex reduce intra-group variability, allowing for greater sensitivity in both imaging and functional assessments.

The contralesional hemisphere is known to have increased compensatory activity in the acute and sub-acute period post-stroke (Weiller et al., 1993; Pineiro et al., 2001; Ward et al., 2003b). Inter-ROI connectivity between sensorimotor regions was compared between treatment & vehicle groups and pooled stroke groups (Figures 81 & 80) to assess whether changes in intrahemispheric connectivity occurred as a result of the loss of bilateral connectivity. No differences were found between any groups. The variances in correlations observed are likely to be due the complexities of the BOLD signal discussed below.

5.5.4   *Considerations when analysing the chronic post-stroke brain*

The process by which focal ischaemic insults result in the destruction, loss of brain tissue and the subsequent neurological impairments are well understood (Dirnagl et al., 1999; Woodruff et al., 2011). However, the loss of brain tissue also has consequences for imaging methodologies that assess structural and functional changes longitudinally. When the primary inflammatory responses are resolved and the dead tissue cleared by the microglia and macrophages, the global architecture of the brain is permanently altered. Compromises in the structural integrity of the brain will cause deformation of primarily the ipsilesional hemisphere, caused by the replacement of the infarct with a fluid-filled cyst and by the IVP pressure gradient (Dereski et al., 1993).

Despite this, there is little literature available that has investigated longitudinal changes in the post-stroke brain, likely due to the cost and duration of such studies. The literature available is variable with many papers focusing on atrophic changes in the cortex and striatum Hara et al. (1993), Fujie et al. (1990) respectively, and

the substantia nigra (Abe et al., 2003) as detailed earlier in this thesis.

These changes are dynamic and occur over several months subsequent to the ischaemic insult. This generates a particular challenge in longitudinal imaging studies, in particular, functional based assessments. Seed-based functional analyses often depend on fitting the data set to normalised structural templates. By not taking into account structural distortions that occur post-stroke, templates (and seed-regions) may incorrectly coregister with the functional data, or the functional area e.g. forelimb area of S1 may either be infarcted, or plastic compensatory mechanisms have remapped the remaining cortical projections (Nudo, 1999). This is an issue in both pre-clinical and clinical investigations and requires further investigation (van den Heuvel and Pol, 2010).

In this study, anatomical MRI data was not analysed for gross structural distortions of the ipsilesional cortex. Analysis techniques such as Voxel Based Morphometry (VBM), Tensor Based Morphometry (TBM) and Voxel Lesion Symptom Mapping (VLSM) allow for additional semi-automated measurements of structure-function relationships in post-stroke brain changes (Crum et al., 2013).

5.5.5 *ROI based analyses for post-stroke resting-state fMRI*

The size and location of the seed ROI has an impact on the correlations derived. The larger the number of voxels within a ROI, the greater the SNR and the smaller the signal variance within, and as such, a larger number of voxels will be significantly correlated

to it. Using a surface coil means that the SNR decreases as a function of distance away from the coil. Subcortical regions therefore have lower SNR compared to cortical areas and cortical seed ROIs will correlate more highly with other cortical regions. Although cortico-cortical connectivity is more prevalent than cortico-striatal connections, it is important to note that SNR challenges may mean that existing networks are not detected.

The global signal is the average of signal fluctuations across the entire brain. Many resting-state MRI studies, where ROI based analyses have been used, have employed global signal regression as a means of nuisance regression of physiological and other sources of noise that are assumed to be uncorrelated to the seed voxel (Desjardins et al., 2001). In van Meer et al. (2010) and van Meer et al. (2012) global signal regression was utilised and both positive and negative resting-state correlations were identified with a seed region in the sensorimotor cortex. One of the outcomes of global signal regression is the generation of anti-correlated networks i.e. $\rho < 0$. Murphy et al. (2009) have comprehensively demonstrated that by regressing out the global signal, the sum of the voxel-wise correlations across the whole brain will by less than or equal to zero. It is therefore purely a mathematical consequence of the regression that anti-correlated networks arise. The size of the ROI used also determines the extent to which noise will become negatively correlated with a larger ROI causing a greater negative correlation (Murphy et al., 2009). By not using global signal regression in the analyses of this thesis, negative BOLD signal correlations were not identified.

Challenges were identified using seed regions within the ischaemic hemisphere and the effect of cortical atrophy several

weeks post stroke (Section 5.4.5). Contamination of the cortical seed ROIs with CSF or white matter in data sets with large ischaemic infarcts delivered challenges in robust group-wise analysis (Figure 72). Both vanMeer et al. (2010) and van Meer et al. (2012) segmented the lesion out of the functional data as well as performing global signal regression to remove the confounds of infarct infiltration into the S1FL ROI used. However, by doing so, two situations arose. Firstly, any ROIs which contained infarcted tissues were truncated, and as such, their SNR reduced, directly affecting any correlations derived. Secondly, the negative connectivity found in both studies is a mathematical consequence of the regression procedure as detailed above. ROI truncation or modification to accommodate the infarcted hemisphere have also been used in human investigations (Rehme et al., 2011; Siegel et al., 2015).

Another challenge with ROI-based analysis in the post-stroke cortex is that the surviving tissue is likely to have remapped its functional representations (Rossini et al., 2003; Lim et al., 2014). Therefore, what represents an intact barrel field or forelimb region in a healthy animal, may not have the same functional representation post-stroke. However the area is still likely to represent the somatosensory region of the cortex as remapping is likely to occur within the volume represented by a single voxel (500μm and more so after spatial filtering). Increases in resolution would reduce the partial volume and infarct contamination effects that were encountered with the 500μm resolution used. However this comes at a cost of a reduction in SNR and increased imaging time. Regression of the CSF signal alone may limit the deleterious effects of the infarct when using ipsilesional or peri-infarct seed

regions.

ROI-based analyses involve a large number of *a priori* assumptions and present several challenged as mentioned above. Independent component analysis (ICA) is a popular method of resting state network analysis which can identify statistically significant networks within a data set (Beckmann et al., 2005). However, networks identified by ICA will still be affected by the infarcts so distinguishing functionally relevant networks from noise is still subject to user interpretation. Graph theory is another method of evaluating brain connectivity whereby the interactions between nodes (representing anatomical brain regions) are evaluated by metrics such as clustering, and small-worldness (Power et al., 2011). Such methods advance ways of understanding intrinsic connectivity changes in the brain and may prove useful in understanding post-stroke recovery mechanisms.

An overall assumption with BOLD imaging of the post stroke brain is that neurovascular coupling and the haemodynamic response function (HRF) are analogous to that of the healthy brain. However there is human evidence of delays in the HRF after stroke (Pineiro et al., 2002; Bonakdarpour et al., 2007). Post-stroke neuronal plasticity is accompanied by haemodynamic and reduced functional hyperaemic response compared to healthy counterparts (Girouard and Iadecola, 2006). A decrease in CBF responses to activation as well a loss of a group mean BOLD signal change but with consistent cerebral blood volume and CBF weighted responses has also been found in chronic post stroke patients (Blicher et al., 2012). This evidence suggests that there exists a dissonance in post-stroke neurovacular coupling.

Although implantation of CTX0E03 stem cells into the peri-infarct region failed to generate any functional recovery, this study was the first to utilise resting-state BOLD imaging for a cellular therapeutic in post-stroke rats. A point of interest is the apparent sensitivity of the resting state BOLD to stab injury via stereotaxic injection. However, as the resting-state was only acquired at one time-point 6 weeks post-transplantation it is difficult to ascertain whether these network impairment were a transient or permanent phenomenon and it is possible that the injury impeded spontaneous recovery.

GENERAL DISCUSSION

Stem cell therapy for ischaemic stroke may reduce the burden of disability 50% of survivors experience (Muir, 2010). Clinical trials of exogenous or autologous stem cells to treat ischaemic stroke are growing in number. However, population heterogeneity and small patient numbers make it difficult to determine the potential of such treatments. Resting-state fMRI may provide a means to assess functional changes following cell transplantation. This thesis detailed a novel attempt at using resting-state fMRI in a pre-clinical model of stroke with transplantation of a GMP cell line, CTX0E03, currently in a Phase 2 clinical trial.

This thesis reports the selection of appropriate longitudinal functional assessments for post-stroke disability, work to develop non-invasive physiological monitoring within a high-field MRI scanner, and a longitudinal study investigation of resting-state network changes both following stroke, and CTX-cell transplantation. In this longitudinal study, no functional improvement was seen with implantation of CTX-cells, in contrast to earlier work (Stroemer et al., 2009; Hassani et al., 2012; Smith et al., 2012) in the same rodent model of stroke. This study confirmed the previous work of van Meer et al. 2010a, 2010b, showing loss of bilateral sensorimotor network connectivity following MCAO. The study also showed that the resting-state sensorimotor network is sensitive to cortical damage caused by stereotaxic injection.

6.1 COMMENTS ON THE LONGITUDINAL STUDY

The longitudinal study detailed in Chapter 5 investigated resting state fMRI as a tool to identify functional recovery following a neural stem cell therapy for ischaemic stroke. Despite the lack of functional improvement following stem cell injection, changes in the resting state sensorimotor network were evident after stereotaxic injection into the caudate nucleus. Damage to the cortex and corpus callosum might impede post-stroke functional recovery and perturb bilateral connectivity or the implantation procedure itself generates an additional co-founder which may outweigh any functional improvements.

The intraluminal filament method is a popular method for MCAO due to its relative ease to perform, and since it generates subcortical infarcts with sensorimotor disability. However, the volumes and distribution of infarcts generated by this method are highly variable. MCAO methods such as distal coagulation, photothrombotic, and topical application of endothelin, can generate small focal lesions in the cortex with lower variability compared to the filament method. By destroying discrete regions of the cortex, e.g. S1FL, specific functional deficits can be observed (Schallert et al., 2000). When using small numbers of animals, such as around n=8 per group as in this study, limiting the inter-subject variance allows for a more robust assessment of a therapeutic agent. It may be the case, that the bimodal and unequal distribution of infarcts across both the MCAO vehicle and CTX-cell treatment groups generated variability greater than the effects of CTX-cell transplantation.

The intra-striatal implantation procedure caused a degree of damage to the brain which may have masked the effect of the cellular therapy. Scarring and bleeding caused by the implantation procedure is likely to have affecting resting-state networks. Further investigations into the effect of stereotaxic injury on resting-state networks would help evaluate the sensitivity of networks to injury. Earlier pilot work indicated that the behavioural tests used (intrinsic to behavioural and functional data) were sensitive enough to detect post-stroke functional recovery and group sizes for the longitudinal study were largely selected on a pragmatic basis and in relation to earlier work. However the sensitivity of the resting-state networks and the tests used (which were not applied in previous studies) suggests that a greater number of animals should be used to identify the effects of CTX-cell transplantation.

6.2 CHALLENGES REGARDING STEM CELL THERAPY FOR ISCHAEMIC STROKE

There are several possibilities as to why the CTX0E03 transplantation conducted in Chapter 5 did not demonstrate the same functional benefits as in previous studies conducted by Stroemer et al. (2009) and Smith et al. (2012). One possibility is that the cells were unsuccessfully transplanted. Although few cells survive post-transplant (Pollock et al., 2006; Stroemer et al., 2009), immunocytochemical staining for the human nuclear antigen (HuNuc) near the transplantation site should demonstrate the presence of any surviving cells to confirm successful transplantation.

Goldman (2016) recently reviewed the prospects of stem cell therapies for a plethora of neurological diseases. The pathological

consequences following an ischaemic insult are multifaceted, involving inammatory, necrotic, and oedematous processes in the acute stage with continued inflammation, and degeneration of neural pathways in the chronic phases (Figure 3, Tamura et al. (1991)). All cell types of the brain are affected by ischaemic stroke. As such, for the intention of cellular replacement, implanted stem cells would be required to not only differentiate into functioning neurons but into all other cells types within the CNS as well. The mechanisms by which neural progenitor cells are driven to their fates are also complex involving numerous molecular signals within a finely controlled environment (Harris et al., 2016). Furthermore, human stroke survivors often suffer from various co-morbidities such as hypertension and Type II Diabetes, which have deleterious effects on neurovascular coupling and function (Simpson et al., 1990; Girouard and Iadecola, 2006). Aside from cellular replacement, there is growing evidence of cellular treatments exerting a beneficial paracrine effect in the host brain, enhancing endogenous repair mechanisms (Carmichael, 2016). CTX0E03 cells are believed to operate by this mechanism (Stroemer et al., 2009; Hicks et al., 2013). Either way, implanted cells must survive for a reasonable amount of time within a deleterious post-stroke brain environment to exert a beneficial effect. This and the frequency of co-morbidities in stroke patients must be taken into account when undertaking BOLD imaging experiments.

Beyond cell replacement, exogenous transplantation of neural stem cells may also have a role in immunomodulation, which in turn influences neurogenesis (Kokaia et al., 2012). Although the mechanisms by which neural stem cells and the immune system interact are well established, it is yet to be elucidated as to whether this can be translated into a clinical environment.

Enhancement of the grafting environment may also improve cell viability. Various scaffolds and matrices for transplanted stem cells (often containing growth factors) have been investigated to improve graft survival and function (Bible et al., 2009; Skop et al., 2014). Scaffold design is complex due to the requirement for substrates to be produced in a sterile envionment and be non-toxic, injectable, biodegradable, and porous for cell and blood vessel integration. Candidate substrates include various gels (Jin et al., 2010), hyaluronic acid (Liang et al., 2013), and microparticles (Aliabadi and Lavasanifar, 2006).

Clinical trials of exogenous or autologous stem cells to treat ischaemic stroke are growing in number. However, the cell type and time of transplantation post-stroke varies greatly among trials (Sinden et al., 2012). Autologous mesenchymal stem cells appear to be the most popular cell type for transplantation (due to astrocytic fate (Kopen et al., 1999), and greater ethical acceptance compared to foetal cells). These are often administered intra-arterially or intravenously in the acute post-stroke period with an aim of neuroprotection. Human bone marrow stromal cells (hBMSCs) administered intra-arterially 60 days post-stroke accumulated in the spleen, reduced systemic inflammation and MHC-II positive cells in the brain (Acosta et al., 2015). The recent clinical trial data from Steinberg et al. (2016) and (Kalladka et al., 2016), both of which involved intracerebral transplantation of bone marrow derived MSCs and neural stem cells respectively, found improvements in functional outcome in small patient groups. However as these studies were open labelled and non-randomised safety trials, the interpretation of the secondary functional assessments should be treated with caution. A large (120 patient) multi-center trial of intravenous bone marrow stem cell treatment delivered in

the sub-acute stages post-stroke conducted by Prasad et al. (2014) showed no beneficial effects on functional outcome.

Although the outlook for stem cell therapy for stroke remains uncertain, there are other neurological diseases which are likely to benefit from cellular therapies. These include myelin specific diseases such as multiple sclerosis where injection of highly migratory glial progenitor cells have been shown to improve myelination (Windrem et al., 2004). Macular degeneration and other ocular diseases are good candidates for stem cell therapy due to the relative ease of being able to observe post-transplantation changes within the eye. These are currently in trial (Song et al., 2015; Schwartz et al., 2015).

6.3 APPROACHES TO RESTING STATE FUNCTIONAL MRI IN STROKE

Resting State fMRI is increasingly used as a clinical investigation due to the absence of task based assessments and the relative ease of acquisition. Pre-clinical work is more challenging due to the requirement to train conscious animals to remain stationary or to develop and optimise anaesthetic regimes which do not cause changes in the BOLD response. In rodents, medetomidine with or without isoflurane is now an accepted method for rs-fMRI imaging experiments with recovery (Weber et al., 2006; Zhao et al., 2008; Kalthoff et al., 2013). Alpha-chloralose and urethane are useful anaesthetics for non-recovery experiments (Hsu and Hedlund, 1998; Williams et al., 2010).

Analysis methods for resting state imaging are seed based, use Independent Component Analysis (ICA) or frequency based analyses such as Partial Directed Coherence (PDC). As described

earlier in this thesis, inter-ROI correlation coefficients are determined, not only by the low frequency BOLD fluctuations, but are also influenced by the SNR and partial volume effects. This is a particular challenge for ischaemic stroke data sets where contamination of the ROIs by the infarction or tissue distortion can cause erroneous network derivation. There appear to be limited solutions for this issue, primarily due to the heterogeneous size and location of ischaemic infarcts and the extent of the subsequent disability, making it difficult to ascertain standard post-stroke network changes. Possible approaches include a standardised method of nuissance regression against infarcts and CSF as well as agreement on ROI usage within the ischaemic hemisphere.

Non-invasive physiological control remains a significant challenge for rodent functional imaging. Although the use of end-tidal and subcutaneous capnography devices is commonly reported (Silva and Koretsky, 2002; Weber et al., 2006; Masamoto et al., 2009b), there tends to be little detail given on the details of the set up (Mirsattari et al., 2005). As demonstrated in Chapter 4, accurate end-tidal capnography within an MRI scanner is challenging due to the long sampling line lengths required. As such, a careful balance between sampling rate, ventilation volume, and respiration rate is required. A standardised methodology with optimal species/strain specific ventilation parameters would be of great benefit to the *in vivo* functional imaging field.

6.4   OTHER USES OF MRI IN ASSESSING STEM CELL THERAPIES

Other MR techniques may provide insight into cell fate and/or host responses to stem cell transplantation. Incorporation of

super-paramagnetic iron oxide particles (SPIOs) into exogenous cells allows for their identification *in vivo* due to the particles generating strong susceptibility gradients in T_2^* weighted images (Bulte et al., 2002; Sykova and Jendelova, 2007). However, the specificity of the ferrous signal to the grafts decreases over time due to the clearance of cells by microglia as well as challenges in identifying SPIO labelled cells from petichial blood post-ischaemia.

ASL uses a 180° inversion pulse to label intra-arterial water and determine CBF by measuring the net magnetisation of tissue after a pre-determined transit time (Detre et al., 1992). With some stem cell lineages reported to be pro-angiogenic (Jiang et al., 2005; Thored et al., 2007; Zhang et al., 2011) including CTX0E03 cells (Hicks et al., 2013), ASL (Arterial Spin Labelling) may be able to detect flow changes or improvements following treatment (Seevinck et al., 2010).

Magnetic resonance spectroscopy imaging (MRSI) measures the levels of metabolites such as lactate and *N*-acetyl-aspartate (NAA, believed to be a marker of neurons (Simmons et al., 1991)). This technique has been used to examine the post stroke brain (Weber et al., 2005). With stem cells purported to have largely neurotrophic actions (Burns and Steinberg, 2011), MRSI may provide evidence for the metabolic responses of the brain to stem cell treatment. However the technique is limited in *in vivo* models due to the large voxel sizes require limiting spatial specificity.

Diffusion tensor imaging (DTI) data was acquired during the longitudinal study (Chapter 5) to assess changes in anatomical connectivity but was not analysed for this thesis. DTI-derived

indices such as Fractional Anisotropy and Mean Diffusivity, allow for inferences on tissue structure via directional biases in tissue water diffusion (Beaulieu, 2002). Successful grafting of neural or oligodendrocyte precursors cells has previously been reported to change the diffusion properties within the brain after transplantation (Gupta et al., 2012), due to remyelination and differentiation into astrocytes and oligodendrocytes. Similar results have been reported in rodent stroke models (Jiang et al., 2006). Novel analysis techniques such as segmentation via k-means clustering (Jones et al., 2015) may provide a greater understanding of the post-stroke brain, especially in the peri-infarct region. Jones et al. (2015) have demonstrated that such methods have shown greater sensitivity to brain tumour infiltration and structural properties at a greater sensitivity compared to conventional anatomical methods. This technique may provide a detailed insight into the structural changes within the peri-infarct region and the transplantation site.

6.4.1 *Other imaging modalities*

The radiotracers ^{18}F-Fludeoxyglucose (FDG) and ^{15}O are highly sensitive markers of brain metabolism frequently used in brain research. The specificity of PET ligands make them a useful investigative tools to understand stem cell fate and responses. Prasad et al. (2014) used FDG PET to identify new regions of FDG uptake following intravenous cell transplantation. Although highly sensitive, the suitability of PET imaging is hindered by limitations in the number of widely available radioligands and the safe number of scans a patient can undertake.

Optical techniques allow for high resolution visualisation of the microvascular and cellular environment within the retina or cortex. Optical Coherence Tomography (OCT), (Huang et al., 1991) and Autoflourescence imaging provide a high resolution assessment suitable for the retina (or cortical layers *in vivo*). These techniques therefore would be preferable in the assessment of stem cell therapeutic efficacy for retinal diseases in humans (Jacobson et al., 2016). Bioluminescene imaging (where cells are labelled with luciferase) allows for longitudinal imaging of cell grafts and their fate and is a useful adjunct with optical imaging techniques (Love et al., 2007).

6.5 CONCLUSIONS

Overall, this thesis has illustrated the challenges and opportunities which arise from longitudinal investigations using post-stroke rodent models. From the selection of appropriate functional assessments; the continuing challenges of non-invasive physiological monitoring; the absence of functional improvement following CTX0E03 transplantation; and the unexpected sensitivity of resting-state fMRI to injury. The former finding opens up a discussion on how resting-state fMRI can be used to assess functional outcomes in post-surgical models and patients. This technique is a powerful and exciting tool to the neuroimaging field and used cautiously in combination with other advanced techniques, will continue to enlighten us into the workings of the brain.

REFERENCES

Abe, O., Nakane, M., Aoki, S., Hayashi, N., Masumoto, T., Kunimatsu, A., Mori, H., Tamura, A. and Ohtomo, K. (2003). MR imaging of postischemic neuronal death in the substantia nigra and thalamus following middle cerebral artery occlusion in rats, *NMR in Biomedicine* **16**(3): 152–9.

Abramsky, O., Carmon, A. and Benton, A. (1971). Masking of and by tactile pressure stimuli, *Perception and Psychophysics* **10**: 353–355.
URL: *http://dx.doi.org/10.3758/BF03207457*

Abrous, D., Koehl, M. and Moal, M. (2005). Adult neurogenesis: From precursors to network and physiology, *Physiological Review* **85**(2): 523–69.

Acosta, S. A., Tajiri, N., Hoover, J., Kaneko, Y. and Borlongan, C. V. (2015). Intravenous bone marrow stem cell grafts preferentially migrate to spleen and abrogate chronic inflammation in stroke., *Stroke* **46**(9): 2616–27.

Adams, H., Davis, P., Leira, E., Chang, K.-C., Bendixen, B., Clarke, W., Woolson, R. and Hansen, M. (1999). Baseline nih stroke scale score strongly predicts outcome after stroke: A report of the trial of org 10172 in acute stroke treatment (toast), *Neurology* **53**(1): 126.
URL: *http://www.neurology.org/content/53/1/126.abstract*

Adamson, J., Beswick, A. and Ebrahim, S. (2004). Is stroke the most common cause of disability?, *J Stroke Cerebrovasc Dis* **13**(4): 171–7.

Aguirre, G., Zarahn, E. and D'esposito, M. (1998). The variability of human, BOLD hemodynamic responses., *Neuroimage* **8**(4): 360–9.

Alaverdashvili, M., Foroud, A., Lim, D. H. and Whishaw, I. Q. (2008). "Learned baduse" limits recovery of skilled reaching for food after forelimb motor cortex stroke in rats: a new analysis of the effect of gestures on success., *Behav. Brain Res.* **188**(2): 281–90.

Alaverdashvili, M. and Whishaw, I. Q. (2008). Motor cortex stroke impairs individual digit movement in skilled reaching by the rat., *Eur. J. Neurosci.* **28**(2): 311–22.

Alexander, S. P. H., Mathie, A. and Peters, J. A. (2008). Guide to receptors and channels (grac), 3rd edition, *British Journal of Pharmacology* **153**(S2): S1–S1.
URL: *http://dx.doi.org/10.1038/sj.bjp.0707746*

Aliabadi, H. M. and Lavasanifar, A. (2006). Polymeric micelles for drug delivery., *Expert Opin Drug Deliv* **3**(1): 139–62.

Allred, R. P., Adkins, D. L., Woodlee, M. T., Husbands, L. C., Maldonado, M. A., Kane, J. R., Schallert, T. and Jones, T. A. (2008). The vermicelli handling test: A simple quantitative measure of dexterous forepaw function in rats, *Journal of Neuroscience Methods* **170**(2): 229 – 244.
URL: *http://www.sciencedirect.com/science/article/pii/S0165027008000502*

Altman, J. and Das, G. (1965). Autoradiographic and histological evidence of postnatal hippocampal neurogenesis in rats., *The Journal of comparative neurology* **124**(3): 319–335.
URL: *http://dx.doi.org/10.1002/cne.901240303*

Amarenco, P., Labreuche, J., Lavallée, P. and Touboul, P. (2004). Statins in stroke prevention and carotid atherosclerosis systematic review and up-to-date meta-analysis, *Stroke* **35**: 2902–2909.

Ames, A., Wright, R., Kowada, M., Thurston, J. and Majno, G. (1968). Cerebral ischemia. II. the no-reflow phenomenon., *Am. J. Pathol.* **52**(2): 437–53.

Arvidsson, A., Collin, T., Kirik, D., Kokaia, Z. and Lindvall, O. (2002). Neuronal replacement from endogenous precursors in the adult brain after stroke., *Nature Medicine* **8**(9): 963–70.

Ashby, F. G. (2011). *Statistical analysis of fMRI data*, MIT press.

Astrup, J., Symon, L., Branston, N. and Lassen, N. (1977). Cortical evoked potential and extracellular k+ and h+ at critical levels of brain ischemia., *Stroke* **8**(1): 51–7.

Attwell, D., Buchan, A., Charpak, S. and Lauritzen, M. (2010). Glial and neuronal control of brain blood flow, *Nature* **468**: 232–243.

Auer, D. P. (2008). Spontaneous low-frequency blood oxygenation level-dependent fluctuations and functional connectivity analysis of the 'resting' brain., *Magn Reson Imaging* **26**(7): 1055–64.

Bandettini, P. A. (2012). Twenty years of functional MRI: the science and the stories., *Neuroimage* **62**(2): 575–88.

Barth, T., Jones, T. and Schallert, T. (1990). Functional subdivisions of the rat somatic sensorimotor cortex., *Behavioural brain research* **39**(1): 73–95.

Barth, T. and Stanfield, B. (1990). The recovery of forelimb-placing behavior in rats with neonatal unilateral cortical damage involves the remaining hemisphere, *The Journal of Neuroscience*

10(10): 3449–3459.
URL: *http://www.jneurosci.org/content/10/10/3449.abstract*

Beart, P. and O'Shea, R. (2007). Transporters for l-glutamate: an update on their molecular pharmacology and pathological involvement., *Br. J. Pharmacol.* **150**(1): 5–17.

Beaulieu, C. (2002). The basis of anisotropic water diffusion in the nervous system - a technical review, *NMR in Biomedicine* **15**(7-8): 435–55.

Beckmann, C. F., Marilena, D., Devlin, J. T. and Smith, S. M. (2005). Investigations into resting-state connectivity using independent component analysis., *Philos. Trans. R. Soc. Lond., B, Biol. Sci.* **360**(1457): 1001–13.

Bederson, J., Pitts, L., Tsuji, M., Nishimura, M., Davis, R. and Bartkowski, H. (1986). Rat middle cerebral artery occlusion: evaluation of the model and development of a neurologic examination., *Stroke, a journal of cerebral circulation* **17**(3): 472–476.

Belluzzi, O., Benedusi, M. and Ackman, J. (2003). Electrophysiological differentiation of new neurons in the olfactory bulb, *The Journal of Neuroscience* **23**: 10411–10418.

Benton, A. L. and Levin, H. S. (1972). An experimental study of 'obscuration', *Neurology* **22**(11).
URL: *http://dx.doi.org/10.1037/h0033609*

Bergmann, O., Liebl, J., Bernard, S., Alkass, K., Yeung, M. S., Steier, P., Kutschera, W., Johnson, L., Landén, M., Druid, H., Spalding, K. L. and Frisén, J. (2012). The age of olfactory bulb neurons in humans., *Neuron* **74**(4): 634–9.

Bermejo, R., Vyas, A. and Zeigler, H. P. (2002). Topography of rodent whisking. two-dimensional monitoring of whisker

movements, *Somatosensory & Motor Research* **19**(4): 341–346.
URL: *http://dx.doi.org/10.1080/0899022021000037809*

Berthois, Y., Katzenellenbogen, J. A. and Katzenellenbogen, B. S. (1986). Phenol red in tissue culture media is a weak estrogen: implications concerning the study of estrogen-responsive cells in culture, *Proceedings of the National Academy of Sciences* **83**(8): 2496–2500.
URL: *http://dx.doi.org/10.1073/pnas.83.8.2496*

Bhasin, A., Srivastava, M., Kumaran, S., Mohanty, S., Bhatia, R., Bose, S., Gaikwad, S., Garg, A. and Airan, B. (2011). Autologous mesenchymal stem cells in chronic stroke., *Cerebrovascular Diseases extra* **1**(1): 93–104.

Bible, E., Chau, D. Y., Alexander, M. R., Price, J., Shakesheff, K. M. and Modo, M. (2009). Attachment of stem cells to scaffold particles for intra-cerebral transplantation., *Nature protocols* **4**(10): 1440–1453.
URL: *http://dx.doi.org/10.1038/nprot.2009.156*

Biernaskie, J., Szymanska, A., Windle, V. and Corbett, D. (2005). Bi-hemispheric contribution to functional motor recovery of the affected forelimb following focal ischemic brain injury in rats, *European Journal of Neuroscience* **21**(4): 989–999.
URL: *http://dx.doi.org/10.1111/j.1460-9568.2005.03899.x*

Biswal, B., Yetkin, Z. F., Haughton, V. M. and Hyde, J. S. (1995). Functional connectivity in the motor cortex of resting human brain using echo planar mri, *Magnetic resonance in Medicine* **34**(4).

Bland, J. and Altman, D. G. (2007). Agreement between methods of measurement with multiple observations per individual.,

Journal of biopharmaceutical statistics **17**(4): 571–582.
URL: *http://dx.doi.org/10.1080/10543400701329422*

Bland, J. M. and Altman, D. (1986). Statistical methods for assessing agreement between two methods of clinical measurement, *The Lancet* **327**(8476): 307–310.
URL: *http://dx.doi.org/10.1016/S0140-6736(86)90837-8*

Bland, J. M. and Altman, D. G. (1999). Measuring agreement in method comparison studies., *Statistical methods in medical research* **8**(2): 135–160.
URL: *http://dx.doi.org/10.1177/096228029900800204*

Blicher, J. U., Stagg, C. J., Jacinta, O., Östergaard, L., J, M. B., Heidi, J., Jezzard, P. and Donahue, M. J. (2012). Visualization of altered neurovascular coupling in chronic stroke patients using multimodal functional mri, *Journal of Cerebral Blood Flow and Metabolism* **32**(11): 2044–54.

Bliss, T., Guzman, R., Daadi, M. and Steinberg, G. K. (2007). Cell transplantation therapy for stroke., *Stroke* **38**(2 Suppl): 817–26.

Bonakdarpour, B., Parrish, T. and Thompson, C. (2007). Hemodynamic response function in patients with stroke-induced aphasia: implications for fMRI data analysis, *Neuroimage* **33**: 322–331.

Bouët, V., Thomas, F., Toutain, J., Divoux, D., Boulouard, M. and Schumann-Bard, P. (2007). Sensorimotor and cognitive deficits after transient middle cerebral artery occlusion in the mouse., *Experimental neurology* **203**(2): 555–567.
URL: *http://dx.doi.org/10.1016/j.expneurol.2006.09.006*

Boynton, G., Engel, S., Glover, G. and Heeger, D. (1996). Linear systems analysis of functional magnetic resonance imaging in human v1., *J. Neurosci.* **16**(13): 4207–21.

Branston, N., Symon, L., Crockard, H. and Pasztor, E. (1974). Relationship between the cortical evoked potential and local cortical blood flow following acute middle cerebral artery occlusion in the baboon., *Exp. Neurol.* **45**(2): 195–208.

Bressler, S. L. and Menon, V. (2010). Large-scale brain networks in cognition: emerging methods and principles, *Trends in Cognitive Science* **14**(6): 277–290.

Brooks, C. M. (1933). Studies on the cerebral cortex, *American Journal of Physiology – Legacy Content* **105**(1): 162–171.
URL: *http://ajplegacy.physiology.org/content/105/1/162*

Brott, T., Adams, H., Olinger, C., Marler, J. and Barsan, W. (1989). Measurements of acute cerebral infarction: a clinical examination scale., *Stroke* **20**: 864–870.

Brown, C. E. and Murphy, T. H. (2008). Livin' on the edge: imaging dendritic spine turnover in the peri-infarct zone during ischemic stroke and recovery., *Neuroscientist* **14**(2): 139–46.

Brozici, M., van der Zwan, A. and Hillen, B. (2003). Anatomy and functionality of leptomeningeal anastomoses: a review., *Stroke* **34**(11): 2750–62.

Bruce, D. (2001). Fifty years since lashley's search of the engram: refutations and conjectures., *J Hist Neurosci* **10**(3): 308–18.

Brus-Ramer, M., Carmel, J. B. and Martin, J. H. (2009). Motor cortex bilateral motor representation depends on subcortical and interhemispheric interactions, *The Journal of Neuroscience* **29**(19): 6196–6206.
URL: *http://dx.doi.org/10.1523/JNEUROSCI.5852-08.2009*

Buñag, R. and Butterfield, J. (1982). Tail-cuff blood pressure measurement without external preheating in awake rats., *Hypertension* **4**: 898–903.

Buchkremer-Ratzmann, I. and Witte, O. (1997). Extended brain disinhibition following small photothrombotic lesions in rat frontal cortex, *Neuroreport* **8**: 519–522.

Buckner, R. and JR, A. (2008). The brain's default network, *Ann. N.Y. Acad. Sci* **1124**: 1–38.

Buerkle, H. and Yaksh, T. L. (1998). Pharmacological evidence for different alpha 2-adrenergic receptor sites mediating analgesia and sedation in the rat., *British Journal of Anaesthesia* **81**(2): 208–215.

Bulte, J. W., Duncan, I. D. and Frank, J. A. (2002). In vivo magnetic resonance tracking of magnetically labeled cells after transplantation., *J. Cereb. Blood Flow Metab.* **22**(8): 899–907.

Burns, T. C. and Steinberg, G. K. (2011). Stem cells and stroke: opportunities, challenges and strategies., **11**(4): 447–61.

Buxton, R. and Frank, L. (1997). A model for the coupling between cerebral blood flow and oxygen metabolism during neural stimulation., *J. Cereb. Blood Flow Metab.* **17**(1): 64–72.

Bylund, D. B. (1988). Subtypes of alpha 2-adrenoceptors: pharmacological and molecular biological evidence converge., *Trends in pharmacological sciences* **9**(10): 356–361.

Calautti, C., Jones, P., Naccarato, M., Sharma, N., Day, D., Bullmore, E., Warburton, E. and Baron, J. C. (2010). The relationship between motor deficit and primary motor cortex hemispheric activation balance after stroke: longitudinal fMRI study., *J. Neurol. Neurosurg. Psychiatr.* **81**(7): 788–92.

Caleo, M. (2015). Rehabilitation and plasticity following stroke: Insights from rodent models., *Neuroscience* **311**: 180–94.

Cammermeyer, J. (1961). The importance of avoiding dark neurons in experimental neuropathology, *Acta Neurpathalogica* **1**: 245–270.
URL: *http://dx.doi.org/10.1007/BF00687191*

Carmichael, S. (2016). Emergent properties of neural repair: elemental biology to therapeutic concepts., *Ann. Neurol.* **79**(6): 895–906.

Carmichael, S., Archibeque, I., Luke, L., Nolan, T., Momiy, J. and Li, S. (2005). Growth-associated gene expression after stroke: evidence for a growth-promoting region in peri-infarct cortex., *Exp. Neurol.* **193**(2): 291–311.

Carter, A. R., Shulman, G. L. and Corbetta, M. (2012). Why use a connectivity-based approach to study stroke and recovery of function?, *Neuroimage* **62**(4): 2271–80.

Celesia, G., Polcyn, R., Holden, J., Nickles, R., Koeppe, R. and Gatley, S. (1984). Determination of regional cerebral blood flow in patients with cerebral infarction. use of fluoromethane labeled with fluorine 18 and positron emission tomography., *Arch. Neurol.* **41**(3): 262–7.

Cerni, C. (2000). Telomeres, telomerase, and myc. an update., *Mutation Research* **462**(1): 31–47.

Collignon, A., Maes, F., Delaere, D., Vandermeulen, D., Suetens, P. and Marchal, G. (1995). Automated multi-modality image registration based on information theory, *Information processing in medical imaging*, Vol. 3, pp. 263–274.

Corbetta, D., Sirtori, V., Moja, L. and Gatti, R. (2010). Constraint-induced movement therapy in stroke patients: systematic review and meta-analysis., *European journal of physical and rehabilitation medicine* **46**(4): 537–544.

Crum, W. R., Giampietro, V. P., Smith, E. J., Gorenkova, N., Stroemer, R. and Modo, M. (2013). A comparison of automated anatomical-behavioural mapping methods in a rodent model of stroke., *Journal of neuroscience methods* **218**(2): 170–183.
URL: *http://dx.doi.org/10.1016/j.jneumeth.2013.05.009*

Curtis, M. A., Kam, M., Nannmark, U., Anderson, M. F., Axell, M. Z., Wikkelso, C., Holtås, S., van Roon-Mom, Willeke M, Thomas, B., Nordborg, C., Frisén, J., Dragunow, M., Faull, R. L. and Eriksson, P. S. (2007). Human neuroblasts migrate to the olfactory bulb via a lateral ventricular extension., *Science* **315**(5816): 1243–9.

da Fonseca, L. M., Gutfilen, B., de Castro, P. H., Battistella, V., Goldenberg, R. C., Tais, K., Chagas, C. L., Wajnberg, E., Maiolino, A., Xavier, S., Andre, C., Rosalia, M. and de Freitas, G. R. (2010). Migration and homing of bone-marrow mononuclear cells in chronic ischemic stroke after intra-arterial injection., *Experimental Neurology* **221**(1): 122–8.

Dancause, N. (2006). Vicarious function of remote cortex following stroke: recent evidence from human and animal studies., *Neuroscientist* **12**(6): 489–99.

Danielian, P. S., White, R., Hoare, S. A., Fawell, S. E. and Parker, M. G. (1993). Identification of residues in the estrogen receptor that confer differential sensitivity to estrogen and hydroxytamoxifen., *Molecular Endocrinology* **7**(2): 232–240.
URL: *http://dx.doi.org/10.1210/mend.7.2.8469236*

Dereski, M., Chopp, M., Knight, R. and Rodolosi, L. (1993). The heterogeneous temporal evolution of focal ischemic neuronal damage in the rat, *Acta Neuropathalogica* **85**: 327–333.

Deschênes, M., Bourassa, J. and Parent, A. (1996). Striatal and cortical projections of single neurons from the central lateral thalamic nucleus in the rat, *Neuroscience* **72**(3): 679 – 687.
URL: *http://www.sciencedirect.com/science/article/pii/0306452296000012*

Desjardins, A., Kiehl, K. and Liddle, P. (2001). Removal of confounding effects of global signal in functional MRI analyses., *NeuroImage* **13**(4): 751–758.
URL: *http://dx.doi.org/10.1006/nimg.2000.0719*

Detante, O., Moisan, A., Dimastromatteo, J., Richard, M., Riou, L., Grillon, E., Barbier, E., Desruet, M., Fraipont, F., Segebarth, C., Jaillard, A., Hommel, M., Ghezzi, C. and Remy, C. (2009). Intravenous administration of 99mTc-HMPAO-labeled human mesenchymal stem cells after stroke: in vivo imaging and biodistribution., *Cell Transplant* **18**(12): 1369–79.

Detre, J. A., Leigh, J. S., Williams, D. S. and Koretsky, A. P. (1992). Perfusion imaging, *Magnetic Resonance in Medicine* **23**(1): 37–45.

Dettmers, C., Young, A., Rommel, T., Hartmann, A., Weingart, O. and Baron, J. (1993). CO_2 reactivity in the ischaemic core, penumbra, and normal tissue 6 hours after acute MCA-occlusion in primates, *Acta Neurochiurgica* **125**(1-4): 150–155.

Dezawa, M., Kanno, H., Hoshino, M., Cho, H., Matsumoto, N., Itokazu, Y., Tajima, N., Yamada, H., Sawada, H., Ishikawa, H., Mimura, T., Kitada, M., Suzuki, Y. and Ide, C. (2004). Specific induction of neuronal cells from bone marrow stromal cells and application for autologous transplantation., *J. Clin. Invest.* **113**(12): 1701–10.

Dijkhuizen, R. M., Singhal, A. B., Mandeville, J. B., Wu, O., Halpern, E. F., Finklestein, S. P., Rosen, B. R. and Lo, E. H. (2003). Correlation between brain reorganization, ischemic damage, and neurologic status after transient focal cerebral ischemia in rats: a functional magnetic resonance imaging study., *J. Neurosci.* **23**(2): 510–7.

Dirnagl, U., Iadecola, C. and Moskowitz, M. (1999). Pathobiology of ischaemic stroke: an integrated view., *Trends in Neurosciences* **22**(9): 391–7.

Disbrow, E., Slutsky, D., Roberts, T. and Krubitzer, L. (2000). Functional MRI at 1.5 tesla: a comparison of the blood oxygenation level-dependent signal and electrophysiology., *Proc. Natl. Acad. Sci. U.S.A.* **97**(17): 9718–23.

Döbrössy and Dunnett (2005). Training specificity, graft development and graft-mediated functional recovery in a rodent model of huntington's disease., *Neuroscience* **132**(3): 543–552.
URL: *http://dx.doi.org/10.1016/j.neuroscience.2005.01.016*

Dohmen, C., Bosche, B., Graf, R., Reithmeier, T., Ernestus, R. I., Brinker, G., Sobesky, J. and Heiss, W. D. (2007). Identification and clinical impact of impaired cerebrovascular autoregulation in patients with malignant middle cerebral artery infarction., *Stroke* **38**(1): 56–61.

Donoghue, J. P., Kerman, K. L. and Ebner, F. F. (1979). Evidence for two organizational plans within the somatic sensory-motor cortex of the rat, *The Journal of Comparative Neurology* **183**(3): 647–663.
URL: *http://dx.doi.org/10.1002/cne.901830312*

Dunn, A. K., Devor, A., Dale, A. M. and Boas, D. A. (2005). Spatial extent of oxygen metabolism and hemodynamic changes

during functional activation of the rat somatosensory cortex, *Neuroimage* **27**(2): 279–290.

Endres, M., Namura, S., M, S., Waeber, C., Zhang, L., T, G., Hyman, B. and Moskowitz, M. (1998). Attenuation of delayed neuronal death after mild focal ischemia in mice by inhibition of the caspase family., *J. Cereb. Blood Flow Metab.* **18**(3): 238–47.

Engelhardt, B. and Sorokin, L. (2009). The blood-brain and the blood-cerebrospinal fluid barriers: function and dysfunction., *Semin Immunopathol* **31**(4): 497–511.

Eriksson, P., Perfilieva, E., T, B., Alborn, A., Nordborg, C., Peterson, D. and Gage, F. (1998). Neurogenesis in the adult human hippocampus., *Nature Medicine* **4**(11): 1313–7.

Ernst, A., Alkass, K., Bernard, S., Salehpour, M., Perl, S., Tisdale, J., Possnert, G., Druid, H. and Frisén, J. (2014). Neurogenesis in the striatum of the adult human brain, *Cell* **156**(5): 1–12.

Fabricius, M., Fuhr, S., Bhatia, R., Boutelle, M. and Hashemi, P. (2006). Cortical spreading depression and peri-infarct depolarization in acutely injured human cerebral cortex, *Brain* **129**: 778–790.

Farr, T. D. and Trueman, R. C. (2011). *Animal Models of Movement Disorders*, Vol. 62 of *Neuromethods*, Humana Press, chapter 6: Functional Assessment of Subcortical Ischemia, pp. 91–114.

Felleman, D. J. and Essen, D. C. (1991). Distributed hierarchical processing in the primate cerebral cortex, *Cereb Cortex* **1**(1): 1–47.

Ferezou, I., Haiss, F., Gentet, L. J., Aronoff, R., Weber, B. and Petersen, C. C. (2007). Spatiotemporal dynamics of cortical sensorimotor integration in behaving mice., *Neuron* **56**(5): 907–23.

Feustel, P., Ingvar, M. and Severinghaus, J. (1981). Cerebral oxygen availability and blood flow during middle cerebral artery occlusion: effects of pentobarbital., *Stroke* **12**(6): 858–63.

Fox, M. D. and Raichle, M. E. (2007). Spontaneous fluctuations in brain activity observed with functional magnetic resonance imaging., *Nature Reviews. Neuroscience* **8**(9): 700–11.

Fox, P. and Raichle, M. (1986). Focal physiological uncoupling of cerebral blood flow and oxidative metabolism during somatosensory stimulation in human subjects., *Proceedings of the National Academy of Sciences of the United States of America* **83**(4): 1140–4.

Fox, P. T. (2012). The coupling controversy, **62**(2): 594–601.

Freret, T., Bouet, V., Toutain, J., Saulnier, R., Palma, P., Bihel, E., Mackenzie, E. T., Roussel, S., Pascale, S. and Touzani, O. (2008). Intraluminal thread model of focal stroke in the non-human primate., *Journal of Cerebral Blood Flow and Metabolism* **28**(4): 786–96.

Freret, T., Valable, S., Chazalviel, L., Saulnier, R., Mackenzie, E. T., Petit, E., Bernaudin, M., Boulouard, M. and Pascale, S. (2006). Delayed administration of deferoxamine reduces brain damage and promotes functional recovery after transient focal cerebral ischemia in the rat, *Eur J Neurosci* **23**(7): 1757–1765.

Friel, K., Barbay, S., Frost, S. and Plautz, E. (2005). Dissociation of sensorimotor deficits after rostral versus caudal lesions in the primary motor cortex hand representation, *Journal of Neurophysiology* **94**: 1312–1324.

Friston, K., Frith, C., Frackowiak, R. and Turner, R. (1995). Characterizing dynamic brain responses with fmri: a multivariate approach., *NeuroImage* **2**: 166–172.

Friston, K., Frith, C., Liddle, P. and Frackowiak, R. (1993). Functional connectivity: the principal-component analysis of large (PET) data sets., *Journal of Cerebral Blood Flow and Metabolism* .

Friston, K., Mechelli, A., Turner, R. and Price, C. (2000). Nonlinear responses in fMRI: the balloon model, volterra kernels, and other hemodynamics., *Neuroimage* **12**(4): 466–77.

Frost, S. B., Barbay, S., Mumert, M. L., Stowe, A. M. and Nudo, R. J. (2006). An animal model of capsular infarct: endothelin-1 injections in the rat., *Behavioural brain research* **169**(2): 206–211.
URL: *http://dx.doi.org/10.1016/j.bbr.2006.01.014*

Frostig, R. D. (2006). Functional organization and plasticity in the adult rat barrel cortex: moving out-of-the-box, *Current Opinion in Neurobiology* **16**(4): 445 – 450. Sensory systems.
URL: *http://www.sciencedirect.com/science/article/pii/S0959438806000778*

Fugl-Meyer, A., Jsk, L., Leyman, I., Olsson, S. and Steglind, S. (1975). The post-stroke hemiplegic patient. 1. a method for evaluation of physical performance, *Scandinavian journal of rehabilitation medicine* **7**(1): 13–31.
URL: *http://europepmc.org/abstract/MED/1135616*

Fujie, W., Kirino, T., Tomukai, N., Iwasawa, T. and Tamura, A. (1990). Progressive shrinkage of the thalamus following middle cerebral artery occlusion in rats., *Stroke* **21**(10): 1485–8.

Fukuda, S. and del Zoppo, G. J. (2003). Models of focal cerebral ischemia in the nonhuman primate., **44**(2): 96–104.

Gage, F. (2000). Mammalian neural stem cells., *Science (New York, N.Y.)* **287**(5457): 1433–1438.

Garcia, A., Doan, N. B., Imura, T., Bush, T. G. and Sofroniew, M. V. (2004). GFAP-expressing progenitors are the principal source of constitutive neurogenesis in adult mouse forebrain., *Nat. Neurosci.* **7**(11): 1233–41.

Gharbawie, O., Auer, R. and Whishaw, I. (2006). Subcortical middle cerebral artery ischemia abolishes the digit flexion and closing used for grasping in rat skilled reaching., *Neuroscience* **137**(4): 1107–18.

Gharbawie, O., Gonzalez, C., Williams, P., Kleim, J. and Whishaw, I. (2005). Middle cerebral artery (MCA) stroke produces dysfunction in adjacent motor cortex as detected by intracortical microstimulation in rats., *Neuroscience* **130**(3): 601–10.

Gibbs, F. and Gibbs, E. (1935). Changes in human cerebral blood flow consequent on alterations in blood gases, *Am. J. Phys* **111**: 557–563.

Ginsberg (1996). The validity of rodent brain-ischemia models is self-evident, *Archives of Neurology* **53**(10): 1065–1067.
URL: + *http://dx.doi.org/10.1001/archneur.1996.00550100151024*

Girouard, H. and Iadecola, C. (2006). Neurovascular coupling in the normal brain and in hypertension, stroke, and alzheimer disease., *J. Appl. Physiol.* **100**(1): 328–35.

Goense, J. B., Ku, S. P., Merkle, H., Tolias, A. S. and Logothetis, N. K. (2008). fMRI of the temporal lobe of the awake monkey at 7T., *Neuroimage* **39**(3): 1081–93.

Goense, J. B., Zappe, A. C. and Logothetis, N. K. (2007). High-resolution fMRI of macaque v1., *Magn Reson Imaging* **25**(6): 740–7.

Goldberg, M. and Ransom, B. (2003). New light on white matter, *Stroke* **34**: 330–332.
URL: *http://dx.doi.org/10.1161/01.STR.0000054048.22626.B9*

Goldman, S. A. (2016). Stem and progenitor Cell-Based therapy of the central nervous system: Hopes, hype, and wishful thinking., *Cell Stem Cell* **18**(2): 174–88.

Gould, E., Vail, N., Wagers, M. and Gross, C. (2001). Adult-generated hippocampal and neocortical neurons in macaques have a transient existence., *Proc. Natl. Acad. Sci. U.S.A.* **98**(19): 10910–7.

Goyal, M., Menon, B. K., van Zwam, W. H., Dippel, D. W., Mitchell, P. J., Demchuk, A. M., Dávalos, A., Majoie, C. B., van der Lugt, A., de Miquel, M. A., Donnan, G. A., Roos, Y. B., Bonafe, A., Jahan, R., Diener, H. C., van den Berg, L. A., Levy, E. I., Berkhemer, O. A., Pereira, V. M., Rempel, J., Millán, M., Davis, S. M., Roy, D., Thornton, J., Román, L. S., Ribó, M., Beumer, D., Stouch, B., Brown, S., Campbell, B. C., van Oosten-brugge, R. J., Saver, J. L., Hill, M. D. and Jovin, T. G. a. (2016). Endovascular thrombectomy after large-vessel ischaemic stroke: a meta-analysis of individual patient data from five randomised trials., *Lancet* **387**(10029): 1723–31.

Grotta, J. C., Noser, E. A., Ro, T., Boake, C., Levin, H., Aronowski, J. and Schallert, T. (2004). Constraint-induced movement therapy, *Stroke* **35**(11 suppl 1): 2699–2701.

Gupta, N., Henry, R., Strober, J. and Kang, S. (2012). Neural stem cell engraftment and myelination in the human brain, *Science translational* .

Gusnard, D. and Raichle, M. (2001). Searching for a baseline: functional imaging and the resting human brain, *Nature Reviews Neuroscience* **2**: 685–696.

Hack, I., Bancila, M., Loulier, K., Carroll, P. and Cremer, H. (2002). Reelin is a detachment signal in tangential chain-migration during postnatal neurogenesis., *Nat. Neurosci.* **5**(10): 939–45.

Hacke, W., Kaste, M., Bluhmki, E., Brozman, M., Dávalos, A., Guidetti, D., Larrue, V., Lees, K. R., Medeghri, Z. and Machnig, T. (2008). Thrombolysis with alteplase 3 to 4.5 hours after acute ischemic stroke, **359**(13): 1317–1329.

Hagemann, G., Redecker, C., T, N., Freund, H. and Witte, O. (1998). Increased long-term potentiation in the surround of experimentally induced focal cortical infarction., *Ann. Neurol.* **44**(2): 255–8.

Hahn, F. (1950). Spin echos, *Physical Review* **80**(4): 580–601.

Hall, C. N., Reynell, C., Gesslein, B., Hamilton, N. B., Mishra, A., Sutherland, B. A., M, O. F., Buchan, A. M., Lauritzen, M. and Attwell, D. (2014). Capillary pericytes regulate cerebral blood flow in health and disease., *Nature* **508**(7494): 55–60.
URL: *http://dx.doi.org/10.1038/nature13165*

Hamilton, N. B., Attwell, D. and Hall, C. N. (2010). Pericyte-mediated regulation of capillary diameter: a component of neurovascular coupling in health and disease., *Frontiers in neuroenergetics* **2**.
URL: *http://dx.doi.org/10.3389/fnene.2010.00005*

Hampson, M., Peterson, B. S., Skudlarski, P., Gatenby, J. C. and Gore, J. C. (2002). Detection of functional connectivity using temporal correlations in MR images, **15**(4): 247–262.

Hampton, D., Rhodes, K., Zhao, C., Franklin, R. and Fawcett, J. (2004). The responses of oligodendrocyte precursor cells, astrocytes and microglia to a cortical stab injury, in the brain., *Neuroscience* **127**(4): 813–20.

Hara, H., Harada, K. and Sukamoto, T. (1993). Chronological atrophy after transient middle cerebral artery occlusion in rats., *Brain Research* **618**(2): 251–60.

Harris, L., Zalucki, O., Piper, M. and Heng, J. I. (2016). Insights into the biology and therapeutic applications of neural stem cells., *Stem Cells Int* **2016**: 1–18.

Hassani, Z., Joanna, O., Pearse, Y., Stroemer, P., Tang, E., Sinden, J., Price, J. and Thuret, S. (2012). Human neural progenitor cell engraftment increases neurogenesis and microglial recruitment in the brain of rats with stroke., *PloS one* **7**(11): 1–9.
URL: *http://dx.doi.org/10.1371/journal.pone.0050444*

He, B. J., Snyder, A. Z., Vincent, J. L., Epstein, A., Shulman, G. L. and Corbetta, M. (2007). Breakdown of functional connectivity in frontoparietal networks underlies behavioral deficits in spatial neglect, **53**(6): 905–918.

He, B. J., Snyder, A. Z., Zempel, J. M., Smyth, M. D. and Raichle, M. E. (2006). Electrophysiological correlates of the brain's intrinsic large-scale functional architecture., *Proc. Natl. Acad. Sci. U.S.A.* **105**(41): 16039–44.

Hedenqvist, P., Roughan, J. V. and Flecknell, P. A. (2000). Sufentanil and medetomidine anaesthesia in the rat and its reversal

with atipamezole and butorphanol, *Laboratory Animals* **34**: 244–251.
URL: *http://dx.doi.org/10.1258/002367700780384762*

Heiss, W. D. (2010). The concept of the penumbra: can it be translated to stroke management?, *International Journal of Stroke* **5**(4): 290–5.

Heiss, W. D. (2016). Malignant MCA infarction: Pathophysiology and imaging for early diagnosis and management decisions., *Cerebrovasc. Dis.* **41**(1-2): 1–7.

Hernández, M., Brenna, R. and Bowman, G. (1978). Cerebral blood flow autoregulation in the rat., *Stroke* **9**(2): 150–156.
URL: *http://dx.doi.org/10.1161/01.STR.9.2.150*

Heubner, O. (1874). *Die luetische Erkrankung der Hirnarterien,* .

Hicks, C., Stevanato, L., Stroemer, R. P., Tang, E., Richardson, S. and Sinden, J. D. (2013). In vivo and in vitro characterization of the angiogenic effect of CTX0E03 human neural stem cells., *Cell transplantation* **22**(9): 1541–1552.
URL: *http://dx.doi.org/10.3727/096368912X657936*

Honey, C. J. and Sporns, O. (2008). Dynamical consequences of lesions in cortical networks, *Human brain mapping* **29**: 802–809.

Honmou, O., Houkin, K., Matsunaga, T., Niitsu, Y., Ishiai, S., Onodera, R., Waxman, S. G. and Kocsis, J. D. (2011). Intravenous administration of auto serum-expanded autologous mesenchymal stem cells in stroke., *Brain: a journal of neurology* **134**(Pt 6): 1790–807.

Horwitz, B., Duara, R. and Rapoport, S. (1984). Intercorrelations of glucose metabolic rates between brain regions: application

to healthy males in a state of reduced sensory input., *J. Cereb. Blood Flow Metab.* **4**(4): 484–99.

Hou, Y., Manns, I. and Jones, B. (2002). Immunostaining of cholinergic pontomesencephalic neurons for 1 versus 2 adrenergic receptors suggests different sleepwake state activities and roles.

Howarth, C., Gleeson, P. and Attwell, D. (2012). Updated energy budgets for neural computation in the neocortex and cerebellum, *Journal of Cerbral Blood Flow and Metabolism* **32**(7): 1222–32.

Hsu, E. and Hedlund, L. (1998). Functional mri of the rat somatosensory cortex: effects of hyperventilation, *Magnetic resonance in Medicine* **40**: 421–426.

Hsu, J. and Jones, T. A. (2006). Contralesional neural plasticity and functional changes in the less-affected forelimb after large and small cortical infarcts in rats., *Exp. Neurol.* **201**(2): 479–94.

Hu, X. and Yacoub, E. (2012). The story of the initial dip in fMRI., *Neuroimage* **62**(2): 1103–8.

Huang, D., Swanson, E., Lin, C., Schuman, J., Stinson, W., Chang, W., Hee, M., Flotte, T., Gregory, K. and Puliafito, C. (1991). Optical coherence tomography., *Science* **254**(5035): 1178–81.

Iadecola, C. and Anrather, J. (2011). The immunology of stroke: from mechanisms to translation, *Nature medicine* **17**(7): 796–809.

Imura, T. and Kornblum, H. (2003). The predominant neural stem cell isolated from postnatal and adult forebrain but not early embryonic forebrain expresses GFAP, *The Journal of Neuroscience* **23**: 2824–2832.

Iwaniuk, A. and Whishaw, I. (2000). On the origin of skilled forelimb movements., *Trends Neurosci* **23**(8): 372–6.

Izumi, Y., Haida, M., Hata, T., Isozumi, K., Kurita, D. and Shinohara, Y. (2002). Distribution of brain oedema in the contralateral hemisphere after cerebral infarction: repeated MRI measurement in the rat., *J Clin Neurosci* **9**(3): 289–93.

Jacobson, S. G., Matsui, R., Sumaroka, A. and Cideciyan, A. V. (2016). Retinal structure measurements as inclusion criteria for stem Cell-Based therapies of retinal degenerations., *Invest. Ophthalmol. Vis. Sci.* **57**(5): 1–9.

Jenkinson, M. (2003). Fast, automated, n-dimensional phase-unwrapping algorithm., *Magn Reson Med* **49**(1): 193–7.

Jezzard, P. and Balaban, R. S. (1995). Correction for geometric distortion in echo planar images from bo field variations, *Magnetic resonance in medicine* **34**(1): 65–73.
URL: *http://dx.doi.org/10.1002/mrm.1910340111*

Jiang, Q., Zhang, Z., Ding, G., Zhang, L., Ewing, J. R., Wang, L., Zhang, R., Li, L., Lu, M., Meng, H., Arbab, A. S., Hu, J., Li, Q., Siamak, P. D., Athiraman, H. and Chopp, M. (2005). Investigation of neural progenitor cell induced angiogenesis after embolic stroke in rat using MRI, *Neuroimage* **28**(3): 698–707.

Jiang, Q., Zhang, Z. G., Ding, G. L., Silver, B., Zhang, L., Meng, H., Lu, M., Siamak, P., Wang, L., Smita, S., Li, L., Hassan, B., Hu, J., Arbab, A. S., Vanguri, P., Ewing, J. R., Ledbetter, K. A. and Chopp, M. (2006). MRI detects white matter reorganization after neural progenitor cell treatment of stroke., *Neuroimage* **32**(3): 1080–9.

Jin, K., Mao, X., Xie, L., Galvan, V., Lai, B., Wang, Y., Gorostiza, O., Wang, X. and Greenberg, D. A. (2010). Transplantation of human neural precursor cells in matrigel scaffolding improves

outcome from focal cerebral ischemia after delayed postischemic treatment in rats., *J. Cereb. Blood Flow Metab.* **30**(3): 534–44.

Jin, K., Wang, X., Xie, L., Mao, X. O., Zhu, W., Wang, Y., Shen, J., Mao, Y., Banwait, S. and Greenberg, D. A. (2006). Evidence for stroke-induced neurogenesis in the human brain., *Proceedings of the National Academy of Sciences of the United States of America* **103**(35): 13198–202.

Johansson, C., Momma, S., Clarke, D., Risling, M., Lendahl, U. and Frisén, J. (1999). Identification of a neural stem cell in the adult mammalian central nervous system., *Cell* **96**(1): 25–34.

Jolkkonen, J., Puurunen, K., Koistinaho, J., Kauppinen, R., Haapalinna, A., Nieminen, L. and Sivenius, J. (1999). Neuroprotection by the alpha2-adrenoceptor agonist, dexmedetomidine, in rat focal cerebral ischemia., *Eur. J. Pharmacol.* **372**(1): 31–6.

Jones, B. E. and Yang, T. (1985). The efferent projections from the reticular formation and the locus coeruleus studied by anterograde and retrograde axonal transport in the rat, *Journal of Comparative Neurology* **242**: 56–92.
URL: *http://dx.doi.org/10.1002/cne.902420105*

Jones, T. L., Byrnes, T. J., Yang, G., Howe, F. A., Bell, B. and Barrick, T. R. (2015). Brain tumor classification using the diffusion tensor image segmentation (D-SEG) technique., *Neuro-oncology* **17**(3): 466–76.

Jørgensen, H., Nakayama, H. and Raaschou, H. (1995). Outcome and time course of recovery in stroke. part II: time course of recovery. the copenhagen stroke study, *Arch Phys Med Rehabil* **76**: 406–412.

Jortner, B. (2006). The return of the dark neuron. a histological artifact complicating contemporary neurotoxicologic evaluation, *Neurotoxicology* **27**: 628–634.

Kalladka, D., Sinden, J., Pollock, K., Haig, C., John, M., Smith, W., Alex, M., Santosh, C., Bath, P. M., Dunn, L. and Muir, K. W. (2016). Human neural stem cells in patients with chronic ischaemic stroke (PISCES): a phase 1, first-in-man study., *Lancet* **388**(10046): 787–96.

Kalra, L. (2010). Stroke rehabilitation 2009: old chestnuts and new insights., *Stroke* **41**(2): 88–90.

Kalthoff, D., Po, C., Wiedermann, D. and Hoehn, M. (2013). Reliability and spatial specificity of rat brain sensorimotor functional connectivity networks are superior under sedation compared with general anesthesia., *NMR in biomedicine* **26**(6): 638–650. **URL:** *http://dx.doi.org/10.1002/nbm.2908*

Kaneko, D., Nakamura, N. and Ogawa, T. (1985). Cerebral infarction in rats using homologous blood emboli: development of a new experimental model., *Stroke* **16**(1): 76–84.

Katsura, K., Kristián, T. and Siesjö, B. (1994). Energy metabolism, ion homeostasis, and cell damage in the brain., *Biochem. Soc. Trans.* **22**(4): 991–6.

Kety, S. and Schmidt, C. (1948). Effects of alterations in the arterial tensions of carbon dioxide and oyxgen on cerebral blood flow and cerebral oxygen consumption of normal young men, **27**(4). **URL:** *http://dx.doi.org/10.1172/JCI101995*

Kim, D., Kim, R., Kim, H., Kim, J., Jun, S., Lee, B., Jo, H., Neto, P. R., Lee, M. and Kim, H. (2015). Longitudinal changes in

resting-state brain activity in a capsular infarct model, *Journal of Cerebral Blood Flow and Metabolism* **35**(1): 11–19.

Kleinfeld, D., Ahissar, E. and Diamond, M. E. (2006). Active sensation: insights from the rodent vibrissa sensorimotor system, *Current Opinion in Neurobiology* **16**(4): 435 – 444.
URL: *http://www.sciencedirect.com/science/article/pii/S0959438806000821*

Kloth, V., Klein, A., Loettrich, D. and Nikkhah, G. (2006). Colour-coded pellets increase the sensitivity of the staircase test to differentiate skilled forelimb performances of control and 6-hydroxydopamine lesioned rats, *Brain Res Bull* **70**(1): 68–80.

Koizumi, J.-i., Yoshida, Y., Nakazawa, T. and Ooneda, G. (1986a). Experimental studies of ischemic brain edema, *Japanese Journal of Stroke* **8**: 1–8.

Koizumi, J., Yoshida, Y., Nakazawa, T. and Ooneda, G. (1986b). Experimental studies of ischemic brain edema, *Nosotchu* **8**(1): 1–8.

Kokaia, Z., Martino, G., Schwartz, M. and Lindvall, O. (2012). Cross-talk between neural stem cells and immune cells: the key to better brain repair [quest], *Nature neuroscience* **15**: 1078–1087.

Konig, J. and Klippel, R. (1963). *A Stereotaxic Atlas of the Forebrain and Lower Parts of the Brain Stem.*, Williams and Wilkins.

Kopen, G., Prockop, D. and Phinney, D. (1999). Marrow stromal cells migrate throughout forebrain and cerebellum, and they differentiate into astrocytes after injection into neonatal mouse brains., *Proc. Natl. Acad. Sci. U.S.A.* **96**(19): 10711–6.

Kornack, D. and Rakic, P. (2001). The generation, migration, and differentiation of olfactory neurons in the adult primate brain., *Proc. Natl. Acad. Sci. U.S.A.* **98**(8): 4752–7.

Kornblum, H. I. (2007). Introduction to neural stem cells, *Stroke* **38**(2): 810–816.

Kågström, E., Smith, M. and Siesjö, B. (1983). Cerebral circulatory responses to hypercapnia and hypoxia in the recovery period following complete and incomplete cerebral ischemia in the rat., *Acta Physiol. Scand.* **118**(3): 281–91.

Langhorne, P., Bernhardt, J. and Kwakkel, G. (2011). Stroke rehabilitation, *The Lancet* **377**(9778): 1693 – 1702.
URL: *http://www.sciencedirect.com/science/article/pii/S0140673611603255*

Langhorne, P., Coupar, F. and Pollock, A. (2009). Motor recovery after stroke: a systematic review., *Lancet Neurol* **8**(8): 741–54.

Lansberg, M., Thijs, V., MW, O., Ali, J., de Crespigny, A., Tong, D., Moseley, M. and Albers, G. (2001). Evolution of apparent diffusion coefficient, diffusion-weighted, and t2-weighted signal intensity of acute stroke., *AJNR Am J Neuroradiol* **22**(4): 637–44.

Larson, C. and Severinghause, J. (1962). Postural variations in dead space and CO2 gradients breathing air and o2., *J Appl Physiol* **17**: 417–20.

Lashley, K. (1950). In search of the engram, *Society of Experimental Biology Symposium No. 4: Physiological mechanisms in animal behaviour* pp. 454–482.

Lassen, N. (1959). Cerebral blood flow and oxygen consumption in man., *Physiol. Rev.* **39**(2): 183–238.

Lassen, N. and Christensen, M. (1976). Physiology of cerebral blood flow, *British Journal of Anaesthesiology* **48**: 719–733.

Lawes, C., Bennett, D., Feigin, V. and Rodgers, A. (2004). Blood pressure and stroke an overview of published reviews, *Stroke* .

Laywell, E., Kukekov, V. and Steindler, D. (1999). Multipotent neurospheres can be derived from forebrain subependymal zone and spinal cord of adult mice after protracted postmortem intervals., *Exp. Neurol.* **156**(2): 430–3.

Lazarini, F. and Lledo, P. (2011). Is adult neurogenesis essential for olfaction?, *Trends in neurosciences* **34**: 20–31.

Lecrux, C., Christopher, M., Weir, C. J., Gallagher, L., Mullin, J., Touzani, O., Muir, K. W., Lees, K. R. and Macrae, M. I. (2008). Effects of magnesium treatment in a model of internal capsule lesion in spontaneously hypertensive rats, *Upd Int Car* **39**(2): 448–454.

Lee, D., Kang, D., Ahn, J., Choi, C., Kim, S. and Suh, D. (2005). Imaging of the ischemic penumbra in acute stroke, *Korean Journal of Radiology* **6**(2): 64–74.

Lee, J. S., Hong, J. M., Moon, G. J., Lee, P. H., Ahn, Y. H., Bang, O. Y. and collaborators, S. (2010). A long-term follow-up study of intravenous autologous mesenchymal stem cell transplantation in patients with ischemic stroke., *Stem Cells* **28**(6): 1099–106.

Leithner, C. and Royl, G. (2014). The oxygen paradox of neurovascular coupling., *Jouranl of Cerebral Blood Flow and Metabolism* **34**(1): 19–29.

Lenzi, G., Frackowiak, R. and Jones, T. (1982). Cerebral oxygen metabolism and blood flow in human cerebral ischemic infarction, *Journal of Cerebral Blood Flow & Metabolism* **2**: 321–335.

Leopold, D. A., Murayama, Y. and Logothetis, N. K. (2003). Very slow activity fluctuations in monkey visual cortex: implications for functional brain imaging., *Cereb. Cortex* **13**(4): 422–33.

Li, P. and Murphy, T. H. (2008). Two-photon imaging during prolonged middle cerebral artery occlusion in mice reveals recovery of dendritic structure after reperfusion., *J. Neurosci.* **28**(46): 11970–9.

Liang, Y., Walczak, P. and Bulte, J. W. (2013). The survival of engrafted neural stem cells within hyaluronic acid hydrogels., *Biomaterials* **34**(22): 5521–9.

Liang, Z., Liu, X. and Zhang, N. (2015). Dynamic resting state functional connectivity in awake and anesthetized rodents., *Neuroimage* **104**: 89–99.

Lim, D. H., M, L. J., Mohajerani, M. H. and Murphy, T. H. (2014). Optogenetic mapping after stroke reveals network-wide scaling of functional connections and heterogeneous recovery of the peri-infarct., *J. Neurosci.* **34**(49): 16455–66.

Lin, A. L., Fox, P. T., Hardies, J., Duong, T. Q. and Gao, J. H. (2010). Nonlinear coupling between cerebral blood flow, oxygen consumption, and ATP production in human visual cortex., *Proc. Natl. Acad. Sci. U.S.A.* **107**(18): 8446–51.

Lindvall, O. and Kokaia, Z. (2011). Stem cell research in stroke how far from the clinic?, *Stroke* **42**(8): 2369–2375.

Littlewood, T. D., Hancock, D. C., Danielian, P. S., Parker, M. G. and Evan, G. I. (1995). A modified oestrogen receptor ligand-binding domain as an improved switch for the regulation of heterologous proteins, *Nucleic Acids Research* **23**(10): 1686–1690. **URL:** *http://dx.doi.org/10.1093/nar/23.10.1686*

Liu, S., Wang, J., Zhu, D., Fu, Y., Lukowiak, K. and Lu, Y. M. (2003). Generation of functional inhibitory neurons in the adult rat hippocampus., *J. Neurosci.* **23**(3): 732–6.

Liu, Z., Chen, C., Li, F. and Shen, J. (2015). Splenic responses in ischemic stroke: New insights into stroke pathology, *CNS neuroscience & Therapeutics* **21**: 320–326.

Logothetis, N., Guggenberger, H., Peled, S. and Pauls, J. (1999). Functional imaging of the monkey brain., *Nature neuroscience* **2**(6): 555–562.
URL: *http://dx.doi.org/10.1038/9210*

Logothetis, N. K. (2003). The underpinnings of the BOLD functional magnetic resonance imaging signal., *J. Neurosci.* **23**(10): 3963–71.

Logothetis, N. K., Pauls, J., Augath, M., Trinath, T. and Oeltermann, A. (2001). Neurophysiological investigation of the basis of the fMRI signal, *Nature* **412**(6843): 150–157.

Lois, C. and Alvarez-Buylla, A. (1994). Long-distance neuronal migration in the adult mammalian brain., *Science* **264**(5162): 1145–8.

Longa, E., Weinstein, P., Carlson, S. and Cummins, R. (1989). Reversible middle cerebral artery occlusion without craniectomy in rats., *Stroke* **20**(1): 84–91.

Lopez, A. D., Mathers, C. D., Ezzati, M., Jamison, D. T. and Murray, C. J. (2006). Global and regional burden of disease and risk factors, 2001: systematic analysis of population health data., *Lancet* **367**(9524): 1747–57.

Love, Z., Wang, F., Dennis, J., Awadallah, A., Salem, N., Lin, Y., Weisenberger, A., Majewski, S., Gerson, S. and Lee, Z. (2007). Imaging of mesenchymal stem cell transplant by bioluminescence and PET, *J Nucl Med* **48**(12): 2011–2020.

Lowe, M., Mock, B. and Sorenson, J. (1998). Functional connectivity in single and multislice echoplanar imaging using resting-state fluctuations., *Neuroimage* **7**(2): 119–32.

Lu, H., Zou, Q., Gu, H., Raichle, M. E., Stein, E. A. and Yang, Y. (2012). Rat brains also have a default mode network., *Proceedings of the National Academy of Sciences of the United States of America* **109**(10): 3979–3984.
URL: *http://dx.doi.org/10.1073/pnas.1200506109*

Lu, X., Huang, B., Zheng, J., Tao, Y. and Yu, W. (2014). Decompressive craniectomy for the treatment of malignant infarction of the middle cerebral artery, *Scientific Reports* **4**: 1–9.

Lukasik, V. M. and Gillies, R. J. (2003). Animal anaesthesia for in vivo magnetic resonance, *NMR in Biomedicine* **16**(8): 459–467.
URL: *http://dx.doi.org/10.1002/nbm.836*

Lundkvist, J. and Lendahl, U. (2001). Notch and the birth of glial cells., *Trends Neurosci* **24**(9): 492–4.

Macrae, I. (1992). New models of focal cerebral ischaemia., *British journal of clinical pharmacology* **34**(4): 302–308.
URL: *http://dx.doi.org/10.1111/j.1365-2125.1992.tb05634.x*

Macrae, I. (2011). Preclinical stroke research–advantages and disadvantages of the most common rodent models of focal ischaemia., *British journal of pharmacology* **164**(4): 1062–1078.
URL: *http://dx.doi.org/10.1111/j.1476-5381.2011.01398.x*

Macrae, I., Robinson, M., Graham, D., Reid, J. and J, M. (1993). Endothelin-1-induced reductions in cerebral blood flow: dose dependency, time course, and neuropathological consequences., *J. Cereb. Blood Flow Metab.* **13**(2): 276–84.

Magnuson, M., Majeed, W. and Keilholz, S. D. (2010). Functional connectivity in blood oxygenation leveldependent and cerebral blood volumeweighted resting state functional magnetic resonance imaging in the rat brain, *Journal of Magnetic Resonance Imaging* **32**(3): 584–592.
URL: *http://dx.doi.org/10.1002/jmri.22295*

Mahoney, F. and Barthel, D. (1965). Functional evaluation: the barthel index, *Maryland state medical journal* **14**: 56–61.

Mangia, S., Giove, F., Tkáč, I. and Logothetis, N. (2008). Metabolic and hemodynamic events after changes in neuronal activity: current hypotheses, theoretical predictions and in vivo NMR experimental findings, *Flow & Metabolism* **29**: 441–463.

Martin, L., NA, A., Brambrink, A. and Kirsch, J. (1998). Neurodegeneration in excitotoxicity, global cerebral ischemia, and target deprivation: a perspective on the contributions of apoptosis and necrosis, *Brain research bulletin* **46**(4): 281–309.

Masamoto, K., Fukuda, M., Vazquez, A. and Kim, S. G. (2009a). Dose-dependent effect of isoflurane on neurovascular coupling in rat cerebral cortex., *Eur. J. Neurosci.* **30**(2): 242–50.

Masamoto, K., Fukuda, M., Vazquez, A. and Kim, S. G. (2009b). Dose-dependent effect of isoflurane on neurovascular coupling in rat cerebral cortex., *Eur. J. Neurosci.* **30**(2): 242–50.

Matthews, J., Altman, D., Campbell, M. and Royston, P. (1990). Analysis of serial measurements in medical research., *BMJ* **300**(6719): 230.

Meng, L. and Gelb, A. W. (2015). Regulation of cerebral autoregulation by carbon dioxide., *Anesthesiology* **122**(1): 196–205.

Merzenich, M., Kaas, J., Wall, J., Nelson, R., Sur, M. and Felleman, D. (1983). Topographic reorganization of somatosensory cortical areas 3b and 1 in adult monkeys following restricted deafferentation., *Neuroscience* **8**(1): 33–55.

Mies, G. and Hossmann, K. (1993). Correlation between peri-infarct DC shifts and ischaemic neuronal damage in rat., *Neuroreport* **4**: 709–711.

Mine, Y., Tatarishvili, J., Oki, K., Monni, E., Kokaia, Z. and Lindvall, O. (2013). Grafted human neural stem cells enhance several steps of endogenous neurogenesis and improve behavioral recovery after middle cerebral artery occlusion in rats., *Neurobiology of disease* **52**: 191–203.
URL: *http://dx.doi.org/10.1016/j.nbd.2012.12.006*

Mirsattari, S. M., Bihari, F., Leung, L., Menon, R. S., Wang, Z., Ives, J. R. and Bartha, R. (2005). Physiological monitoring of small animals during magnetic resonance imaging., *J. Neurosci. Methods* **144**(2): 207–13.

Mišić, B. and Sporns, O. (2016). From regions to connections and networks: new bridges between brain and behavior., *Current Opinion in Neurobiology* **40**: 1–7.

Modo, M., Stroemer, R., Tang, E., Patel, S. and Hodges, H. (2003). Effects of implantation site of dead stem cells in rats with stroke damage., *Neuroreport* **14**(1): 39–42.
URL: *http://dx.doi.org/10.1097/01.wnr.0000053066.88427.c2*

Modo, M., Stroemer, R., Tang, E., Veizovic, T., Sowniski, P. and Hodges, H. (2000). Neurological sequelae and long-term behavioural assessment of rats with transient middle cerebral artery occlusion., *Journal of neuroscience methods* **104**(1): 99–9109.
URL: *http://dx.doi.org/10.1016/S0165-0270(00)00329-0*

Montoya, C., LJ, C., Pemberton, K. and Dunnett, S. (1991). The "staircase test": a measure of independent forelimb reaching and grasping abilities in rats., *Journal of neuroscience methods* **36**(2-3): 219–228.
URL: *http://dx.doi.org/10.1016/0165-0270(91)90048-5*

Mostany, R., Chowdhury, T. G., Johnston, D. G., Portonovo, S. A., Carmichael, S. and Carlos, P. (2010). Local hemodynamics dictate long-term dendritic plasticity in peri-infarct cortex., *J. Neurosci.* **30**(42): 14116–26.

Muir, K. W. (2010). Stem cells in stroke management, *Reviews in Clinical Gerontology* **21**: 125–140.

Murphy, K., Birn, R., Handwerker, D. and Jones, T. (2009). The impact of global signal regression on resting state correlations: are anti-correlated networks introduced?, *Neuroimage* **44**: 893–905.

Nakai, T., Hayashi, M., Ichihara, K., Wakabayashi, H. and Hoshi, K. (2002). Noradrenaline release in rat locus coeruleus is regulated by both opioid and alpha(2) -adrenoceptors., *Pharmacological research : the official journal of the Italian Pharmacological Society* **45**(5): 407–412.

Napoli, D. M. (2001). Systemic complement activation in ischemic stroke, *Stroke* **32**: 1444.

Nedergaard, M. and Hansen, A. (1993). Characterization of cortical depolarizations evoked in focal cerebral ischemia., *J. Cereb. Blood Flow Metab.* **13**(4): 568–74.

Neumann-Haefelin, T., Bosse, F., Redecker, C. and Müller, H. (1999). Upregulation of GABA a-receptor 1-and 2-subunit mR-

NAs following ischemic cortical lesions in rats, *Brain research* **816**: 234–237.

Nguyen, Q.-T. and Kleinfeld, D. (2005). Positive feedback in a brainstem tactile sensorimotor loop, *Neuron* **45**(3): 447 − 457.
URL: *http://www.sciencedirect.com/science/article/pii/S0896627305000140*

Nudo, R. (1999). Recovery after damage to motor cortical areas., *Curr. Opin. Neurobiol.* **9**(6): 740–7.

Nudo, R., Wise, B., F, S. and Milliken, G. (1996). Neural substrates for the effects of rehabilitative training on motor recovery after ischemic infarct, *Science* **272**: 1791–1796.

O'Brien, M., Waltz, A. and Jordan, M. (1974). Ischemic cerebral edema. distribution of water in brains of cats after occlusion of the middle cerebral artery., *Arch. Neurol.* **30**(6): 456–60.

Ogawa, S., Lee, T., Kay, A. and Tank, D. (1990). Brain magnetic resonance imaging with contrast dependent on blood oxygenation., *Proceedings of the National Academy of Sciences of the United States of America* **87**(24): 9868–72.

Ogawa, S., Lee, T., Nayak, A. S. and Glynn, P. (1990). Oxygenation sensitive contrast in magnetic resonance image of rodent brain at high magnetic fields, *Magnetic resonance in Medicine* **14**: 68–78.

Olsson, M., Nikkhah, G., Bentlage, C. and Bjö rklund, A. (1995). Forelimb akinesia in the rat parkinson model: differential effects of dopamine agonists and nigral transplants as assessed by a new stepping test., *The Journal of neuroscience : the official journal of the Society for Neuroscience* **15**(5 Pt 2): 3863–3875.

Ord, E., Shirley, R., van Kralingen, J. C., Graves, A., D, M. J., Wilkinson, M., Christopher, M., Macrae, M. I. and Work, L. M.

(2012). Positive impact of pre-stroke surgery on survival following transient focal ischemia in hypertensive rats, *J Neurosci Meth* **211**(2): 305–308.

Orset, C., Macrez, R., Young, A. R., Panthou, D., Eduardo, A., Maubert, E., Agin, V. and Vivien, D. (2007). Mouse model of in situ thromboembolic stroke and reperfusion., *Stroke* **38**(10): 2771–8.

Osborne, K. A., Shigeno, T., Balarsky, A. M., Ford, I., McCulloch, J., Teasdale, G. M. and Graham, D. I. (1987). Quantitative assessment of early brain damage in a rat model of focal cerebral ischaemia., *Journal of Neurology, Neurosurgery & Psychiatry* **50**(4): 402–410.
URL: *http://dx.doi.org/10.1136/jnnp.50.4.402*

Pantoni, L., Garcia, J. and Gutierrez, J. (1996). Cerebral white matter is highly vulnerable to ischemia., *Stroke* **27**: 1641–6.

Parent, J. M. (2003). Injury-induced neurogenesis in the adult mammalian brain., *The Neuroscientist* **9**(4): 261–72.

Parent, J. M., Vexler, Z. S., Gong, C., Derugin, N. and Ferriero, D. M. (2002). Rat forebrain neurogenesis and striatal neuron replacement after focal stroke., *Annals of Neurology* **52**(6): 802–13.

Pasztor, E., Symon, L., Dorsch, N. and Branston, N. (1973). The hydrogen clearance method in assessment of blood flow in cortex, white matter and deep nuclei of baboons., *Stroke* **4**(4): 556–67.

Patel, U. (1983). Non-random distribution of blood vessels in the posterior region of the rat somatosensory cortex, *Brain Res* **289**(1-2): 65–70.

Pauling, L. and Coryell, C. (1936). The magnetic properties and structure of hemoglobin, oxyhemoglobin and carbonmonoxyhemoglobin., *Proc. Natl. Acad. Sci. U.S.A.* **22**(4): 210–6.

Pawela, C. P., Biswal, B. B., Cho, Y. R., Kao, D. S., Li, R., Jones, S. R., Schulte, M. L., Matloub, H. S., Hudetz, A. G. and Hyde, J. S. (2008). Resting-state functional connectivity of the rat brain., *Magnetic resonance in medicine* **59**(5): 1021–1029.
  URL: *http://dx.doi.org/10.1002/mrm.21524*

Paxinos, G. and Watson, C. (2006). *The Rat Brain in Stereotaxic Coordinates: Hard Cover Edition*, Elsevier Science.
  URL: *http://books.google.co.uk/books?id=oprYfdDbh58C*

Petersen, C. (2007). The functional organization of the barrel cortex, *Neuron* **56**(2): 339–355.

Petreanu, L., Huber, D., Sobczyk, A. and Svoboda, K. (2007). Channelrhodopsin-2assisted circuit mapping of long-range callosal projections, *Nat Neurosci* **10**(5): 663–668.

Picard, D. (1993). Steroid-binding domains for regulating the functions of heterologous proteins in cis., *Trends in Cell Biology* **3**(8): 278–80.

Pineiro, R., Pendlebury, S., H, J. and Matthews, P. (2001). Functional MRI detects posterior shifts in primary sensorimotor cortex activation after stroke: evidence of local adaptive reorganization?, *Stroke* **32**(5): 1134–9.

Pineiro, R., Pendlebury, S., H, J. and Matthews, P. (2002). Altered hemodynamic responses in patients after subcortical stroke measured by functional MRI., *Stroke* **33**(1): 103–9.

Poldrack, R., Mumford, J. and Nichols, T. (2011). *Handbook of Functional MRI Data Analysis*, Cambidge University Press.
  URL: *http://books.google.co.uk/books?id=VjwBnVRwuD8C*

Pollock, A., Farmer, S. E., Brady, M. C., Langhorne, P., Mead, G. E., Mehrholz, J. and van Wijck, F. (2014). Interventions for improving upper limb function after stroke., *The Cochrane database of systematic reviews* **11**: CD010820.

Pollock, K., Stroemer, P., Patel, S., Stevanato, L., Hope, A., Miljan, E., Dong, Z., Hodges, H., Price, J. and Sinden, J. D. (2006). A conditionally immortal clonal stem cell line from human cortical neuroepithelium for the treatment of ischemic stroke., *Experimental neurology* **199**(1): 143–155.
  URL: *http://dx.doi.org/10.1016/j.expneurol.2005.12.011*

Potter, K., Buck, A. and Self, W. (2012). Stab injury and device implantation within the brain results in inversely multiphasic neuroinflammatory and neurodegenerative responses, *Journal of Neural Engineering* **9**: 1–14.

Power, J., Cohen, A., Nelson, S., Wig, G. and Barnes, K. (2011). Functional network organization of the human brain, *Neuron* **72**: 665–678.

Prasad, K., Sharma, A., Garg, A., Mohanty, S., Bhatnagar, S., Johri, S., Singh, K. K., Nair, V., Sarkar, R. S., Gorthi, S. P., Hassan, K. M., Prabhakar, S., Marwaha, N., Khandelwal, N., Misra, U. K., Kalita, J. and Nityanand, S. a. (2014). Intravenous autologous bone marrow mononuclear stem cell therapy for ischemic stroke: a multicentric, randomized trial., *Stroke* **45**(12): 3618–24.

Puig, J., Pedraza, S. and Blasco, G. (2010). Wallerian degeneration in the corticospinal tract evaluated by diffusion tensor imaging

correlates with motor deficit 30 days after middle cerebral artery, *American Journal of Neuroradiology* **31**: 1324–1330.

Qü, M., Mittmann, T., Luhmann, H., Schleicher, A. and Zilles, K. (1998). Long-term changes of ionotropic glutamate and GABA receptors after unilateral permanent focal cerebral ischemia in the mouse brain, *Neuroscience* **85**(1): 29–43.

Raichle, M. E., Ann, M., Snyder, A. Z., Powers, W. J., Gusnard, D. A. and Shulman, G. L. (2001). A default mode of brain function, *PNAS* **98**(2): 676–682.

Rasmussen, P. M., Jespersen, S. N. and Østergaard, L. (2014). The effects of transit time heterogeneity on brain oxygenation during rest and functional activation, *Journal of Cerebral Blood Flow & Metabolism* .
URL: *http://dx.doi.org/10.1038/jcbfm.2014.213*

Rehme, A., Eickhoff, S., Wang, L., Fink, G. and Grefkes, C. (2011). Dynamic causal modeling of cortical activity from the acute to the chronic stage after stroke, *Neuroimage* **55**: 1147–1158.

Reviews, C. (2013). Organised inpatient (stroke unit) care for stroke, **9**.

Ridker, P., Cook, N., Lee, I. and Gordon, D. (2005). A randomized trial of low-dose aspirin in the primary prevention of cardio-vascular disease in women, *New England Journal of Medicine* **352**(13): 1293–1304.

Rossini, P., Calautti, C., Pauri, F. and Baron, J. (2003). Post-stroke plastic reorganisation in the adult brain, *The Lancet Neurology* **2**(8): 493–502.
URL: *http://www.sciencedirect.com/science/article/pii/S147444220300485X*

Roy, C. and Sherrington, C. (1890). On the regulation of the blood-supply of the brain., *J. Physiol. (Lond.)* **11**(1-2): 85–158.17.

Sacco, R. L., Kasner, S. E., Broderick, J. P., Caplan, L. R., Connors, J., Culebras, A., Elkind, M. S., George, M. G., Hamdan, A. D., Higashida, R. T., Hoh, B. L., Janis, L., Kase, C. S., Kleindorfer, D. O., Lee, J. M., Moseley, M. E., Peterson, E. D., Turan, T. N., Valderrama, A. L., Vinters, H. V., , , , and and (2013). An updated definition of stroke for the 21st century: a statement for healthcare professionals from the american heart Association/American stroke association., *Stroke* **44**(7): 2064–89.

Saha, B., Jaber, M. and Gaillard, A. (2012). Potentials of endogenous neural stem cells in cortical repair., *Frontiers in cellular neuroscience* **6**: 1–10.
   URL: *http://dx.doi.org/10.3389/fncel.2012.00014*

Sakoh, M., Røhl, L., Gyldensted, C., Gjedde, A. and Østergaard, L. (2000). Cerebral blood flow and blood volume measured by magnetic resonance imaging bolus tracking after acute stroke in pigs: comparison with [(15)O]H(2)O positron emission tomography., *Stroke* **31**(8): 1958–64.

Samuels, E. R. and Szabadi, E. (2008). Functional neuroanatomy of the noradrenergic locus coeruleus: Its roles in the regulation of arousal and autonomic function part II: physiological and pharmacological manipulations and pathological alterations of locus coeruleus activity in humans, *Current Neuropharmacology* **6**: 254–285.
   URL: *http://dx.doi.org/10.2174/157015908785777193*

Sanai, N., Berger, M. S., M, G. J. and Arturo, A. (2007). Comment on "Human neuroblasts migrate to the olfactory bulb via a lateral ventricular extension"., *Science* **318**(5849): 393.

Sanai, N., Nguyen, T., Ihrie, R., Mirzadeh, Z. and Tsai, H. (2011). Corridors of migrating neurons in the human brain and their decline during infancy, *Nature* **478**: 382–387.

Saver, J. L., Albers, G. W., Dunn, B., Johnston, K. C. and Fisher, M. a. (2009). Stroke therapy academic industry roundtable (STAIR) recommendations for extended window acute stroke therapy trials., *Stroke* **40**(7): 2594–600.

Savola, J.-M., Ruskoaho, H., Purrunen, J., Salonen, J. S. and KRKI, N. T. (1986). Evidence for medetomidine as a selective and potent agonist 2-adrenoreceptors, *Journal of Autonomic Pharmacology* **6**(4): 275–284.
URL: *http://dx.doi.org/10.1111/j.1474-8673.1986.tb00654.x*

Schaar, K. L., Brenneman, M. M. and Savitz, S. I. (2010). Functional assessments in the rodent stroke model, *Experimental & Translational Stroke Medicine* **2**(1): 1–13.
URL: *http://dx.doi.org/10.1186/2040-7378-2-13*

Schacter, D., Buckner, R., Koutstaal, W., Dale, A. and Rosen, B. (1997). Late onset of anterior prefrontal activity during true and false recognition: an event-related fMRI study., *Neuroimage* **6**(4): 259–69.

Schallert, T. (2006). Behavioral tests for preclinical intervention assessment., *NeuroRx : the journal of the American Society for Experimental NeuroTherapeutics* **3**(4): 497–504.
URL: *http://dx.doi.org/10.1016/j.nurx.2006.08.001*

Schallert, T., Fleming, S., Leasure, J., Tillerson, J. and Bland, S. (2000). CNS plasticity and assessment of forelimb sensorimotor outcome in unilateral rat models of stroke, cortical ablation, parkinsonism and spinal cord injury., *Neuropharmacology*

39(5): 777–787.
URL: *http://dx.doi.org/10.1016/S0028-3908(00)00005-8*

Schallert, T. and Whishaw, I. Q. (1984). Bilateral cutaneous stimulation of the somatosensory system in hemidecorticate rats., *Behavioral neuroscience* **98**(3): 518–540.

Scheinin, M., Lomasney, J. and Hayden-Hixson, D. (1994). Distribution of 2-adrenergic receptor subtype gene expression in rat brain, *Molecular Brain Research* **24**: 133–149.

Schiene, K., Bruehl, C., Zilles, K., Qü, M., Hagemann, G., Kraemer, M. and Witte, O. (1996). Neuronal hyperexcitability and reduction of GABAA-receptor expression in the surround of cerebral photothrombosis., *J. Cereb. Blood Flow Metab.* **16**(5): 906–14.

Schlaug, G., Siewert, B., Benfield, A., Edelman, R. and Warach, S. (1997). Time course of the apparent diffusion coefficient (ADC) abnormality in human stroke., *Neurology* **49**(1): 113–9.

Schmid-Elsaesser, R., Zausinger, S., Hungerhuber, E., Baethmann, A. and Reulen, H. (1998). A critical reevaluation of the intraluminal thread model of focal cerebral ischemia: evidence of inadvertent premature reperfusion and subarachnoid hemorrhage in rats by laser-Doppler flowmetry., *Stroke* **29**(10): 2162–70.

Schölvinck, M. L., Maier, A., Ye, F. Q., Duyn, J. H. and Leopold, D. A. (2010). Neural basis of global resting-state fMRI activity., *Proc. Natl. Acad. Sci. U.S.A.* **107**(22): 10238–43.

Schwartz, S., Regillo, C., Lam, B. and Eliott, D. (2015). Human embryonic stem cell-derived retinal pigment epithelium in patients with age-related macular degeneration and stargardt's macular dystrophy: follow-up of two , *The Lancet* **385**: 509–516.

Schwarz, A. J., Danckaert, A., Reese, T., Gozzi, A., Paxinos, G., Watson, C., V, M. E. and Bifone, A. (2006). A stereotaxic MRI template set for the rat brain with tissue class distribution maps and co-registered anatomical atlas: application to pharmacological MRI., *NeuroImage* **32**(2): 538–550.
URL: *http://dx.doi.org/10.1016/j.neuroimage.2006.04.214*

Seevinck, P. R., Deddens, L. H. and Dijkhuizen, R. M. (2010). Magnetic resonance imaging of brain angiogenesis after stroke, *Nato Adv Sci Inst Se* **13**(2): 101–111.

Seitz, R., Azari, N., Knorr, U., Binkofski, F., Herzog, H. and Freund, H. (1999). The role of diaschisis in stroke recovery., **30**(9): 1844–50.

Sharkey, J., Ritchie, I. and Kelly, P. (1993). Perivascular microapplication of endothelin-1: a new model of focal cerebral ischaemia in the rat., *J. Cereb. Blood Flow Metab.* **13**(5): 865–71.

Shen, L., Li, Y., Chen, J., Zhang, J., Vanguri, P., Borneman, J. and Chopp, M. (2006). Intracarotid transplantation of bone marrow stromal cells increases axon-myelin remodeling after stroke., **137**(2): 393–9.

Shuaib, A., Lees, K., Lyden, P. and Grotta, J. (2007). NXY-059 for the treatment of acute ischemic stroke, *New England Journal of Medicine* **357**: 562–71.

Siegel, J. S., Snyder, A. Z., Ramsey, L., Shulman, G. L. and Corbetta, M. (2015). The effects of hemodynamic lag on functional connectivity and behavior after stroke., *J. Cereb. Blood Flow Metab.* **0**: 1–15.

Sigler, A., Mohajerani, M. H. and Murphy, T. H. (2009). Imaging rapid redistribution of sensory-evoked depolarization through

existing cortical pathways after targeted stroke in mice., *Proc. Natl. Acad. Sci. U.S.A.* **106**(28): 11759–64.

Silva, A. C. and Koretsky, A. P. (2002). Laminar specificity of functional MRI onset times during somatosensory stimulation in rat, *Proceedings of the National Academy of Sciences.* **99**: 15182–7.

Simmons, M., Frondoza, C. and Coyle, J. (1991). Immunocytochemical localization of n-acetyl-aspartate with monoclonal antibodies., *Neuroscience* **45**(1): 37–45.

Simpson, R., Phillis, J. and Buchannan, J. (1990). A comparison of cerebral blood flow during basal, hypotensive, hypoxic and hypercapnic conditions between normal and streptozotocin diabetic rats., **531**(1-2): 136–42.

Sinclair, M. D. (2003). A review of the physiological effects of alpha2-agonists related to the clinical use of medetomidine in small animal practice., *The Canadian veterinary journal. La revue vétérinaire canadienne* **44**(11): 885–897.

Sinden, J. D., Vishnubhatla, I. and Muir, K. W. (2012). *Prospects for stem cell-derived therapy in stroke*, Vol. 201, Sciencedirect.

Sist, B., Jesudasan, S. and Winship, I. (2012). *Diaschisis, Degeneration, and Adaptive Plasticity After Focal Ischemic Stroke*, InTech, chapter 1, pp. 1–28.

Skop, N. B., Calderon, F., Cho, C. H., Gandhi, C. D. and Levison, S. W. (2014). Improvements in biomaterial matrices for neural precursor cell transplantation., *Mol Cell Ther* **2**(1): 19.

Smith, E. J., Stroemer, R., Gorenkova, N., Nakajima, M., Crum, W. R., Tang, E., Stevanato, L., Sinden, J. D. and Modo, M. (2012). Implantation site and lesion topology determine efficacy of a human neural stem cell line in a rat model of chronic stroke.,

Stem cells (Dayton, Ohio) **30**(4): 785–796.
URL: *http://dx.doi.org/10.1002/stem.1024*

Smith, S. M. (2002). Fast robust automated brain extraction., *Human Brain Mapping* **17**(3): 143–55.

Smits, E., Gordon, D., Witte, S., Rasmusson, D. and Zarzecki, P. (1991). Synaptic potentials evoked by convergent somatosensory and corticocortical inputs in raccoon somatosensory cortex: substrates for plasticity., *J. Neurophysiol.* **66**(3): 688–95.

Soleman, S., Yip, P. K., Duricki, D. A. and Moon, L. (2012). Delayed treatment with chondroitinase ABC promotes sensorimotor recovery and plasticity after stroke in aged rats, *Brain* **135**(4): 1210–1223.

Song, W., Park, K., Kim, H., Lee, J., Choi, J. and Chong, S. (2015). Treatment of macular degeneration using embryonic stem cell-derived retinal pigment epithelium: preliminary results in asian patients, *Stem cell reports* **4**: 860–872.

Steinberg, G. K., Kondziolka, D., Wechsler, L. R., Lunsford, L., Coburn, M. L., Billigen, J. B., Kim, A. S., Johnson, J. N., Bates, D., King, B., Case, C., Michael, M., Yankee, E. W. and Schwartz, N. E. (2016). Clinical outcomes of transplanted modified bone Marrow-Derived mesenchymal stem cells in stroke: A phase 1/2a study., *Stroke* **47**: 1–15.

Steiner, L. and Andrews, P. (2006). Monitoring the injured brain: ICP and CBF, *British journal of anaesthesia* **97**(1): 26–38.

Stevanato, L., Corteling, R. L., Stroemer, P., Hope, A., Heward, J., Miljan, E. A. and Sinden, J. D. (2009). c-MycERTAM transgene silencing in a genetically modified human neural stem cell line

implanted into MCAo rodent brain, *BMC Neuroscience* **10**: 1–13.
URL: *http://dx.doi.org/10.1186/1471-2202-10-86*

Stowe, A. M., Plautz, E. J., Ines, E., Frost, S. B., Barbay, S., Zoubina, E. V., Dancause, N., Taylor, M. D. and Nudo, R. J. (2007). VEGF protein associates to neurons in remote regions following cortical infarct, *Journal of Cerebral Blood Flow & Metabolism* **27**(1): 76–85.

Stroemer, P., Patel, S., Hope, A., Oliveira, C., Pollock, K. and Sinden, J. (2009). The neural stem cell line CTX0E03 promotes behavioral recovery and endogenous neurogenesis after experimental stroke in a dose-dependent fashion., *Neurorehabilitation and neural repair* **23**(9): 895–909.
URL: *http://dx.doi.org/10.1177/1545968309335978*

Stroemer, R., Kent, T. and Hulsebosch, C. (1995). Neocortical neural sprouting, synaptogenesis, and behavioral recovery after neocortical infarction in rats, *Stroke* **26**(11): 2135–2144.
URL: *http://stroke.ahajournals.org/content/26/11/2135.abstract*

Strohl, K. P., Thomas, A. J., St. Jean, P., Schlenker, E. H., Koletsky, R. J. and Schork, N. J. (1997). Ventilation and metabolism among rat strains, *Journal of Applied Physiology* **82**(1): 317–323.
URL: *http://jap.physiology.org/content/82/1/317*

Sykova, E. and Jendelova, P. (2007). *In vivo tracking of stem cells in brain and spinal cord injury*, Vol. 161, Sciencedirect.

Symposium, I. S. (2016). Middle cerebral artery - superior division.
URL: *http://www.strokecenter.org/professionals/stroke-diagnosis/stroke-syndromes/middle-cerebral-artery-superior-division/*

Takahashi, K., Tanabe, K., Ohnuki, M., Narita, M. and Ichisaka, T. (2007). Induction of pluripotent stem cells from adult human fibroblasts by defined factors, *Cell* **131**: 861–872.

Tamura, A., Graham, D., J, M. and Teasdale, G. (1981). Focal cerebral ischaemia in the rat: 1. description of technique and early neuropathological consequences following middle cerebral artery occlusion., *Journal of Cerebral Blood Flow and Metabolism* **1**(1): 53–60.

Tamura, A., Tahira, Y., Nagashima, H., Kirino, T., Gotoh, O., Hojo, S. and Sano, K. (1991). Thalamic atrophy following cerebral infarction in the territory of the middle cerebral artery., *Stroke* **22**(5): 615–8.

Thanvi, B. and Robinson, T. (2006). Sporadic cerebral amyloid angiopathyan important cause of cerebral haemorrhage in older people, *Age and Ageing* **35**(6): 565–571.
URL: *http://ageing.oxfordjournals.org/content/35/6/565.abstract*

Thawley, V. and Waddell, L. S. (2013). Pulse oximetry and capnometry, *Topics in Companion Animal Medicine* **28**(3): 124–128.
URL: *http://dx.doi.org/10.1053/j.tcam.2013.06.006*

Thored, P., Wood, J., Arvidsson, A., Cammenga, J., Kokaia, Z. and Lindvall, O. (2007). Long-Term neuroblast migration along blood vessels in an area with transient angiogenesis and increased vascularization after stroke, *Stroke* **38**(11): 3032–3039.

Thulborn, K., Carpenter, P. and Just, M. (1999). Plasticity of language-related brain function during recovery from stroke., *Stroke* **30**(4): 749–54.

Tian, P., Teng, I. C., May, L. D., Kurz, R., Lu, K., Scadeng, M., Hillman, E. M., Crespigny, A. J., E, D. H., Mandeville, J. B.,

Marota, J. J., Rosen, B. R., Liu, T. T., Boas, D. A., Buxton, R. B., Dale, A. M. and Devor, A. (2010). Cortical depth-specific microvascular dilation underlies laminar differences in blood oxygenation level-dependent functional MRI signal, *Proc Natl Acad Sci* **107**(34): 15246–15251.

Trueman, R. C., Harrison, D. J., Dwyer, D. M., Dunnett, S. B., Hoehn, M. and Farr, T. D. (2011). A critical Re-Examination of the intraluminal filament MCAO model: Impact of external carotid artery transection, *Translational Stroke Research* **2**(4): 651–661.
URL: *http://dx.doi.org/10.1007/s12975-011-0102-4*

Tuunanen, P. I. and Kauppinen, R. A. (2005). Effects of oxygen saturation on BOLD and arterial spin labelling perfusion fMRI signals studied in a motor activation task., *NeuroImage* **30**(1): 102–109.

Uccelli, A., Moretta, L. and Pistoia, V. (2008). Mesenchymal stem cells in health and disease., *Nature Reviews, Immunology* **8**(9): 726–36.

Vallone, F., Lai, S., Spalletti, C., Panarese, A., Alia, C., Micera, S., Caleo, M. and Di Garbo, A. (2016). Post-Stroke longitudinal alterations of Inter-Hemispheric correlation and hemispheric dominance in mouse Pre-Motor cortex., *PLoS ONE* **11**(1): 1–26.

van den Heuvel, M. P. and Pol, H. E. (2010). Exploring the brain network: a review on resting-state fmri functional connectivity., *European neuropsychopharmacology* **20**(8): 519–34.

van Meer, M. P., Otte, W. M., van der Marel, K., Nijboer, C. H., Kavelaars, A., van der Sprenkel, J. W., Viergever, M. A. and Dijkhuizen, R. M. (2012). Extent of bilateral neuronal network reorganization and functional recovery in relation to stroke

severity., *The Journal of neuroscience : the official journal of the Society for Neuroscience* **32**(13): 4495–4507.
URL: *http://dx.doi.org/10.1523/JNEUROSCI.3662-11.2012*

van Meer, M. P., van der Marel, K., Otte, W. M., Berkelbach van der Sprenkel, J. W. and Dijkhuizen, R. M. (2010). Correspondence between altered functional and structural connectivity in the contralesional sensorimotor cortex after unilateral stroke in rats: a combined resting-state functional MRI and manganese-enhanced MRI study., *Journal of Cerebral Blood Flow and Metabolism* **30**(10): 1707–1711.
URL: *http://dx.doi.org/10.1038/jcbfm.2010.124*

van Zijl, P. C., Hua, J. and Lu, H. (2012). The BOLD post-stimulus undershoot, one of the most debated issues in fMRI., *Neuroimage* **62**(2): 1092–102.

vanMeer, M., vanderMarel, K., Wang, K., Otte, W., ElBouazati, S., Roeling, T., Viergever, M., BerkelbachvanderSprenkel, J. and Dijkhuizen, R. (2010). Recovery of sensorimotor function after experimental stroke correlates with restoration of resting-state interhemispheric functional connectivity., *The Journal of neuroscience : the official journal of the Society for Neuroscience* **30**(11): 3964–3972.
URL: *http://dx.doi.org/10.1523/JNEUROSCI.5709-09.2010*

Veinante, P. and Deschênes, M. (1999). Single- and multi-whisker channels in the ascending projections from the principal trigeminal nucleus in the rat., *J Neurosci Official J Soc Neurosci* **19**(12): 5085–95.

Vendrame, M., Cassady, J., Newcomb, J., Butler, T., Pennypacker, K., Zigova, Z., Sanberg, C., Sanberg, P. and Willing, A. (2004). Infusion of human umbilical cord blood cells in a rat model of

stroke dose-dependently rescues behavioral deficits and reduces infarct volume, *Stroke* **35**(10): 2390–2395.
URL: *http://dx.doi.org/10.1161/01.STR.0000141681.06735.9b*

Virley, D., Beech, J. S., Smart, S. C., Williams, S. C., Hodges, H. and Hunter, J. A. (2000). A temporal MRI assessment of neuropathology after transient middle cerebral artery occlusion in the rat: Correlations with behavior, *J Cereb Blood Flow Metabolism* **20**(3): 563–582.

von Kummer, R., Dzialowski, I. and Gerber, J. (2015). Therapeutic efficacy of brain imaging in acute ischemic stroke patients., *J Neuroradiol* **42**(1): 47–54.

Ward, N., Brown, M., Thompson, A. and Frackowiak, R. (2003a). Neural correlates of outcome after stroke: a cross-sectional fMRI study., *Brain : a journal of neurology* **126**(Pt 6): 1430–1448.

Ward, N. S., Brown, M. M., Thompson, A. J. and Frackowiak, R. S. J. (2003b). Neural correlates of motor recovery after stroke: a longitudinal fMRI study, *Brain* **126**(11): 2476–2496.
URL: *http://dx.doi.org/10.1093/brain/awg245*

Watson, B. D., Dietrich, D. W., Busto, R., Wachtel, M. S. and Ginsberg, M. D. (1985). Induction of reproducible brain infarction by photochemically initiated thrombosis, *Annals of Neurology* **17**(5): 497–504.

Weber, R., Pedro, R. and Hoehn, M. (2005). Present status of magnetic resonance imaging and spectroscopy in animal stroke models, *J. Neurosci* **26**(5): 591–604.

Weber, R., Pedro, R., Justicia, C., Wiedermann, D., Strecker, C., Sprenger, C. and Hoehn, M. (2008). Early prediction of functional recovery after experimental stroke: functional magnetic

resonance imaging, electrophysiology, and behavioral testing in rats., *Journal of Neuroscience* **28**(5): 1022–9.

Weber, R., Pedro, R., Wiedermann, D., van Camp, N. and Hoehn, M. (2006). A fully noninvasive and robust experimental protocol for longitudinal fMRI studies in the rat., *NeuroImage* **29**(4): 1303–1310.
URL: *http://dx.doi.org/10.1016/j.neuroimage.2005.08.028*

Wegener, S., Weber, R. and P, R. (2005). Temporal profile of t2-weighted MRI distinguishes between pannecrosis and selective neuronal death after transient focal cerebral ischemia in the rat, *Journal of Cerebral Blood Flow and Metabolism* **26**: 38–47.

Weiller, C., Ramsay, S., Wise, R., Friston, K. and Frackowiak, R. (1993). Individual patterns of functional reorganization in the human cerebral cortex after capsular infarction., *Ann. Neurol.* **33**(2): 181–9.

Weishaupt, N., Silasi, G. and Colbourne, F. (2010). Secondary damage in the spinal cord after motor cortex injury in rats, *Journal of Neurotrauma* **27**: 1387–1397.

Weisskoff, R. M. and Kiihne, S. (1992). MRI susceptometry: Image based measurement of absolute susceptibility of MR contrast agents and human blood, *Magnetic Resonance in Medicine* **24**(2): 375–383.

Wells, A. J., Vink, R., Blumbergs, P. C., Brophy, B. P., Helps, S. C., Knox, S. J. and Turner, R. J. J. (2012). A surgical model of permanent and transient middle cerebral artery stroke in the sheep., *PLoS ONE* **7**(7): e42157.

Westlake, K. and Nagarajan, S. (2011). Functional connectivity in relation to motor performance and recovery after stroke, *Frontiers in Systems Neuroscience* **5**: 1–12.

Whishaw, I. and Pellis, S. (1990). The structure of skilled forelimb reaching in the rat: a proximally driven movement with a single distal rotatory component., *Behav Brain Res* **41**(1): 49–59.

Whishaw, I. Q. and Gorny, B. (1994). Arpeggio and fractionated digit movements used in prehension by rats, *Behav Brain Res* **60**(1): 15–24.

Whishaw, I., WT, O. and Dunnett, S. (1986). The contributions of motor cortex, nigrostriatal dopamine and caudate-putamen to skilled forelimb use in the rat., *Brain J Neurology* **109 (Pt 5)**: 805–43.

Whiteley, W. N., Emberson, J., Lees, K. R., Blackwell, L., Albers, G., Bluhmki, E., Brott, T., Cohen, G., Davis, S., Donnan, G., Grotta, J., Howard, G., Kaste, M., Koga, M., von Kummer, R., Lansberg, M. G., Lindley, R. I., Lyden, P., Olivot, J. M., Parsons, M., Toni, D., Toyoda, K., Wahlgren, N., Wardlaw, J., Del Zoppo, G. J., Sandercock, P., Hacke, W. and Baigent, C. (2016). Risk of intracerebral haemorrhage with alteplase after acute ischaemic stroke: a secondary analysis of an individual patient data meta-analysis., *Lancet Neurol* pp. 1–9.

Williams, K. A., Magnuson, M., Majeed, W., LaConte, S. M., Peltier, S. J., Hu, X. and Keilholz, S. D. (2010). Comparison of -chloralose, medetomidine and isoflurane anesthesia for functional connectivity mapping in the rat, *Magnetic Resonance Imaging* **28**(7): 995–1003.
URL: *http://dx.doi.org/10.1016/j.mri.2010.03.007*

Windrem, M., Nunes, M. and Rashbaum, W. (2004). Fetal and adult human oligodendrocyte progenitor cell isolates myelinate the congenitally dysmyelinated brain, *Nature medicine* **10**: 93–97.

Witte, O., Bidmon, H., Schiene, K., Redecker, C. and Hagemann, G. (2000). Functional differentiation of multiple perilesional zones after focal cerebral ischemia., *J. Cereb. Blood Flow Metab.* **20**(8): 1149–65.

Wolf, S., Thompson, P., Winstein, C. and Miller, J. (2010). The EXCITE stroke trial comparing early and delayed constraint-induced movement therapy, *Stroke* .

Woodruff, T., Thundyil, J., Tang, S. and Sobey, C. (2011). Pathophysiology, treatment, and animal and cellular models of human ischemic stroke, *Molecular Neurodegeneration* **6**: 1–19.

Woolsey, T. A. and der Loos, H. (1970). The structural organization of layer IV in the somatosensory region (S i) of mouse cerebral cortex the description of a cortical field composed of discrete cytoarchitectonic units, *Brain Res* **17**(2): 205–242.

Yan, C. and Zang, Y. (2010). DPARSF: a MATLAB toolbox for "Pipeline" data analysis of Resting-State fMRI., *Front Syst Neurosci* **4**: 1–7.

Yozbatiran, N., Der-Yeghiaian, L. and Cramer, S. C. (2008). A standardized approach to performing the action research arm test, *Neurorehabilitation and Neural Repair* **22**(1): 78–90.
URL: *http://nnr.sagepub.com/content/22/1/78.abstract*

Zhang, L., Schallert, T., Zhang, Z., Jiang, Q., Arniego, P., Li, Q., Lu, M. and Chopp, M. (2002). A test for detecting long-term sensorimotor dysfunction in the mouse after focal cerebral

ischemia., *Journal of neuroscience methods* **117**(2): 207–214.
URL: *http://dx.doi.org/10.1016/S0165-0270(02)00114-0*

Zhang, P., Li, J., Liu, Y., Chen, X., Lu, H., Kang, Q., Li, W. and Gao, M. (2011). Human embryonic neural stem cell transplantation increases subventricular zone cell proliferation and promotes periinfarct angiogenesis after focal cerebral ischemia, *Neuropathology* **31**(4): 384–391.

Zhao, F., Zhao, T., Zhou, L., Wu, Q. and Hu, X. (2008). BOLD study of stimulation-induced neural activity and resting-state connectivity in medetomidine-sedated rat, *Neuroimage* **39**(1): 248–60.